Peptide and Monoclonal Antibody Mediated Targeting of Nanoconjugates in Cancer Chemotherapy

A thesis submitted in the fulfillment of the requirements for degree of

Doctor of Philosophy

Hitesh Kulhari
M. Pharm.

School of Applied Sciences
College of Science, Engineering and Health
RMIT University, Australia

March 2015

Declaration

I certify that except where due acknowledgement has been made, the work is that of the author alone; the work has not been submitted previously, in whole or in part, to qualify for any other academic award; the content of the thesis is the result of work which has been carried out since the official commencement date of the approved research program; and, any editorial work, paid or unpaid, carried out by a third party is acknowledged; and ethics procedures and guidelines have been followed.

Date: March 25, 2015 **Hitesh Kulhari**

This Thesis is

Dedicated to

MY WIFE

Who never once allowed me to believe that it couldn't be done.

I am eternally grateful to you for your immense Love and Care.

Acknowledgements

"In the name of GOD, the most gracious and the most merciful"

I would like to begin my acknowledgement by first acknowledging the creator who made all life possible and without whom I wouldn't be here. I am indeed so much indebted to him, nothing but his help leads to our destination.

A journey is easier when you travel together. Interdependence is certainly more valuable than independence. This thesis is the result of three years of work whereby I have been accompanied and supported by many people. It is a pleasant aspect that I have now the opportunity to express my gratitude for all of them.

Since my first day of Ph.D. duration I felt, I have been given unique opportunities... and taken advantage of them. This includes working at the IICT for two years and the one year at RMIT. So first of all I want to thank Dr. Laxmi Kantham, Director, CSIR-IICT and Prof. Suresh Bhargava, Pro Vice-chancellor, RMIT University who started the IICT-RMIT Joint Research Centre and gave me an opportunity to join this PhD programme.

With a deep sense of gratitude, I wish to express my sincere thanks to both of my *supervisors, Prof. David Adams* and *Dr. Ramakrishna Sistla* for their immense help in planning and executing the works in time.

I would like to express my deepest gratitude to my supervisor *Dr. Ramakrishna Sistla*, for his excellent guidance, caring, patience, and providing me with an excellent atmosphere for doing research. He took me on the process of learning and made himself available even through his very heavy work load. What I know today about the process of research, I learned from Dr. Sistla. His company and assurance at the time of crisis would be remembered lifelong. I believe that one of the main gains of two years at IICT was working with Dr. Sistla and gaining his trust and guidance.

The confidence and dynamism with which *Prof. David Adams* guided the work requires no elaboration. He has been a tremendous mentor for me. His understanding, encouraging and personal guidance have provided a good basis for the present thesis. His valuable suggestions as final words during the course of work are greatly acknowledged. His research aptitude, zeal for work and innovative ideas would be remembered by me. I also want to thank you for letting my defense be an enjoyable moment, and for your brilliant comments and suggestions.

I owe my sincere gratitude to *Dr. Madhusudhana Kuncha and Mr. Syed Fareed Ahmed* for their sincere help during animal studies at IICT.

The cooperation I received from labmates at IICT specially *Shweta*, *Mayank, Deepthi, Rasika, Sudeep, Srinivas Chinde* is gratefully acknowledged.

I wish I would never forget the company I had from my juniors of IICT laboratory. I enjoyed my work with the company of *Vishnu Kiran, Nishant, Vinay Das, Laxmi, Bharathi, Harshini, Raju, Riyaz, Sravani, Nikhila, Dileep* and *Samrat.* They will always be within my sweet memories.

The episodes of acknowledgement would not be complete without the mention of my colleagues *Rajan* and *Indu* for their love, support, space and time I occupied.

A special group from the RMIT is not mentioned yet, because they deserve their own part: the NBRL group. I praise the enormous amount of help and teaching by *Prof. Vipul Bansal & Dr. Ravi Shukla.* I specially thank them for the help extended to me when I approached them and the valuable discussion that I had with them during the course of research.

I greatly appreciate *Dr. Suzzane Rogers* for her generous time to read the drafts of my manuscripts. She is always ready to help with a smile.

I would like to thank administrative and technical staff member of RMIT University, especially Dr. Lisa Dias, who have been kind enough to advice and help in their respective role.

Needless to say, that I am grateful to my entire lab buddies at the RMIT made it a convivial place to work. In particular, I would like to thank *Srinu, Praveen, Jampu, Suresh, Vishal and Amanda*. I should also appreciate the kind help and support of *Dr. Rajesh Ramanathan, Dr. Sarvesh Soni* and *Dr. Selvakannan Periasamy* during my stay at Melbourne.

I will be failing in my duty if I do not mention the laboratory staff of MCP division and BIOSAFE for their timely help. I specially thank *Laxman, Chinna* and *Rajesh* for their help during this study.

I will not forget to memorize the small wonders of nature as they sacrificed their lives during the course of this study.

A special thanks to my family. Words cannot express how grateful I am to my parents for all of the sacrifices that you've made on my behalf. Your prayer for me was what sustained me thus far. I would

also like to thank my parent in-laws. They were always supporting and encouraging me with their best wishes. I would also like to thank all of my brothers, sister and in-laws who supported me in my life, and incented me to strive towards my goal.

At the end I would like to express appreciation to my beloved wife *Deep Pooja* and loving daughter Dyuti (Teesha). Deep, who spent sleepless nights with and was always my support in the moments when there was no one to answer my queries. No word can express heartfelt thanks to her without whose motivation, support and encouragement, my all efforts would have been in vain. Her positive attitude always helped me to choose the best option, to take some big decisions and to do the best during each and every step of my carrier. I am heartily thankful to her for being so co-operative in this long journey.

Teesha, my little cute angel, a source of endless joy and love. I am deeply sorry for the time we spent apart. You have inspired me in ways that you may never understand. The day you came into my life is the happiest day of my life. I look forward to watching you grow and achieve your goals. Teeshu, you are my biggest accomplishment. I thank God for you.

The chain of my gratitude would be definitely incomplete if I would forget to thank M/s TherDose Pharma Pvt. Ltd, Hyderabad for providing the anticancer drugs- docetaxel, paclitaxel and gemcitabine hydrochloride.

Hitesh Kulhari

Abstract

Cancer is one of the most common causes of the death. Currently used anticancer drugs have shown to be effective against various cancers. However, these anticancer drugs cannot differentiate between tumor cells and normal cells. These agents kill both types of cells resulting in severe side effects. Poor physico-chemical properties of anticancer drugs and development of chemo-resistance in cancer cells aggravate the problems. Over the past one decade, nanotechnology-based formulations have been explored to overcome the limitations of anticancer drugs. These nanomedicines have shown promises to deliver drugs effectively to the cancer cells. In this research work, efforts have been made to improve the specificity of the drug loaded nanocarriers towards tumor cells. Cancer cells over express some receptors than normal cells. Therefore, nanocarriers attached with a ligand, having high affinity to particular receptor, could be target to cancer cells. In this context, two peptides (bombesin and cyclic RGDfK) and a monoclonal antibody, trastuzumab, were used as targeting ligand. Polymeric nanoparticles were used as drug carriers. Polymers such as poly(lactic-co-glycolic acid) (PLGA), D-α-tocopheryl polyethylene glycol succinate (TPGS), dendrimers and poly(glutamic acid) (PGA) were used for the preparation of nanoparticles. The selection of the polymers depended on the physicochemical properties of drug, desired particle size range, target tissue and the functional group available on the surface for conjugation with targeting ligand.

Bombesin conjugated PLGA nanoparticles showed the potential to improve the delivery of a hydrophobic anticancer drug, docetaxel, in gastrin releasing peptide receptors over expressing breast and prostate cancer cells. Trastuzumab conjugated dendrimers demonstrated high specificity towards human epidermal growth factor 2

receptors over expressing breast cancer cells. cRGDfK conjugated TPGS nanomicelles showed significant cytotoxicity and anti-angiogenic activity of encapsulated docetaxel to integrin receptors over expressing prostate cancer cells. As integrin receptors have also been over expressed in other cancers such as ovarian, brain, lung and breast cancers, cRGDfK conjugated nanoparticles were investigated for the targeting of drugs to ovarian and brain cancers. cRGDfK conjugated PLGA nanoparticles were investigated for the delivery of hydrophilic gemcitabine hydrochloride to ovarian cancer. In a separate study, cRGDfK was conjugated to PGA nanoparticles for selective targeting of hydrophobic camptothecin to integrin over expressing brain tumor cells.

In summary, this thesis presents a research done with regards to preparation of anticancer drugs loaded different nanoparticles, bioconjugation of targeting ligand on the surface of nanoparticles and evaluation of anticancer activities of these ligand mediated targeted drug delivery systems in cancer cells. The study revealed that the nanoparticle-based targeted formulations better control over the growth of cancer than plain drugs.

Table of Contents

LIST OF FIGURES

LIST OF TABLES

LIST OF SCHEMES

LIST OF ABBREVIATIONS

AFM	Atomic Force Microscopy
AO	Acridine orange
AUC	Area under the curve
BBN	Bombesin
FITC	5(6)-Carboxy-2′,7′-dichlorofluorescein diacetate
Cl	Total clearance
C_{max}	Peak plasma concentration
CPT	Camptothecin
cRGDfK	Cyclo(Arg-Gly-Asp-D-Phe-Lys)
Carboxy-DCFDA	Carboxy-2', 7'-dichlorofluorescein diacetate
DMEM	Dulbecco’s modified eagle medium
DMSO	Dimethyl sulfoxide
DTX	Docetaxel
EB	Ethidium bromide
EDC	1-Ethyl-3-(3-dimethylaminopropyl) carbodiimide
FBS	Fetal bovine serum
FITC	Fluorescein isothiocyanate
GBM	Glioblastoma multiforme
GEM	Gemcitabine hydrochloride
GRP	Gastrin-releasing peptide
HPLC	High performance liquid chromatography
MAL-PEG-NHS	Maleimide-poly(ethylene) glycol-N-hydroxysuccinimide

MES	2-(n-morpholino) ethanesulfonic acid
MRT	Mean residence time
MTT	3-(4, 5- dimethylthiazol-2-yl)-2, 5-diphenyl tetrazolium bromide
NHS	N-hydroxysuccinimide
PA	Phenyl alanine
PAE	Phenyl alanine ester
PAMAM	Poly(amidoamine)
PGA	Poly (glutamic) acid
PGA-PA	Poly (glutamic acid)-phenyl alanine conjugate
PK	Pharmacokinetic
PLGA	Poly (lactic-co-glycolic acid)
ROS	Reactive oxygen species
SD	Standard deviation
SEM	Scanning Electron Microscopy
$t_{1/2}$	Plasma half-life
TEM	Transmission Electron Microscopy
C_{max}	Time to reach peak plasma concentration
TZ	Trastuzumab
UPLC	Ultra performance liquid chromatography
VEGF	Vascular endothelial growth factor
XPS	X-ray Photoelectron Spectroscopy
XRD	X-ray Diffraction

CHAPTER

Introduction

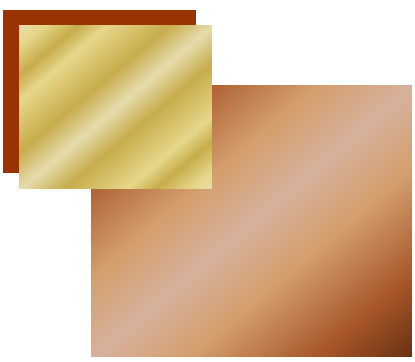

1.1. Overview

The objective of this study was to develop nanocarrier based cellular targeting system for active targeting of anticancer drugs and to improve the therapeutic efficacy of chemotherapy by enhancing the bioavailability of the drug, decreasing the total dose requirements and dosing frequency. In this introductory chapter, the role of chemotherapy in cancer treatment, problems associated with current cancer chemotherapy and advantages of nanotechnology based targeted drug delivery systems in the delivery of anticancer drugs are reviewed. Typically, a targeted drug delivery system is composed of two basic components-first a nanocarrier and second a targeting ligand. The nanocarrier is required to carry the drug molecules while the ligand is needed for selective targeting of the drug-loaded nanocarrier to the cancer cells. This chapter summarizes the different nanocarrier systems with specific emphasis on polymeric nanoparticles, surfactant based nanomicelles and dendrimers which have been used in research. Similarly, various targeting ligands have been summarized with their potential target receptors while three ligands namely bombesin peptide, cRGDfK peptide and trastuzumab monoclonal antibody have been discussed in detail.

1.2. Cancer and cancer treatment

Cancer is a leading cause of death across the world. As per the GLOBOCAN 2012 report by The International Agency for Research on Cancer (IARC) of the World Health Organization (WHO), about 14.1 million new cases were diagnosed and 8.2 million cancer-related deaths occurred in 2012. IARC also estimated an increase of this number to 19.3 million new cancer cases every year by 2025. Lung cancer is the most commonly diagnosed cancer with 13% of total diagnosed cases followed by breast cancer (11.9%) and colorectal cancer (9.7%) (IAFRO, 2013).

Cancer is a group of diseases characterized by uncontrolled growth and spread of abnormal cells. Based on origin, cancer can be categorized as:

- Carcinoma: starts in the skin or tissues that line or cover internal organs.
- Leukemia: in blood forming tissues.
- Lymphoma and myeloma: cancer in the immune system
- Sarcoma: cancer in bone, cartilage, muscles, blood vessels or other connective tissues.

Commonly used cancer treatment approaches include surgery, chemotherapy and radiation therapy. Surgery is the first treatment option in the case of early stages of cancer and when removal of the tumour from the body is possible. However, none of these therapies are sufficient to cure cancer. Therefore, a combined approach is used to provide more effective treatment than a single therapy. Chemotherapy helps to shrink the tumour and is followed by radiation therapy. High-energy radiation such as X-rays and gamma rays are used in radiation therapy. This therapy may work either by directly damaging the DNA of cancer cells making them unable to divide further or by an indirect approach by generating free radicals which damage DNA. (Bernier et al., 2004; Bhaskar et al., 2012) In chemotherapy, anticancer agents are used to kill cancer cells. Recently, some other therapeutic approaches such as hormone therapy and immunotherapy have been designed to treat cancer (Sioka et al., 2009).

1.3. Chemotherapy

Chemotherapy involves the use of chemical substances to destroy cancer cells. As a common mechanism, chemotherapeutic agents impair mitosis and thereby inhibit cell division. Anticancer agents are broadly classified as (Payne and David, 2008):

a) *Alkylating agents:* Alkylating agents causes the cross-linking between two strands of DNA and thereby prevent replication of DNA. eg. Cyclophosphamide, mechlorethamine.

b) *Antimetabolites:* These drugs have structural similarity to the biomolecules needed for the synthesis of RNA and DNA. Thus, these compounds act as fake substrate and enter in cell cycle during s-phase of cell cycle and block synthesis of RNA and DNA. eg. Methotrexate, 5-Fluorouracil.

c) *Natural products:* These compounds are obtained from natural sources. Eg. Taxanes (docetaxel, paclitaxel), camptothecin, vinca alkaloids (vinblastin, vincristine) and podophyllotoxins (etoposide, teniposide)

d) *Antibiotics:* Daunorubicin, doxorubicin, bleomycin

e) *Hormones and antagonists:* Corticosteroids (prednisone, dexamethasone), androgen (testosterone propionate), anti-androgen (flutamide), estrogens (ethinyloestradiol), anti-estrogens (tamoxifen), progesterone derivative (megestrol acetate) and aromatase inhibitors (anastrazole).

f) *Enzyme*s: L-asparaginase

g) *Monoclonal antibodies:* Trastuzumab, cetuximab, bevacizumab, rituximab

1.4. Problems with current cancer chemotherapy

Current anticancer chemotherapy suffers with following major drawbacks:

a) *Non-specificity*: Although available anticancer drugs are effective to kill cancer cells, they can't differentiate between a normal cell and a cancer cell. This non-selectivity of anticancer drugs leads to systemic toxicity and severe side effects (Ross et al., 2004).

b) *Tumor resistance to cancer cells*: Cancer cells shows inherent and some acquired resistance towards anticancer drugs including altered apoptosis

regulation, increased DNA damage repair, alteration in metabolism, under-expression of topoisomerase II or topoisomerase II gene mutations,decreased uptake of water-soluble drugs and increased energy-dependent efflux of hydrophobic anticancer drugs (Krishna and Mayer, 2000). Energy-dependent efflux of hydrophobic anticancer drugs by tumor cells is due to over expression of glycoproteins involved in the efflux of drugs. Due to this efflux, patients are needed to be exposed to high dosages of anticancer drugs.

c) *Inability to across protective lining of tissues*: Anticancer drugs can't cross the protective lining of some tissues. For example, the brain is well protected by the blood brain barrier (BBB) and anticancer drugs are unable to cross BBB to provide therapeutic effects in brain cancer (Elsabahy M, Wooley, 2012).

d) *Aggregation or precipitation due to poor aqueous solubility (Cho et al., 2008)*

e) *In vivo degradation (Parveen et al., 2012)*

f) *Short circulation half-life and*

g) *Low therapeutic indices (Cho et al., 2008; Parveen et al., 2012)*

1.5. Targeted drug delivery systems (TDDS)

In the past decade, targeted drug delivery systems have shown potential to overcome the problems of anticancer drugs. These TDDS deliver anticancer drugs specifically to cancer cells with a minimum or low toxicity to normal cells. TDDS make use of differences in the chemical and structural biology of normal and cancer cells (Brannon-Peppas and Blanchette, 2012). Tumor cells demonstrate leakiness of blood vessels, poor lymphatic drainage in tumor tissues and enhanced vascular permeability. Other biochemical differences between two types of cells are lower pH and oxygen level (hypoxia) in cancer cells than normal cells. Most of the TDDS are based on the nanotechnology. Nanoparticles are small particles with a nanometre

size. Because of small size, nanoparticles especially particles below 200 nm can extravasate through the leaky vasculature of blood vessels of the tumor (~400 nm) and accumulate in the tumor tissues (Peer et al., 2007). This phenomenon is called blood circulation and extravasations (Bae and Park, 2011). Since cancer cells grow faster than normal cells, they require more nutrients and oxygen supply which leads to induction of angiogenesis. This induced angiogenesis results in increase in permeability of blood vessels in tumor tissue (Danhier et al., 2012). Because of enhanced permeability, nanoparticles enter more into tumor tissues but are trapped or retained in the tumor bed due to poor lymphatic drainage. Therefore, this phenomenon is also called as enhanced permeability and retention (EPR) effect (Peer et al., 2007; Brannon-Peppas and Blanchette, 2012).

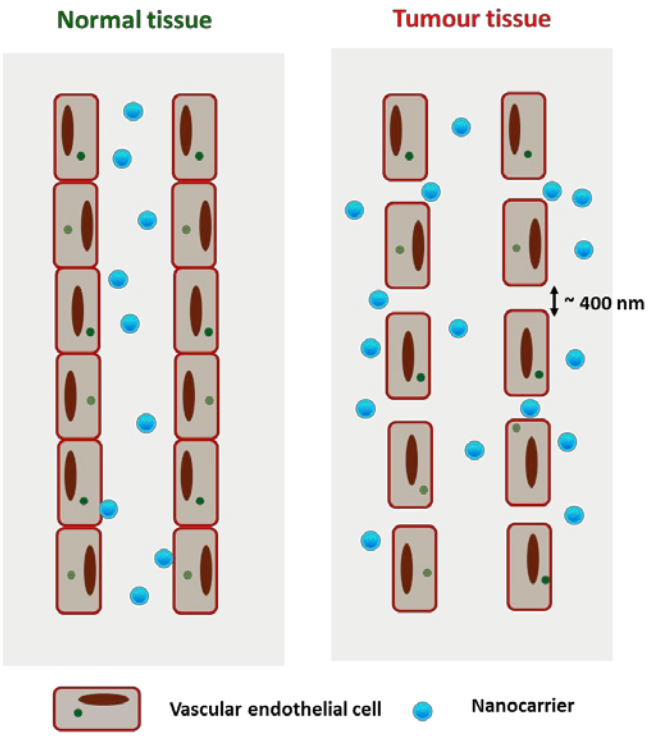

Figure 1.1: Enhanced permeability and retention (EPR) effect on the transport of nanoparticles through a normal vasculature and leaky vasculature

A size between 10-200 nm is the most preferable size range for nanoparticles to get the advantage of EPR effect for anticancer drug delivery. These nanoparticles

are not small enough to be excreted by the kidney (< 6 nm) or large enough to be rapidly recognized and trapped by the reticulo-endothelial system (RES) (>300 nm) (Michelle Longmire et al., 2008). Therefore, nanoparticles with this size range are circulated more in the blood after intravenous administration which provides more opportunity to accumulate in tumor tissues. However, this EPR is not effective enough to produce a significant improvement on the efficacy of anticancer formulations. EPR shows only 20-30% specificity towards tumor cells than other tissues (Kobayashi et al., 2014).

A more effective approach which is currently being explored is active targeting of anticancer drugs to cancer cells (Sinha et al., 2006). The backbone of this concept is over expression or up regulation of some receptors on the surface of tumor cells than normal cells. These receptors are generally absent or present at very low frequency on normal cells (Shin et al., 2013). Therefore, anticancer drugs directed to these receptors provide a unique opportunity of selective and specific delivery of drugs to cancer cells (Sinha et al., 2006; Kularatne and Low, 2010). Most of the current TDDS are based ligand-mediated targeted delivery. In this strategy, a ligand is conjugated on the surface of nanoparticles which directs nanoparticles to particular receptors. Therefore, a TDDS is composed of two important tools-a nanocarrier system which carries drug molecules and a targeting ligand.

Internalization of TDDS in cancer cells

After binding to a target receptor, nanoparticles are taken up by cancer cells through receptor-mediated endocytosis. This process is also called as clathrin-mediated endocytosis and responsible for uptake of essential nutrients such as cholesterol, iron. Cholesterol is taken up by cells through low density lipoprotein receptors while iron enters into cells via transferrin receptors. Similarly, targeted

nanoparticles are engulfed through particular receptors and form early endosomes. Drug encapsulated in nanoparticles is released due to degradation of nanoparticles, triggered by pH or enzymes. Detached receptors are recycled on the surface of cells extracellularly.

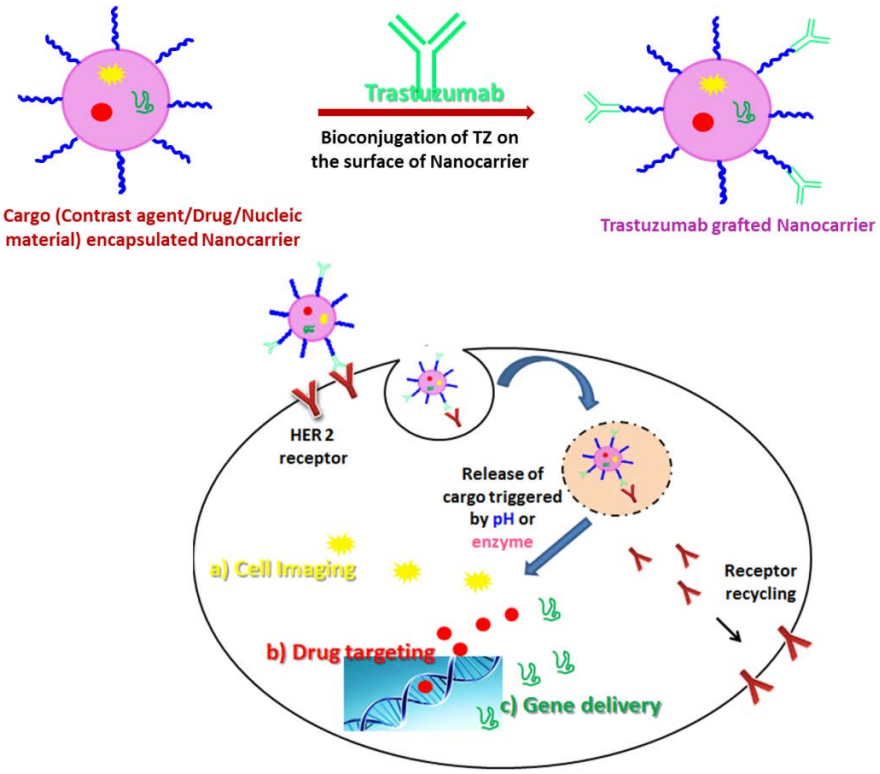

Figure 1.2: Bioconjugation and internalization of trastuzumab conjugated nanocarriers. Conjugated nanoparticles bind to HER2 receptors over expressed on the cancer cells and enter via receptor-mediated endocytosis. After internalization, the encapsulated molecule (imaging or drug or gene) is released by enzymatic or pH based activities in lysosomes. Receptors are recycled whereas encapsulated molecule is exposed to its target. (This figure is taken from Kulhari et al., 2014)

1.6. Types of nanoparticles

Nanoparticles enhance the aqueous solubility of hydrophobic drugs, controlled drug release, protect drug from degradation and improved bioavailability. Nanoparticles can be modified for targeted delivery of drugs and thereby reduce total dosage requirements and reduce side effects. Nanoparticles allow rapid-formulation

development and can be formulated in different ways according to route of administration.

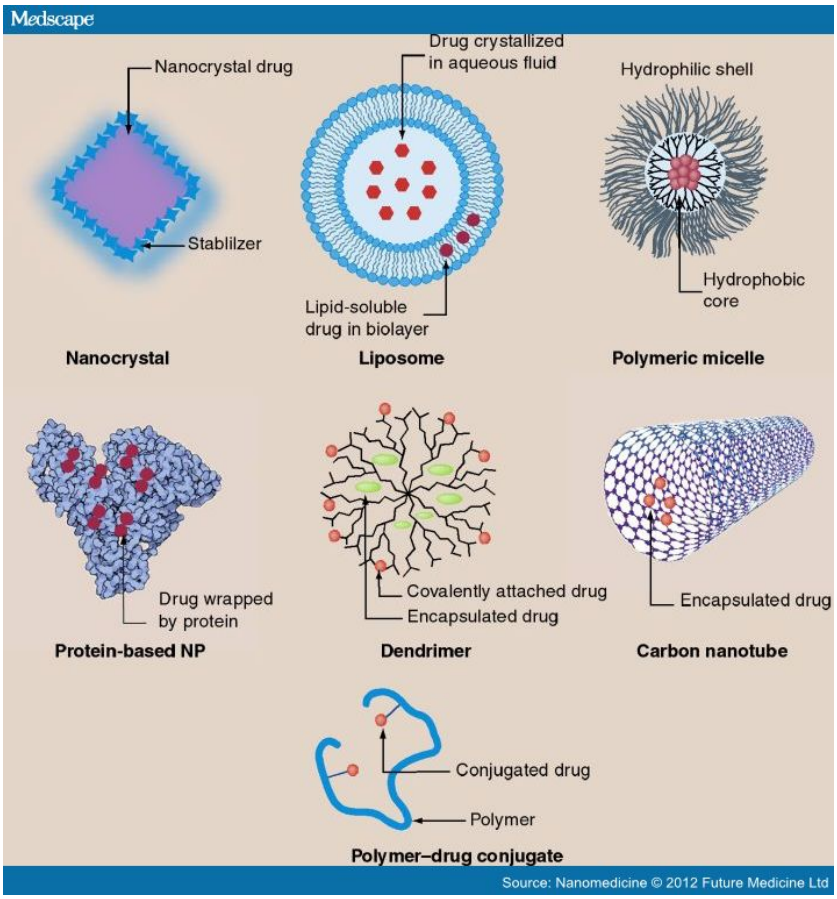

Figure 1.3: Different types of nanocarrier systems currently being explored as carrier system for anticancer drugs. This figure is taken from Bamrungsap et al., 2012.

Based on material used for nanoparticles-matrix, NPs can be categorized as follows:

a) Polymeric nanoparticles: Polymeric nanoparticles contain a polymer as matrix. Polymer may be a single (linear or branched) or a graft copolymer. Commonly used polymeric materials are D, L-lactide co-glycolide (PLGA), polylactide(PLA), polyethyleneimine (PEI), poly(glutamic) acid (PGA), poly(acrylic) acid, poly(ethylene glycol) (PEG) etc.

b) Carbohydrate and protein based nanoparticles: Apart from synthetic polymers some carbohydrate based high molecular weight compounds have been investigated

as drug delivery carrier. These include dextran, chitosan, gelatin, bovine serum albumin etc.

c) Lipid-based nanoparticles: Lipid nanoparticles are composed of a lipid, an emulsifier and water. These nanoparticles can be converted into different form such as liposomes, niosomes, solid lipid nanoparticles, lipid nanostructures, nanoemulsions, self-emulsifying nanoparticles etc.

d) Inorganic nanoparticles: The use of inorganic nanoparticles for thernostic applications in cancer is emerging as a new area. The unique physicochemical properties of inorganic nanoparticles such as extremely small size (<50 nm), high surface reactivity, stability in biological fluids and presence of surface plasmon response, make them suitable for imaging, diagnostic and drug delivery applications. There are types of inorganic nanoparticles: metal nanoparticles and ceramic nanoparticles. Metal nanoparticles are composed of a metal such as gold, silver, iron oxide or titanium (Song et al., 2009). Mesoporous silica nanoparticles (MSNs) are example of ceramic nanoparticles. MSNs are highly biocompatible and does not show change in porosity with pH. MSNs are highly stable and do not exhibit swelling in physiological conditions.

e) Dendrimers: Dendrimers are synthetic organic compounds with nanoscale structural design with very low polydispersity (Mw/Mn< 1.01-1.05) and high surface functionality. The structure of dendrimers contains three basic components: a central core, branches with lots of void spaces and terminal surface group (Figure 3). The unique structure of dendrimers makes them ideal nanocarrier system for delivery of contrast agents, drugs and genes. Based on core materials dendrimers are further classified as poly (propylene imine) dendrimers, poly (ethylene) imine dendrimers, poly(amido amine) (PAMAM) dendrimers and peptide dendrimers.

f) Surfactant based nanomicelles: Nanomicelles synthesized using surfactants such as pluronics, D-α-tocopheryl polyethylene glycol succinate (TPGS) have been used as potential drug delivery carrier.

In this PhD research work, three types of nanoparticles were prepared for the development of TDDS- a) polymeric nanoparticles using PLGA and PGA polymers, b) nanomicelles using TPGS and c) PAMAM dendrimers

1.6.1. Polymeric nanoparticles

Polymer-based nanoparticles effectively carry encapsulated drugs or proteins or contrast agents to target particular cells. The advantages and other common properties of polymeric nanoparticles are shown in figure 1.4.

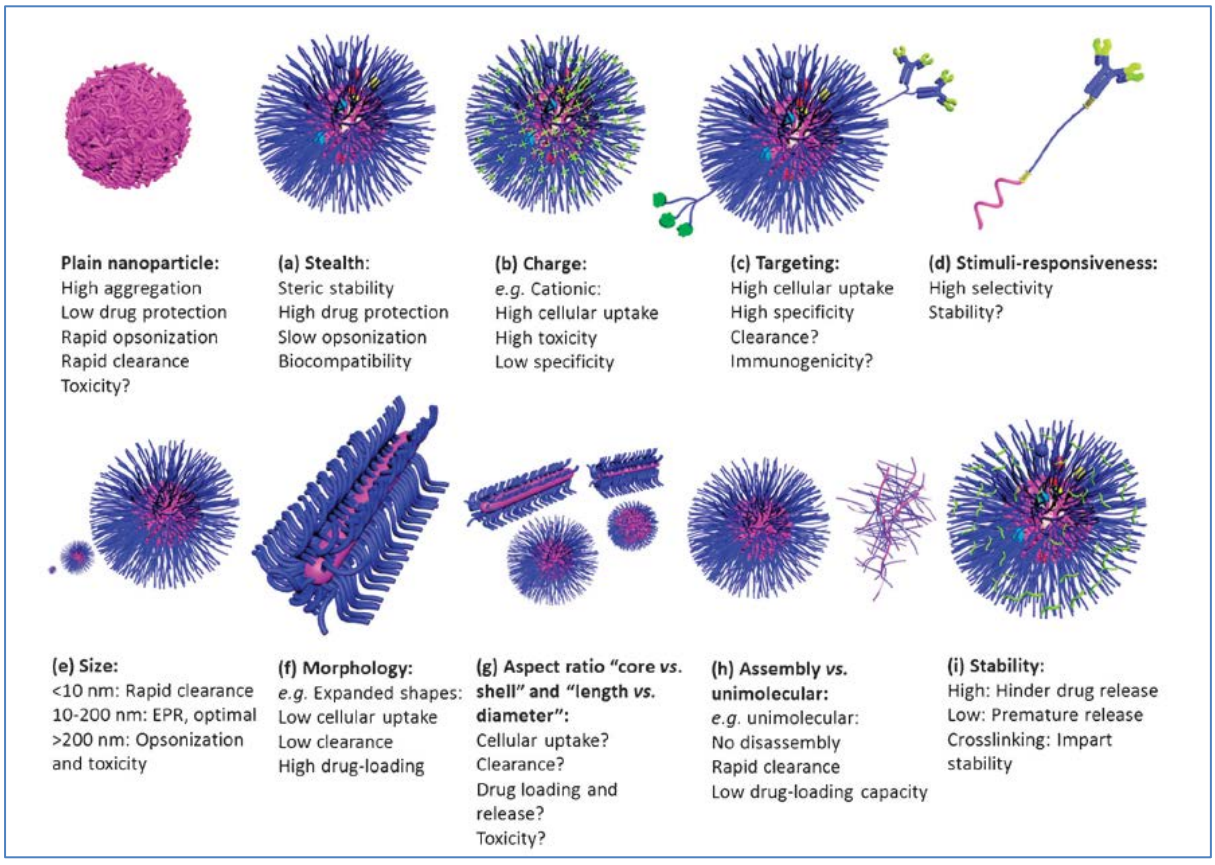

Figure 1.4: Characteristics of polymeric nanoparticles: (a) stealth: imparts biocompatibility, steric stability and protection of the encapsulated drug and reduces the opsonization and clearance of nanoparticles, but may also reduce the cellular uptake and endosomal escape capabilities, (b) charge: cationic character enhances

cellular uptake and endosomal escape, but subject to uncontrolled tissue distribution and often associated with toxicity, (c) targeting: enhances cellular uptake and specificity, but sometimes can accelerate the clearance and/or immunogenicity, (d) stimuli responsiveness: controls the dynamics of nanoparticles with possibility of releasing their cargoes at specific sites (selectivity). The stability and responsiveness of these materials under physiological and pathological conditions may vary and may result in premature release of the drug. (e) size: 100 nm particles is optimal for delivery, being large enough to avoid renal clearance and small enough to reduce clearance and toxicity, (f) morphology: expanded morphology results in higher drug-loading capacity, lower clearance and cellular uptake, (g) aspect ratio: the shell vs. core volume and length vs. diameter can greatly affect the cellular uptake, clearance, drug loading and release, and toxicity, (h) assembly vs. unimolecular structures: unimolecular structures are more stable (no dissociation) but can be cleared rapidly depending on the size and usually have low drug-loading capacity, and (i) stability: intermediate stability to circumvent physiological barriers and at the same time be able to release the drug at the target sites is required and can be achieved with different methods, for instance, by crosslinking. This figure is taken from Elsabahy and Wooley, 2012.

Methods of preparation of polymeric nanoparticles

Polymers based nanoparticles can be prepared by several techniques including solvent displacement, double emulsification, salting out, dialysis, ionic-gelation and super critical fluid technology.

a) Solvent displacement method

It is one of the oldest but highly effective methods for the preparation of polymeric nanoparticles. In this method, drug and polymer are dissolved in a volatile, water-miscible organic solvent and then transferred into aqueous phase containing surfactant as stabilising agent (Astete and Sabliov, 2006). For the preparation of surfactant-free nanoparticles, normal distilled water or phosphate buffer is used as aqueous phase (Tomoda et al., 2014). The dispersion may be homogenised or ultra-sonicated followed by evaporation of solvent by either stirring on magnetic stirrer or

under reduced pressure. Commonly used organic solvents are ethyl acetate, acetone, chloroform and dichloromethane.

b) Double emulsification method

This method is used for the encapsulation of hydrophilic drugs. The drug is dissolved in water and added to the organic phase to prepare water-in-oil (w/o) emulsion. Thereafter, this primary emulsion is added into the large aqueous phase containing the surfactant solution to produce water-in-oil-in-water w/o/w type double emulsion. This double emulsion system is stirred to evaporate organic solvent and to get drug loaded nanoparticles.

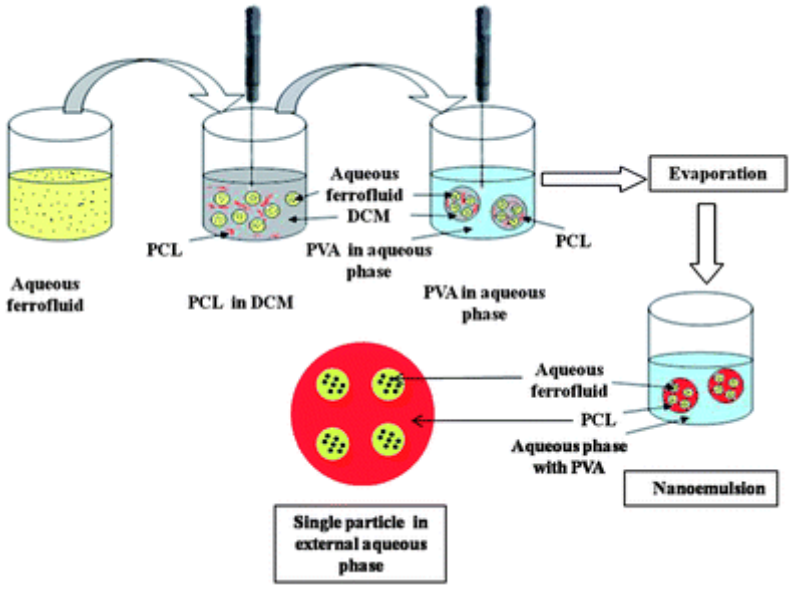

Figure 1.5: Emulsification process based on the modified double emulsion evaporation method. This figure is taken from Ahmed et al., 2012.

c) Emulsification/ solvent diffusion

Emulsification/ solvent diffusion is modified solvent evaporation method where polymer is dissolved in a partially water-soluble solvent such as propylene carbonate. Then, it is saturated with water until to themodynamic equilibrium of both the solvents. To allow the diffusion of the solvent, the dispersed phase is diluted with the dispersion medium. This method is generally used to prepare nanospheres or

nanocapsules. High drug encapsulation efficiency, batch to batch reproducibility, no need for homogenisation and easy scale-up are major advantages of this technique. However, it also suffers from disadvantages of leakage of water-soluble drugs and requirement of high volumes of water to be eliminated from suspension.

d) Dialysis

In dialysis method, the polymer and drug are dissolved in dimethyl sulfoxide (DMSO) or dimethyl formamide (DMF), emulsified with aqueous phase and placed in a dialysis tubing molecular weight cut off 12000-14000 Da (Jeon et al., 2000). Then, the whole assembly is placed in dialysis medium (water). As solvents DMSO/DMF and water, passes across the dialysis tubing, the solubility of polymer is decreased and it aggregates in the form of small homogenous particles.

e) Salting out

This method is based on the separation of water miscible solvent from aqueous solution using electrolytes or non-electrolytes (Konan et al., 2002). Initially, the polymer and drug are dissolved in a water miscible solvent like acetone and subsequently emulsified in aqueous solution containing a salting out agent and a stabilizer (Eley et al., 2004). Commonly used salting out agents includes either electrolytes such as calcium chloride, magnesium chloride, magnesium acetate or non-electrolyte like sucrose. As the organic solvent defuses through the aqueous phase, nanoparticles are formed. This technique is easy to scale up and produces nanoparticles with high efficiency. However, it is suitable for only water-insoluble or lipophilic drugs (Astete and Sabliov, 2006).

f) Ionic gelation method

Ionic gelation method is used for the hydrophilic polymers such as poly glutamic acid (PGA), sodium alginate, chitosan and gelatin. In this method, the

polymer in study is crossed-linked with an oppositely charged polymer to coacervates to a particle size in the nano-range. eg. Hellmers et al., (2013) synthesized PGA-chitosan composite nanoparticles by ionic gelation method for the delivery of doxorubicin.

g) Rapid expansion of supercritical solution

In this technique, the polymer is dissolved in supercritical fluid to form solution which is rapidly expanded across an orifice or a capillary nozzle into a liquid solvent or ambient air to form nanoparticles. Imran ul-haq et al., (2010) synthesized poly(lactic acid) nanoparticles by rapid expansion of supercritical CO_2 solution.

1.6.1.1. PLGA based nanoparticles

PLGA is a biodegradable polymer composed of two monomer units- lactic acid and glycolic acid. After degradation of PLGA, both the monomer units enter into Kreb's cycle and are degraded completely in the body (Avnesh et al., 2010). It provides excellent biodegradability and biocompatibility to PLGA and hence PLGA has been approved for therapeutic applications. The properties of PLGA depend upon the percentage of each monomer unit. PLGA containing 50:50 ratios of lactic and glycolic acid is degraded faster than any other compositions.

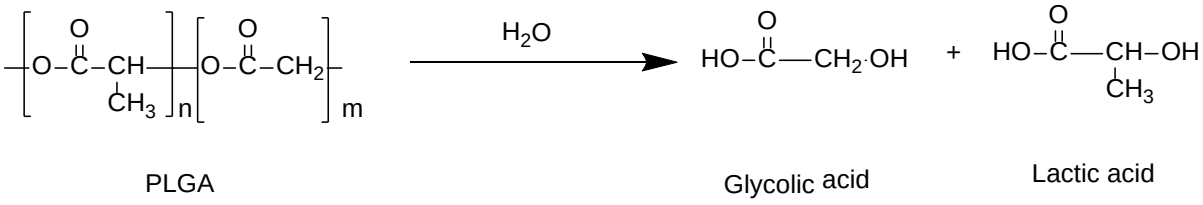

Figure 1.6: Biodegradation of PLGA in aqueous biological environment

PLGA is one of the mostly explored polymers in the area of drug delivery. Drugs from different categories such as anticancer agents, anti-diabetic drugs, anti-psychotic, hormones and toxoids have been delivered using PLGA-based drug delivery systems. Nanotechnology-based preparations have been used for the

delivery of anticancer agents to explore the inherent advantages of nanocarrier systems such as EPR, bypass multi drug resistance etc. Docetaxel, paclitaxel, 5-fluorouracil, etoposide, camptothecin, cisplatin, xanthone, triptorelin, and doxorubicin have been successfully encapsulated in PLGA nanoparticles.

1.6.1.2. Poly(glutamic) acid (PGA)

PGA is a water soluble poly amino acid comprising monomer units of D- and L-glutamic acid. These units are linked together via amine bonding between γ-carboxylic acid and α-amino acid groups. PGA can be synthesized either chemically or microbiologically. Chemical synthesis method produces α-PGA while γ-PGA is obtained by certain strains of *Bacillus*. PGA is a non-toxic, non-immunogenic, biodegradable and biocompatible polymer. PGA nanoparticles are prepared by either dialysis or ionic gelation method as described earlier.

PGA has been used as drug delivery carrier for the delivery of anticancer drugs. Anticancer drugs are either conjugated with a polymer or encapsulated in a polymer matrix. Anticancer drugs delivered by using PGA as the polymeric backbone include paclitaxel (Markovsky et al., 2014), docetaxel (Lollo et al., 2014), doxorubicin (Cao et al., 2011; Markovsky et al., 2014), idarubicin (Wadhwa and Mumper, 2012), cisplatin (Xiong et al., 2012) and plitidepsin (Gonzalo et al., 2013).

1.6.2. Surfactant-based nanomicelles

Amphiphilic molecules, with a hydrophilic and a hydrophobic part, have unique properties of getting self-assembled when exposed to a solvent. Above a particular concentration i.e. critical micellar concentration (CMC), these molecules form aggregates or cluster called micelles (Trivedi and Compella, 2010). These micelles have several properties such as small size (10-100 nm), increased drug solubility, enhanced tissue penetration and longer circulation time which are suitable

for their applications as drug delivery carrier system (Li et al., 2013; Torchilin, 2007; Nishiyama and Kataoka, 2006). Pluronic F127, F68 and P123 are commonly explored surfactants or copolymers for the delivery of anticancer drugs (Kabanov et al., 2002; Batrakova and Kabanov AV, 2008; Hu et al., 2012). Recently, D-α-tocopheryl polyethylene glycol succinate (TPGS) have also identified as pharmaceutically safe surfactant which could be used as nanocarrier system.

1.6.2.1. D-α-tocopheryl polyethylene glycol succinate (TPGS)

TPGS is a PEG derivative of natural vitamin E. It is synthesized by esterification of Vit E succinate with PEG. The molecular weight of TPGS depends upon the length of PEG chain. Generally, the molecular weight of TPGS containing PEG1000 is 1513. A hydrophobic part (Vit E) and a hydrophilic part (PEG) provide an amphiphilic nature to TPGS with a hydrophilic-lipophilic balance 13.2 and a critical micellar concentration 0.02% w/w. Above CMC value, TPGS forms micelles with nano-size range (< 50 nm) and with very low polydispersity. TPGS is highly stable in wide range of pH. TPGS has been used as solubilizer, non-ionic surfactant, emulsifier, absorption and permeability enhancer and nutritional supplement. The oral lethal dose 50 for TPGS is >7g/kg for adult rates and therefore, TPGS has been approved by FDA as a pharmaceutically safe adjuvant. In addition, TPGS is also an inhibitor of P-gp, a protein strongly involved in multi-drug resistance.

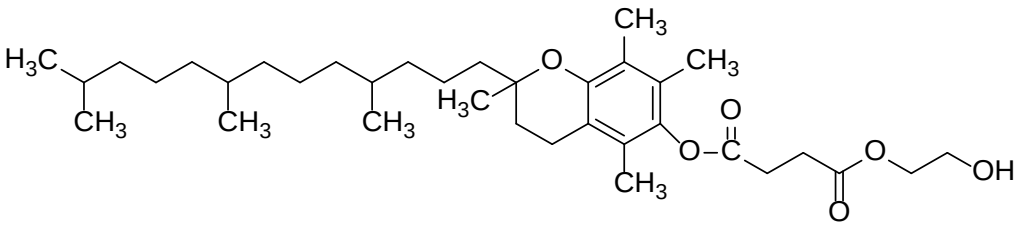

Figure 1.7: Chemical structure of D-α-tocopheryl polyethylene glycol 1000 succinate

These unique properties of TPGS make it an important tool for the delivery of lipophilic drugs by improving their absorption and bioavailability. TPGS has been used in the delivery of various anticancer drugs as solubilizer (Pooja et al., 2014), nanocarrier system (Mu et al., 2005; Mi et al., 2011), stabilizer in polymer or lipid-based nanoparticles formulation (Mu and Feng, 2002; Feng et al., 2007; Zhai et al., 2008; Katragadda et al., 2011; Muthu et al., 2004, 2011). TPGS has also been conjugated directly with anticancer drugs to synthesized prodrugs (Cao and Feng., 2008; Lee and Feng; 2005).

Methods of preparation of Nanomicelles

There are two methods for the preparation of TPGS nanomicelles-

a) *Solubilisation above CMC value*

Self-assembled TPGS nanomicelles could be prepared by solubilizing TPGS in water above its CMC value.

b) Solvent-casting method

This method is generally used to increase the drug loading if hydrophobic drugs. In this method, TPGS and drug are solubilized in organic solvent and then extracted with water under stirring or reduced pressure to form drug loaded nanomicelles.

1.6.3. Dendrimers

Dendrimers are unique architecture polymers and have been used as potential drug delivery carrier system. Dendrimers are three-dimensional, highly branched monodisperse macromolecules with defined size, mass, topology and surface chemistry. Dendrimers are composed of a unique tree- like branched structure originating from a central core with branching out with the increase in generation number (Svenson and Tomalia, 2005; Mignani et al., 2013).

Therefore, a typical dendrimer structure contains four components:

(i) A central core

(ii) Branch units attached to the core and called as generation.

(iii) Terminal surface functional groups attached to the outmost generation

(iv) Void spaces

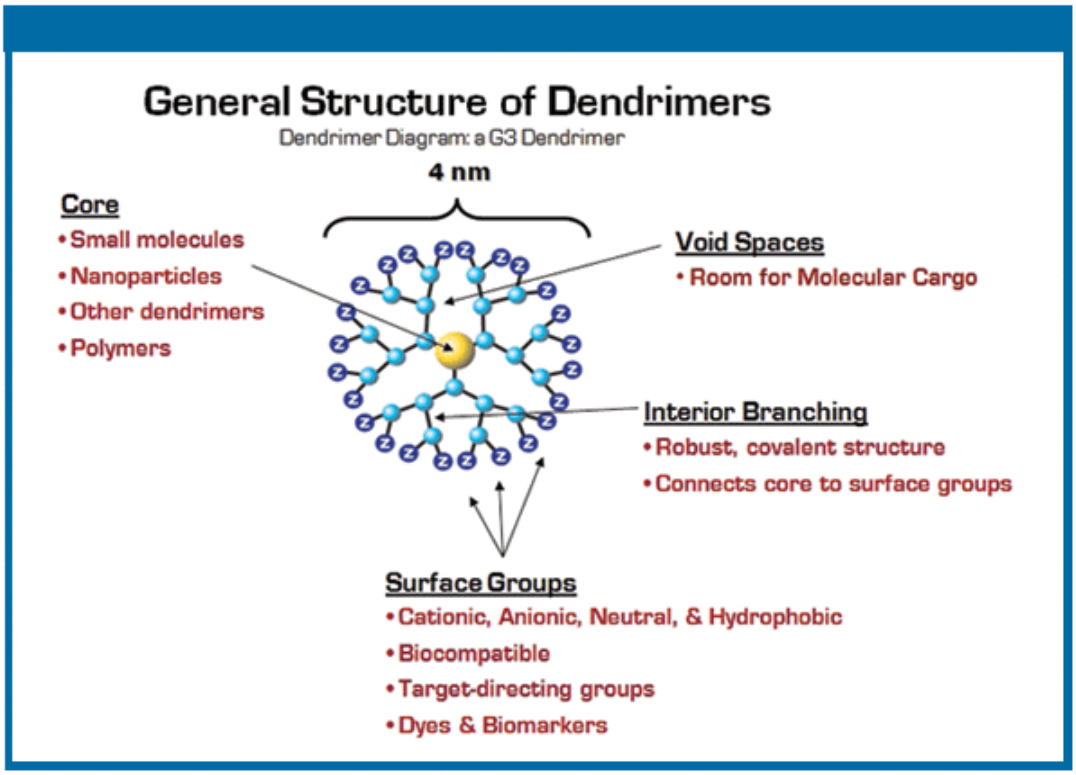

Figure 8: Schematic diagram of a typical dendrimer molecule. This figure is taken from Tolia and Hannah, 2008.

Advantages of dendrimers as drug delivery system:

- Dendrimers are highly monodisperse system (Mw/Mn< 1.01-1.05) and can be synthesized with high purity.
- Dendrimers not only carry a drug but can also enhance the solubility of lipophilic drugs.
- Improve the oral bioavailability of both hydrophilic and lipophilic drugs.
- Free terminal surface groups provide an opportunity of easy surface modification to develop a targeted drug delivery system.

- These surface groups can also be modified as stimuli responsive to release drugs (Ramireddy et al., 2012).
- Because small size, dendrimers avoid the RES uptake and enhance the resident time of drug in the blood circulation (Mignani et al., 2013)
- Dendrimers have also shown enhanced permeability and retention effect for the passive targeting of anticancer drugs.
- Biocompatibility and opportunity to deliver multiple drugs at a time.
- outstanding capability to be used with different routes of administration (Gupta et al., 2006)

Methods of preparation of dendrimers-based formulations

Dendrimer based nanomedicines can be prepared by two methods:

a) *Encapsulation in interiors cavities*:

Drug molecules can be encapsulated into empty internal cavities or void spaces present between branching units. The hydrophobic nature of these cavities makes them suitable for the encapsulation of lipophilic drugs (Svenson, 2009). In these cavities, drug may be present as an entrapped molecule or may be bound through electrostatic interactions. Although, electrostatic interactions are mostly observed between drug-molecules present on the surface of dendrimers. High density of functional groups on the surface of dendrimers has been explored to enhance the solubility of hydrophobic drugs using electrostatic interactions.

For the preparation of drug loaded dendrimers formulations, an excess amount of drug is added to the dendrimer solution and kept shaking overnight using an orbital shaker. Thereafter, the formulation is allowed to stand for 24 h to equilibrate the dendrimers-drug complex followed by filtration through a suitable filter, usually 0.22 or 0.45 µm (Chauhan et al., . 2004)

b) Covalent conjugation

This technique is used for the site-specific and controlled release of the drug. Drug molecule is covalently conjugated to the free surface groups of the dendrimers. The drug is released by chemical or enzymatic cleavage of chemical bonds between drug and dendrimers (Ramireddy et al., 2012). Cancer cells have lower pH and higher glutathione reductase level than normal cells. Therefore, in case of anticancer drugs, covalent conjugation technique is used to make pH-sensitive or glutathione reductase triggered release of drug from the dendrimers-drug complexes.

Dendrimers in the delivery of anticancer drugs

For the delivery of anticancer drugs, dendrimers have been used as both solubility enhancer and carrier system. Kojima et al., (2000) used PEG conjugated PAMAM dendrimers for the encapsulation of adriamycin and methotrexate. Similarly, Bhadra et al., (2003) used PEGylated PAMAM dendrimers for encapsulation of 5-fluorouracil. Camptothecin has been encapsulated using polyester dendrimers (Morgan et al., 2006), 1,3,5 triazine based dendrimers (Steffensen et al., 2006) and poly (etherhydroxylamine) PEHAM dendrimers (Tomalia et al., 2006). Various research groups have encapsulated cisplatin using G3.5 PAMAM dendrimers (Malik et al., 1999; Kulhari et al., 2013). Other anticancer drugs, encapsulated using dendrimers, include doxorubicin (Gillies and Frechet, 2005), etoposide (Sideratou et al., 2010) and taxanes (Pooja et al., 2014).

Apart from physical encapsulation, anticancer drugs have also been conjugated on the surface to form dendrimer-drug conjugate. Doxorubicin was covalently conjugated to polyester dendrimers through an acid-labile hydrazone bond (Padilla De Jesús et al., 2002). Dendrimers, based on amino apidic acid and β-glutamic acids, have been coupled with epirubicin to improve solubility and stability

of the drug (Pasut et al., 2005). Paclitaxel was conjugated to PAMAM dendrimers to improve its cytotoxicity (Majorosetal., 2006; Khandare et al., 2006). Recently, Zhang et al., (2014) conjugated peptide dendrimers to doxorubicin via an enzyme-sensitive linker to target ovarian cancer.

1.7. Physicochemical characterization of TDDS

Nanoparticles based formulations are characterized by several instrumental techniques:

a) Dynamic light scattering: Nanoparticle size, polydispersity and zeta potential are measured by dynamic light scattering techniques. This technique is also known as photon correlation spectroscopy. Nanoparticles are dispersed in buffer or distilled water and measured for above parameters using a Zeta sizer Nano ZS.

b) Surface morphology: Shape and surface morphology of nanoparticles are determined by scanning electron microscopy (SEM), transmission electron microscopy (TEM), atomic force microscopy (AFM) and small angle neutron scattering (SANS) analysis

c) Fourier transform infrared (FTIR) analysis: Chemical interactions between drug molecules, excipients and matrix of nanoparticles are determined by FTIR analysis. FTIR is also used for confirmation of binding of a targeting ligand on the surface of nanoparticles.

d) Differential scanning calorimetry (DSC): DSC is a thermo-analytical technique and used for the determination of physical state of drug inside the nanoparticles. It is also used for the thermal stability of nanoparticles.

e) X-ray diffraction analysis (XRD): XRD is used to study the crystalline materials. Most of the anticancer drugs are crystalline in nature. However, after encapsulation in nanocarrier matrix, physical state is transformed to amorphous or

disordered crystalline or solid solution. Therefore, XRD is used to determine the physical sate of drug in nanoparticles.

f) High performance liquid chromatography (HPLC): HPLC is used for both characterization and determination of drug content in nanoparticles. Therefore, HPLC is an analytical tool for the estimation of drug encapsulation efficiency and drug loading. Release of encapsulated drug from nanoparticles at different time period is also studied using a HPLC system.

1.8. Targeting ligand

A targeting ligand is a molecule which has high affinity towards receptors overexpressing on the surface of cancer cells. Therefore, nanoparticles could be directed specifically to the cancer cells by decorating their surface with a targeting ligand. A targeting ligand can be conjugated to the nanoparticles either directly or through a spacer between nanoparticles and a targeting ligand. A variety of molecules have been explored as potential targeting ligand. These include:

- ✓ Low molecular weight compounds eg. Folic acid, β-hydroxy butyric acid
- ✓ Peptides and proteins: Lectins, transferrin, RGD peptides, bombesin, somatostatin
- ✓ Antibodies: EGFR targeting antibodies, monoclonal antibodies such as trastuzumab, cetuximab etc
- ✓ Nucleic acids: Aptamers
- ✓ Monosaccharide sugars: Mannose, lactose, galactose, glucose
- ✓ Polysaccharides: Hyaluronic acid

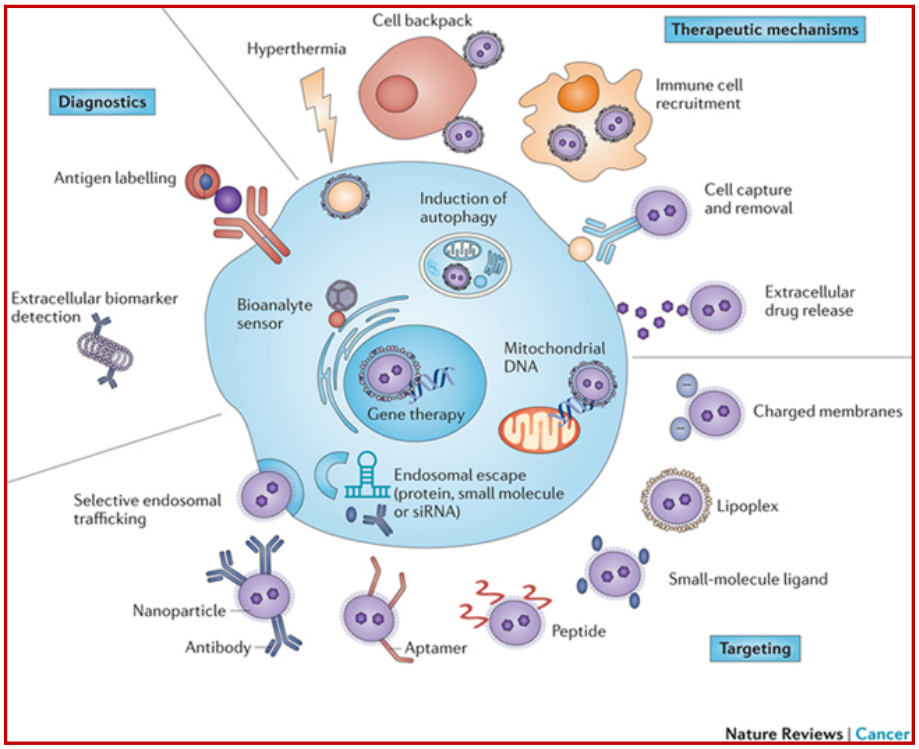

Figure 1.9: Nanomaterial strategies from the point-of-view of the cell. This figure summarizes unique targeting, diagnostic and therapeutic mechanisms related to the cancer cell. This figure is taken from Schroeder et al., 2011.

1.8.1. Peptides

A peptide is a chain of amino acids. Initially, peptides were recognised as hormones or vaccines which act through g-protein coupled receptors. However, with the increasing knowledge of peptide chemistry and functionality, peptides have been used as drug carrier, targeting ligand and proteases substrate. Cell penetrating peptides found their application as drug delivery carrier to overcome the problem of passage through the cellular plasma membrane barrier. As targeting ligand peptides have several advantages of high specificity, small size and possibility of large scale synthesis by chemical methods. Peptides like bombesin, Tat, PIVO-8, PIVO-24, LyP-1 and RGD-based peptides have been successfully used as targeting ligand for cancer imaging and therapy (Chang et al., 2009; Luo et al., 2010; Danhier et al., 2012; Karmali et al., 2009; Zhang et al., 2012; Stott Reynolds et al., 2015; Cheng et

al., 2014; Li et al., 2014; Zhan et al., 2010). In this PhD research work, two peptides- bombesin and cyclo (-Arg-Gly-Asp-D-Phe-Lys) have been used as targeting ligands.

1.8.1.1. Bombesin

Bombesin receptors are a type of G-protein coupled receptors and have 4 subtypes- BB1, BB2, BB3 and BB4. BB1 is known as the neuromedin B (NMB) receptor because of its affinity towards mammalian ligand NMB. BB2 receptor with high affinity to mammalian gastrin releasing peptide (GRP) is called as GRP receptor (Jenson et al., 2008). Among bombesin receptors, in particular BB2 have been found to be over expressed in several cancers (Table 1.1).

Table 1.1: Different types of bombesin receptors, their agonist, physiological role and over expression in cancer

Bombesin Receptor	Agonist	Physiological role	Over expression in cancer	References
BB1 (NMB)	Neuromedin B	Urogenital and gastrointestinal smooth muscles contraction	Small cell lung cancer cells, non-small cell lung cancer, Colon cancer	Reubi et al., 2002; Moody et al., 1995; Matusiak et al., 2005
BB2 (GRP)	Bombesin	Stimulation of acid secretion, pancreatic exocrine and enteric peptide hormones, gut motility, Stimulation of immune response	Breast, prostate, lung, colon, glioblastoma, neuroblastoma, head and neck squamous cell cancers	Gugger and Reubi, 1999; Markwalder and Reubi, 1999; Reubi et al., 2004; Fleischmann el., 2005; Jensen et al., 2008;
BB3	MK-50946 and Bantag-1	Regulation of blood glucose level, energy balance and weight control	Testis, lung and ovarian cancer	Moreno et al, 2013

Role of bombesin peptide (BBN) in cancer

Bombesin (BBN) is a 14-amino acid peptide and has structural similarity with GRP naturally present in human. BBN was originally isolated from a frog Bombina bombina by Antansi et al., in 1971. Gargosky et al., then found that the C-terminal peptide ligand containing 7 to 9 amino acids sequence is sufficient to achieve receptors-mediated response of bombesin. Since then several analogues of BBN have been synthesized to target GRP receptors for the imaging, diagnosis and for the treatment of cancer.

BBN in imaging and diagnosis

Bombesin analogues have been conjugated with radionuclide and fluorescent substances for the imaging and diagnostic of cancers. Wagh et al. (2012), synthesized ^{111}In-labelled BBN conjugates, comprising 2-nitroimidazole as pharmacophore, for the imaging of PC3 human prostate cancer cells. Abiraj et al. (2011), constructed and evaluated BBN antagonist (PEG_4-D- Phe-Gln-Trp-Ala-Val-Gly-His-Sta-Leu-NH_2) based radioligands for single, photon emission computed tomography (SPECT) and positron emission tomography (PET) nuclear imaging in PC3 tumour bearing nude mice. Chanda et al., (2010) used radiolabelled gold nanoparticles-BBN conjugate for the imaging of prostate cancer cells and to study the BBN-mediated biodistribution of nanocarrier. Mendoza-Sanchez et al., (2010) used 99m Tc-labelled gold nanoparticles and then conjugated with Lys3-bombesin for the imaging of GRP-receptors in vivo in athymic mice with PC3 induced tumours.

BBN in targeting of cancer

Yang et al., (2013) synthesized chimeric peptide by conjugating BBN with a mitochondrial-disrupting peptide B28 to enhance the selectivity and toxicity of B28 against bombesin receptor over expressing prostate cancer cells. BBN conjugated

B28 peptide was found to be 10 time more cytotoxic with specifically accumulation in mitochondria than unconjugated B28. In an interesting study, Cascato et al., (2008) evaluated in vitro and in vivo targeting potential of two GRP receptors antagonists (Demobesin 1 and Demobesin 4) in comparison to an agonist. The results demonstrated that GRP receptor antagonists could be a better targeting agent than GRP receptors agonist. Accardo et al (2012) synthesized doxorubicin loaded liposomes for the targeting of GRP receptors over expressing prostate cancer cells.

1.8.1.2. Arg-Gly-Asp (RGD) based peptides

Integrin receptors have been recognised as potential targets for delivery of anticancer drugs. Integrins are cell adhesion receptors for extracellular matrix proteins, enzymes like proteases, immunoglobulins and cytokines (Wang et al., 2013). Integrins are heterodimeric trans-membrane glycoproteins composed of two subunits α and β. There are 18 α-subunits and 8 β-subunits which form 24 different types of functional integrins (Desgrosellier and Cheresh, 2010). Integrins are overexpressed in different cancer and therefore consider potential target for drug delivery applications. Among all integrins, $\alpha_v\beta_3$ is specifically involved in metastasis, tumour proliferation and angiogenesis (Danhier et al., 2012).

Peptides containing an RGD moiety preferentially bind to the $\alpha_v\beta_3$ receptor and have been used as targeting ligand for therapeutic application in cancer. Anticancer drugs such as doxorubicin (Murphy et al., 2008; Zhou et al., 2012), paclitaxel (Danhier et al., 2009, 2012; Zhan et al., 2010), docetaxel (Ray et al., 2012), gemcitabine (Xu et al., 2012), cisplatin (Graf et al., 2012) and geldanamycin (Borgman et al., 2009) have been targeted to $\alpha_v\beta_3$ receptor over expressing cancer cells. Apart from drug delivery, RGD-based peptides have also been explored for imaging of integrin receptors over expressing cancer cells in vitro and in vivo.

(Schmieder et al., 2008; Pike et al., 2010; Nasonkla et al., 2006; Tsiapa et al., 2013; Shen et al., 2013; Yang et al., 2011). cRGDfK is a cyclic peptide with a sequence cyclo (-Arg-Gly-Asp-D-Phe-Lys) and molecular weight 603.7 Da. more stable than linear peptide. The lysine residue with free amine group provides an opportunity for chemical coupling with nanoparticles.

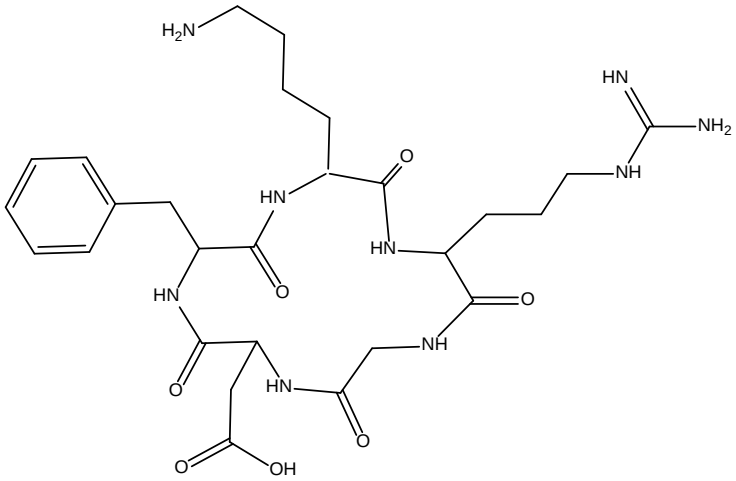

Figure 1.10: Chemical structure of cRGDfK, a RGD-based cyclic peptide that binds to $\alpha_v\beta_3$ receptor over expressing cancer cells

1.8.2. Monoclonal antibody: Trastuzumab

Trastuzumab (TZ) is a recombinant humanized monoclonal antibody that binds with extracellular domain IV of human epidermal growth factor receptor HER2 (Valabrega et al., 2007). HER2 receptors have been found to over express in 15-20% of breast cancer and TZ is one of the first line treatment drugs for HER2 positive breast cancer (Colozza et al., 2006). TZ is also the standard care of treatment for metastatic gastric cancer (Boku et al., 2014). Although TZ was developed as a drug, it is being tested as targeting ligand for the delivery of various anticancer drugs and nucleic materials (Yousefpour et al., 2011; Shukla et al., 2008; Steinhauser et al., 2008). I have published a review article describing the role of TZ as anticancer drug and as targeting ligand. Please refer appendices.

1.9. Anticancer drugs used in the research work

1.9.1. Docetaxel (DTX)

IUPAC name: 1,7β,10β-trihydroxy-9-oxo-5β,20-epoxytax-11-ene-2α,4,13α-triyl 4-acetate 2-benzoate 13-{(2R,3S)-3-[(tert-butoxycarbonyl)amino]-2-hydroxy-3-phenylpropanoate}

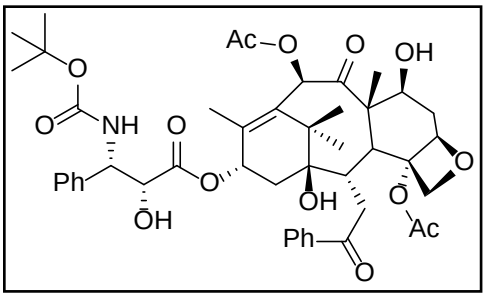

Chemical formula: $C_{43}H_{53}NO_{14}$

Molecular mass: 807.87 g/mol;

Meting point: 176-178 °C

Category: Semisynthetic, taxane derivative.

Physical state: White crystalline powder

Solubility: insoluble in water, freely soluble in ethanol, sparingly soluble in acetonitrile, soluble in acetone, methanol and ethyl acetate.

Clinical applications: DTX has been approved by the FDA for treatment of locally advanced or metastatic breast cancer, gastric cancer, head and neck cancer, hormone-refractory prostate cancer and non-small-cell lung cancer.

Mechanism: DTX disrupt the microtubule assembly and inhibits the cell division leading to apoptosis and cell death (Musumeci et al., 2006; Oliveira et al., 2013).

Plasma half-life: 86 h

Protein binding: >98%

Metabolism: Hepatic

Excretion: Biliary

Side effects: Taxotere is the marketed formulation of DTX which is formulated with a high concentration of Tween® 80 (40 g/L) which causes severe side effects like hypersensitivity reactions, cumulative fluid retention, nausea, fatigue, hair loss, peripheral neuropathy, and anaemia (Gelderblom et al., 2001; Lee et al., 2011)

1.9.2. Gemcitabine hydrochloride (GEM)

IUPAC name: 4-amino-1-(2-deoxy-2,2-difluoro-β-D-erythro-pentofuranosyl)pyrimidin-2(1H)-on

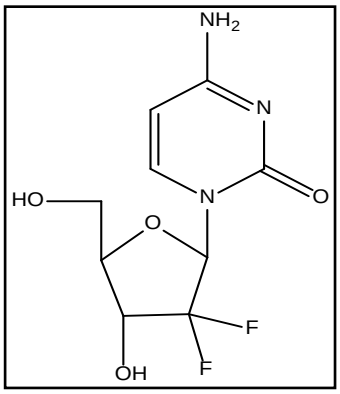

Chemical formula: $C_9H_{11}F_2N_3O_4$. HCl

Molecular mass: 299.66 g/mol; Meting point:

Category: Nucleoside analogue

Physical state: White to off-white solid, crystalline.

Solubility: Soluble in water, slightly soluble in methanol, and practically insoluble in ethanol and polar organic solvents.

Clinical applications: GEM has been approved by Food and Drug Administration (FDA) for the treatment of breast cancer (with paclitaxel), non-small cell lung cancer (with cisplatin), ovarian cancer and pancreatic cancer.

Mechanism: GEM is a prodrug and phosphorylated by deoxycytidine kinase to gemcitabine monophosphate followed by gemcitabine di- and triphosphates. Gemcitabine triphosphate is incorporated into DNA chain by DNA polymerase that results to termination of chain elongation. GEM also inhibits DNA polymerase. By another mechanism, diphosphate analogue of GEM binds with ribonucleotide reductase and inactivates the enzyme irreversibly. Ribonucleotde reductase is an essential enzyme for DNA replication and repair (Mini et al., 2006).

GEM half-life: 8-17 min (Joshi et al., 2014)

Protein binding: <10%

Side effects: GEM is reported to cause leukopenia, thrombocytopenia and anemia by suppressing bone marrow function. GEM also causes pulmonary, renal (haemolytic uremic syndrome) and hepatotoxicity. Being embryotoxic, GEM can cause fetal malformations (cleft palate, incomplete ossification) when given to pregnant woman.

1.9.3. Camptothecin (CPT)

Camptothecin (CPT) is a plant quinolone alkaloid obtained from bark and stem of Camptotheca acuminata, a Chinese tree (Amna et al., 2013).

IUPAC name: (S)-4-ethyl-4-hydroxy-1H-pyrano[3',4':6,7]indolizino[1,2-b]quinoline-3,14-(4H,12H)-dione

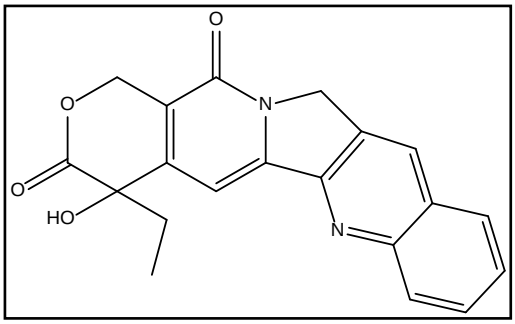

Mol. Wt.: 348.35 g/mol

Chemical formula: $C_{20}H_{16}N_2O_4$

Solubility: Poorly soluble in water (logP=1.74)

Melting point: 275-277 °C

Physical state: CPT is found as yellowish, solid powder. CPT is present in two inter-convertible forms; lactone (active form) and carboxylate (inactive form) (Zou et al., 2013).

Mechanism of action: CPT binds to the topoisomerase I and DNA complex, stabilizes it and prevents DNA re-ligation and therefore resulting in DNA damage followed by apoptosis (Amna et al., 2013).

Pharmacokinetics:

Protein binding: high plasma protein binding. Lactone form and carboxylate form bind about 81% and 98% to human serum albumin, respectively (Schluep et al., 2006).

Toxicity: Acute oral toxicity (LD50 in miceis 50.1 mg/kg

Clinical applications:

CPT has shown a broad spectrum of anticancer activity against different cancers in human including breast, lung, prostate, colon, stomach, ovarian carcinomas and melanoma (Venditto and Simanek, 2010).

1.10. Focus area of this research work

Ligand mediated nanoparticles is attractive research area for the targeted delivery of anticancer drugs to tumor cells. Bombesin has been reported to bind with the GRP receptors. Human breast cancer cells such MDA-MB-231 over express the GRP receptors. The initial objective of the study was to develop BBN-conjugated PLGA nanoparticles for the delivery of DTX. During the formulation optimization, I observed, surprisingly, that BBN-conjugated PLGA nanoparticles were more stable than unconjugated nanoparticles. Therefore, the major focus of Chapter 2 was to find out the possible mechanisms behind the higher stability of BBN-conjugated PLGA over unconjugated nanoparticles. In chapter 3, BBN-conjugated PLGA nanoparticles were explored for the delivery of DTX to GRP-over expressing breast cancer cells. As prostate cancer cells also over express the GRP receptors, in a separate study (chapter 4), the anticancer activity of these nanoparticles was studied against two human prostate cancer cells DU145 and PC3 cells along with biodistribution studies in male Balb/c mice.

In chapter 5, TZ was conjugated to dendrimers for the delivery of DTX to HER2-postive cancer cells. Although antibody conjugated nanoparticles have been reported for the delivery of anticancer drugs, the major focus was to study the pharmacokinetic profile of DTX loaded in TZ-conjugated dendrimers. In chapter 6-8, I explored the potential of integrin receptor-binding peptide, cRGDfK as targeting ligand. As integrin receptors have been found to be over-expressed in more than one cancer, the efficacy of cRGDfK-conjugated nanoparticles (as targeted delivery system) was studied against prostate cancer (chapter 6), ovarian cancer (chapter 7) and brain cancer (Chapter 8).

1.11. References

- Abiraj K, Mansi R, Tamma ML, Fani M, Forrer F, Nicolas G, Cescato R, Reubi JC, Maecke HR. Bombesin antagonist-based radioligands for translational nuclear imaging of gastrin-releasing peptide receptor-positive tumors. *J Nucl Med* 2011;**52(12)**:1970-8.
- Amna T, Barakat NAM, Shamshi Hassan M, Khil M, Kim HY. Camptothecin loaded poly(ε-caprolactone)nanofibers via one-step electrospinning and their cytotoxicity impact. *Colloids Surf A* 2013;**431**:1-8.
- Astete CE, Sabliov CM. Synthesis and characterization of PLGA nanoparticles. *J Biomater Sci Polymer Edn* 2006;**17**:247-89.
- Bae YH, Park K. Targeted drug delivery to tumors: myths, reality and possibility. *J Control Release* 2011;**153(3)**:198-205.
- Bamrungsap S., Zhao Z., Chen T., Wang L, Li C, Fu T, Tan W. Nanotechnology in Therapeutics. Nanomedicine 2012;7(8):1253-71.
- Baskar R, Lee KA, Yeo R, Yeoh KW. Cancer and radiation therapy: current advances and future directions. *Int J Med Sci* 2012;**9(3):**193-9.
- Batrakova EV, Kabanov AV. Pluronic block copolymers: evolution of drug delivery concept from inert nanocarriers to biological response modifiers. *J Control Release* 2008;**130(2)**:98-106.
- Bernier J, Hall EJ, Giaccia A. Radiation oncology: a century of achievements. *Nat Rev Cancer* 2004;**4(9):**737-47.
- Bhadra D, Bhadra S, Jain S, Jain NK. A PEGylated dendritic nanoparticulate carrier of fluorouracil. *Int J Pharm* 2003;**257**:111-24.
- Boku N. HER2-positive gastric cancer. *Gastric Cancer* 2014;**17**:1-12.
- Borgman MP, Aras O, Geyser-Stoops S, Sausville EA, Ghandehari H. Biodistribution of HPMA copolymer-aminohexylgeldanamycin-RGDfK conjugates for prostate cancer drug delivery. *Mol Pharm* 2009;**6**:1836-47.
- Brannon-Peppas L, Blanchette JO. Nanoparticle and targeted systems for cancer therapy. *Adv Drug Deliv Rev* 2012;**64**:206-12.
- Cao N, Cheng D, Zou S, Ai H, Gao J, Shuai X. The synergistic effect of hierarchical assemblies of siRNA and chemotherapeutic drugs co-delivered into hepatic cancer cells. *Biomaterials* 2011;**32(8)**:2222-32.

- Cao N, Feng SS. Doxorubicin conjugated to D-alpha-tocopheryl polyethylene glycol 1000 succinate (TPGS): conjugation chemistry, characterization, in vitro and in vivo evaluation. *Biomaterials* 2008;**29**:3856-65.
- Cescato R, Maina T, Nock B, Nikolopoulou A, Charalambidis D, Piccand V, Reubi JC. Bombesin receptor antagonists may be preferable to agonists for tumor targeting. *J Nucl Med* 2008;**49(2)**:318-26.
- Chanda N, Kattumuri V, Shukla R, Zambre A, Katti K, Upendran A, Kulkarni RR, Kan P, Fent GM, Casteel SW, Smith CJ, Boote E, Robertson JD, Cutler C, Lever JR, Katti KV, Kannan R. Bombesin functionalized gold nanoparticles show in vitro and in vivo cancer receptor specificity. *Proc Natl Acad Sci USA* 2010;**107(19)**:8760-5.
- Chang DK, Chiu CY, Kuo SY, Lin WC, Lo A, Wang YP, Li PC, Wu HC. Antiangiogenic targeting liposomes increase therapeutic efficacy for solid tumors. *J Biol Chem* 2009;**284**:12905-16.
- Chauhan AS, Jain NK, Diwan PV, Khopade AJ. Solubility enhancement of indomethacin with poly(amidoamine) dendrimers and targeting to inflammatory regions of arthritic rats. *J Drug Target* 2004;**12(9-10)**:575-83.
- Cheng Y, Dai Q, Morshed RA, Fan X, Wegscheid ML, Wainwright DA, Han Y, Zhang L, Auffinger B, Tobias AL, Rincón E, Thaci B, Ahmed AU, Warnke PC, He C, Lesniak MS. Blood-brain barrier permeable gold nanoparticles: an efficient delivery platform for enhanced malignant glioma therapy and imaging. *Small* 2014;**10(24)**:5137-50.
- Cho K, Wang X, Nie S, Chen ZG, Shin DM. Therapeutic nanoparticles for drug delivery in cancer. *Clin Cancer Res* 2008;**14(5)**:1310-6.
- Colozza M, de Azambuja E, Cardoso F, Bernard C, Piccart MJ. Breast cancer: achievements in adjuvant systemic therapies in the pre-genomic era. *The Oncologist* 2006;**11(2)**:111-25.
- Danhier F, Pourcelle V, Marchand-Brynaert J, Jérôme C, Feron O, Préat V. Targeting of Tumor Endothelium by RGD-Grafted PLGA-Nanoparticles Methods. *Enzymol* 2012;**508**:157-75.
- Danhier F,Vroman B, Lecouturier N, Crokart N, Pourcelle V, Freichels H, Jérôme C, Marchand-Brynaert J, Feron O, Préat V. Targeting of tumor endothelium by RGD-grafted PLGA-nanoparticles loaded with paclitaxel. *J Control Release* 2009;**140**:166-73.

- de Oliveira R, Zhao P, Li N, de Santa Maria LC, Vergnaud J, RuizJ, Astruc D, Barratt G. Synthesis and in vitro studies of gold nanoparticles loaded with docetaxel. *Int J Pharm* 2013;**454**:703-11.
- Desgrosellier JS, Cheresh DA. Integrins in cancer: biological implications and therapeutic opportunities. *Nat Rev Cancer* 2010;**10(1)**:9-22.
- Eley JG, Pujari VD, McLane J. Poly (lactide-co-glycolide) nanoparticles containing coumarin-6 for suppository delivery: in vitro release profile and in vivo tissue distribution. *Drug Deliv* 2004;**11(4)**:255-61.
- Elsabahy M, Wooley KL. Design of polymeric nanoparticles for biomedical delivery applications. *Chem Soc Rev* 2012;**41(7)**:2545-61.
- Feng SS, Zhao LY, Zhang ZP, Bhakta G, Win KY, Dong YC, et al. Chemotherapeutic engineering: Vitamin E TPGS-emulsified nanoparticles of biodegradable polymers realized sustainable paclitaxel chemotherapy for 168 h in vivo. *Chem Eng Sci* 2007;**62**:6641-48.
- Fleischmann A, Waser B, Gebbers JO, et al. Gastrin-releasing peptide receptors in normal and neoplastic human uterus: involvement of multiple tissue compartments. *J Clin Endocrinol Metab* 2005;**90**:4722-29.
- Gelderblom H, Verweij J, Nooter K, Sparreboom A. Cremophor EL: the drawbacks and advantages of vehicle selection for drug formulation. *Eur J Cancer* 2001;**37**:1590-98.
- Gillies ER, Fréchet JMJ. pH-responsive copolymer assemblies for controlled release of doxorubicin. *Bioconjug Chem* 2005;**16**:361-68.
- Gonzalo T, Lollo G, Garcia-Fuentes M, Torres D, Correa J, Riguera R, Fernandez-Megia E, Calvo P, Avilés P, GuillénMJ, Alonso MJ. A new potential nano-oncological therapy based on polyamino acid nanocapsules. *J Control Release* 2013;**169(1-2)**:10-6.
- Graf N, Bielenberg DR, Kolishetti N, Muus C, Banyard J, Farokhzad OC, Lippard SJ. α(V)β(3) integrin-targeted PLGA-PEG nanoparticles for enhanced anti-tumor efficacy of a Pt(IV) prodrug. *ACS Nano* 2012;**6(5)**:4530-9.
- Gugger M, Reubi JC. GRP receptors in non-neoplastic and neoplastic human breast. *Am J Pathol* 1999;**155**:2067-76.
- Gupta U, Agashe HB, Asthana A, Jain NK. A review of in vitro-in vivo investigations on dendrimers: the novel nanoscopic drug carriers. *Nanomedicine* 2006;**2(2)**:66-73.

- Hellmers F, Ferguson P, Koropatnick J, Krull R, Margaritis A. Characterization and in vitro cytotoxicity of doxorubicin-loaded γ-polyglutamic acid-chitosan composite nanoparticles. *Biochem Eng J* 2013;**75**:72-8.
- Hu HQ, Yu JH, Li YY, Zhao J, Dong HQ. Engineering of a novel pluronic F127/graphenenanohybrid for pH responsive drug delivery. *J Biomed Mater Res Part A* 2012,**100(1)**:141-48.
- Imran ul-haq M, Acosta-Ramírez A, Mehrkhodavandi P, Signorell R. Influence of polydispersity of poly(lactic acid) on particle formation by rapid expansion of supercritical CO_2 solutions. *J Supercrit Fluids* 2010;**51**:376-83.
- International Agency for Research on Cancer. Latest World Cancer Statistics Global Cancer Burden Rises to 14.1 Million New Cases in 2012: Marked Increase in Breast Cancers must be Addressed. *World Health Organization* 2013;**223**: 1-3.
- Jensen RT, Battey JF, Spindel ER, Benya RV. International Union of Pharmacology. LXVIII. Mammalian bombesin receptors: nomenclature, distribution, pharmacology, signaling, and functions in normal and disease states. *Pharmacol Rev* 2008;**60(1)**:1-42.
- Jeon HJ, Jeong YI, Jang MK, Park YH, Nah JW. Effect of solvent on the preparation of surfactant-free poly(DL-lactide-co-glycolide) nanoparticles and norfloxacin release characteristics. *Int J Pharm* 2000;**207(1-2)**:99-108.
- Joshi G, Kumar A, Sawant K. Enhanced bioavailability and intestinal uptake of Gemcitabine HCl loaded PLGA nanoparticles after oral delivery. *Eur J Pharm Sci* 2014;**60**:80-9.
- Kabanov AV, Batrakova EV, Alakhov VY. Pluronic block copolymers as novel polymer therapeutics for drug and gene delivery. *J Control Release* 2002;**82**:189-212.
- Karmali PP, Kotamraju VR, Kastantin M, Black M, Missirlis D, Tirrell M, Ruoslahti E. Targeting of albumin-embedded paclitaxel nanoparticles to tumors. *Nanomedicine* 2009;**5**:73-82.
- Katragadda U, Teng Q, Rayaprolu BM, Chandran T, Tan C. Multi-drug delivery to tumor cells via micellarnanocarriers. *Int J Pharm* 2011;**419**:281-86.
- Khandare JJ, Jayant S, Singh A, Chandna P, Wang Y, Vorsa N, Minko T. Dendrimer versus linear conjugate: influence of polymeric architecture on the delivery and anticancer effect of paclitaxel. *Bioconjug Chem* 2006;**17**:1464-72.

- Kobayashi H, Watanabe R, Choyke PL. Improving Conventional Enhanced Permeability and Retention (EPR) Effects; What Is the Appropriate Target? *Theranostics* 2014;**4(1)**:81–9.
- Kojima C, Kono K, Maruyama K, Takagishi T. Synthesis of polyamidoamine dendrimers having poly(ethylene glycol) grafts and their ability to encapsulate anticancer drugs. *Bioconjug Chem* 2000;**11**:910-17.
- Konan YN, Gurny R, Allemann E. Preparation and characterization of sterile and freeze-dried sub-200 nm nanoparticles. *Int J Pharm* 2002;**233(1-2)**:239-52.
- Krishna R, Mayer LD. Multidrug resistance (MDR) in cancer. Mechanisms, reversal using modulators of MDR and the role of MDR modulators in influencing the pharmacokinetics of anticancer drugs. *Eur J Pharm Sci* 2000;**11(4)**:265-83.
- Kularatne SA, Low PS. Targeting of nanoparticles: folate receptor. *Methods Mol Biol* 2010;**624**:249-65.
- Kulhari H, Pooja D, Rompicharla SVK, Sistla R, Adams DJ. Biomedical Applications of trastuzumab: as a therapeutic agent and a targeting ligand. Medicinal Research Reviews 2015;35:849–76.
- Lee SW, Yun MH, Jeong SW, In CH, Kim JY, Seo MH, et al. Development of docetaxel-loaded intravenous formulation, nanoxel-pm using polymer-based delivery system. *J Control Release* 2011;**155(2)**:262–71.
- Li J, Liu F, Shao Q, Min Y, Costa M, Yeow EK, Xing B. Enzyme-responsive cell-penetrating peptide conjugated mesoporous silica quantum dot nanocarriers for controlled release of nucleus-targeted drug molecules and real-time intracellular fluorescence imaging of tumor cells. *Adv Healthc Mater* 2014;**3(8)**:1230-9.
- Li YY, Li L, Dong HQ, Cai XJ, Ren TB. Pluronic F127 nanomicelles engineered with nuclear localized functionality for targeted drug delivery. *Mater Sci Eng C Mater Biol Appl* 2013;**33(5)**:2698-707.
- Lollo G, Rivera-Rodriguez GR, Bejaud J, Montier T, Passirani C, Benoit JP, García-Fuentes M, Alonso MJ, Torres D. Polyglutamic acid-PEG nanocapsules as long circulating carriers for the delivery of docetaxel. *Eur J Pharm Biopharm* 2014;**87(1)**:47-54.
- Longmire M, Choyke PL, Kobayashi H. Clearance Properties of Nano-sized Particles and Molecules as Imaging Agents: Considerations and Caveats. *Nanomedicine* 2008;**3(5)**:703-17.

- Luo G, Yu X, Jin C, Yang F, Fu D, Long J, Xu J, Zhan C, Lu W. LyP-1-conjugated nanoparticles for targeting drug delivery to lymphatic metastatic tumors. *Int J Pharm* 2010;**385**:150-56.
- Majoros IJ, Myc A, Thomas TP, Mehta CB, Baker Jr JR. PAMAM dendrimer-based multifunctional conjugate for cancer therapy: synthesis, characterization, and functionality. *Biomacromolecules* 2006;**7**:572-79.
- Malik N, Evagorou EG, Duncan R. Dendrimer-platinate: a novel approach to cancer chemotherapy. *Anticancer Drugs* 1999;**10**:767-76.
- Markovsky E, Baabur-Cohen H, Satchi-Fainaro R. Anticancer polymeric nanomedicine bearing synergistic drug combination is superior to a mixture of individually-conjugated drugs. *J Control Release* 2014;**187**:145-57.
- Markwalder R, Reubi JC. Gastrin-releasing peptide receptors in the human prostate: relation to neoplastic transformation. *Cancer Res* 1999;**59**:1152-59.
- Matusiak D, Glover S, Nathaniel R, Matkowskyj K, Yang J, Benya RV. Neuromedin B and its receptor are mitogens in both normal and malignant epithelial cells lining the colon. *Am J Physiol Gastrointest Liver Physiol* 2005;**288**:718-28.
- Mendoza-Sánchez AN, Ferro-Flores G, Ocampo-García BE, Morales-Avila E, de M Ramírez F, De León-Rodríguez LM, Santos-Cuevas CL, Medina LA, Rojas-Calderón EL, Camacho-López MA. Lys3-bombesin conjugated to 99mTc-labelled gold nanoparticles for in vivo gastrin releasing peptide-receptor imaging. *J Biomed Nanotechnol* 2010;**6(4)**:375-84.
- Mi Y, Liu YT, Feng SS. Formulation of Docetaxel by folic acid-conjugated D-alpha-tocopheryl polyethylene glycol succinate 2000 (Vitamin E TPGS(2k)) micelles for targeted and synergistic chemotherapy. *Biomaterials* 2011;**32**:4058-66.
- Mignani S, El Kazzouli S, Bousmina M, Majoral JP. Expand classical drug administration ways by emerging routes using dendrimer drug delivery systems: a concise overview. *Adv Drug Deliv Rev* 2013;**65(10):**1316-30.
- Mini E, Nobili S, Caciagli B, Landini I, Mazzei T. Cellular pharmacology of gemcitabine. Ann Oncol 2006;**17 (Suppl 5)**:v7–v12.
- Moody TW, Fagarasan M, Zia F. Neuromedin B stimulates arachidonic acid release, c-fos gene expression, and the growth of C6 glioma cells. *Peptides* 1995;**16**:1133-40.

- Moreno P, Mantey SA, Nuche-Berenguer B, Reitman ML, Gonzalez N, , Coy DH, Jensen RT. Comparative Pharmacology of Bombesin Receptor Subtype-3, Nonpeptide Agonist MK-5046, a Universal Peptide Agonist, and Peptide Antagonist Bantag-1 for Human Bombesin Receptors. *Pharmacol ExpTherap* 2013;**347(1)**:100-16.
- Morgan MT, Nakanishi Y, Kroll DJ, Griset AP, Carnahan MA, Wathier M, Oberlies NH, Manikumar G, Wani MC, Grinstaff MW. Dendrimer-encapsulated camptothecins: increased solubility, cellular uptake, and cellular retention afford enhanced anticancer activity in vitro. *Cancer Res* 2006;**66**:11913-21.
- Mu L, Elbayoumi TA, Torchilin VP. Mixed micelles made of poly(ethylene glycol)-phosphatidylethanolamine conjugate and D-alpha-tocopheryl polyethylene glycol 1000 succinate as pharmaceutical nanocarriers for camptothecin. *Int J Pharm* 2005;**306**:142-49.
- Mu L, Feng SS. Vitamin E TPGS used as emulsifier in the solvent evaporation/extraction technique for fabrication of polymeric nanospheres for controlled release of paclitaxel (Taxol (R)). *J Control Release* 2002;**80**:129-44.
- Mu L, Seow PH, Ang SN, Feng SS. Study on surfactant coating of polymeric nanoparticles for controlled delivery of anticancer drug. *Colloid Polym Sci* 2004;**283**:58-65.
- Murphy EA, Majeti BK, Barnes LA, Makale M, Weis SM, Lutu-Fuga K, Wrasidlo W, Cheresh DA. Nanoparticle-mediated drug delivery to tumor vasculature suppresses metastasis. *Proc Natl Acad Sci USA* 2008;**105**:9343-48.
- Musumeci T, Ventura CA, Giannone I, Ruozi B, Montenegro L, Pignatello R, Puglisi G. PLA/PLGA nanoparticles for sustained release of docetaxel. *Int J Pharm* 2006;**325**:172-79.
- Muthu MS, Kulkarni SA, Xiong J, Feng SS. Vitamin E TPGS coated liposomes enhanced cellular uptake and cytotoxicity of docetaxel in brain cancer cells. *Int J Pharm* 2011;**421**:332-40.
- Nasongkla N, Bey E, Ren J, Ai H, Khemtong C, Guthi JS, Chin SF, Sherry AD, Boothman DA, Gao J. Multifunctional polymeric micelles as cancer-targeted, MRI-ultrasensitive drug delivery systems. *Nano Lett* 2006;**6**:2427-30.
- Nishiyama N, Kataoka K. Current state, achievements, and future prospects of polymeric micelles as nanocarriers for drug and gene delivery. *Pharmacol Ther* 2006;**112(3)**:630-48.

- Padilla De Jesús OL, Ihre HR, Gagne L, Fréchet JMJ, Szoka Jr FC. Polyester dendritic systems for drug delivery applications: in vitro and in vivo evaluation. *Bioconjug Chem* 2002;**13**:453-61.
- Parveen S, Misra R, Sahoo SK. Nanoparticles: a boon to drug delivery, therapeutics, diagnostics and imaging. *Nanomedicine* 2012;**8(2)**:147-66.
- Pasut G, Scaramuzza S, Schiavon O, Mendichi R, Veronese FM. PEG-epirubicin conjugates with high drug loading. *J Bioactive Compatible Polym* 2005;**20**:213-30.
- Peer D, Karp JM, Hong S, Farokhzad OC, Margalit R, Langer R. Nanocarriers as an emerging platform for cancer therapy. *Nat Nanotech* 2007;**2**:751-60.
- Pike DB, Ghandehari H. HPMA copolymer-cyclic RGD conjugates for tumor targeting. *Adv Drug Delivery Rev* 2010;**62**:167-183.
- Pooja D, Kulhari H, Singh MK, Mukherjee S, Rachamalla SS, Sistla R. Dendrimer-TPGS mixed micelles for enhanced solubility and cellular toxicity of taxanes. *Colloids Surf B* 2014;**121**:461-8.
- Ramireddy RR, Raghupathi KR, Torres DA, Thayumanavan S. Stimuli sensitive amphiphilic dendrimers. *New J Chem* 2012;**36**:340-49.
- Ray A, Larson N, Pike DB, Grüner M, Naik S, Bauer H, Malugin A, Greish K, Ghandehari H. Comparison of active and passive targeting of docetaxel for prostate cancer therapy by HPMA copolymer-RGDfK conjugates. *Mol Pharm* 2011;**8(4)**:1090-9.
- Reubi JC, Korner M, Waser B, et al. High expression of peptide receptors as a novel target in gastrointestinal stromal tumours. *Eur J Nucl Med Mol Imaging* 2004;**31**:803-10.
- Reubi JC, Wenger S, Schmuckli-Maurer J, Schaer JC, Gugger M. Bombesin receptor subtypes in human cancers: detection with the universal radioligand (125)I-[D-TYR(6), beta-ALA(11), PHE(13), NLE(14)] bombesin(6-14). *Clin Cancer Res* 2002;**8**:1139-46.
- Ross JS, Schenkein DP, Pietrusko R, Rolfe M, Linette GP, Stec J, Stagliano NE, Ginsburg GS, Symmans WF, Pusztai L, Hortobagyi GN. Targeted therapies for cancer. *Am J Clin Pathol* 2004;**122(4)**:598-609.
- Sarah P, David M. Mechanisms of anticancer drugs. In: Gleeson MJ, Clarke RC, editors. Scott-Brown's Otorhinolaryngology: Head and Neck Surgery. Volume 3, 7thed. Great Britain: Butterworth & Co;2008,134.

- Schluep T, Cheng J, Khin KT, Davis ME. Pharmacokinetics and biodistribution of the camptothecin-polymer conjugate IT-101 in rats and tumor-bearing mice. *CancerChemother Pharmacol* 2006;**57(5)**:654-62.
- Schmieder AH, Caruthers SD, Zhang H, Williams TA, Robertson JD, Wickline SA, Lanza GM. Three-dimensional MR mapping of angiogenesis with alpha5beta1(alpha nu beta3)-targeted theranostic nanoparticles in the MDA-MB-435 xenograft mouse model. *FASEB J* 2008;**22**:4179-89.
- Schroeder A, Heller DA, Winslow MM, Dahlman JE, Pratt GW, Langer R, Jacks T, Anderson DG. Treating metastatic cancer with nanotechnology. *Nat Rev Cancer* 2011;**12(1)**:39-50.
- Shen JM, Gao FY, Yin T, Zhang HX, Ma M, Yang YJ, Yue F. cRGD-functionalized polymeric magnetic nanoparticles as a dual-drug delivery system for safe targeted cancer therapy. *Pharmacol Res* 2013;**70(1)**:102-15.
- Shin SJ, Beech JR, Kelly KA. Targeted nanoparticles in imaging: paving the way for personalized medicine in the battle against cancer. *Integr Biol* 2013;**5(1)**:29-42.
- Shukla R, Thomas TP, Desai AM, Kotlyar A, Park SJ, Baker Jr JR. HER2 specific delivery of methotrexate by dendrimer conjugated anti-HER2 mAb. *Nanotechnology* 2008;**19**:1-7.
- Sideratou Z, Kontoyianni C, Drossopoulou GI, Paleos CM. Synthesis of a folate functionalized PEGylated poly(propylene imine) dendrimer as prospective targeted drug delivery system. *Bioorg Med Chem Lett* 2010;**20(22)**:6513-7.
- Sinha R, Kim GJ, Nie S, Shin DM. Nanotechnology in cancer therapeutics: bioconjugated nanoparticles for drug delivery. *Mol Cancer Ther* 2006;**5(8)**:1909-17.
- Sioka C, Kyritsis AP. Chemotherapy, hormonal therapy, and immunotherapy for recurrent meningiomas. *J Neurooncol* 2009;**92(1)**:1-6.
- Steffensen MB, Hollink E, Kuschel F, Bauer M, Simanek EE. Dendrimers based on [1,3,5]-triazines. *J Polym Sci A Polym Chem* 2006;**44**:3411-33.
- Steinhauser IM, Langer K, Strebhardt KM, Spänkuch B. Effect of trastuzumab-modified antisense oligonucleotide-loaded human serum albumin nanoparticles prepared by heat denaturation. *Biomaterials* 2008;**29(29)**:4022-28.
- Stott Reynolds TJ, Schehr R, Liu D, Xu J, Miao Y, Hoffman TJ, Rold TL, Lewis MR, Smith CJ. Characterization and evaluation of DOTA-conjugated

Bombesin/RGD-antagonists for prostate cancer tumor imaging and therapy. *Nucl Med Biol* 2015;**42(2)**:99-108.

- Svenson S, Tomalia DA. Dendrimers in biomedical applications--reflections on the field. *Adv Drug Deliv Rev* 2005;**57(15)**:2106-29.
- Svenson S. Dendrimers as versatile platform in drug delivery applications. *Eur J Pharm Biopharm* 2009;**71(3)**:445-62.
- Tolia GT, Choi HH. The role of dendrimers in topical drug delivery. *Pharmaceutical Technology* 2008;**32.11**: 88-98.
- Tomalia DA, Swanson DR, Huang B, Pulgam VR, Heinzelmann JR, Svenson S, Reyna LA, Zhuravel MA, Chauhan AS, DeMattei CR. Dendritic polymers with enhanced amplification and interior functionality. *Dendritic Nanotechnologies Inc.* 2006; PCT Patent WO2006-115547.
- Tomoda K, Yabuki N, Terada H, Makino K. Surfactant free preparation of PLGA nanoparticles: The combination of antisolvent diffusion with preferential solvation. *Colloids Surf A* 2014;**457**:88-93.
- Torchilin VP. Micellarnanocarriers: pharmaceutical perspectives. *Pharm Res* 2007;**24(1)**:1-16.
- Trivedi R, Kompella UB. Nanomicellar formulations for sustained drug delivery: strategies and underlying principles. *Nanomedicine* 2010;**5(3)**:485-505.
- Tsiapa I, Loudos G, Varvarigou A, Fragogeorgi E, Psimadas D, Tsotakos T, Xanthopoulos S, Mihailidis D, Bouziotis P, Nikiforidis GC, Kagadis GC. Biological evaluation of an ornithine-modified (99m)Tc-labeledRGD peptide as an angiogenesis imaging agent. *Nucl Med Biol* 2013;**40(2)**:262-72.
- Valabrega G, Montemurro F, Aglietta M. Trastuzumab: mechanism of action, resistance and future perspectives in HER2-overexpressing breast cancer. *Ann Oncol* 2007;**18(6)**:977-84.
- VendittoVJ, Simanek EE. Cancer therapies utilizing the camptothecins: a review of the in vivo literature. *Mol Pharm* 2010;**7(2)**:307-49.
- Wadhwa S, Mumper RJ. Polypeptide conjugates of D-penicillamine and idarubicin for anticancer therapy. *J Control Release* 2012;**158(2)**:215-23.
- Wagh NK, Zhou Z, Ogbomo SM, Shi W, Brusnahan SK, Garrison JC. Development of hypoxia enhanced 111In-labeled Bombesin conjugates: design, synthesis, and in vitro evaluation in PC-3 human prostate cancer. *Bioconjug Chem* 2012;**23(3)**:527-37.

- Wang F, Li Y, Shen Y, Wang A, Wang S, Xie T. The Functions and Applications of RGD in Tumor Therapy and Tissue Engineering. *Int J Mol Sci* 2013;**14(7)**:13447-62.
- Xiong Y, Jiang W, Shen Y, Li H, Sun C, Ouahab A, Tu J. A poly(γ, L-glutamic acid)-citric acid based nanoconjugate for cisplatin delivery. *Biomaterials* 2012;**33(29)**:7182-93.
- Xu W, Luo T, Li P, Zhou C, Cui D, Pang B, Ren Q, Fu S. RGD-conjugated gold nanorods induce radiosensitization in melanoma cancer cells by downregulating alpha(v)beta expression. *Int J Nanomed* 2012;**7**:915-24.
- Yang H, Cai H, Wan L, Liu S, Li S, Cheng J, Lu X. Bombesin analogue-mediated delivery preferentially enhances the cytotoxicity of a mitochondria-disrupting peptide in tumor cells. *PLoS One* 2013;**8(2)**:e57358.
- Yang X, Hong H, Grailer JJ, Rowland IJ, Javadi A, Hurley SA, Xiao Y, Yang Y, Zhang Y, Nickles RJ, Cai W, Steeber DA, Gong S. cRGD-functionalized, DOX-conjugated, and ^{64}Cu-labeled superparamagnetic iron oxide nanoparticles for targeted anticancer drug delivery and PET/MR imaging. *Biomaterials* 2011;**32(17)**:4151-60.
- Yousefpour P, Atyabi F, Vasheghani-Farahani E, Movahedi AA, Dinarvand R. Targeted delivery of doxorubicin-utilizing chitosan nanoparticles surface-functionalized with anti-Her2 trastuzumab. *Int J Nanomed* 2011;**6**:1977-90.
- YY Song, F Schmidt-Stein, S Bauer, P Schmuki. Amphiphilic TiO_2 nanotube arrays: an actively controllable drug delivery system. *J Am Chem Soc* 2009;**131**:4230-32.
- Zhai GX, Wu J, Zhao XB, Yu B, Li H, Lu YH, et al. A liposomal delivery vehicle for the anticancer agent gossypol. *Anticancer Res* 2008;**28**:2801-05.
- Zhan C, Gu B, Xie C, Li J, Liu Y, Lu W. Cyclic RGD conjugated poly(ethylene glycol)-co-poly(lactic acid) micelle enhances paclitaxel anti-glioblastoma effect. *J Controlled Release* 2010;**143**:136-42.
- Zhang C, Pan D, Luo K, Li N, Guo C, Zheng X, Gu Z. Dendrimer–doxorubicin conjugate as enzyme-sensitive and polymeric nanoscale drug delivery vehicle for ovarian cancer therapy. *Polym Chem* 2014;**5**:5227-35.
- Zhang F, Niu G, Lin X, Jacobson O, Ma Y, Eden HS, He Y, Lu G, Chen X. Imaging tumor-induced sentinel lymph node lymphangiogenesis with LyP-1 peptide. *Amino Acids* 2012;**42(6)**:2343-51.

- Zhou D, Zhang G, Gan Z. c(RGDfK) decorated micellar drug delivery system for intravesical instilled chemotherapy of superficial bladder cancer. *J Control Release* 2013;**169(3)**:204-10.
- Zou HY, Zhao DX, Yang ZZ. A theoretical study on mechanism of the anticancer drug camptothecin's E-ring-opening. *J Mol Graph Model* 2013;**43**:58-65.

CHAPTER

Optimization, characterization & stability of Bombesin conjugated Poly (D,L-lactic-co-glycolic acid) nanoparticles

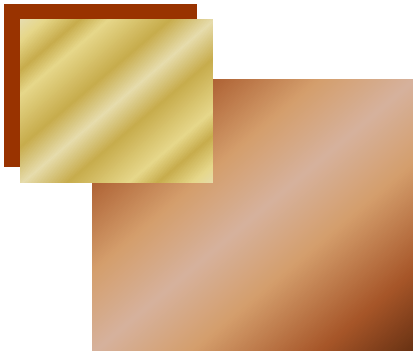

2.1. Background

Nanoparticles are promising carriers for several biomedical applications such as imaging, diagnostics and drug delivery (Davis et al., 2008; Arruebo et al., 2009; Koi et al., 2012. In drug delivery, their applications are mostly explored in development of targeted drug delivery systems especially for anticancer drugs. Because of small size, nanoparticles can easily enter into the cancer cells through the leaky vasculature (passive targeting). In addition, the surface of nanoparticles can be easily manipulated to give receptor-specific targeted system (Ruoslahti et al., 2010).

The efficacy of the nanoparticulate systems is very much dependant on three basic surface properties such as size, surface charge and hydrophobicity (Muller, 1997; Jiang et al., 2009). These parameters affect stability as well as *in vivo* performance like translocation to target site, binding and cellular uptake (Petros and DeSimone; 2010). Nanoparticles are colloidal systems that range in size range 10-1000 nm and their stability is mainly determined by the surface chemistry. The physical stability of colloidal systems is explained by their aggregation and coagulation behavior.

According to DLVO theory, the stability of nanoparticles depends on the balance between attractive Van der Waals and repulsive electrostatic forces due to double layer of counter ions (Derjaguin and Landau, 1941; Verwey et al., 1948). Among three different types of Van der Waals forces (Keesom, Debije and London), London forces i.e. induced dipole – induced dipole, are mainly responsible for attraction and aggregation of nanoparticles. The strength of electrostatic repulsion forces depends on the distance from the nanoparticle surface. Electrostatic forces

are expressed in terms of Nernst potential and Zeta potential (ζ). The Nernst potential is the potential difference between the actual nanoparticle surface and electroneutral region. The zeta potential or electrokinetic potential is the potential difference between shear plane and electroneutral region. Nernst potential has little effect in colloidal stabilization and is not practically assessable. Thus zeta potential is an important parameter of electrostatic repulsion. When the electrostatic repulsive forces dominate the attractive Van der Waal forces, the system remains stable and in dispersed state. Thus high zeta potential value (more negative or positive) indicates more the colloidal stability of nanoparticles. But, practically attractive forces are found to be stronger compared to repulsive forces and nanoparticles tend to form aggregates within seconds.

Surface hydrophobicity is another major cause of the instability of nanoparticles. It also affects the behavior of nanoparticles in aqueous environment and decides the fate and transport of nanoparticles (Muller, 1997). The hydrophobicity plays an important role in the interaction of nanoparticles with the bio-membranes (Li et al., 2008; Kim et al., 2013; Xiao and Wiesner, 2012).

Several approaches can be used to increase the stability of nanoparticles (Chen et al.,2010). First, by forming an electric double layer around nanoparticles i.e. charge or electrostatic stabilization. Second, by adsorption or chemically attachment of polymeric molecule on the nanoparticle surface (steric stabilizer) i.e. steric stabilization (Luckham, 1996). Third, combination of both electrostatic and steric stabilization i.e. electrosteric stabilization. Generally, steric stabilization or electrosteric stabilization approaches are used in nanoparticle stabilization because of its several advantages- electrolyte insensitivity, redispersibility of nanoparticles,

can accommodate high concentration and suitability to multiphase systems (Ortega-Vinuesa et al., 1996; Russel et al., 1992; Birdi, 2008).

The primary objective of this investigation was to develop a sterically stabilized bombesin (BBN) peptide conjugated biodegradable polymeric nanoparticles based system for cancer targeting. Several targeting ligands have been conjugated to nanoparticles for the delivery of anticancer drugs (Liang et al., 2011; Zheng et al, 2010; Dhar et al., 2008). However, surface conjugation changes the dimension and other physicochemical parameters such as surface charge, which are directly related to the stability of nanoparticle. Hence, the colloidal stability of unconjugated polymeric nanoparticles (PNP) and BBN conjugated nanoparticles (BPNP) was studied in the presence of electrolytes and physiological conditions. The nanoparticle stabilization and aggregation mechanisms were investigated in detail. This study also provides insight about the selection of method for the determination of stability factor.

2.2. Experimentation

2.2.1. Materials

Poly (D,L-lactic-co-glycolic acid) (PLGA) containing a free carboxyl end group (uncapped) with L/G molar ratio of 50:50, Bombesin, Sodium cholate, 1-Ethyl-3-(3-dimethylaminopropyl)carbodiimide (EDC), N-Hydroxysuccinimide (NHS), 2-(n-morpholino) ethanesulfonic acid (MES) and N-[tris(hydroxymethyl)methyl]-2-aminoethane sulfonic acid (TES) were purchased from Sigma-Aldrich (Mumbai, India). Bradford reagent was purchased from Biomatik (Hyderabad, India). Rose Bengal dye and other chemicals were of analytical grade and were purchased from s. d. fine-chem Ltd. (Hyderabad, India).

2.2.2. Preparation of PLGA nanoparticles

PLGA nanoparticles (PNP) were prepared by a modified solvent evaporation (nano-precipitation) method. PLGA (20 mg) was dissolved in 2 mL acetone and then quickly poured in 20 mL of deionised water containing different concentrations (0.1%, 0.25% and 0.5% w/v) of surfactants (polyvinyl alcohol, Tween® 20 and sodium cholate). The dispersion was sonicated for 2 minutes in an ice bath. The organic phase was evaporated off by magnetic stirring at 1000 rpm for 3 h. Finally, the dispersion was centrifuged at 15000 rpm for 20 minutes at 4 °C. Nanoparticles were washed thrice with deionised water, lyophilized and stored at 2-8 °C.

2.2.3. Bioconjugation of BBN to PLGA nanoparticle

Ten milligrams of PNP were dispersed in 5 ml of MES buffer (0.1 M) and incubated with 497.95 µM of EDC and NHS each. The dispersion was kept on gentle stirring for one hour at room temperature. To this, 100, 250 and 500 µl of BBN solution (1 mg/ml) was added, mixed well and kept for further stirring of 6 h. BBN conjugated nanoparticles (BPNP) were collected after centrifugation at 10000 rpm for 10 min and washed thrice with distilled water. The conjugation efficiency was determined by measuring BBN in supernatant by Bradford protein assay. The absorbance was measured at 595 nm using microplate reader (Synergy 4, Biotek).

2.2.4. Effect of pH and buffer on conjugation efficiency

The effect of pH and buffer medium on the peptide conjugation efficiency was studied using 0.1 M MES buffer pH 6.2, phosphate buffer saline pH 7.4 (PBS) and 0.1 M TES buffer pH 8.2.

2.2.5. Nanoparticle characterization

Nanoparticles were characterized for particle size, zeta potential, surface morphology and chemical interactions between the molecules. Mean particle diameter (PD), polydispersity index (PDI) and zeta potential of both PNP and BPNP were measured by proton correlation spectroscopy using Zetasizer Nano-ZS (Malvern instrument Ltd., Malvern, UK). Samples were diluted 10 times with distilled water and analyzed at 25 °C with a backscattering angle of 173°.

Surface morphology of nanoparticles was determined by scanning electron microscopy (SEM) analysis. The samples were sputtered on thin film of gold and scanned using SEM machine (SEM-LEOS 1430VP, LEO Electron Microscopy Ltd, U.K) equipped with tungsten filament. The chemical interaction between amine group of BBN and carboxylic group of PNP was studied by Fourier transform infrared (FTIR) analysis. FTIR analysis was carried out by potassium bromide (KBr) pellet technology. An amount (3 mg) of nanoparticles was mixed with the 100 mg of KBr using a mortar and pestle. The mixture was filled in the die and pressed using 15 ton laboratory Hydraulic Pellet Press. The formed pellet was placed in the pellet holder and scanned using FTIR (Perkin Elmer, Spectrum one) spectrophotometer in the range of wave number 450 to 4000 cm^{-1}.

2.2.6. Colloidal and serum stability studies

2.2.6.1. Stability of nanoparticles in serum and physiological conditions

Stability of PNP and BPNP with time was tested in bovine serum (1% v/v), PBS and physiological saline (NS) as per earlier reports (Lazzari et al., 2012; Chaudhari et al., 2012). A stock solution (1 mg/ml) of nanoparticles was prepared in distilled water. Aliquot (0.5 ml) of the stock solution was taken and diluted with 4.5

mL of study medium. The samples were stored at room temperature and particle size, polydispersity and zeta potential were determined.

2.2.6.2. Salt induced aggregation of nanoparticles

Salt induced aggregation of nanoparticles was studied by the method reported previously (Chaudhari et al., 2012). Both nanoparticles were dispersed in 0.1 to 1 M sodium sulphate solutions and the optical density of the dispersions was measured at 595 nm by UV/VIS spectrophotometer (Perkin Elmer, Lambda 25, UK).

2.2.6.3. Determination of Fuchs or stability factor

Stability or Fuchs factor was determined by two different methods. *a) On the basis of optical density:* The optical density of nanoparticle suspension was determined at 595 nm using UV/VIS spectrometer. The total aggregation measurement time was 200 s. *b) On the basis of average hydrodynamic diameter:* The nanoparticles were dispersed in varying concentration of salts solutions (NaCl and $CaCl_2$). The hydrodynamic diameter of nanoparticles and aggregates was determined as a function of time by dynamic light scattering method.

The Fuchs factor (W) for every electrolyte concentration was calculated using following equation:

$$W = \frac{K_f}{K_s} = \frac{(dAbs/dt)_f}{(dAbs/dt)_s} \qquad \text{…….. (Equation 1)}$$

Where, K_f is the fastest aggregation-kinetic constant and K_s is slower aggregation-kinetic constant**.**

These rate constants can be calculated from following equation:

$$\frac{dAbs}{dt} = \frac{(0.5C_2 - C_1)\, N^2{}_0\, l}{2.3}\, k \qquad \text{…….. (Equation 2)}$$

Where; C_1 and C_2 are scattering cross-sections of a monomer and a diamer, respectively, N_0 is the initial particle concentration, and l is the optical path length.

Similarly, the W was calculated for particle diameter studies by replacing the absorbance with particle diameter in equation 1.

2.2.7. Surface hydrophobicity of nanoparticles

Surface hydrophobicities of PNP and BPNP were determined by Rose Bengal dye adsorption test as reported earlier (Jung et al., 2002). The nanoparticles were dispersed in different concentration of dye solutions (5- 40 µg/ml) and incubated at 25 °C for 3 h. Nanoparticle dispersion was centrifuged at 15000 rpm for 1 h and amount of dye adsorbed on the nanoparticle surface was determined indirectly by measuring unbound dye in supernatant at 542 nm using UV-VIS spectrophotometer.

The binding constant (K) of Rose Bengal for PNP and BPBP was determined by Scatchard transformation:

r/a = KN-Kr …….. (Equation 3)

Where; r = where r is the amount of Rose Bengal adsorbed per mg nanoparticles (mg/mg); a is equilibrium concentration of Rose Bengal (mg/ml); K is the binding constant (ml /mg); and N is the maximum amount bound (mg/mg).

2.2.8. Peptide desorption studies

The integrity of the chemical bond between nanoparticle and BBN was tested by measuring the release of BBN from the nanoparticles surface. Ten milligram of BPNP were dispersed in 5 mL of PBS, mixed well and kept on mechanical shaker. At scheduled time intervals, the nanoparticles were centrifuged at 10000 rpm for 5 minutes and supernatant was estimated for BBN content.

2.3. Results and discussion

2.3.1. Optimization of PLGA nanoparticles using different surfactants

PLGA nanoparticles were prepared by solvent evaporation method. PLGA was dissolved in acetone and transferred to aqueous surfactant solution to get o/w emulsion. The formed emulsion was stirred to evaporate the organic phase and form drug encapsulated nanosized particles. PLGA nanoparticles preparations have been reported with or without surfactant solutions (Dailey et al., 2003; Wang et al., 2009). However, nanoparticles prepared without surfactant were found to be less stable compared to with surfactant nanoparticles. In this study, PLGA nanoparticles were prepared using three different surfactants: PVA, Tween 20 and sodium cholate, at three different concentrations (0.1%, 0.25% and 0.5% w/v). The observed mean particle size and zeta potential of the different formulations are shown in Table 1.

Nanoparticles prepared with sodium cholate were of smaller size (< 100 nm) compared to PVA (102.65-119.82 nm) and Tween 20 (109.33-149.92 nm). Among the various formulations prepared with sodium cholate (F3, F6 and F9), F6 formulation showed the smallest size (86.15 ± 2.47 nm). Both increase and decrease in surfactant concentration produced larger nanoparticles. It can be attributed to adsorption of surfactant molecules on nanoparticle surface at higher concentration. On the other side, low surfactant concentration may be insufficient to keep particle separate leading to agglomeration of small particles.

The zeta potential observed for various formulations ranged from -23.3 to-24.2 mV for PVA, -21.8 to -34.7 mV for Tween 20 and -27.6 to -36.5 mV for sodium cholate. So formulation F6 was considered as optimized formulation because of the smallest size and good zeta potential value (Figure 2.1).

Table 2.1: Optimization of PLGA nanoparticle prepared with different surfactants (Mean ± SD, n=3)

Formulation	Surfactant	Size (nm)	PDI	Zeta Potential (mV)
F1	0.5% PVA	110.64 ± 1.28	0.12 ± 0.05	-24.2 ± 2.6
F2	0.5% Tween 20	115.90 ± 2.42	0.07 ± 0.01	-21.8 ± 3.1
F3	0.5% Sod. cholate	91.12 ± 1.53	0.18 ± 0.02	-36.5 ± 3.7
F4	0.25% PVA	119.82 ± 3.46	0.11 ± 0.02	-23.3 ± 1.2
F5	0.25% Tween 20	109.33 ± 1.54	0.07 ± 0.02	-24.5 ± 2.8
F6	0.25% Sod. cholate	86.15 ± 2.47	0.11 ± 0.03	-34.2 ± 2.3
F7	0.1% PVA	102.65 ± 4.07	0.13 ± 0.04	-23.7 ± 2.3
F8	0.1% Tween 20	149.92 ± 3.28	0.33 ± 0.05	-34.7 ± 3.5
F9	0.1% Sod. cholate	98.42 ± 1.89	0.20 ± 0.04	-27.6 ± 4.1

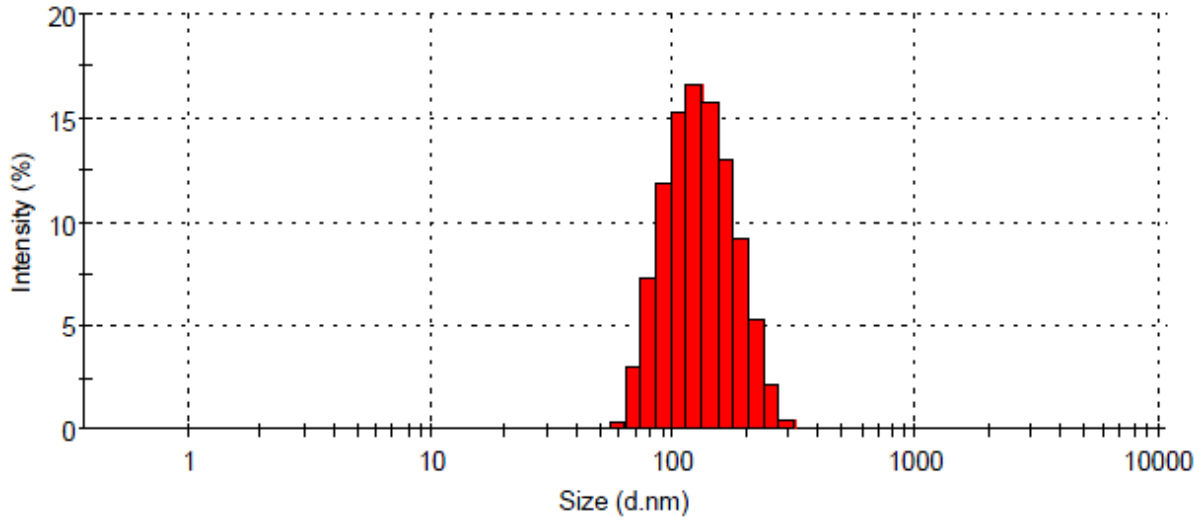

a)

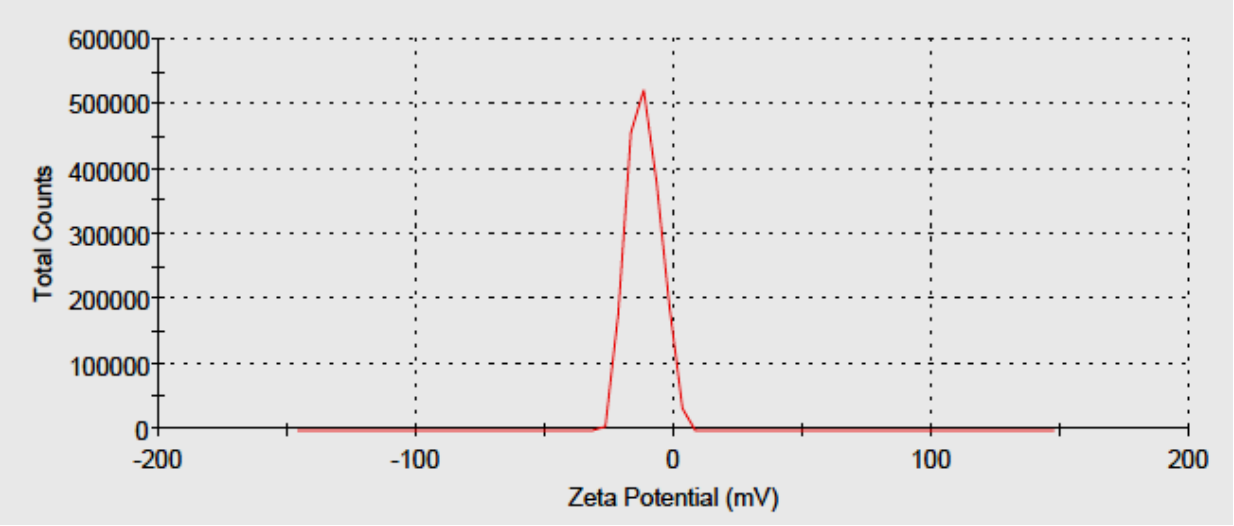

b)

Figure 2.1: a) Particle diameter and b) zeta potential of bombesin conjugated PLGA nanoparticles (BPNP) measured by Dynamic light scattering method

2.3.2. Conjugation of BBN to PNP surface

Bombesin was conjugated to the PNP surface by well known EDC/NHS reaction. The free carboxylic group on nanoparticle surface was activated by EDC/NHS and allowed to react with free amine group present on BBN. The conjugation was carried out in three different peptide/polymer ratios (Table 2.2). As the peptide concentration was increased, the size of the particles was also increased. But, the zeta potential was changed from -34.2 mV to -9.1 mV. The surface charge of PLGA nanoparticle is due to presence of negatively charged carboxylic group on the surface. During conjugation, this carboxylic group interacts with positive amine group of BBN and overall surface charge moves towards neutrality.

The conjugation efficiency was decreased with the increase in peptide concentration in reaction mixture. This can be explained by the steric hindrance on the nanoparticle surface at higher peptide concentration. However, the peptide

conjugation to per mg of nanoparticle was increased. The BBN conjugated to per mg of nanoparticles was 4.75 µg, 9.06 µg, and 19.13 µg for BPNP1, BPNP2 and BPNP3; respectively. The slight variation in pH and buffer medium did not show significant difference in conjugation efficiency and other physicochemical parameters. Hence, it is suggested that BBN conjugation to nanoparticles can be carried out in the pH range 6.2-8.2.

Table 2.2: Characterization of Bombesin conjugated PLGA Nanoparticles (Mean ± SD, n=3)

Formulation	Particle diameter (nm)	Polydispersity index	Zeta potential (mV)	Conjugation efficiency (%)
PNP	86.15 ± 2.47	0.11 ± 0.04	-34.2 ± 2.9	-
BPNP 1	101.32 ± 3.96	0.22 ± 0.02	-15.7 ± 1.8	94.47 ± 0.62
BPNP 2	112.59 ± 2.15	0.19 ± 0.04	-11.3 ± 1.5	90.59 ± 2.11
BPNP 3	129.72 ± 4.06	0.31 ± 0.03	-9.1 ± 2.6	76.52 ± 1.84

2.3.3. SEM analysis

The surface morphology was studied using scanning electron microscope (Figure 2.2). Nanoparticles were spherical in shape and well dispersed in the dispersion medium. The average particle size was in the range of 100-150 nm.

2.3.4. FTIR analysis

Binding of BBN to the nanoparticle surface was confirmed by the FTIR analysis. FTIR spectra of pure BBN showed characteristic peaks at 3299, 1647 and 1533 cm^{-1} corresponding to -NH stretching, C=O stretching (amide I) and -CN stretching (amide II), respectively (Figure 2.3). The characteristic carboxylic group

peak of PNP was appeared at 1760 cm^{-1}. The other peaks of PNP were observed at 3392 (-OH stretching), 2938 (-CH stretching) and at 1082 cm^{-1} (-C-O stretching**).** In BPNP FTIR spectra, the carboxylic group peak was disappeared and amide bond peak was appeared at 1650 cm^{-1} which confirmed the formation of amide bond between carboxylic group of PNP and amine group of BBN.

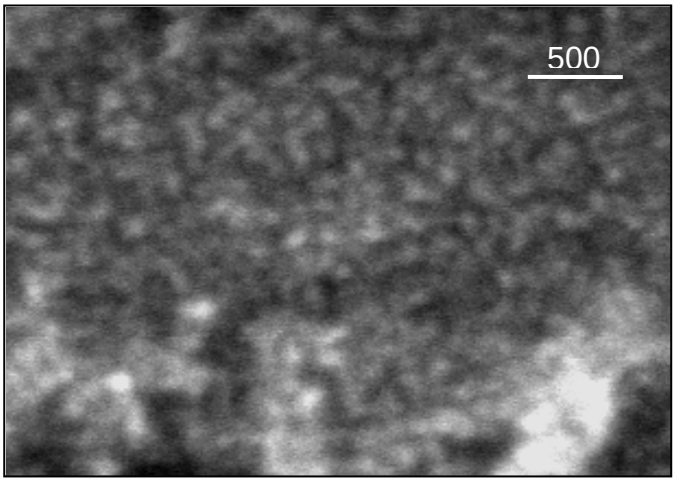

Figure 2.2: Scanning electron microscopy (SEM) of bombesin conjugated PLGA nanoparticles (BPNP). Size-scale is represented in nm.

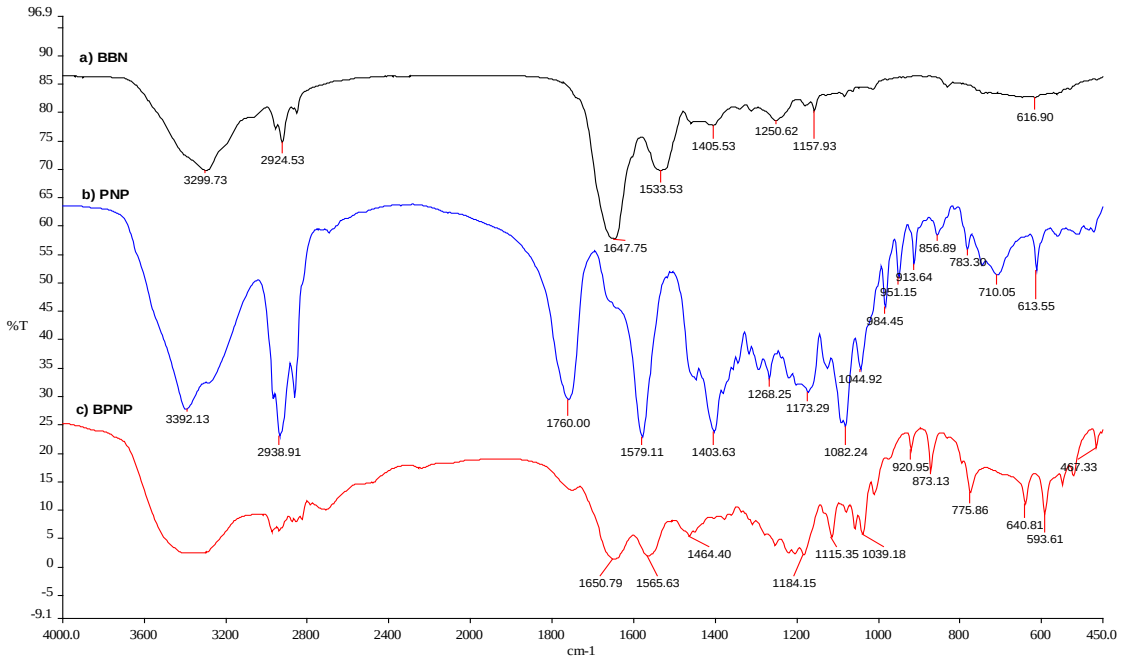

Figure 2.3: FTIR spectra of a) Bombesin, b) PLGA nanoparticle and c) Bombesin conjugated PLGA nanoparticles

2.3.5. Colloidal stability of nanoparticles in serum and physiological conditions

Colloidal stability of nanoparticles was determined in distilled water, NS, and PBS and was expressed as change in particle size (Figure 2.4) and PDI (Figure 2.5) with time. After intravenous administration, the size and charge of nanoparticles are mainly determined by the adsorbed serum components (Lourenco et al., 1996). Hence, a similar study was also carried out in 1% bovine serum. Both PNP and BPNP were to be found stable in all four medium up to 24 h. The observed particle size of PNP was 221.3, 217.6, 131.5 and 130.9 nm in DW, NS, PBS and serum, respectively. In case of BPNP, the particle size was 258.8, 277, 171.3 and 158.2 nm in DW, NS, PBS and serum, respectively. Although, an increase in particle size was observed with nanoparticles dispersed in DW and NS, no agglomeration was observed. Nanoparticles were dispersible and stable in the medium. Similar effect was observed on PDI after dispersion in to different medium. After 24 h, the PDI for both PNP and BPNP was below 0.3 in serum and PBS. In NS and distilled water, the PDI was more than 0.5 for PNP and BPNP.

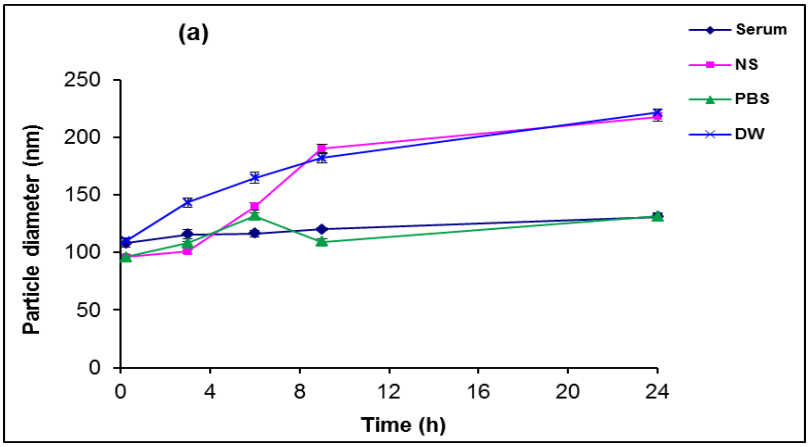

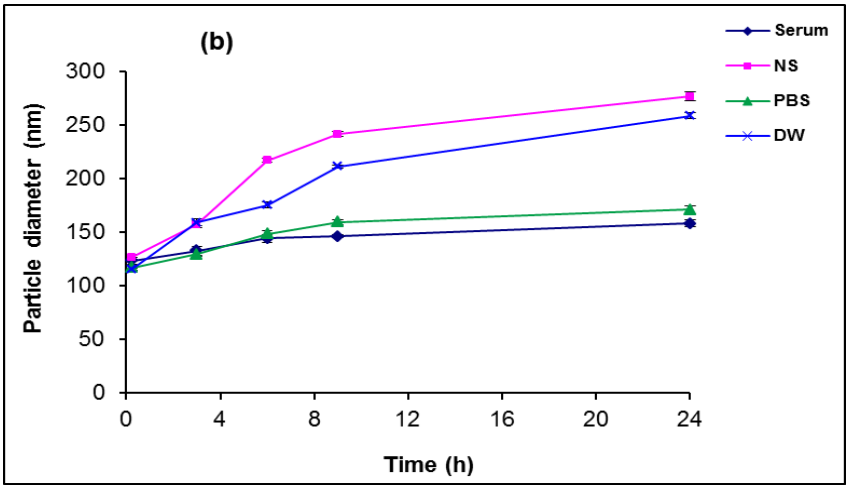

Figure 2.4: Change in particle size of a) polymeric nanoparticle (PNP) and b) Bombesin conjugated PLGA nanoparticles (BPNP) with time in different medium (n=3)

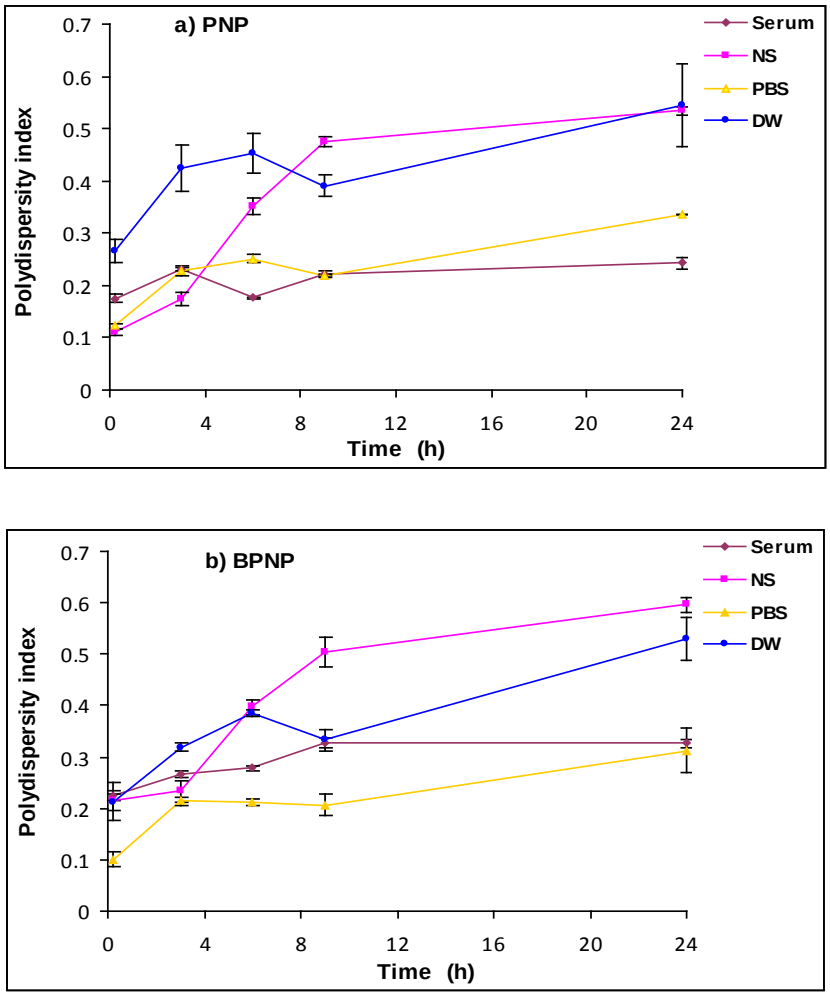

Figure 2.5: Change in polydispersity of a) polymeric nanoparticle (PNP) and b) Bombesin conjugated PLGA nanoparticles (BPNP) with time in different medium (n=3)

2.3.6. Salt induced aggregation of nanoparticles

Nanoparticles were incubated in increased concentration of sodium sulphate to evaluate their aggregation resistance property (Figure 2.6). The critical flocculation concentration (CFC) of PNP and BPNP in Na_2SO_4 was 0.4M and 0.7M. The results showed that nanoparticles were stable through electrostatic forces and addition of Na_2SO_4 solution resulted in destruction of electrostatic double layer. The increase in CFC of BPNP may be to steric stabilization of nanoparticles by the BBN.

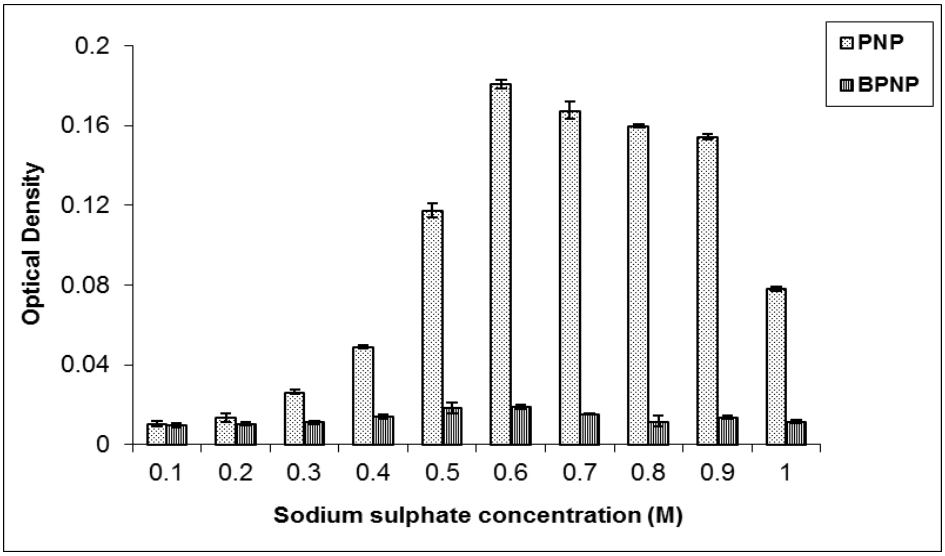

Figure 2.6: Change in optical density of PNP and BPNP dispersion with sodium sulphate concentration (n=3)

2.3.7. Determination of stability or Fuchs factor (W)

Aggregation-kinetics studies were performed to determine the stability or Fuchs factor. According to DLVO theory, the aggregation of a lyophobic colloidal system increases with increase in electrolyte concentration. Generally the optical density increases with the increase in aggregation. Hence the measurement of optical density of the colloidal system provides insight about the stability of nanoparticles. The change in the optical densities of PNP and BPNP with the time

were measured (Figure 2.7). The curves were found steeper in $CaCl_2$ than in NaCl and the steepness was increased with the concentration.

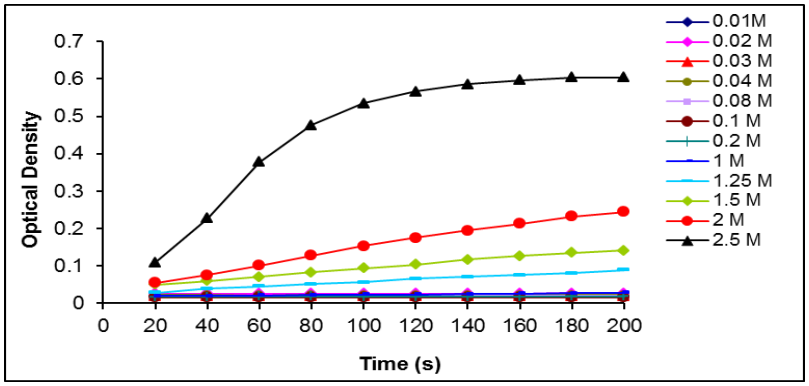

a)

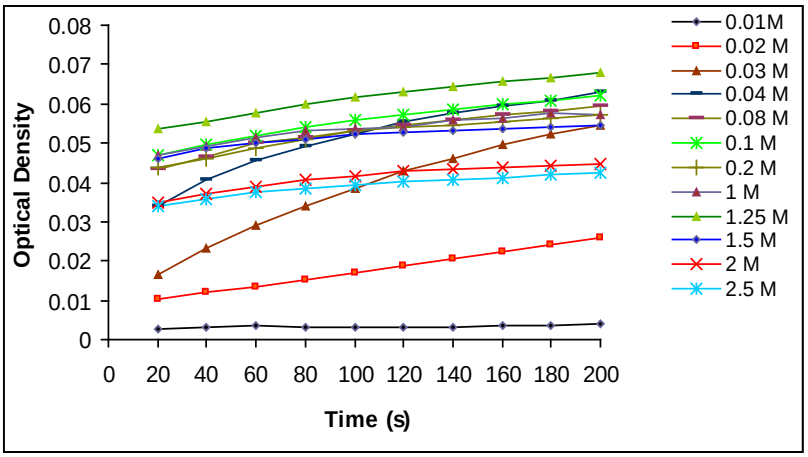

b)

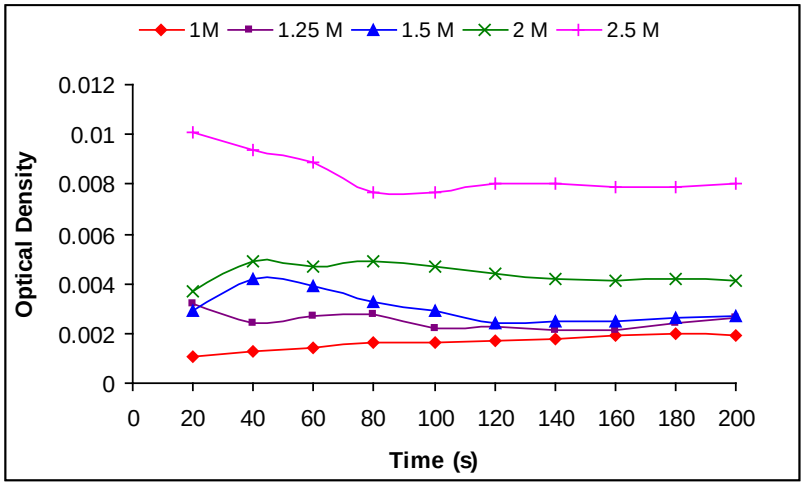

c)

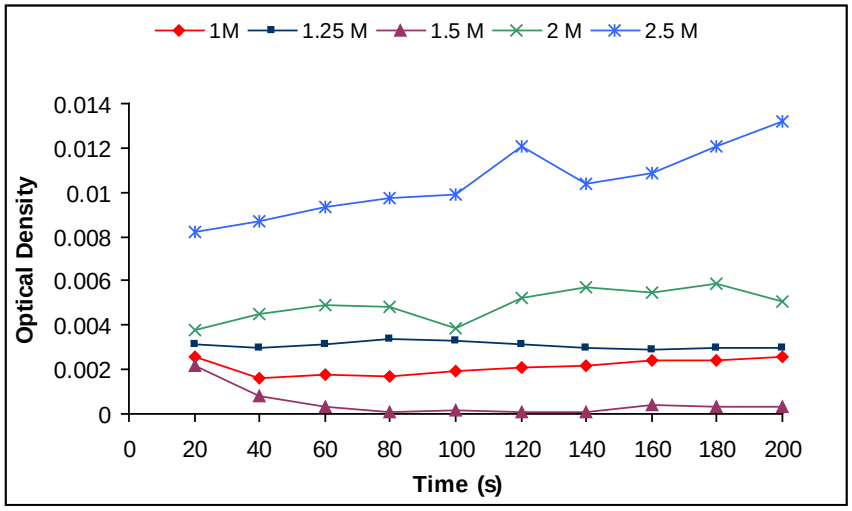

d)

Figure 2.7: Change in optical density with time: a) PNP in NaCl; b) PNP in $CaCl_2$; c) BPNP in NaCl; and d) BPNP in $CaCl_2$

But, these curve provide only a general picture of stability and difficult to differentiate the effect of little variation in electrolyte concentration. Therefore, the data were treated to calculate the Fuchs factor for individual electrolyte concentration (Equation 1 and 2).

Fuchs factor is related to the number of collisions that must occur between two colliding particles before they stuck completely. The value W =1 indicates the complete instability of colloidal system while W= ∞ means the total stability (Fuchs, 1934). Further, for the determination of exact CFC, the Fuchs factor was plotted against the electrolyte concentration (Figure 2.8). For PNP, the CFC was observed 1.5M for NaCl and 30 mM for $CaCl_2$. For BPNP, the optical density values were negative at lower concentration of both NaCl and $CaCl_2$. At higher concentration (> 1M), the CFC was not observed up to 2.5 M concentration of both NaCl and $CaCl_2$. However, the minimum observed W value was 4.2 and 1.8 in NaCl and $CaCl_2$. All above data indicated that both PNP and BPNP showed faster aggregation in $CaCl_2$

than NaCl. It is because of the faster neutralization of negative surface charge of nanoparticles by the divalent Ca^{+2} ions than monovalent Na^{+1}. The BPNP showed more stability than PNP. It may be due to presence of bombesin peptide on the surface which may affect the surface properties on nanoparticles in two ways. First, BBN is hydrophilic in nature and may reduce the surface hydrophobicity of nanoparticle. Second, the nanoparticle stabilization mechanism might have switched to steric from electrostatic.

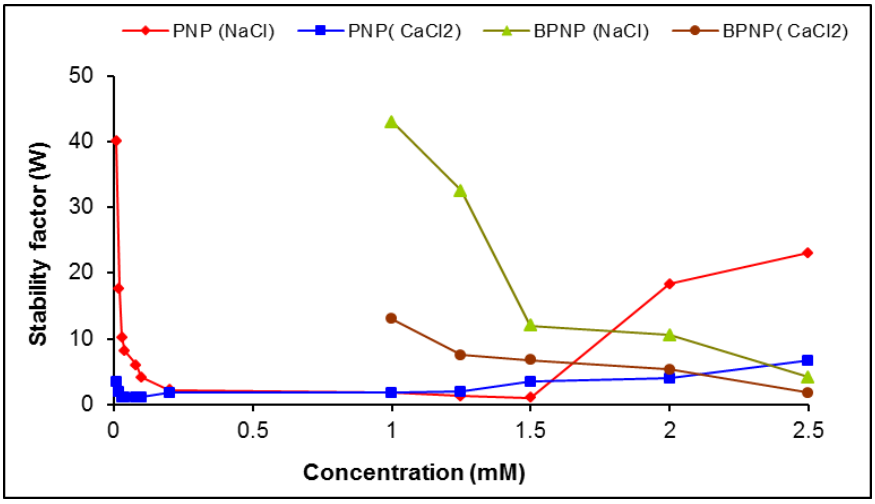

Figure 2.8: Stability or Fuchs factor (W,) determined by optical density method, as a function of electrolyte concentration

To confirm the stabilization mechanism, nanoparticles were incubated with low and high electrolyte concentrations. At low ionic strength, electrostatic stabilization is sufficient to stabilize the particles. The thickness of electric double layer is about 5-10 nm and elecreostatic repulsion forces are able to counteract the attractive Van der Waals forces. But as the ionic strength is increased (> 0.1M), the thickness of double layer is reduced (< 1 nm) and Van der Waals forces dominates over electrostatic forces and particles tends to form agglomerates (Napper, 1983).

But, as mentioned earlier, the optical density values were found to be negative at lower concentrations. Hence a different method (based on particle diameter) was used to determine the stability factor. The concept was that the negative values may be because of very dilute solution used in optical density method. But the diameter of a particle is independent on its concentration. The change in particle diameters of PNP and BPNP with time are shown as Figure 2.9.

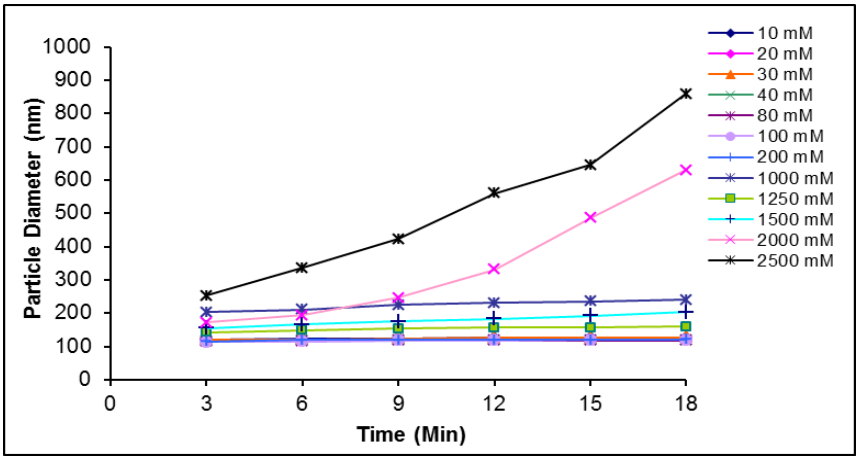

a)

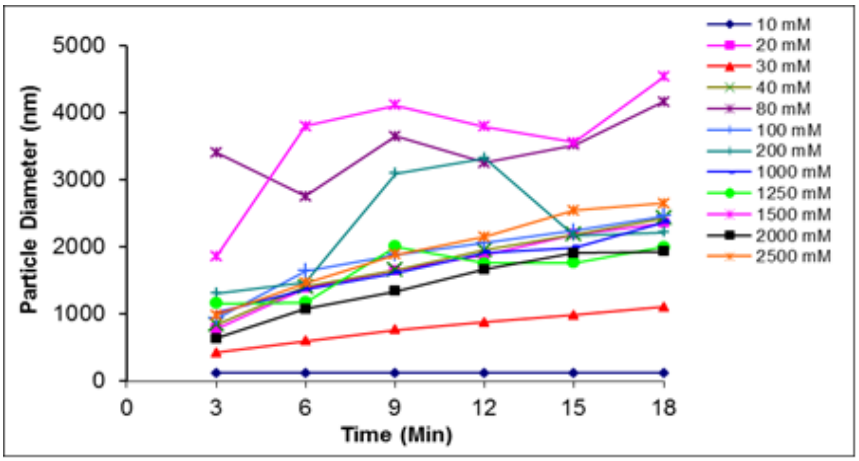

b)

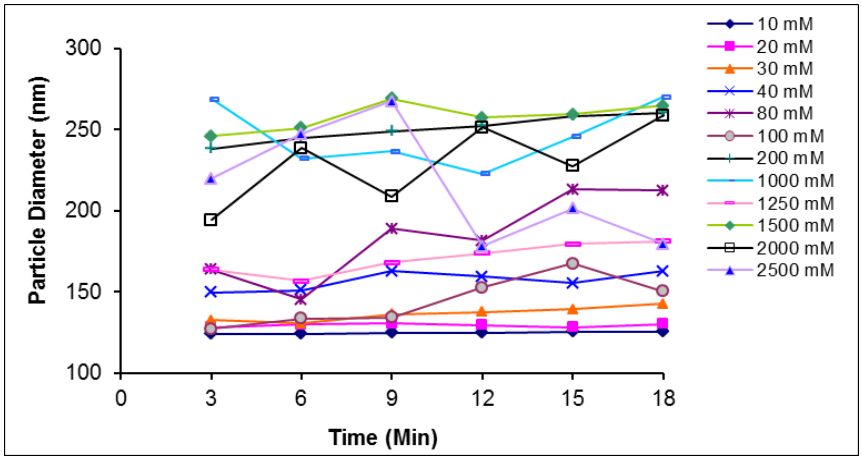

c)

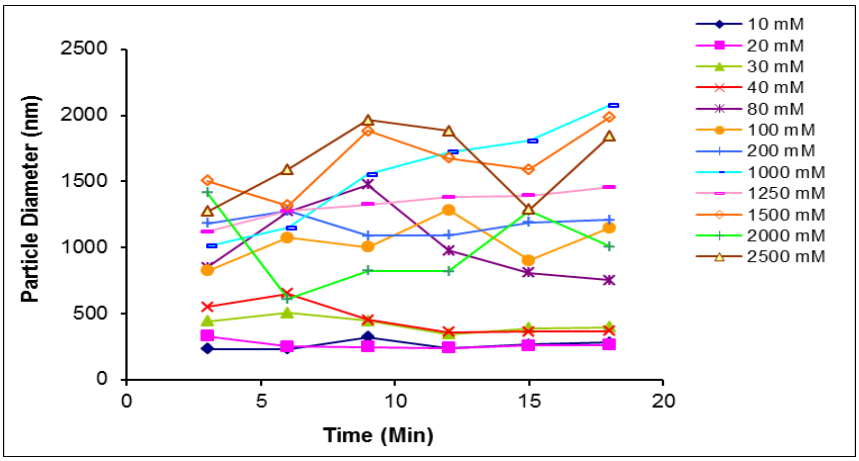

d)

Figure 2.9: Change in particle diameter with time: a) PNP in NaCl; b) PNP in $CaCl_2$; c) BPNP in NaCl; and d) BPNP in $CaCl_2$

The stability factor was calculated and plotted against electrolytes concentration (Figure 2.10). The CFC values observed for different solutions were as follows: 1.5M for PNP in NaCl, 0.08M for PNP in $CaCl_2$, 0.1M for BPNP in $CaCl_2$. CFC was not observed for BPNP in NaCl. The results indicated that CFC value observed in particle diameter method was similar (1.5M) for PNP in NaCl and slightly higher (0.08M v/s 0.03M) for PNP in $CaCl_2$. Again, CFC was not observed for BPNP

in NaCl. It confirmed that BPNP were stabilized by both electrostatic and steric stabilization. The massive difference in particle size measured in NaCl and $CaCl_2$ solution could be explained by rapid and more neutralization of negative charge of nanoparticles by Ca^{+2} ions than monovalent Na^{+} ion.

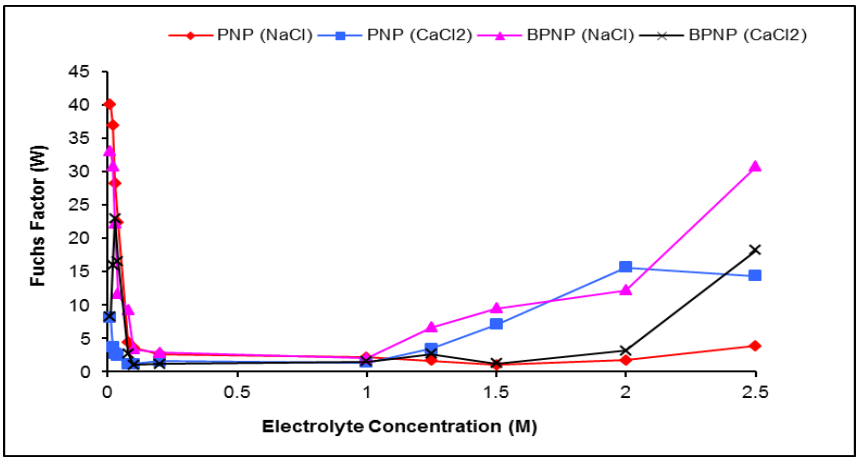

Figure 2.10: Stability or Fuchs factor (W), determined by particle diameter method, as a function of electrolyte concentration

Although the methods used in the assessment of stability of the formulations are different in nature, the optical density value is concentration dependent whereas particle size of nanoparticle is independent of concentration of the sample. In our study, the results were found to be independent of method used which indicates that both the methods can be used as complementary. When the sample quantity is less or for costly formulation, particle diameter measurement could be a better approach than optical density measurement. For less expensive or concentrated samples, optical density measurement is more suitable.

A separate study was carried out to determine the nanoparticle-aggregation mechanism. The PNP and BPNP dispersed in 0.08M $CaCl_2$ were diluted four times with distilled water and vortexed for 5 min. The size of PNP was not changed significantly but in case of BPNP, it was reduced to half (similar to 0.03M). It suggest

that PNP were aggregated by coagulation (irreversible) while BPBP formed floccules which were reversible at some extant.

2.3.8. Surface hydrophobicity of nanoparticles

Hydrophobicity of nanoparticle plays an important role in fate and transport in biological system. Adsorption of organic dye such as rose bengal on nanoparticle surface is good indicator of hydrophobicity of nanoparticles (Jung et al., 2002; Thiele et al., 2003). The binding constant (K) of rose bengal was 0.018 for PNP and 0.011 for BPBP which indicated that BPNP were more hydrophilic than PNP. The results were in good agreement with change in surface potential.

2.3.9. Bombesin desorption studies

Bombesin release from the nanoparticle surface was determined to check the stability of the conjugate (Figure 2.11). About 12.76% of BBN was released after 24 h indicating the stability of the bonding between peptide and nanoparticles. However, 9.35% of BBN was released in very first hour of the study. It may be due to release of BBN present on nanoparticle surface not conjugated covalently but was only adsorbed or entangled with conjugated BBN.

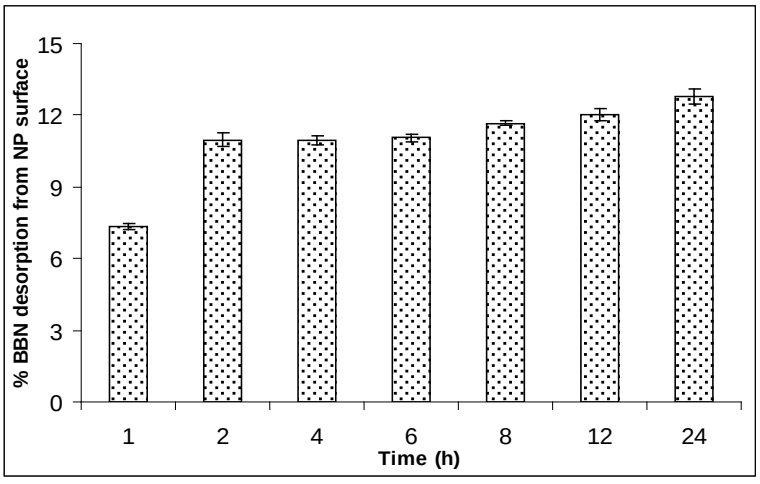

Figure 2.11: Percent release of BBN from nanoparticle surface with time (n=3)

2.4. Conclusion

The assessment of colloidal stability is an important tool in the development of effective and efficient drug delivery system. In the present research work, bombesin conjugated biodegradable polymeric nanoparticles (BPNP) were prepared, characterized and their stability was determined in various physiological conditions. The change in optical density and particle diameter were used as stability indicators and were compared. Both the methods showed similar results. However, for dilute and costly formulations particle diameter determination was found better than optical density measurement. The formulations were further investigated for stabilization and aggregation mechanisms. Unconjugated and peptide conjugated nanoparticles were stabilized by two different mechanisms-electrostatic and electro-steric stabilization, respectively. Similarly, particle aggregation mechanisms for PNP and BPNP were also different. PNP were aggregated by coagulation process whereas BPNP formed floccules. All the above results were well supported by surface hydrophobicity studies and peptide desorption studies. Thus bombesin, which was grafted on nanoparticles as targeting ligand, also improved the stability of nanoparticles.

2.5. References

- Arruebo M, Valladares M, Gonzalez-Fernandez A. Antibody conjugated nanoparticles for biomedical application. *J Nano Mat* 2009;1-24.
- Birdi K. Handbook of surface and colloid chemistry. CRC Press, 2008.
- Chaudhari KR, Kumar A, Khandelwal VKM, Ukawala M, Manjappa AS, Mishra AK, Monkkonen J, Murthy RSR. Bone metastasis targeting: a novel approach to reach bone using zoledronate anchored PLGA nanoparticle as carrier system loaded with docetaxel. *J Control Release* 2012;**158(3)**:470-78.

- Chaudhari KR, Ukawala M, Manjappa AS, Kumar A, Mundada PK, Mishra AK, Mathur R, Mönkkönen J, Murthy RSR. Opsonization, biodistribution, cellular uptake and apoptosis study of PEGylated PBCA nanoparticle as potential drug delivery carrier. *Pharm Res* 2012;**29(1)**:53-68.
- Chen KL, Smith BA, Ball WP, Fairbrother DH. Assessing the colloidal properties of engineered nanoparticles in water: case studies from fullerene C60 nanoparticles and carbon nanotubes. *Environ Chem* 2010;**7(1)**:10-27.
- Dailey L, Kleemann E, Wittmar M, Gessler T, Schmehl T, Roberts C, Seeger W, Kissel T. Surfactant-free, biodegradable nanoparticles for aerosol therapy based on branched polysters, DEAPA-PVAL, g-PLGA. *Pharm Res* 2003;**20**:2011-20.
- Davis ME, Chen Z, Shin DM. Nanoparticle therapeutics: an emerging treatment modality for cancer. *Nat Rev Drug Discov* 2008;**7**:771-82.
- Derjaguin BV, Landau LD. Theory of the stability of strongly charged lyophobic sols and of the adhesion of strongly charged particles in the solution of electrolytes. *Acta Physicochim* 1941;**14**:633-62.
- Dhar S, Gu FX, Langer R, Farokhzad OC, Lippard SJ. Targeted delivery of cisplatin to prostate cancer cells by aptamer functionalized Pt(IV) prodrug-PLGAPEG nanoparticles. *Proc Natl Acad Sci* 2008;**105**:17356-61.
- Jiang J, Oberdo¨rster G, Biswas P. Characterization of size, surface charge, and agglomeration state of nanoparticle dispersions for toxicological studies. *J Nanopart Res* 2009;**11**:77–89.
- Jung T, Kamm W, Breitenbach A, Klebe G, Kissel T. Loading of Tetanus Toxoid to biodegradable nanoparticles from branched poly(sulfobutyl-polyvinyl alcohol)-g-(lactide-co-glycolide) nanoparticles by protein adsorption: a mechanistic study. *Pharm Res* 2002;**19**:1105-13.

- Kim ST, Saha K, Kim C, Rotello VM. The Role of surface functionality in determining nanoparticle cytotoxicity. *Accounts of Chem Res* 2013;**46(3)**:681-91.
- Koi KY, Saravanakumar G, Park JH, Park K. Hyaluronic acid-based nanocarriers for intracellular targeting: Interfacial interactions with proteins in cancer. *Colloid surf B* 2012;**99**:82-94.
- Lazzari S, Moscatelli D, Codari F, Salmona M, Morbidelli M, DiomedeL. Colloidal stability of polymeric nanoparticles in biological fluids. *J Nanopart Res* 2012;**14(920)**:2-10.
- Li Y, Chen X, Gu N. Computational investigation of interaction between nanoparticles and membranes: hydrophobic/hydrophilic effect. *J Phys Chem B* 2008;**112**:16647-53.
- Liang C, Yang Y, Ling Y, Huang Y, Li T, Li X. Improved therapeutic effect of folate-decorated PLGA-PEG nanoparticles for endometrial carcinoma. *Bioorg Med Chem* 2011;**19**:4057-66.
- Lourenco C, Teixeira M, Simoes S, Gaspar R. Steric stabilization of nanoparticles: size and surface properties. *Int J Pharm* 1996;**138**:1-12.
- Luckham PF. Recent advances in polymers at surfaces: The steric effect. *Curr Opin Colloid & Interface Sci* 1996;**1(1)**:39-47.
- Müller RH. Surface Hydrophobicity: determination by rose bengal (RB) adsorption methods. In: Müller RH, Mehnert W, editors. Particle and surface characterization methods. 280S, Germany: Medpharm Scientific Publishers; 1997;215-28.
- Napper DH. Polymeric stabilization of colloidal dispersions. Academic Press London, 1983.

- Ortega-Vinuesa J, Martın-Rodrıguez A, Hidalgo-Alvarez R. Colloidal stability of polymer colloids with different interfacial properties: mechanisms. *J Colloid Interface Sci* 1996;**184(1)**:259-67.
- Petros RA, DeSimone JM. Strategies in the design of nanoparticles for therapeutic applications. *Nat Rev Drug Discov* 2010;**9**:615-27.
- Ruoslahti E, Bhatia SN, Sailor MJ. Targeting of drugs and nanoparticles to tumors. *J Cell Bio* 2010;**188(6)**:759-68.
- Russel WB, Saville DA, Schowalter WR. Colloidal dispersions. Cambridge University Press, 1992.
- Thiele L, Merkle P, Walter E. Phagocytosis and phagosomal fate of surface-modified microparticles in dendritic cells and macrophages. *Pharm Res* 2003;**20(2)**:221-8.
- Verwey EJW, Overbeek JTG, Van Nes K. Theory of the stability of lyophobic colloids: the interaction of sol particles having an electric double layer. Elsevier New York, 1948.
- Wang YC, Wu YT, Huang HY, Yang CS. Surfactant-free formulation of poly(Lactic/Glycolic) acid nanoparticles encapsulating functional polypeptide: a technical note. *AAPS Pharm Sci Tech* 2009;**10**:1263-67.
- Xiao Y, Wiesner MR. Characterization of surface hydrophobicity of engineered nanoparticles. *J Hazard Mater* 2012;**215–216**:146-51.
- Zheng Y, Yu B, Weecharangsan W, Piao L, Darby M, Mao Y, Koynova R, Yang X, Li H, Xu S, Lee LJ, Sugimoto Y, Brueggemeier RW, Lee RJ. Transferrin-conjugated lipid-coated PLGA nanoparticles for targeted delivery of aromatase inhibitor 7alpha-APTADD to breast cancer cells. *Int J Pharm* 2010;**390**:234-41.

CHAPTER

Bombesin conjugated and docetaxel loaded PLGA nanoparticles: Characterization and cytotoxicity against breast cancer

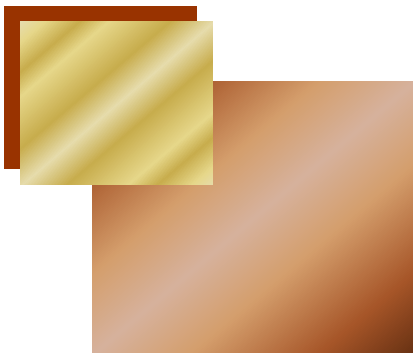

3.1. Background

Nanoparticle mediated targeted drug delivery has attracted lot of attention in last one decade especially for anticancer drug delivery. Conventional use of anticancer drugs is often hampered by non-specific toxicity and side effects in non-targeted tissues. Nanoparticle mediated intracellular delivery of anticancer drugs provides the advantages of increased local drug delivery due to EPR effect, specificity, controlled drug release and avoidance of systemic drug toxicity. Apart from passive targeting, nanoparticles also offer an opportunity of active targeting through surface modification (Byrne et al., 2008; Danhier et al., 2010).

Currently various small chemicals such as folic acid (Oliveira et al., 2013), beta hydroxybutyric acid (Venishetty et al., 2013) and biomolecules like mannose-6-phosphate (Prakash et al.,2010), galactose (Pimm et al., 1993; David et al., 2004), peptides (Kim et al., 2012), glycoproteins (Mo and Lim, 2005), aptamers (Yu et al., 2011) and monoclonal antibodies (Xu et al., 2012) are being used for active targeting of anticancer drugs (Byrne et al., 2008; Oliveira et al., 2013; Xu et al., 2012). However, physiologically occurring or regulatory peptides have several unique advantages that make them attractive as targeting ligand. For e.g. peptides are small molecules with high permeability and biocompatibility. The small size of a peptide minimizes the overall size of nanoconjuagte while still maintaining high surface density (number of peptides per nanoparticle). Further, peptides are usually hydrophilic in nature and can't cross (less than 0.1% of total injected peptide) the blood brain barrier. This property of peptide gives an extra benefit when peripheral tumors are the desired targets (Reubi, 2003; Wang and Thanou, 2010; Yu et al., 2010). Various peptides such as K237, RGD, LyP-1, I4R have been conjugated to nanocarriers to target tumor neovasculature, endothelium, lymphatic metastatic

tumors and other tumor tissues [8,16-18]. (Kim et al., 2012; Yu et al., 2010; Danhier et al., 2009; Luo et al., 2010).

The primary objective of this study was to develop BBN-conjugated biodegradable polymeric drug delivery system for anticancer drug. BBN, a tetradecapeptide, was first isolated from the skin of the frog Bombina bombina (Anatasi et al, 1971). BBN contains a mammalian counterpart called gastrin releasing peptide (GRP). BBN and GRP show structural and functional similarities especially on C-terminus residue. Because of this, BBN and its analogues may be used to target BBN receptor subtype 2 i.e. GRP receptors. GRP receptors have been found over expressed on lung, breast, ovarian and prostate cancer cells (Sancho et al., 2011).

DTX is a semi-synthetic, taxane derived, highly potent anticancer drug. It has shown broad spectrum anti-tumor activity against prostate, breast, pancreatic, lung, gastric and hepatic carcinomas (Hwang, 2012; Zhao and astruc, 2012; Xu et al., 2009). DTX binds irreversibly to the β-actin and stabilizes the microtubule assembly which is responsible for inhibition of cell division and finally cell death (Musumeci et al., 2006).

In this study, BBN was conjugated to PLGA nanoparticles for targeted delivery of DTX in GRP receptor over-expressing breast cancer cells. PLGA has been approved by US FDA and European Medicine Agency (EMA) for use in various therapeutic applications in human. Chemically, it is a cyclic dimer of two monomers namely lactic acid and glycolic acid. Both monomers are endogenous and by-products of normal metabolic pathways in the body. This provides excellent biocompatibility and biodegradability to PLGA and makes the polymer of choice for drug delivery system development (Danhier et al., 2012). PLGA nanoparticles

provide the advantages of high structural stability, availability of free surface groups for bioconjugation and require less number of excipients than lipid based nanoparticulate systems. On the other hand, they also avoid the problem of rapid agglomeration and surface drug loading of inorganic nanocarriers (Soppimath et al., 2001; Jong et al., 2008). BBN was covalently coupled to the PLGA nanoparticle surface using EDC/NHS chemistry. The nanoconjugate was physico-chemically characterized and studied for in vitro cytotoxicity studies.

3.2. Experimentation

3.2.1. Materials

Docetaxel was obtained as gift sample from TherDose pharma pvt ltd (Hyderabad, India). Poly (D, L-lactic-co-glycolic acid, 50:50 Molecular weight ~ 30000-60000) (PLGA) and Bombesin were purchased from Sigma Aldrich (St. Louis, MO, USA). HPLC grade solvents were purchased from Merck specialties (Mumbai, India). MDAMB-231 (breast cancer) cell line was obtained from American Type Culture Collection (ATCC, Manassas, USA). Dulbecco's modified eagle's medium (DMEM), 3-(4, 5- dimethylthiazol-2-yl)-2, 5-diphenyl tetrazolium bromide (MTT), Trypsin, EDTA were purchased from Sigma Chemicals Co (St. Louis, MO, USA). Fetal bovine serum (FBS) was purchased from Gibco, USA. 96 well flat bottom tissue culture plates were purchased from Tarson Ltd (Mumbai, India).

3.2.2. Preparation of DTX loaded nanoparticles

PLGA nanoparticles were prepared by a modified solvent evaporation (nanoprecipitation) method (Kulhari et al., 2014). Five milligrams of DTX was dissolved in 5 ml of PLGA solution (10 mg/ml in acetone) and then quickly poured in 50 mL distilled water with 0.25% w/v sodium cholate. The dispersion was briefly sonicated for 2 minutes in an ice bath and kept on stirring. After 3 h, the dispersion

was centrifuged (15000 rpm) for 30 minutes to separate DTX loaded nanoparticles (DNP) from free DTX. Nanoparticles were washed thrice with distilled water, lyophilized and stored at 2-8 °C. Blank nanoparticles (BNP) were prepared using same procedure but without DTX.

3.2.3. Bioconjugation of BBN to DTX loaded nanoparticles

Twenty milligrams of DNP were dispersed in 5 ml 0.1M MES buffer (pH 6.2) and incubated with 14.62 mg NHS and 191.22 mg EDC. The dispersion was kept on gentle stirring for 1 h at room temperature. To this, 0.5 mg of BBN was added, mixed well and kept for further stirring overnight. BBN-conjugated DTX loaded nanoparticles (BDNP) were collected after centrifugation at 10000 rpm for 10 min and washed thrice with distilled water. Conjugation efficiency was determined by estimating free or unconjugated BBN content in the supernatant.

BBN was quantified using standard Bradford protein assay. A calibration curve of standard range of 0.5 -10 µg/ml was prepared using standard BSA stock solution (2 mg/ml). The supernatant was diluted and absorbance was measured at 595 nm using microplate reader (Synergy 4, Biotek, USA).

3.2.4. Nanoparticle characterization

Mean particle size and zeta potential of BNP and DNP were measured by proton correlation spectroscopy using Malvern Zetasizer Nano-ZS (Malvern instrument Ltd., Malvern, UK). Samples were diluted 1: 9 with distilled water and analyzed at 25 $^{\circ}$C with a backscattering angle of 173°. Surface morphology of nanoparticles was examined by atomic force microscopy (AFM) using Digital Nanoscope IV (Veeco Instruments, Santa Barbara, CA). A drop of sample was placed on metal substrate, air dried for 24 h and scanned for analysis.

DSC scans were carried out on DSC-Q100 (TA Instruments, USA). The samples were scanned from 30 °C to 200 °C at a speed of 10 °C/min, under nitrogen environment. The thermal properties of DTX, BNP, DNP and BDNP were investigated by TGA analyzer (TGA/SDTA 851^e Mettler Toledo, Switzerland). A weighed amount of the compound was placed in a crucible and heated from 25 °C to 650 °C with a heating rate 10 °C/min in nitrogen environment. The change in weight was plotted as a function of temperature.

X-ray diffractograms of DTX, DNP and BDNP were obtained using X-ray diffractometer (D8 Advance, Bruker, Germany) equipped with Cu-Kα X-ray radiation source, at 40 KV and 30 mA. The diffraction angle (2θ) was measured at 2 to 50° at a scanning speed of 2°/min and step time 13.6 s.

3.2.5. Analytical method

DTX content was measured using high performance liquid chromatography (HPLC) with photodiode array detector (Waters, USA). An octadecylsilane column (Shodex, 250 x 4.6 mm, 5 µm) was used for analysis and column temperature was maintained at 25 °C ± 5 °C. The mobile phase, acetonitrile (60%) and water (40%), was pumped at a flow rate of 1.0 ml/min and monitored at a wavelength of 229 nm. The calibration graph was rectilinear in the concentration range of 0.5-10 µg/ml with a correlation coefficient of 0.999. The inter-intraday accuracy and precision was within a relative standard deviation (RSD) of ≤ 5%.

3.2.6. Drug loading and encapsulation efficiency

Lyophilized DNP (10 mg) were completely dissolved in 2 mL acetonitrile, centrifuged and supernatant was analyzed for DTX content using HPLC. Drug loading and encapsulation efficiency were determined as follows:

$$\% \text{ Drug loading} = (W_D \text{ in NP}/W_{NP}) \times 100$$

$$\% \text{ Encapsulation efficiency} = (W_D \text{ in NP}/W_I) \times 100$$

Whereas W_{NP}: weight of nanoparticles; W_D: weight of DTX; W_I: Initial weight of DTX

3.2.7. In vitro drug release

To study the DTX release profile, pure DTX, Taxotere, DNP and BDNP (containing 1 mg of DTX) were suspended in 1 mL distilled water and placed in a dialysis tubing (12,000-14000 molecular weight cutoff, Sigma Aldrich, USA). The tubing were placed individually into 75 mL release media at 37 $^{\circ}$C and kept for stirring at 100 rpm. The phosphate buffer saline (PBS, pH 7.4) and sodium acetate buffer (SAB, pH 5.0) containing 0.5% Tween® 80 were used as release media. An aliquot of one ml was withdrawn from the release medium at different time intervals and was replaced with same volume of fresh medium. The total release medium was replaced every 3rd hour with fresh medium. The samples were appropriately diluted, filtered through 0.22 µm nylon filter and analyzed for DTX content by HPLC as described above.

3.2.8. Cell culture

MDA-MB-231 human breast cancer cell line was grown as adherent in DMEM medium supplemented with 10% fetal bovine serum, 100 µg/ml penicillin, 200 µg/ml streptomycin and 2 mM L-glutamine. The culture was maintained in a humidified atmosphere with 5% CO_2. Dilutions were made with sterile PBS to get required concentration. Formulations were filtered with 0.22 µm sterile filter before adding to the wells containing cells.

3.2.9. In-vitro cytotoxicity studies

Cytotoxicity of formulations was determined by MTT assay based on mitochondrial reduction of yellow MTT tetrazolium dye to a highly colored blue formazan product. 1x10^4 Cells (counted by Trypan blue exclusion dye method) in 96

well plates were incubated with formulations and standard Erlotinib with series of concentrations for 48 h at 37 °C in DMEM with 10% FBS medium. Then the above media was replaced with 90 µl of fresh serum free media and 10 µl of MTT reagent (5 mg/ml) and plates were incubated at 37 °C for 4 h. After removing the media, 200 µl of DMSO was added and incubated at 37 °C for further 10 min. The absorbance at 570 nm was measured using spectrophotometer (Spectramax Plus, Molecular Devices, USA). The mean % of cell viability relative to that of untreated cells was estimated from data of three individual experiments. The half maximal inhibitory concentration (IC50) of each compound was calculated by curve fitting method.

3.2.10. Statistical analysis

All the studies were performed in triplicate and results are expressed as Mean ± SD (standard deviation). Statistical significance was analyzed using student t-test for two groups and one way ANOVA for multiple groups. The p value less than 0.05 were considered as significant.

3.3. Result and discussion

3.3.1. Preparation of blank and DTX loaded PLGA nanoparticles

BNP and DNP were prepared using sodium cholate, an anionic surfactant. Nano-precipitation or solvent displacement method was used for nanoparticle preparation because of its simplicity and high drug loading efficiency. The prepared nanoparticles showed very narrow size distribution and low polydispersity. The size of BNP was 92.71 ± 1.46 nm with 0.083 PDI while the DNP showed particle diameter 111.35 ± 2.19 nm with 0.152 PDI (Table 1).

Table 3.1: Physicochemical characterization of nanoparticles: particle size, size distribution, zeta-potential and drug encapsulation efficiency. Data represent Mean ± SD, n=6.

Formulation	Particle Diameter (nm)	Polydispersity Index (PDI)	Zeta Potential (mV)	Drug Loading (%)	Encapsulation Efficiency (%)
BNP	92.71 ± 1.46	0.08 ± 0.02	-28.7 ± 2.76	-	-
DNP	111.35 ± 2.19	0.15 ± 0.04	-26.9 ± 2.55	8.03 ± 1.4	81.38 ± 2.45
BDNP	136 ± 3.95	0.24 ± 0.05	-11.5 ± 1.34	7.52 ± 0.63	83.27 ± 1.74

3.3.2. Drug loading and encapsulation efficiency

DTX loading and encapsulation efficiency of PLGA nanoparticles were determined at two drug/polymer (D/P) ratios- 5 %w/w and 10 %w/w (Table 3.1). Initially, 5 %w/w DTX was added to polymer solution and observed DTX loading and encapsulation efficiency were 4.58% and 96.12%. Because of high drug encapsulation efficiency, drug to polymer ratio was increased to 10 %w/w. At this level, drug loading was found to be 8.03% whereas encapsulation efficiency was 81.38%. Thus 10 %w/w D/P ratio was considered as optimum level for DTX loading in PLGA nanoparticles.

3.3.3. Bioconjugation of BBN to DNP

Bombesin was conjugated on DNP surface by an EDC/NHS reaction. About 18.2 µg of BBN was conjugated to per mg of nanoparticles. The conjugation efficiency was 72.8%.

3.3.4. Physicochemical characterization of nanoparticles

Bombesin surface conjugation was characterized in terms of mean particle diameter, polydispersity index and zeta potential. After BBN conjugation, the size of nanoparticles was increased to 136 ± 3.95 nm (Figure 3.1a) with 0.247 polydispersity

index while the zeta potential was decreased to -11.5 mV (Table 3.1). The change in surface potential confirmed the conjugation between BBN and PLGA nanoparticles. AFM analysis showed that BDNP were spherical in shape (Figure 3.1b). The average particle size observed with AFM analysis was 142.35 ± 8.91 nm (n=5).

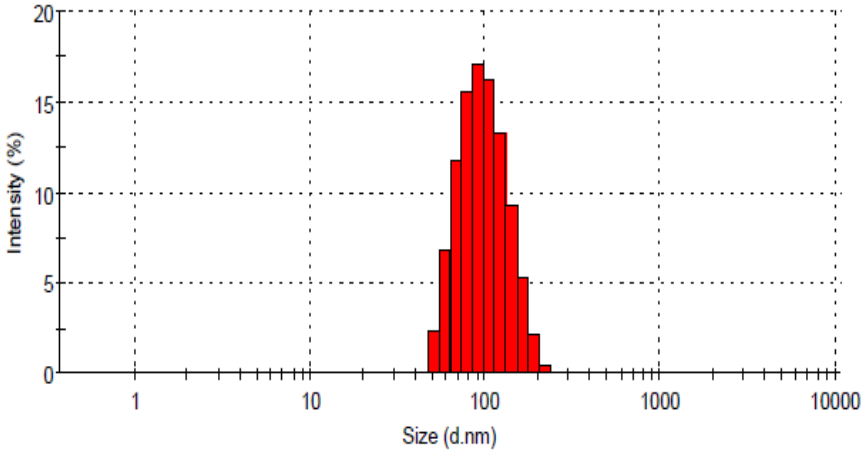

a)

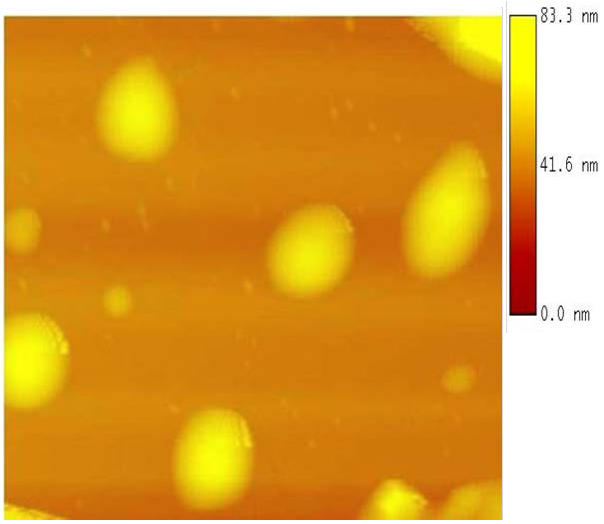

b)

Figure 3.1a-b: Particle size and surface morphology of BBN conjugated nanoparticles (BDNP) determined by a) Dynamic light scattering and b) Atomic force microscopy analysis.

FTIR analysis was carried out to confirm the surface group interaction between -NH_2 group of BBN and –COOH group of DNP (Figure 3.2). FTIR spectra of pure BBN showed two characteristic peaks at 3299 cm^{-1} (free amine group) and 1647 cm^{-1} (carbonyl group of peptide bond). DNP showed characteristic carbonyl peak of carboxylic group at 1761 cm^{-1}. BDNP showed amide bond peaks at 1646 cm^{-1} and 1566 cm^{-1} indicating the conjugation between BBN and DNP. As BBN also shows the amide bond peaks, absence of carboxylic group peak of PLGA nanoparticles in BDNP confirmed the conjugation of BBN to the DNP.

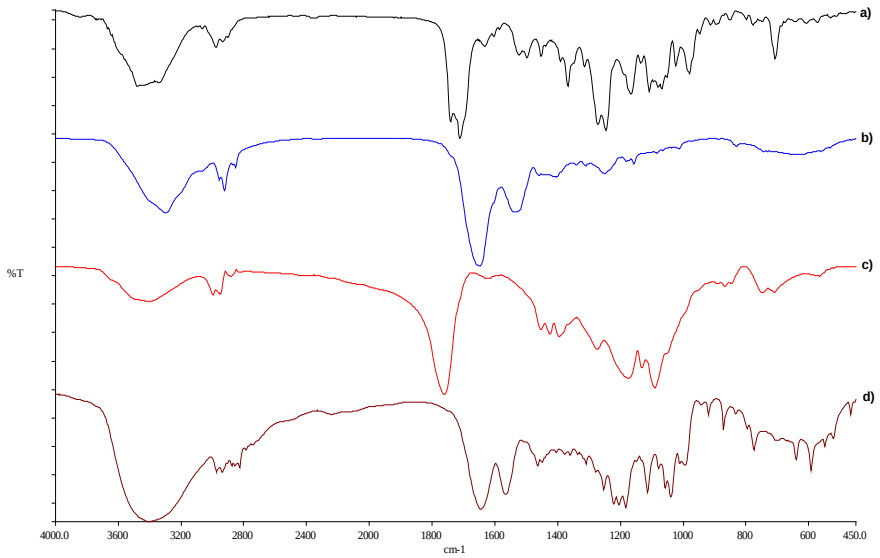

Figure 3.2: FTIR spectra of a) Docetaxel, b) Bombesin, c) Docetaxel loaded PLGA nanoparticle (DNP) and d) Bombesin conjugated DNP nanoparticles (BDNP)

The physical state of DTX as pure compound and inside the nanoparticles was determined by DSC analysis (Figure 3.3). The melting endothermic peak of pure DTX was appeared at 178.7 $^{\circ}C$. However this peak was not observed in nanoparticle formulation. DNP formulation showed only glass transition temperature (Tg) peak of PLGA at 50.4 °C. It suggested two important things: first, the pure DTX was present as crystalline form but in nanoparticles it was transformed to amorphous or

disordered crystalline or to the solid solution state. Second, the nanoparticle preparation method used in this study, does not affects the properties of the PLGA.

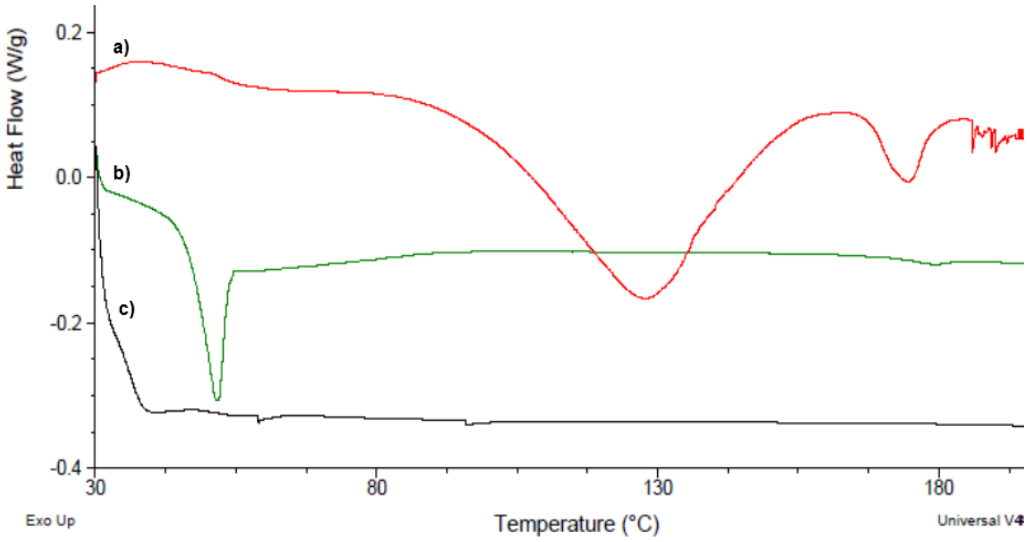

Figure 3.3: Differential scanning calorimetry (DSC) spectra of a) Docetaxel b) PLGA and c) DTX loaded PLGA nanoparticles

` The thermal behaviour of DTX, PLGA, DNP and BDNP was studied using thermo gravimetric analyzer. Figure 3.4 shows the thermal degradation behaviour of DTX, BNP, DNP and BDNP. The weight loss in pure DTX was started about 200 °C while in case of BNP and DNP it occurred after 300 °C. BDNP formulation showed an early degradation at 220 °C.

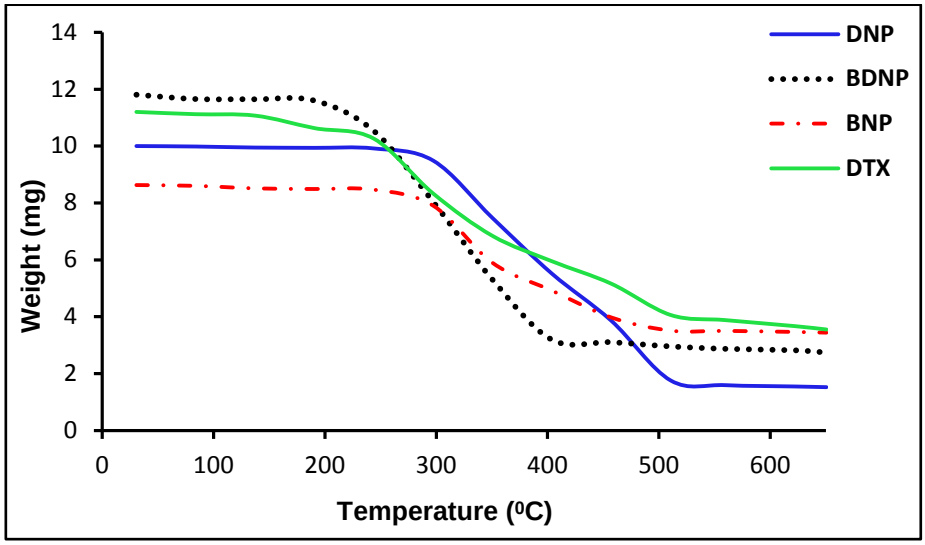

Figure 3.4: Thermo gravimetric analysis (TGA) of pure DTX, blank nanoparticles (BNP), DTX loaded nanoparticles (DNP) and bombesin conjugated DNP (BDNP)

XRD spectra of pure DTX showed characteristic sharp peaks between 2 to 20°, confirming the crystalline state of DTX (Figure 3.5). In DTX loaded nanoparticle spectra, the sharp peaks of DTX were disappeared and a hump was observed from 10 to 22° which indicated that in nanoparticle formulation DTX was present in its amorphous form rather than crystalline. In BDNP spectra, the some sharp peaks were appeared which may be because of BBN present on nanoparticle surface.

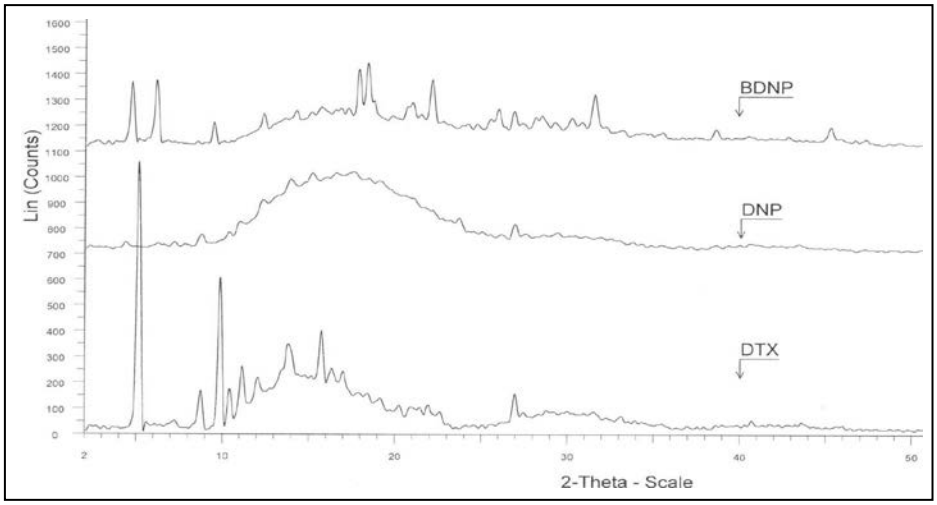

Figure 3.5: Powder X-ray diffraction (PXRD) analysis of pure DTX, DNP and BDNP

3.3.5. In vitro drug release

In vitro release of DTX from pure drug suspension, Taxotere and nanoparticles was performed in PBS (Figure 3.6a) and SAB (Figure 3.6b). From pure drug suspension and Taxotere, DTX was released completely within 10 h in both PBS and SAB. The nanoparticle formulations showed biphasic pattern of DTX release. About 21% of drug was released in first 24 h but after that only 11% and 15.3% DTX was released in next 96 h from DNP and BDNP formulations, respectively. The initial faster drug release may be due to the release of drug present on the surface or near to the periphery of the nanoparticles (Fredenberg et al., 2011). The drug release was slightly higher in BDNP than from DNP which may be because of hydrophilic nature of BBN present on the surface. A similar kind of

pattern was observed in SAB. But the overall release of DTX from nanoparticles was more in SAB (36.2%) compared to PBS (31.57%). It can be explained by the faster degradation of PLGA at acidic pH (Yoo et al., 2005). This faster degradation of nanoparticles and hence increased DTX release in acidic pH than PBS would provide the advantage of maximum drug release in cancer cells.

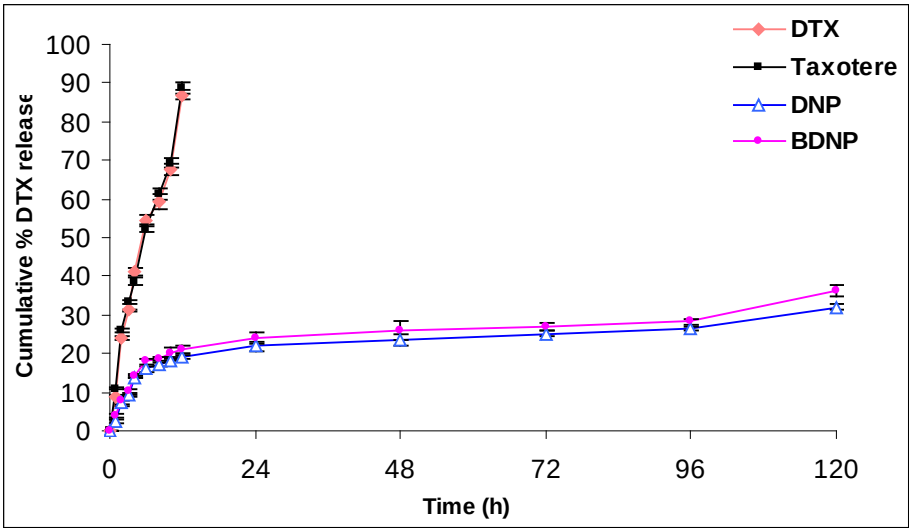

a)

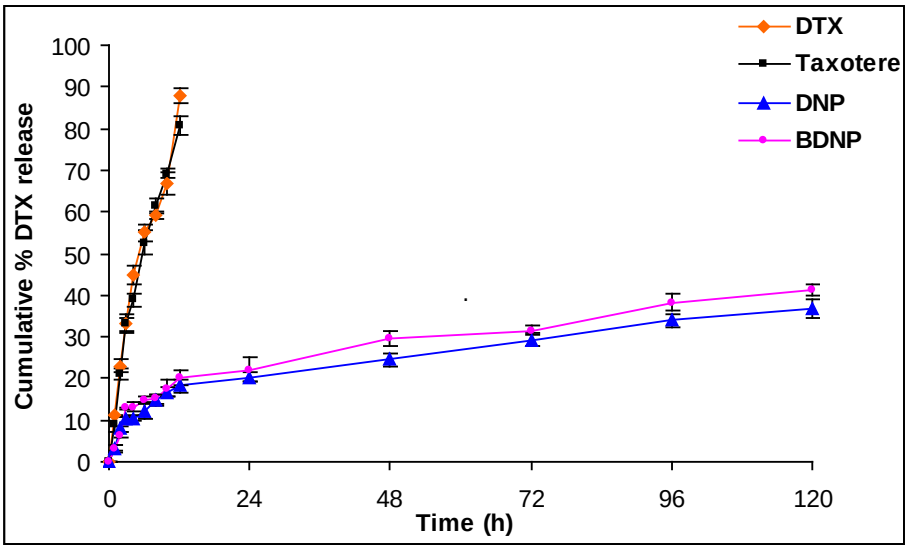

b)

Figure 3.6a-b: In vitro drug release studies of different DTX formulations in a) PBS and b) SAB (Mean ± SD; n=3)

3.3.6. Cytotoxicity studies

The anticancer activity of DTX, Taxotere, DNP and BDNP was studied by MTT assay against MDA-MB-231 human breast cancer cells (Figure 3.7 and 3.8). MDA-MB-231 cells were selected for in vitro cytotoxicity study for three reasons. First, these cells are reported to over express GRP receptors (Chao et al., 2009). Second, MDA-MB-231 cells are triple negative cells- estrogen receptor negative, progesterone receptor negative and human epidermal growth factor 2 (HER 2) receptor negative. So the hormonal and trastuzumab therapy may not be useful for the treatment of these cells. Third, MDA-MB-231 cells show intermediate response to the chemotherapy (Holliday and Speirs, 2011). So the effect of peptide conjugated formulation can be clearly observed from the effect of unconjugated formulation. The IC50 value for both free DTX and Taxotere was more than the highest tested concentration (375 ng/ml). Both DNP and BDNP showed more cellular toxicity than free DTX and Taxotere. The IC50 value for DNP and BDNP was 142.23 ± 18.95 and 35.53 ± 5.91.

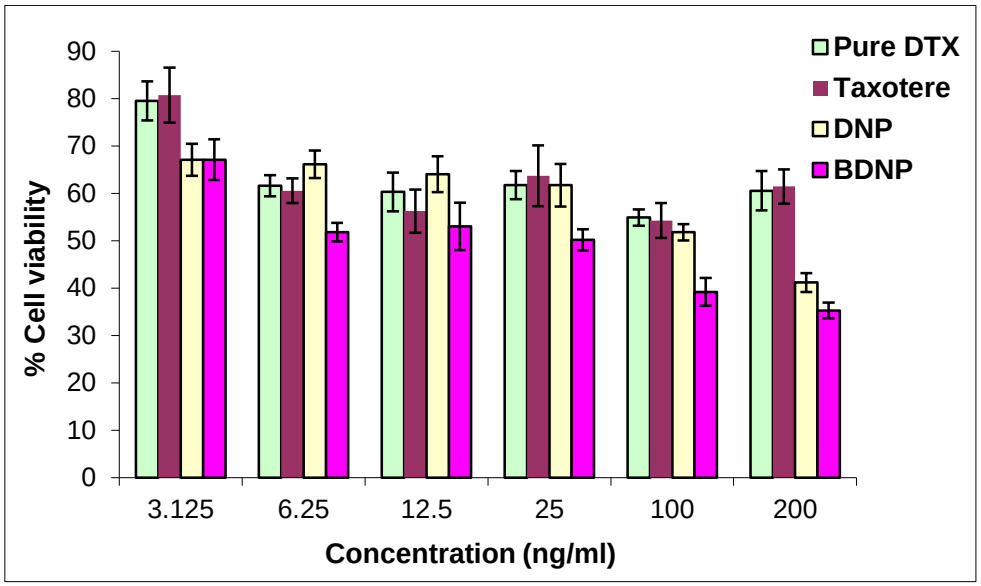

Figure 3.7: Cell viability studies of DTX, Taxotere, DTX loaded nanoparticles (DNP) and BBN conjugated-DTX loaded nanoparticles (BDNP) (Mean ± SD; n=3)

At low concentration of 3.125 ng/ml, both DNP and BDNP showed significant cytotoxicity compared to either pure DTX or Taxotere. However, the difference of cytotoxic potential of DTX was insignificant between DNP and BDNP. Significant improvement in cytotoxicity was observed with BDNP compared to DNP in a dose-dependent manner from 6.25 to 100 ng/ml. At higher concentration (200 ng/ml), BDNP could not enhance the cytotoxicity over DNP. The significant increase in toxicity of DNP compared to free DTX or Taxotere can be attributed to passive targeting of nanoparticles. Several anticancer drugs including dexamethasone, paclitaxel, vincristine, curcumin, etoposide, campatothecin, 5-fluorouracil, doxorubicin and cisplatin have been successfully delivered and passively targeted by encapsulation in PLGA nanoparticles (Acharya and Sahoo, 2011). BDNP were 4 times more toxic ($p < 0.001$) than DNP which may be due to receptor-mediated endocytosis of nanoparticles. The enhanced cellular internalization of actively targeted BDNP resulted in enhanced cytotoxicity of DTX.

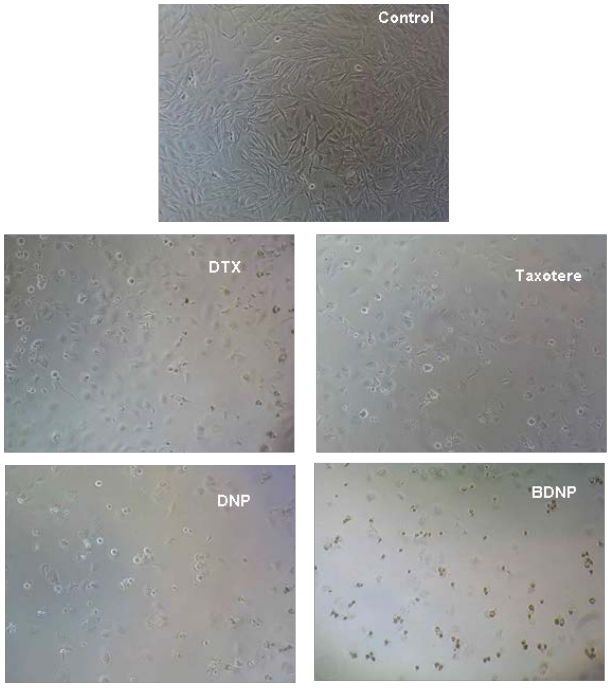

Figure 3.8: Phase contrast images of MDA-MB-231 cells treated with control, free DTX, Taxotere, DNP and BDNP after 48 h

3.4. Conclusion

Targeted drug delivery systems have shown a great advance in delivery of anticancer drugs exclusively to cancer cells. In this study, Bombesin peptide was first time conjugated with biodegradable polymeric nanoparticles for the delivery of an anti-cancer drug, DTX, to breast cancer cells. The breast cancer cell lines used in this study were low to intermediate chemotherapy responsive. The peptide conjugated nanoparticles showed significantly higher in vitro cytotoxicity to the targeted cells than free DTX. As per the generalized and well accepted concept, nanoparticles of less than 200 nm size with hydrophilic surface exhibits improved EPR effect due to longer retention of nanocarriers in the blood stream. Because of small size, sustained drug release and enhanced and targeted delivery, the developed drug delivery system has great potential to deliver anticancer drugs to GRP receptor over-expressing and to low chemotherapy-responsive cells.

3.5. References

- Acharya S, Sahoo SK. PLGA nanoparticles containing various anticancer agents and tumour delivery by EPR effect. *Adv Drug Deliv Rev* 2011;**63**:170.
- Anastasi A, Erspamer V, Vucci M. Isolation and structure of Bombesin and alytesn, two analogous active peptides from the skin of European amphibians Bombina and Alytes. *Experientia* 1971;**27**:166-7.
- Byrne JD, Betancourt T, Brannon-Peppas L. Active targeting schemes for nanoparticle systems in cancer therapeutics. *Adv Drug Deliv Rev* 2008;**60**:1615-26.
- Chao C, Ives K, Hellmich HL, Townsend CM Jr, Hellmich MR. Gastrin-releasing peptide receptor in breast cancer mediates cellular migration and interleukin-8 expression. *J Surg Res* 2009;**156(1)**:26-31.

- Danhier F, Ansorena E, Silva JM, Coco R, Le Breton A, Preat V. PLGA-based nanoparticles: an overview of biomedical applications. *J Control Release* 2012;**161**:505-22.
- Danhier F, Feron O, Préat V. To exploit the tumor microenvironment: Passive and active tumor targeting of nanocarriers for anti-cancer drug delivery. *J Control Release* 2010;**148**:135-46.
- Danhier F, Vroman B, Lecouturier N, Crokart N, Pourcelle V, Freichels H, Jerome C, Marchand-Brynaert J, Feron O, Préat V. Targeting of tumor endothelium by RGD-grafted PLGA-nanoparticles loaded with paclitaxel. *J Control Release* 2009;**140**:166-73.
- David A, Kopeckova P, Minko T, Rubinstein A, Kopecek J. Design of a multivalent galactoside ligand for selective targeting of HPMA copolymer-doxorubicin conjugates to human colon cancer cells. *Eur J Cancer* 2004;**40**:148-57.
- De Jong WH, Borm PJ. Drug delivery and nanoparticles:applications and hazards. *Int J Nanomedicine 2008*;**3(2)**:133-49.
- Fredenberg S, Wahlgren M, Reslow M, Axelsson A. The mechanisms of drug release in poly(lactic-co-glycolic acid)-based drug delivery systems-a review. *Int J Pharm* 2011;**415**:34-52.
- Holliday DL, Speirs V. Choosing the right cell line for breast cancer research. *Breast Cancer Res* 2011;**13**:1-7.
- Hwang C. Overcoming docetaxel resistance in prostate cancer: a perspective review. *Ther Adv Med Oncol* 2012;**4**:329-40.
- Kim JH, Bae SM, Na MH, Shin H, Yang YJ, Min KH, Choi KY, Kim K, et al. Facilitated intracellular delivery of peptide-guided nanoparticles in tumor tissues. *J Control Release* 2012;**157**:493-9.

- Kulhari H, Kulhari DP, Singh MK, Sistla R. Colloidal stability and physicochemical characterization of bombesin conjugated biodegradable nanoparticles. *Colloids Surf A* 2014;**443**:459-66.
- Luo G, Yu X, Jin C, Yang F, Fu D, Long J, Xu J, Zhan C, Lu W. LyP-1-conjugated nanoparticles for targeting drug delivery to lymphatic metastatic tumors. *Int J Pharm* 2010;**385 (1–2)**:150-6.
- Manjappa AS, Chaudhari KR, Venkataraju MP, Dantuluri P, Nanda B, Sidda C, Sawant KK, Murthy RSR. Antibody derivatization and conjugation strategies: application in preparation of stealth immunoliposome to target chemotherapeutics to tumor*. J Control Release* 2011;**150(1)**:2-22.
- Mo Y, Lim LY. Paclitaxel-loaded PLGA nanoparticles: potentiation of anticancer activity by surface conjugation with wheat germ agglutinin. *J Control Release* 2005;**108**:244-62.
- Musumeci T, Ventura CA, Giannone I, Ruozi B, Montenegro L, Pignatello R, Puglisi G. PLA/PLGA nanoparticles for sustained release of docetaxel. *Int J Pharm* 2006;**325**:172-9.
- Oliveira R, Zhao P, Li N, Maria LCS, Vergnaud J, Ruiz J, Astruc D, Barratt G. Synthesis and in vitro studies of gold nanoparticles loaded with docetaxel. *Int J Pharm* 2013;**454(2)**:703-11.
- Pimm M, Perkins A, Duncan R, Ulbrich K. Targeting of N-(2-hydroxypropyl)methacrylamide copolymer-doxorubicin conjugate to the hepatocyte galactose-receptor in mice: visualisation and quantification by gamma scintigraphy as a basis for clinical targeting studies. *J Drug Target* 1993;**1**:125-31.
- Prakash J, Beljaars L, Harapanahalli AK, Zeinstra-Smith M, de Jager-Krikken A, Hessing M, Steen H, Poelstra K. Tumor-targeted intracellular delivery of

anticancer drugs through the mannose-6-phosphate/insulin-like growth factor II receptor. *Int J Cancer* 2010;**126(8)**:1966-81.

- Reubi JC. Peptide receptors as molecular targets for cancer diagnosis and therapy. *Endocr Rev* 2003; **24**:389-427.
- Sancho V, Flrio AD, Moody TW, Jensen RT. Bombesin receptor-mediated imaging and Cytotoxicity: review and current status. *Curr Drug Deliv* 2011;**8(1)**:79-134.
- Soppimath KS, Aminabhavi TM, Kulkarni AR, Rudzinski WE. Biodegradable polymeric nanoparticles as drug delivery devices. *J Control Release* 2001;**70(1-2)**:1-20.
- Venishetty VK, Samala R, Komuravelli R, Kuncha M, Sistla R, Diwan PV. β-Hydroxybutyric acid grafted solid lipid nanoparticles:A novel strategy to improve drug delivery to brain. *Nanomed Nanotech Biol Med* 2013;**9**:388-97.
- Wang M, Thanou M. Targeting nanoparticles to cancer. *Pharmacol Res* 2010;**62(2)**:90-9.
- Xu S, Olenyuk BZ, Okamoto CT, Hamm-Alvarez SF. Targeting receptor-mediated endocytotic pathways with nanoparticles: rationale and advances. *Adv Drug Deliv Rev* 2013;**65**:121-38.
- Xu Z, Chen L, Gu W, Gao Y, Lin L, Zhang Z, Xi Y, Li Y. The performance of docetaxel-loaded solid lipid nanoparticles targeted to hepatocellular carcinoma. *Biomaterials* 2009;**30**:226-32.
- Yoo JY, Kim JM, Seo KS, Jeong YK, Lee HB, Khang G. Characterization of degradation behavior for PLGA in various pH conditions by simple liquid chromatography method. *Biomed Mater Eng* 2005;**15(4)**:279-88.
- Yu C, Hu Y, Duan J, Yuan W, Wang C, Xu H, Yang SD. Novel aptamer-nanoparticle bioconjugates enhances delivery of anticancer drugs to MUC1-positive cancer cells invitro. *PLoS One* 2011;**6**: e24077.

- Yu DH, Lu Q, Xie J, Fang C, Chen H. Peptide-conjugated biodegradable nanoparticles as a carrier to target paclitaxel to tumor neovasculature. *Biomaterials* 2010;**31(8)**:2278-92.
- Zhang XX, Eden HS, Chen X. Peptides in cancer nanomedicine: Drug carriers, targeting ligands and protease substrates. *J Control Release* 2012;**159**:2-13.
- Zhao P, Astruc D. Docetaxel nanotechnology in anticancer therapy. *ChemMedChem* 2012;**7**:952-72.

CHAPTER

Bombesin-conjugated nanoparticles: In vitro cytotoxicity against prostate cancer, pharmacokinetic and tissue-distribution studies

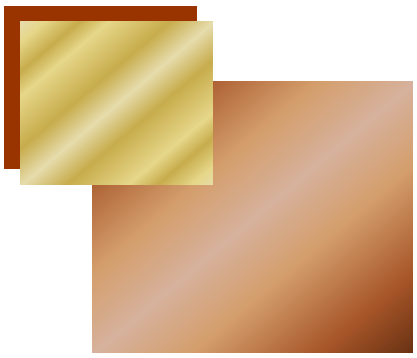

4.1. Background

Prostate cancer is one of the leading causes of cancer related death in men. Surgery, radiation and chemotherapy are approaches available for the treatment of prostate cancer (Fong et al., 2012; Guan and Chen, 2006). Generally prostate cancer is treated with surgery or radiation therapy. Chemotherapy is the treatment of choice when cancer recurs or when a patient's tumor can be controlled at an earlier stage by manipulating its growth signals (Salvador-Morales et al., 2009). Chemotherapy for prostate cancer treatment includes hormone therapy, vaccines and chemical agents. Hormone therapy is used in androgen-dependent prostate cancer (Namiki et al., 2012). Provenge®, the only cancer therapeutic vaccine, is approved by the FDA for use in men with metastatic prostate cancer that does not respond to hormone therapy (Cheever and Higano, 2011). Of the anticancer drug docetaxel (DTX), in combination with prednisolone, is approved for the treatment of metastatic hormone-refractory or castration-resistant prostate cancer (Aragon-Ching and Dahut, 2007). This androgen-independent or androgen-insensitive cancer spreads throughout the body, beyond the prostate alone, and continues to grow, even when testosterone is inhibited (Kwon et al., 2012).

DTX is a semi-synthetic analogue of paclitaxel and is used to treat various cancers, including prostate cancer. It binds with β-tubulin and inhibits mitotic progression and cell proliferation leading to cell death (Hwang, 2012). In refractory, advanced disease with poor prognosis, prostate cancer cells exhibits high levels of Bcl-2 expression. DTX inactivates this pro-survival protein and promotes apoptosis (Bray et al., 2009; Kraus et al., 2003). But, water insolubility, toxicity to normal cells and drug resistance are three major constraints in the therapeutic applications of DTX (Hwang, 2012; Tannock et al., 2004). DTX is soluble in water at only microgram

levels. Therefore, the use of the non-ionic surfactant polysorbate 80, which can cause severe anaphylactic hypersensitivity reactions, is required (Loos et al., 2003).

Nanoparticle-mediated targeted DTX delivery may help to overcome all these inherent problems (Salvador-Morales et al., 2009; Sanna and Sechi, 2012). Nanoparticle formulations, irrespective of the method of preparation, enhance the solubility of poorly-water soluble agents by converting drug micro-particles to nanoparticles and thus increasing the overall effective surface area (Yarnell, 2012; Merisko-Liversidge and Liversidge, 2008). Site-specific delivery using specific targeting ligands further decreases total dose requirements. In addition, ligand-based targeting of drug encapsulated nanoparticles reduces non-specific uptake into normal cells. Nanoparticles enter tumor cells via endocytotic processes, increasing intracellular drug concentrations and overcoming efflux-pump mediated drug resistance (Dong and Mumper, 2010).

In this study, DTX was encapsulated in biodegradable and well characterised poly (lactic-co-glycolic acid) (PLGA) nanoparticles. Bombesin was ligated to the nanoparticle surface for site-specific delivery of drug to prostate cancer cells. Bombesin is a tetradeca peptide that has high binding-affinity for gastrin-releasing peptide (GRP) receptors (Cornelio et al., 2007; Jensen et al., 2008). Human prostate cancer cell lines such as PC3 and DU145 have been reported to over-express GRP receptors (Accardo et al., 2012; De vesser et al., 2007; Reile et al., 1994). Therefore, site-specific delivery of DTX may improve the therapeutic potential of DTX. In a previous study, BBN conjugated PLGA nanoparticles demonstrated a significant improvement in the cytotoxic efficacy of DTX against GRP over-expressing breast cancer cells (Kulhari et al., 2014). Here, the anticancer activity of these formulations were evaluated against prostate cancer cells which also over-express GRP

receptors. Also, the pharmacokinetic and tissue distribution profiles of BBN conjugated, DTX loaded PLGA nanoparticles were studied and compared to those of Taxotere®, a marketed formulation of DTX.

4.2. Experimentation

4.2.1. Preparation and characterization of bombesin conjugated PLGA nanoparticles

DTX loaded PLGA nanoparticles (DNP) and bombesin-conjugated DNP (BDNP) were prepared as per previously optimized method (Kulhari et al., 2014). Mean particle diameter and zeta potential of DNP and bombesin conjugated DNP (BDNP) were measured by the dynamic light scattering method using a particle-size analyser Zetasizer Nano-ZS (Malvern Instrument Ltd., UK). Nanoparticle surface morphology was examined using transmission electron microscopy (FEI Tecnai, G112, Philips, USA).

4.2.2. Cell culture

DU145 human prostate cancer cells were grown in DMEM medium supplemented with 10% FBS, 0.3% sodium bicarbonate, 10 mL/L antibiotic/antimycotic solution (10,000 U/mL penicillin, 10 mg/mL streptomycin and 25 µg/mL amphotericin B), 1 mL of 2 mM L-glutamine and 1 mL of 100 mM sodium pyruvate.

PC3 human prostate cancer cell line was grown in RPMI-1640 medium supplemented with 10% FBS, 2 mM glutamine, penicillin (100 U/mL), and streptomycin (0.1 mg/mL). Cells were cultured in a CO_2 incubator at 37 ºC with a 90% humidified and 5% CO_2 atmosphere.

4.2.3. In vitro cytotoxicity studies

The cytotoxicity of DTX, DNP and BDNP against DU145 and PC3 human prostate cancer cells was evaluated using a tetrazolium-based calorimetric MTT assay. Cells were seeded into 96 well plates at a density of 5×10^3 cells per well. After overnight incubation, cells were treated with DTX, DNP and BDNP at concentrations ranging from 1-10000 ng/mL. After 48 h, the media was replaced with 90 µL fresh serum free media and 10 µL MTT (5 mg/mL in PBS). Plates were incubated at 37 ºC for another 4 h. Thereafter, media was discarded and 150 µL of DMSO was added in each well to dissolve purple formazan crystals. The absorbance of samples was measured at 570 nm using a SpectraMax plus 384 UV-Visible plate reader (Molecular Devices, Sunnyvale, CA, USA). Half maximal inhibitory concentration (IC_{50}) values were determined by the Probit analysis software package of MicroSoft-excel.

4.2.4. Cellular uptake studies

Coumarin-loaded PLGA nanoparticles (CPN) were prepared and conjugated with BBN (BCPN) for comparative cellular uptake studies. Coumarin-6 is a hydrophobic florescent dye and therefore, has been used as model compound to study the uptake of hydrophobic drugs. In this study, we encapsulated coumarin-6 into PLGA nanoparticles in place of DTX and then conjugated BBN to the nanoparticles to study role of BBN in the uptake of nanoparticles. For quantitative studies, 1×10^5 cells per well were seeded in 12 well plates and allowed to adhere for 24 h. Cells were incubated with coumarin-6, CPN, and BCPN formulations for time intervals of 0.5, 1, 3 and 6 h. After removal of culture media, cells were washed twice with cold PBS and observed under a fluorescence microscope (Olympus Corp., U-LH100HG, Japan).

4.2.5. Apoptosis assay by acridine orange and ethidium bromide double staining

PC3 Cells (1×10^5 cells/well) were grown in 12 well plates and incubated overnight. Next day, cells were treated with DTX, DNP or BDNP, equivalent to 100 ng/mL DTX. After 24 h, cells were washed with PBS and fixed with 4% of paraformaldehyde. Cells were washed twice with PBS and stained with a solution of AO and EB (5 µg/mL of each). After 30 min of incubation, cells were again washed with PBS and observed under a fluorescence microscope (Nikon, Japan).

4.2.6. Wound healing scratch assay

PC3 cells (5×10^5 cells/mL) were seeded in petri-dishes and allowed to grow to 80% confluence. Wounds were created with sterile 250 µL pipette tips. Cells were incubated with DTX, DNP or BDNP, equivalent to 100 ng/mL DTX. The zone of wound healing was observed at 0, 12 and 24 h using a bright field microscope. The percentage of wound closure was determined by measuring the wound area using Image J analysis software.

4.2.7. Clonogenic assay

For colony formation assays, PC3 cells were seeded at a density of 500 cells per well in a 6 well plate. From days 3 to 8, cells were incubated with DTX, DNP or BDNP. Then, media was removed and cells incubated in fresh media without drug. On day 14, cells were washed with PBS, fixed with 4% formaldehyde and stained with 0.5% w/v methylene blue. Cells were washed and photographs captured using a digital camera.

4.2.8. Animal study protocols

The animal experimental protocol for this study was approved by the Institutional Animal Ethics Committee (IAEC) of the CSIR-Indian Institute of

Chemical Technology, Hyderabad and all the studies performed on the animals were in accordance with the guidelines of the Committee for the Purpose of Control and Supervision of Experiments on Animals (CPCSEA). Male BALB/c mice weighing between 20-25 g were used for the pharmacokinetic and tissue distribution studies. Animals were kept in polypropylene cages under standard laboratory conditions (12:12 h light/ dark cycle) at 24 °C.

4.2.9. Bio-analytical method

For the determination of DTX content in plasma and tissue samples, an analytical method was validated using a HPLC system (Waters, USA) equipped with a C18 column (Grace, 250 x 4.6 mm, 5 µm) and a photodiode array detector. The mobile phase consisted of acetonitrile (48%) and 0.1% orthophosphoric acid (52%). A volume of 5 µL paclitaxel (PTX) solution (1 mg/ml) was used as an internal standard. The flow rate was maintained at 1 mL/min. Peaks were monitored at 230 nm λ_{max}. Retention times were 9.1 and 11.2 min for DTX and PTX, respectively.

4.2.10. Pharmacokinetic and tissue distribution studies

Ninety six animals were randomly divided to three treatment groups (n=32). Four animals were used separately as normal controls. The treatment groups received Taxotere®, DNP and BDNP, respectively. Taxotere®, DNP and BDNP were administered intravenously (tail vein) at a dose of 10 mg/Kg body weight of the loaded drug. Blood samples were collected by retro-orbital venous plexus puncture with the aid of glass heparinized capillary tubes at different time intervals. Blood samples were centrifuged at 4,000 rpm for 10 min to separate plasma from cell mass. The supernatant (plasma) was separated and analyzed for DTX content. After blood collection, animals were euthanized by cervical dislocation, and tissues (heart,

liver, spleen, lung, brain and kidney) were harvested, rinsed in buffer, weighed and frozen at –80 °C until analysis.

4.2.11. Plasma and tissue sample processing

Plasma and tissue samples were processed and analyzed for DTX content as reported previously by Wang et al (2012). After the addition of 1 ml of normal saline, the tissue samples were homogenized using a tissue homogenizer. A volume of 200 µL of plasma or tissue sample was extracted with 250 µL of methanol and 250 µL of acetonitrile, vortexed for one minute and finally centrifuged at 15,000 rpm for 15 min. The supernatant was separated, filtered through a 0.22 µm filter and analyzed by HPLC as described above.

4.2.12. Determination of pharmacokinetic parameters & statistical analysis

Non-compartmental analysis with WinNolin software was used to estimate pharmacokinetic parameters of different DTX formulations. The peak plasma concentration (C_{max}) and time to reach C_{max} (t_{max}) were determined directly from the observed concentration versus time profiles. Area under curve (AUC) and area under first moment curve (AUMC) were calculated using the linear trapezoidal rule. Mean residence time (MRT) was calculated by dividing AUMC by AUC.

Results are expressed as the mean ± SD (standard deviation) of at least four experiments (n=4). Statistical significance was assessed using the Student's t-test or Dunnett's test for multiple comparisons with $p < 0.05$ as the minimal level of significance.

4.3. Results and discussion

4.3.1. Characterization of nanoparticles

Mean particle diameter and zeta potential of DTX loaded PLGA nanoparticles (DNP) were 98.52 ± 2.31 nm and –29.06 ± 1.57 mV, respectively. DTX

encapsulation efficiency was 79.52 ± 2.08%. Bombesin was grafted onto nanoparticle surfaces by carbodiimide chemistry with a conjugation efficiency of 77.39%. After conjugation of BBN, nanoparticle size was increased to 115.74 ± 1.86 nm while potential was decreased to −12.6 ± 0.95 mV; thus confirming grafting of BBN. TEM analysis of BDNP showed that nanoparticles were spherical in shape and uniform in size (Figure 4.1).

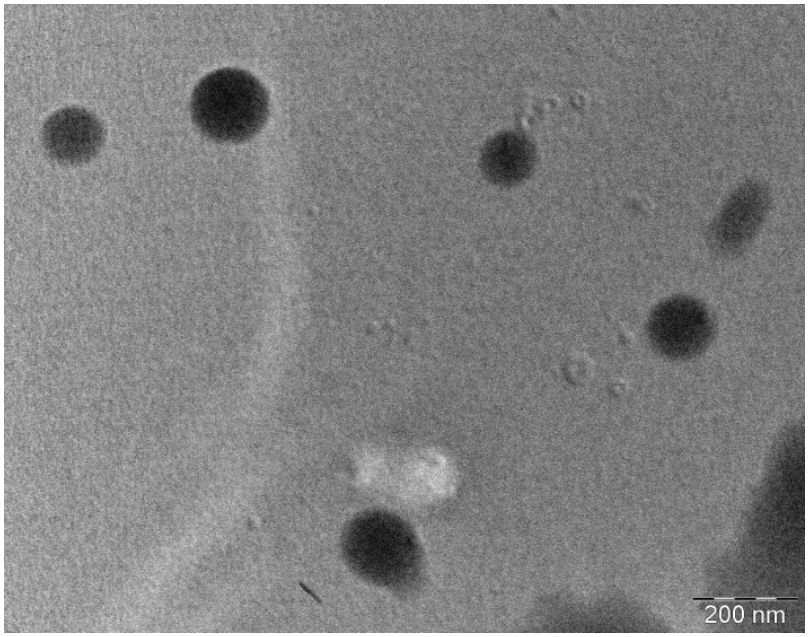

Figure 4.1: Transmission electron microscopy of bombesin grafted docetaxel loaded PLGA nanoparticles (BDNP)

4.3.2. In vitro cytotoxicity studies

Prostate cancer is basically of two types: localized and advanced metastasized. Localised prostate cancer can be treated by either radical prostatectomy or radiation therapy. Advanced and metastasized is usually treated by androgen deprivation therapy. However, long-term deprivation of androgen results in the development of resistance in the cancer cells i.e. androgen-independent cancer. This androgen-independent prostate cancer has increased proliferation and invasion capacity and spreads beyond prostate (Carrión-Salip et al., 2012; Saraon et al.,

2011). Chemotherapy like taxanes has shown significant potential in controlling the androgen-independent prostate cancer (Schrijvers, 2007). However, to avoid the non-specific toxicity, in this study we developed targeted nanocarrier system for the delivery of DTX and evaluated their potential against androgen-independent human prostate cancer cells DU145 and PC3. In this study, The cell viability of human prostate cancer cells (DU145 and PC3) exposed to different DTX formulations was investigated and results are presented in Figure 4.2. All three formulations showed concentration-dependent toxicities to both cell lines. At very low concentration (1 ng/mL), there was no significant difference in viability of cells when treated with DTX, DNP or BDNP. However, as the drug concentration level was increased, the viabilities of the cells treated with nanoparticle formulations were decreased rapidly in comparison to native DTX. Between nanoparticle formulations, bombesin grafted nanoparticles exhibited higher toxicity than unconjugated nanoparticles.

After 48 h incubation, the IC_{50} values against DU145 cells for DTX, DNP and BDNP were 241.89, 126.04 and 77.41 ng/mL, respectively (Table 4.1).

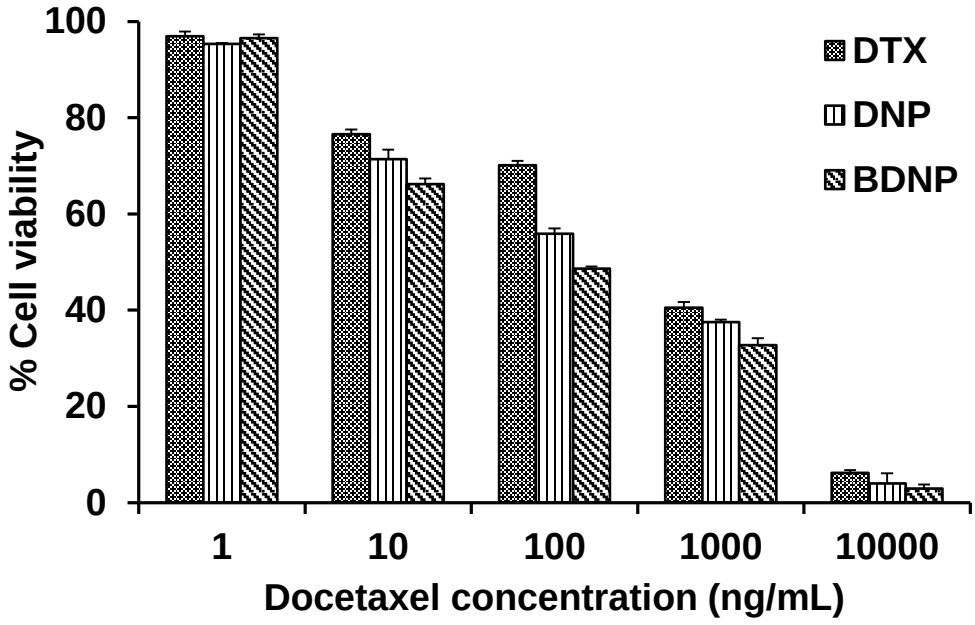

a)

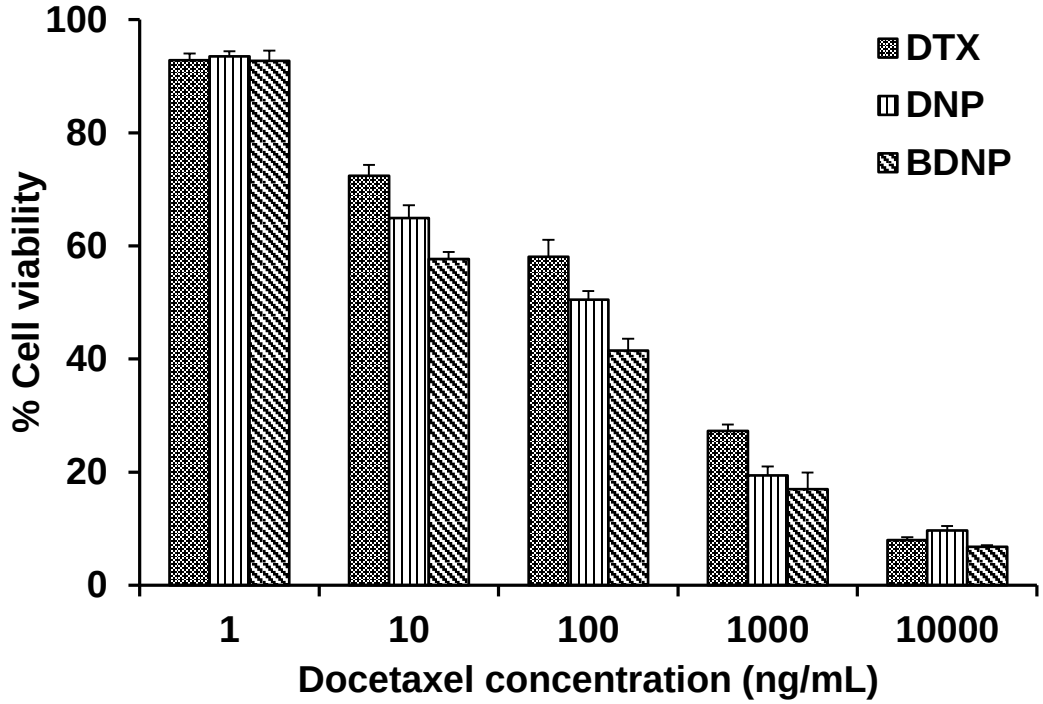

b)

Figure 4.2 a-b: Growth inhibition of human prostate cancer cells, DU145 (A) and PC3 (B) after 48 h exposure of docetaxel (DTX), DTX loaded nanoparticles (DNP) and bombesin conjugated DNP (BDNP) (mean ± SD, n=4)

For PC3 cells, IC_{50} values were 122.95, 74.44 and 45.02 ng/mL for DTX, DNP and BDNP, respectively. The enhanced cytotoxicity of BDNP in comparison to DNP can be attributed to increased cellular uptake of BDNP through receptor-mediated endocytosis. Human prostate cancer cells have been reported to over-express GRP receptors compared to normal cells (Markwalder and Reubi, 1999). Both PC3 and DU145 cells express high levels of GRP receptors (Accardo et al., 2012; De Visser et al., 2007; Reile et al., 1994; Yang et al., 2013). Therefore BBN grafted nanoparticles would be expected to be taken up more by the cancer cells, leading to increased intracellular DTX delivery.

To confirm this, a separate study was performed using coumarin loaded nanoparticles. PC3 cells were used for further experiments as they are more

sensitive to the formulations than DU145 cells. It would be worth mentioning that both PC3 and DU145 cells are androgen-independent and show no expression of androgen receptors or prostate specific antigens which are characteristics to prostate cancer (Sancho et al., 2011). Therefore, GRP-mediated targeting and enhanced cytotoxicity of DTX using BDNP could be very promising in the treatment of androgen-independent prostate cancer. Figure 3 shows the change in the morphology of PC3 cells treated with DTX, DNP and BDNP. Control cells were observed as polygonal to spindle in shape, whilst treated cells were mostly rounded.

Table 4.1: IC50 values of different DTX formulations against DU145 and PC3 human prostate cancer cells after 48 h incubation. (Mean ± SD; n=4).

Formulation	IC50 value (ng/mL)	
	DU145	**PC3**
DTX	241.89 ± 1.3	122.95 ± 2.7
DNP	126.04 ± 2.1	74.44 ± 1.9
BDNP	77.41 ± 1.7	45.01 ± 1.6

DTX: Docetaxel; DNP: Docetaxel loaded PLGA nanoparticles; BDNP: Bombesin grafted DNP

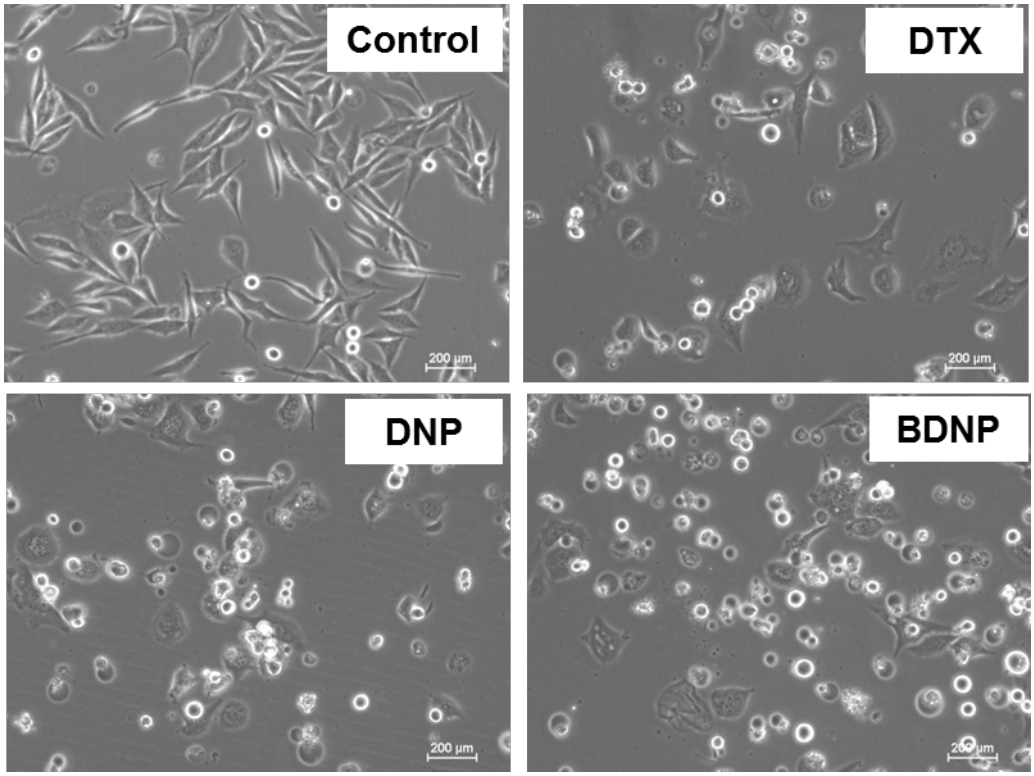

Figure 4.3: Phase contrast images of PC3 human prostate cancer cells after treatment with docetaxel (DTX), DTX loaded nanoparticles (DNP) and bombesin-conjugated DNP (BDNP). Untreated cells are shown as control. Cells treated with DTX formulations showed a significant change in morphology

4.3.3. Cellular uptake studies

Florescence microscopy provided preliminary evidence of cellular internalization of nanoparticles. Coumarin-6 loaded PLGA nanoparticles (CPN) and BBN grafted CPN (BCPN) were separately formulated for cellular uptake studies. CPN were prepared by the same method reported in section 2.2, except that 3 mg of coumarin-6 was used instead of DTX. Figure 4.4 shows the fluorescent microscopic images of PC3 cells following incubation with coumarin-6, CPN or BCPN. A time-dependent cellular uptake of the different formulations was observed (Figure 3). Non-encapsulated coumarin-6 was barely taken up by cells even after 3 h. Cells incubated with BCPN showed higher fluorescence at all the time points than

unconjugated nanoparticles (CPN). The higher cellular uptake of BCPN than CPN may be attributed to increased interaction of BCPN to the cell surface through GRP receptors (Yang et al., 2013).

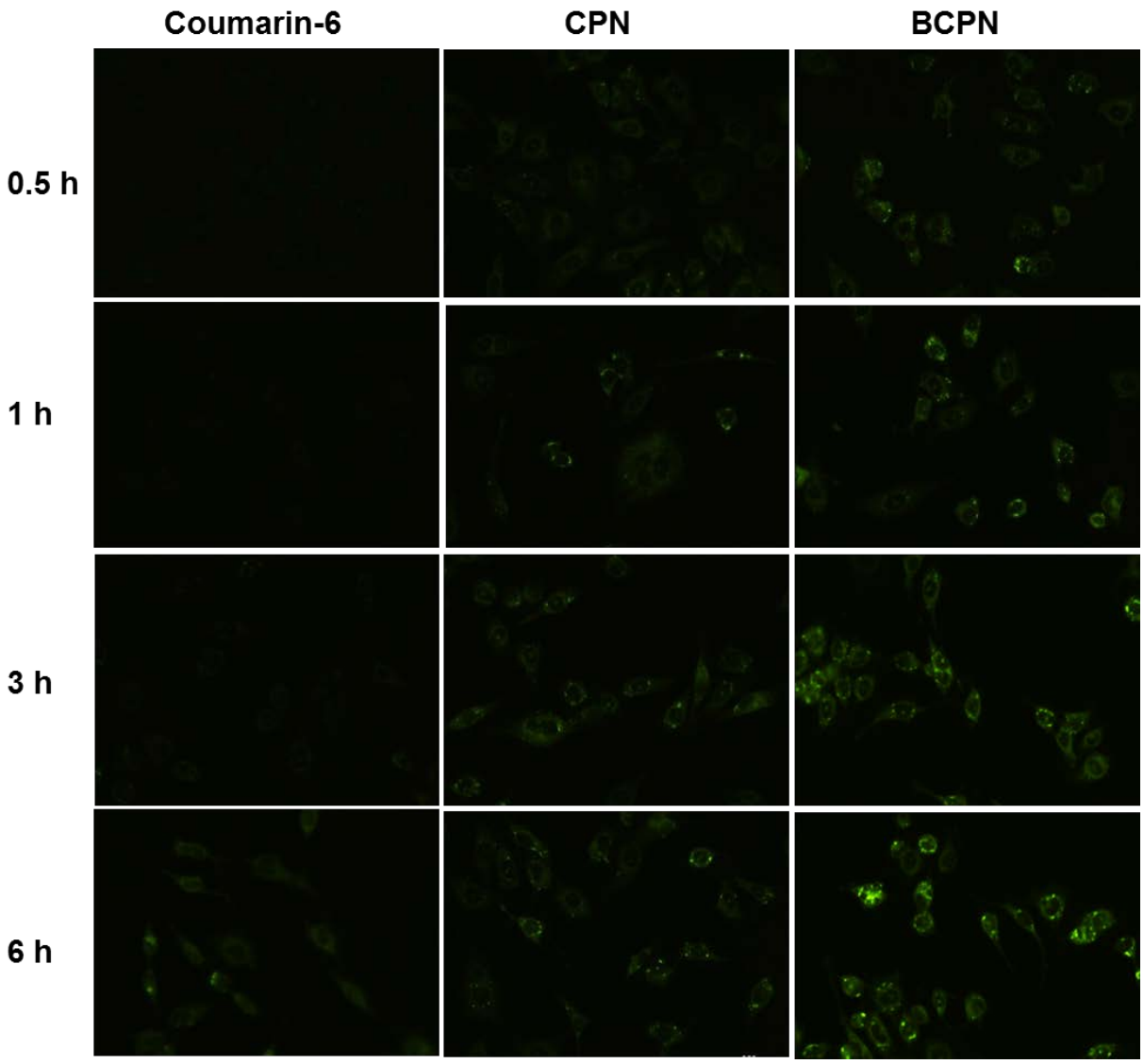

Figure 4.4: In vitro cellular uptake of coumarin-6, coumarin-6 loaded PLGA nanoparticles (CPN) and bombesin-conjugated CPN (BCPN) by PC3 prostate cancer cells after incubation for different times (0.5, 1, 3 and 6 h).

4.3.4. AO/EB assay

Induction of apoptosis by DTX formulations was studied using the AO/EB assay. This double staining method visualizes the nuclear changes and apoptotic body formation that are characteristic of apoptosis (Paul et al., 2013). Intact live cell

membranes are permeable to AO, producing green fluorescence after excitation. In contrast, EB can only enter cells through damaged cell membranes and produces orange fluorescence. Therefore, live cells can be discriminated from dead cells by AO/EB staining on the basis of membrane integrity (Huang et al., 2011). Figure 4.5 shows the fluorescent microscopic images of untreated cells and cells treated with DTX, DNP or BDNP. Untreated cells appeared green in colour while treated cells were dark orange-red colour. BDNP treated cells showed higher apoptosis and decreased cell numbers compared to DNP and DTX, suggesting superior apoptosis-induction capability of BDNP. This could also be explained by the enhanced intracellular delivery of DTX by BDNP than other formulations.

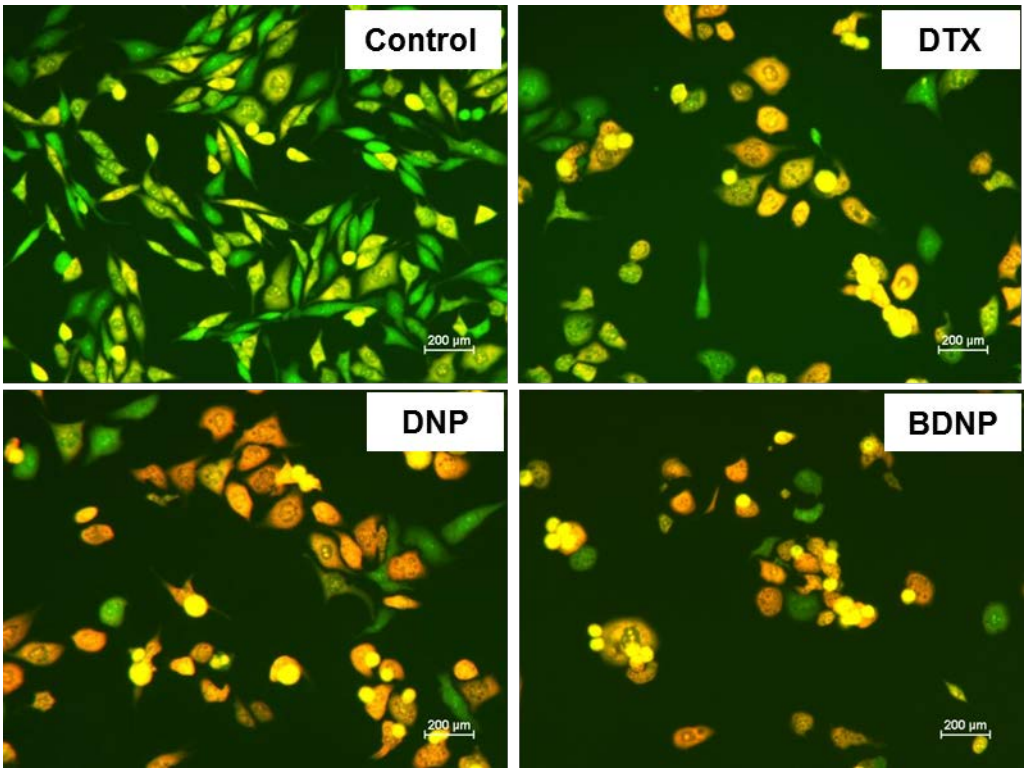

Figure 4.5: Induction of apoptosis studies using acridine orange and ethidium bromide double staining of PC3 human prostate cancer cells after treatment with docetaxel (DTX), DTX loaded nanoparticles (DNP) or bombesin conjugated DNP (BDNP). Untreated cells are shown as control

4.3.5. Wound healing scratch assay

Angiogenesis is an important step for the growth of cancer cells especially when tumor size reaches about 2 mm^3. Angiogenesis involves the formation of new blood vessels from existing blood vessels. Therefore, the inhibition of angiogenesis is complementary to anti-proliferation activity of anticancer drugs (Danhier et al., 2012). The effect of different DTX formulations on the migration of PC3 cells was determined by the wound healing scratch assay. In control experiments, the wound zone was completely filled with cells after 24 h; while a clear wound zone was observed in cells incubated with DTX, DNP and BDNP formulations (Figure 4.6a). However, among these DTX formulations, inhibition of cell migration was greatest with BDNP. The percentage of wound closure was found 93.6, 45.2, 29.4 and 11.3% for untreated (control), DTX-, DNP- and BDNP-treated cells, respectively (Figure 4.6b). The enhanced anti-angiogenic activity of BDNP may be attributed to higher cellular uptake and therefore increased intracellular delivery of DTX.

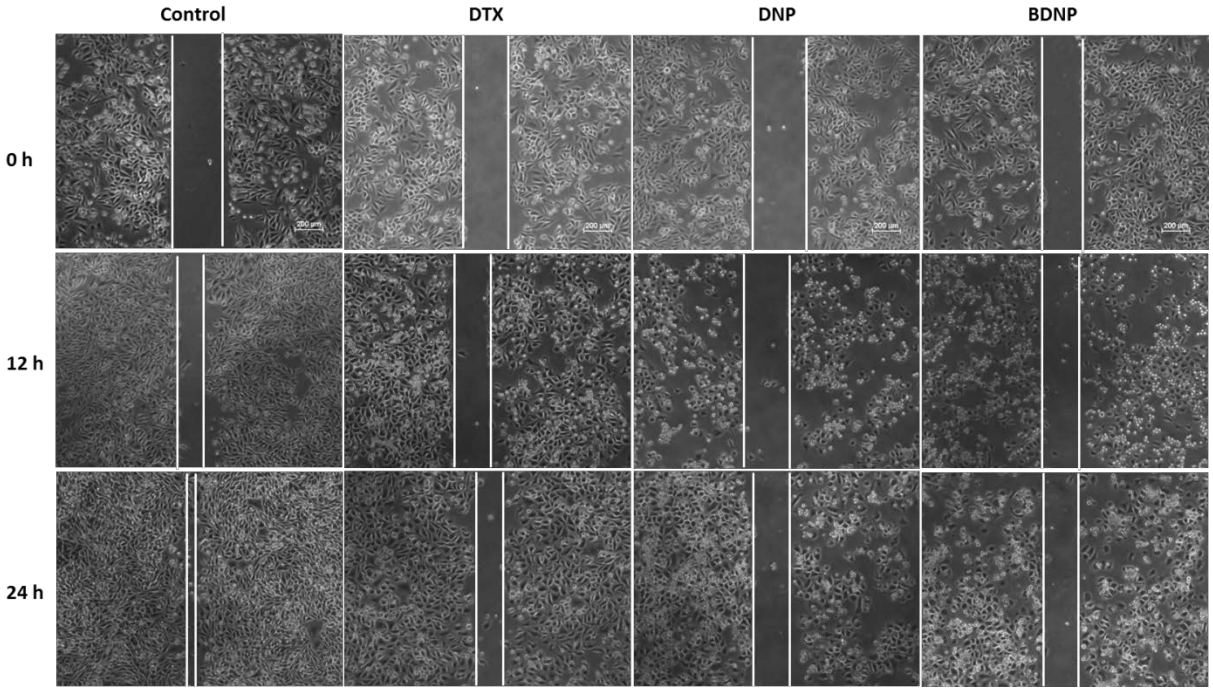

a)

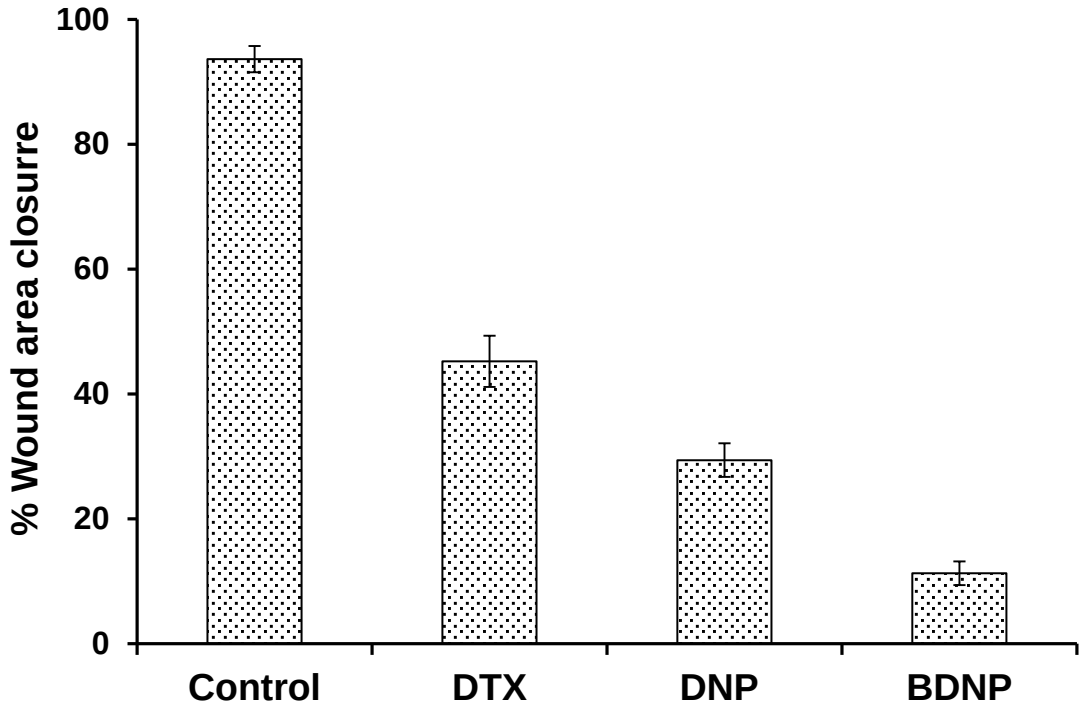

b)

Figure 4.6 a-b: Wound healing scratch assay. (a) Bright field images of PC3 human prostate cancer cells. Untreated cells migrated promptly towards the wound area. Migration was inhibited in cells treated with DTX, DNP and BDNP. The wound area remained practically unchanged, even after 24 h, in cells treated with BDNP, reflecting anti-angiogenic activity. (b) Quantitative determination of % wound area closure.

4.3.6. Clonogenic assay

The potential long-term anti-cancer effects of the DTX formulations under study were examined by a colony formation assay. The three formulations showed a significant reduction in colony number compared to control or untreated cells (Figure 4.7). The nanoparticle-based formulations, DNP and BDNP, showed superior colony formation inhibition activities against PC3 cells over DTX alone. These results can be explained by sustained release of DTX from DNP and BDNP as observed in our previous study.

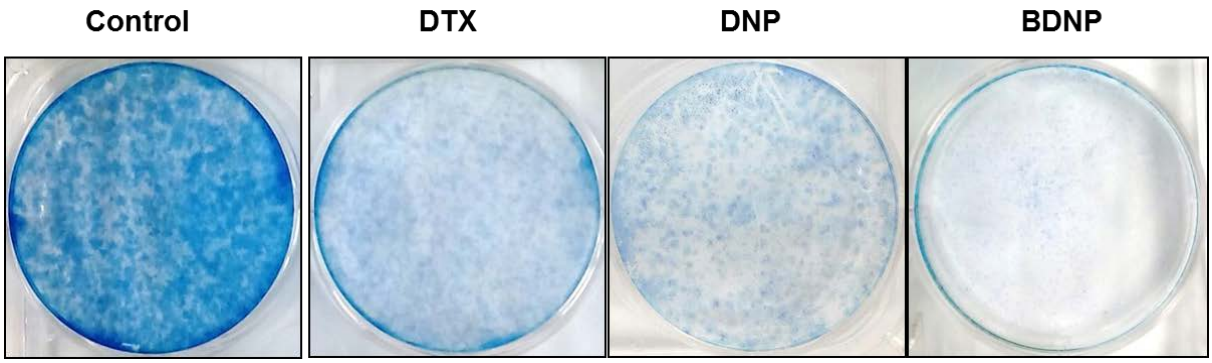

Figure 4.7: Clonogenic assay. DTX formulations showed a significant control over the colony formation inhibition activity of PC3 human prostate cancer cells

4.3.7. Pharmacokinetic studies

In drug delivery, the understanding of pharmacokinetic and biodistribution of formulations helps to predict their efficacy. In case of anticancer drugs, these studies are also used to determine the possible toxicities of encapsulated drugs. PK data aid to determine the dose and dose regimen for the encapsulated drugs to maintain the concentration of the drug within the therapeutic window for improved therapeutic effect and decreased side effects.

For pharmacokinetic studies, Taxotere® or the nanoparticle formulations DNP and BDNP were administered to Balb/c mice at a dose of 10 mg/Kg body weight by tail vein injection. The time course of plasma drug concentrations is shown in Figure 6a, with the corresponding pharmacokinetic parameters reported in Table 4.2. Compared to nanoparticle formulations, following Taxotere® injection a rapid decline in DTX concentration occurred and after 8 h, plasma DTX concentration was below the detection level (Figure 4.8). In DNP and BDNP treated mice DTX plasma half-life was longer than Taxotere® treated mice (Table 2). The area under the curve ($AUC_{0-\infty}$) for Taxotere®, DNP and BDNP concentrations were 29.52, 108.68 and 137.21 µg/mL/h, respectively. A significant increase in AUC for DTX nanoparticles can be

attributed to slow release of drug from nanoparticles. Decreased clearance of DTX may be another reason for the extended blood circulation time when delivered via DNP or BDNP. In comparison to Taxotere®, with DNP and BDNP, clearance of DTX was decreased by 3.68 and 4.65 times. Increased plasma half-life and decreased clearance also lead to longer mean residence time of DNP (3.76 h) and BDNP (4.32 h) (Table 4.2). Therefore, the DTX encapsulated PLGA nanoparticles showed better DTX pharmacokinetic (PK) profiles than Taxotere®. However, it was also noted that there was no significant ($p > 0.05$) difference between PK profiles of DNP and BDNP. This suggests surface functionalization with BBN does not alter the stability and circulation of nanoparticles in blood. This could be due to the low density of BBN (0.7%, determined by XPS analysis) on the surface of nanoparticles.

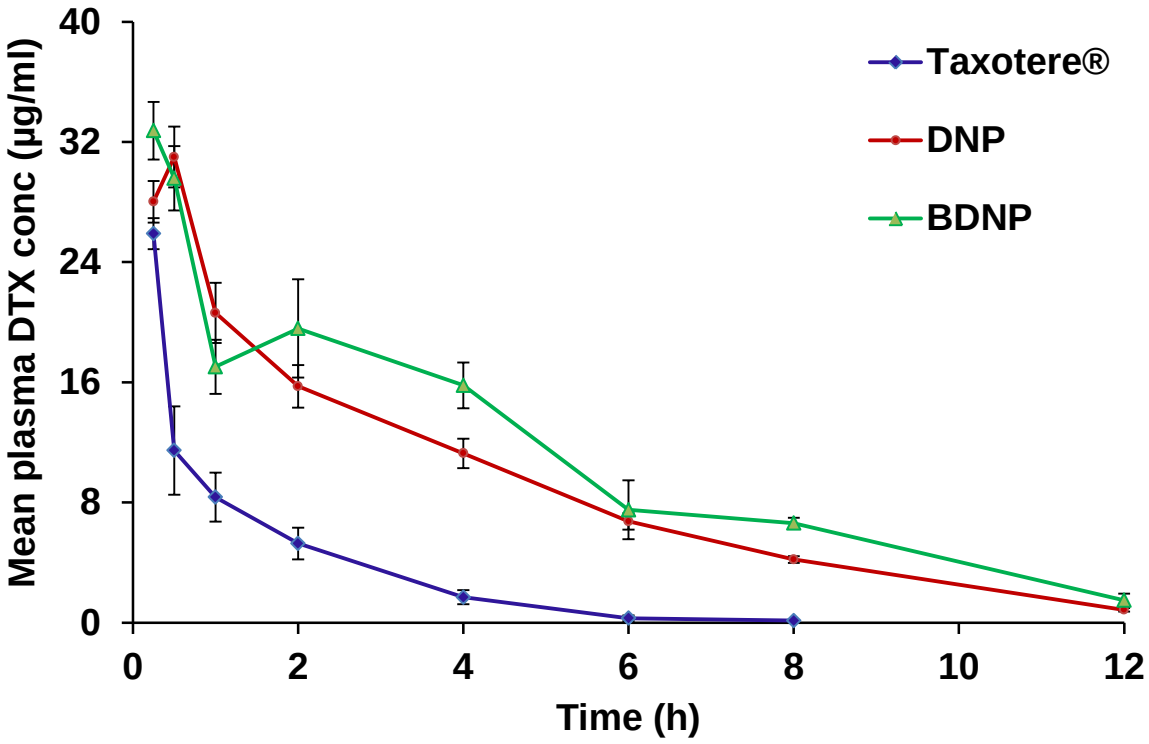

Figure 4.8: Pharmacokinetic profiles of Taxotere®, DNP and BDNP administered intravenously to Balb/c mice at a dose of 10 mg/Kg body weight by tail vein injection (Mean ± SD, n=4).

4.3.8. Tissue-distribution of different DTX formulations

Distribution of DTX after intravenous administration of Taxotere®, DNP and BDNP was estimated in different body tissues including heart, brain, kidney, liver, lung and spleen. Tissue distribution profiles of Taxotere®, DNP and BDNP are shown in Figure 4.9a-c. Both DNP and BDNP showed a rapid and high drug distribution to spleen, lung and liver. This could be a reason why the plasma-concentration curves of the two nanoparticle formulations were not significantly different. From Figure 4.9a it is clear that the relative distribution of Taxotere® was higher in kidney (3.4 µg/g) than other tissues. This could explain the rapid clearance of DTX with Taxotere® (Table 4.2). The DNP formulation was highly distributed to spleen (4.6 µg/g) (Figure 4.9b) while BDNP accumulated in lungs (4.8 µg/g) (Figure 4.9c).

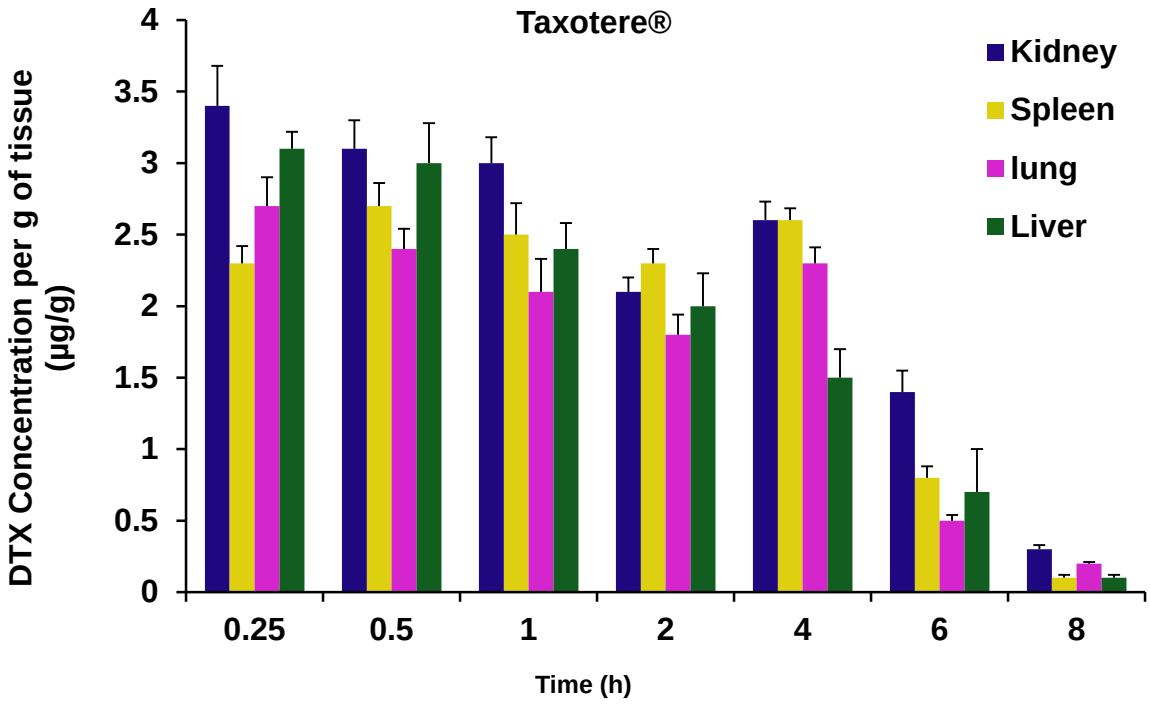

a)

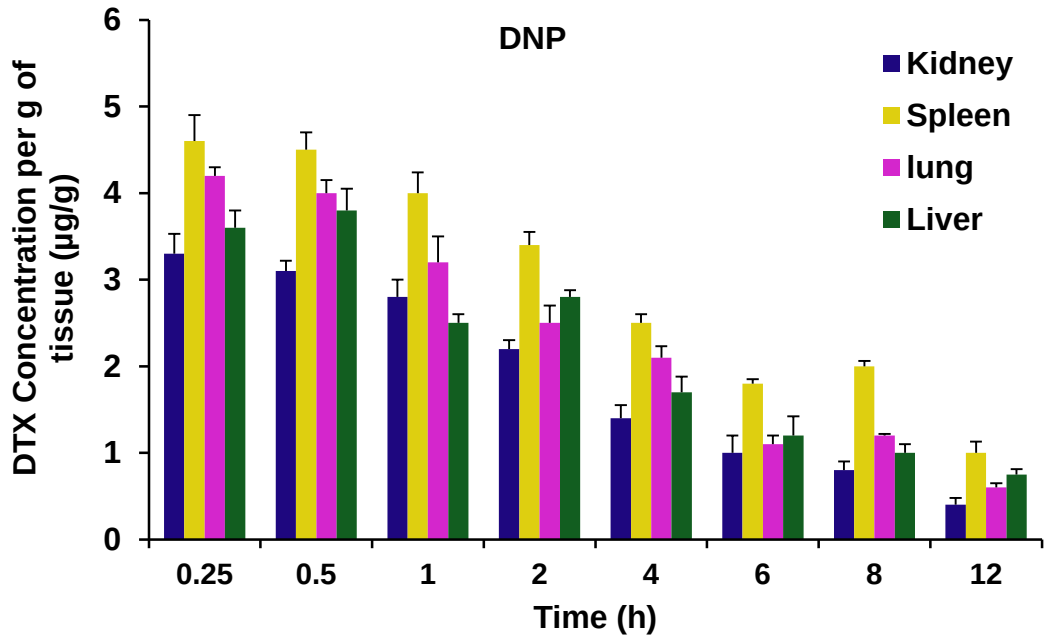

b)

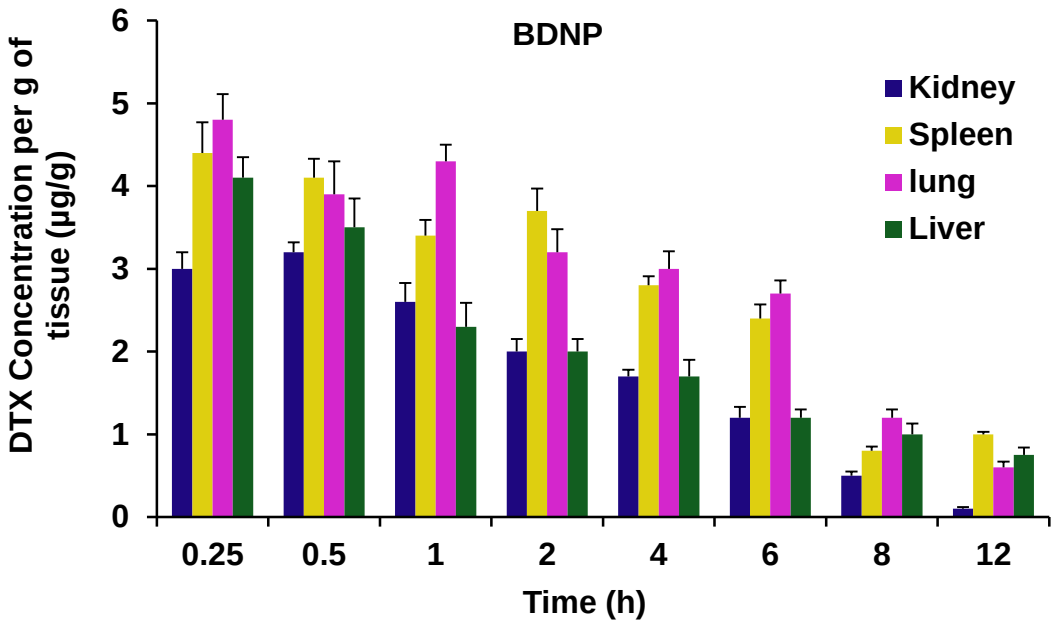

c)

Figure 4.9 a-c: Tissue distribution profiles of DTX in kidney, spleen, lung and liver after intravenous administration of Taxotere® (a), DNP (b) or BDNP (c) (Mean ± SD, n=4).

Table 4.2: Pharmacokinetic parameters of DTX after intravenous administration of Taxotere®, DNP and BDNP at a dose of 10 mg/Kg body weight in Balb/c mice. Data are represented as Mean ± SD; n=4.

Pharmacokinetic Parameter	**Taxotere®**	**DNP**	**BDNP**
$AUC_{0-\infty}$ (µg/ml/h)	29.52±3.21	108.68±5.92**	137.21±5.37**, ###
MRT (h)	1.39±0.16	3.76±0.28	4.32±0.198*,ns
Cl (ml/h)	8.46±1.15	2.3±0.3*	1.82±0.21**,ns
Terminal half life (h)	1.3±0.2	2.5±0.14	2.94±0.11
C_{max}	25.9±3.72	31±4.57	32.75±2.98
t_{max}	0.25±0.04	0.5±0.08	0.25±0.05

Statistical analysis: ns Not Significant, * p<0.05, ** p<0.005, *** p<0.0005, # p<0.05, ## p<0.005, ### p<0.0005,

**** Indicates comparison with Taxotere®;***

 # Indicates comparison with DNP

Thus, BDNP decreased the accumulation of nanoparticles in liver, spleen and kindey than Taxotere®. It can be explained by the size of the BDNP (115 nm). Because of the small size (< 400 nm), nanoparticles escape the uptake by reticulo-endothelial organs like liver and spleen. But, they had enough large size (> 6 nm) to avoid filter through kidney (Longmire et al., 2008).[32] Interesting, drug was not detected in brain at all-time points after administration of any of the formulations. Therefore, the targeted drug delivery system provides the advantage of avoiding on-specific targeting to brain with the drug being distributed only to peripheral tissues. Variable drug levels were observed in heart tissues making it difficult to draw a clear conclusion.

4.4. Conclusion

In summary**,** bombesin-mediated cellular recognition and uptake of nanoparticles leads to increases in the anti-proliferative, apoptotic and migration-inhibiting activities of DTX in PC3 androgen-independent human prostate cancer cells with high expression of GRP receptors. In clonogenic assays, nanoparticle formulations also show long-term control over growth of cancer cells. Pharmacokinetic data suggest longer blood circulation times and higher plasma concentrations of BDNP compared to Taxotere®. Therefore, BBN mediated targeted delivery of docetaxel could be a potential approach for the GRP over expressing prostate cancer.

4.5. References

- Accardo A, Salsano G, Morisco A, Aurilio M, Parisi A, Maione F, et al. Peptide-modified liposomes for selective targeting of bombesin receptors over-expressed by cancer cells: a potential theranostic agent. *Int J Nanomed* 2012,**7**:2007-17.
- Aragon-ChingJB, Dahut WL. Chemotherapy in Androgen-Independent Prostate Cancer (AIPC): What's next after taxane progression? *Cancer Therapy* 2007,**5**:151-60.
- Bray K, Chen HY, Karp CM, May M, Ganesan S, Karantza-Wadsworth V, DiPaola RS, White E. Bcl-2 modulation to activate apoptosis in prostate cancer. *Mol Cancer Res* 2009,**7**:1487-96.
- Carrión-Salip D, Panosa C, Menendez JA, Puig T, Oliveras G, Pandiella A, De Llorens R, Massaguer A. Androgen-independent prostate cancer cells circumvent EGFR inhibition by overexpression of alternative HER receptors and ligands. Int J Oncol 2012,41(3):1128-38.

- Cheever MA, Higano CS. PROVENGE (Sipuleucel-T) in prostate cancer: the first FDA-approved therapeutic cancer vaccine. *Clin Cancer Res* 2011,**17**:3520-6.
- Cornelio D, Roesler R, Schwartsmann G. Gastrin-releasing peptide receptor as a molecular target in experimental anticancer therapy. *Ann Oncol* 2007,**18**:1457-66.
- Danhier F, Le Breton A, Préat V. RGD-based strategies to target alpha(v) beta(3) integrin in cancer therapy and diagnosis. *Mol Pharm* 2012,**9**:2961-73.
- De Visser M, van Weerden WM, de Ridder CM, Reneman S, Melis M, Krenning EP, et al. Androgen-dependent expression of the gastrin-releasing peptide receptor in human prostate tumor xenografts. *J Nucl Med* 2007,**48**:88-93.
- Dong X, Mumper RJ. Nanomedicinal strategies to treat multidrug-resistant tumors: current progress. *Nanomedicine* 2010,**5**:597-615.
- Fong MK, Hare R, Jarkowski A. A new era for castrate resistant prostate cancer: a treatment review and update. *J Oncol Pharm Pract* 2012,**18**:343-54.
- Guan X, Chen L. Current opinions on the treatment of androgen-independent prostate cancer. *National J Androl* 2006,**12**:1021-5.
- Huang HL, Li ZZ, Liang ZH, Yao JH, Liu YJ. Synthesis, cellular uptake, apopotosis, cytotoxicity, cell cycle arrest, interaction with DNA and antioxidant activity of ruthenium (II) complexes. *Eur J Med Chem* 2011,**46**:3282-90.
- Hwang C. Overcoming docetaxel resistance in prostate cancer: a perspective review. *Ther Adv Med Oncol* 2012,**4:**329-40.
- Jensen R, Battey J, Spindel E, Benya R. International Union of Pharmacology. LXVIII. Mammalian bombesin receptors: nomenclature, distribution, pharmacology, signaling, and functions in normal and disease states. *Pharmacol Rev* 2008,**60**:1-42.

- Kraus LA, Samuel SK, Schmid SM, Dykes DJ, Waud WR, Bissery MC. The mechanism of action of docetaxel (Taxotere®) in xenograft models is not limited to bcl-2 phosphorylation. *Invest New Drugs* 2003,**21**:259-68.
- Kulhari H, Pooja D, Shrivastava S, VGM N, Sistla R. Peptide conjugated polymeric nanoparticles as a carrier for targeted delivery of docetaxel. *Colloids Surf B: Biointerfaces* 2014,**117**:166-73.
- Kwon GT, Jung JI, Song HR, Woo EY, Jun JG, Kim JK, et al. Piceatannol inhibits migration and invasion of prostate cancer cells: possible mediation by decreased interleukin-6 signaling. *J Nutr Biochem* 2012,**23**:228-38.
- Longmire M, Choyke PL, Kobayashi H. Clearance Properties of Nano-sized Particles and Molecules as Imaging Agents: Considerations and Caveats. *Nanomedicine (Lond)* 2008,**3**:703–17.
- Loos WJ, Baker SD, Verweij J, Boonstra JG, Sparreboom A. Clinical pharmacokinetics of unbound docetaxel: role of polysorbate 80 and serum proteins. *Clin Pharmacol Ther* 2003,**74**:364-71.
- Markwalder R, Reubi JC. Gastrin-releasing peptide receptors in the human prostate relation to neoplastic transformation. *Cancer Res* 1999,**59**:1152-9.
- Marques RB, van Weerden WM, Erkens-Schulze S, de Ridder CM, Bangma CH, Trapman J, Jenster G. The human PC346 xenograft and cell line panel: a model system for prostate cancer progression. *Eur Urol* 2006,**49**:245-57.
- Merisko-Liversidge EM, Liversidge GG. Drug nanoparticles: formulating poorly water-soluble compounds. *Toxicol Pathol* 2008,**36**:43-8.
- Namiki M, Ueno S, Kitagawa Y. Role of hormonal therapy for prostate cancer: perspective from Japanese experiences. *Transl Androl Urol* 2012,**1**:160-72.

- Paul A, Das S, Das J, Samadder A, Khuda-Bukhsh AR. Cytotoxicity and apoptotic signalling cascade induced by chelidonine-loaded PLGA nanoparticles in HepG2 cells in vitro and bioavailability of nano-chelidonine in mice in vivo. *Toxicol Lett* 2013,**222**:10-22.
- Reile H, Armatis PE, Schally AV. Characterization of high-affinity receptors for bombesin/gastrin releasing peptide on the human prostate cancer cell lines PC-3 and DU-145: internalization of receptor bound 125I-(Tyr4) bombesin by tumor cells. *Prostate* 1994,**25**:29-38.
- Salvador-Morales C, Gao W, Ghatalia P, Murshed F, Aizu W, Langer R, Farokhzad OC. Multifunctional nanoparticles for prostate cancer therapy. *Expert Rev Anticancer Ther* 2009,**9**:211-21.
- Sancho V, Di Florio A, Moody TW, Jensen RT. Bombesin receptor-mediated imaging and cytotoxicity: review and current status. *Curr Drug Deliv* 2011,**8**:79-134.
- Sanna V, Sechi M. Nanoparticle therapeutics for prostate cancer treatment. *Maturitas* 2012,**73**:27-32.
- Saraon P, Jarvi K, Diamandis EP. Molecular alterations during progression of prostate cancer to androgen independence. Clin Chem 2011,57:1366–75.
- Schrijvers D. Androgen-independent prostate cancer. Recent Results in Cancer Research 2007,175:239-49.
- Tannock IF, de Wit R, Berry WR, Horti J, Pluzanska A, Chi KN, et al. Docetaxel plus prednisone or mitoxantrone plus prednisone for advanced prostate cancer. *N Engl J Med* 2004,**351**:1502-12.
- Wang L, Liu Z, Liu D, Liu C, Juan Z, Zhang N. Docetaxel-loaded-lipid-based-nanosuspensions (DTX-LNS): preparation, pharmacokinetics, tissue distribution and antitumor activity. *Int J Pharm* 2011, **413**:194-201.

- Yang H, Cai H, Wan L, Liu S, Li S, Cheng J, et al. Bombesin analogue-mediated delivery preferentially enhances the cytotoxicity of a mitochondria-disrupting peptide in tumor cells. *PloS One* 2013,**8**:e57358.
- Yarnell A. Nanoparticles boost drug solubility. *Chem Eng News* 2012,**90**:30-1.

5

CHAPTER

Trastuzumab conjugated PAMAM dendrimers for the selective delivery of docetaxel to HER2 positive breast cancer

5.1. Background

According to the GLOBCON 2012 report of The International Agency for Research on Cancer (IARC), the specialized cancer agency of the World Health Organization, breast cancer is the second most common diagnosed cancer worldwide. In 2012, 1.7 million new cases were diagnosed, and over 5 million women died of breast cancer. Since 2008, estimates of breast cancer incidence have increased by more than 20%, while mortality has increased by 14% (Ferlay et al., 2013; Bray et al., 2008). An estimated, 20% of breast cancers are HER2 positive (Senkusa et al., 2014). That is, they express high levels of the human epidermal growth factor receptor-type 2. HER2 stimulates the growth of breast cancer cells. HER2 positive breast cancer tends to be more aggressive and to spread more quickly than HER2 negative tumours. HER2 positive breast cancer can also be difficult to treat with hormone therapies used for other types of breast cancer. Younger women are more likely to present with HER2 positive breast cancer than older women (Senkusa et al., 2014; Figueroa-Magalhaes et al., 2014).

Both adjuvant and neoadjuvant chemotherapies play important roles in the management of HER2-positive breast cancer. The latest and one of the biggest clinical trials conducted by Roche and the Breast International Group confirmed that one year of Herceptin (Trastuzumab) treatment remains the gold standard of care for the patients with early-stage HER2-positive breast cancer. Trastuzumab (TZ) is a humanized monoclonal antibody and has been approved by the Food and Drug Administration for the treatment of HER2-positive breast cancer. It binds with HER2 receptors on breast cancer cells and blocks downstream signaling leading to antibody dependent cellular toxicity (Figueroa-Magalhaes et al., 2014; Pinto et al., 2013; Gennari et al., 2004; Gschwind et al., 2004).

Clinical trials have also been carried out to optimize chemotherapeutic combinations and regimens. As a result, the combination of TZ with other chemotherapeutic agents has significantly improved disease-free survival rates and overall survival rates. Taxanes and anthracyclines are the most commonly used anticancer drugs for the treatment of breast cancer. TZ in combination with docetaxel (DTX) is synergistic (Moreno-Aspitia and Perez, 2009). DTX is a semi-synthetic analog of paclitaxel and has been used as a first-line treatment for various cancers, including breast, lung, ovarian, brain and prostate cancers (Zhao and Astruc, 2012; Kulhari et al., 2014; Feng et al., 2009; Mosallaei et al., 2013).

Dendrimers are hyper-branched, nano-sized and multi-functionality carrier systems. The unique structure of dendrimers allows delivering of more than one drug at a time. Dendrimers contain open internal cavities and free functional groups on the surface (Kulhari et al., 2011, 2013, 2015; Chauhan et al., 2004). In the current study DTX was loaded into the internal cavities of dendrimers through non-covalent interactions and TZ was conjugated to free amine groups on their surface. This dendrimer-mediated drug delivery system was designed to use TZ as a targeting ligand for the site-specific delivery of DTX to HER2-positive breast cancer cells. Although reports are available on conjugation of TZ to a nanocarrier system, (Shukla et al., 2008; Yousefpour et al., 2011; Kim et al., 2012; Miyano et al., 2010; Isabel et al., 2006), preclinical studies have not so far been reported.

5.2. Experimentation

5.2.1. Materials

G4 PAMAM dendrimers with diaminobutane core were purchased from NanoSynthons, Mt Pleasant, MI. Trastuzumab was purchased from Nava Sanjivani Drugs, Hyderabad. Maleimide-poly(ethylene) glycol-N-hydroxysuccinimide (Mal-PEG-

NHS) was purchased from Thermo Fisher Scientific. Docetaxel was obtained as gift from TherDose Pharma Pvt. Ltd. (Hyderabad, India). High performance liquid chromatography (HPLC) grade solvents were purchased from Merck specialties (Mumbai, India). Nylon membrane filters of pore size 0.22 µm were obtained from Pall India Pvt. Ltd. (Mumbai, India). Fluorescein isothiocyanate (FITC), dialysis tubing (Molecular weight cut off 2000), Dulbecco's modified eagle medium (DMEM), trypsin–EDTA, antibiotic/anti-mycotic solution, phosphate buffer saline (Ca^{2+}, Mg^{2+} free), 3-(4, 5- dimethylthiazol-2-yl)-2, 5-diphenyl tetrazolium bromide (MTT), dimethyl sulfoxide (DMSO), annexin V-FITC apoptosis detection kit, acridine orange and ethidium bromide were purchased from Sigma Aldrich (St. Louis, MO, USA). Fetal bovine serum (FBS) was purchased from Gibco, USA. Cell culture plastic wares were purchased from Tarson Ltd (Mumbai, India).

5.2.2. Synthesis and characterization of FITC labelled TZ conjugated PAMAM dendrimers

FITC labeled TZ conjugated PAMAM dendrimers were synthesized by a four step chemical reaction: a) synthesis of FITC conjugated dendrimers b) Conjugation of heterocross-linker to FITC labeled dendrimers c) Thiolation of TZ d) Bioconjugation of thiolated TZ to dendrimers.

a) Synthesis of FITC conjugated dendrimers

FITC labeled G4 PAMAM dendrimers were prepared by a previously reported method (Yellepeddi et al., 2008). Dendrimers (15 mg) were dissolved in phosphate buffer saline (PBS, pH 7.4) and mixed with 465 µL of FITC solution (5 mg/mL in acetone). The mixture was stirred overnight. The solution was then dialyzed against PBS for 24 h to remove unconjugated or untrapped FITC. The molar ratio of FITC conjugation to dendrimers was determined from absorbance at 495 nm using a UV-

VIS spectrophotometer. For qualitative analysis, samples were scanned in the wavelength-range of 200-800 nm. The FITC labeled dendrimer solution was lyophilized and used for further reactions.

b) Conjugation of NHS-PEG-MAL to FITC labeled dendrimers

27µL of NHS ester of PEG-MAL (100 mg/mL in DMSO) was added to FITC conjugated dendrimer solution in PBS, pH 8 and stirred for 30 minutes at room temperature. Synthesis of Dend-PEG-MAL was characterized by ^{1}H NMR spectroscopy. PEGylated dendrimers were dissolved in D_2O and scanned using Avance 500 NMR.

c) Thiolation of TZ

Eighty four milligrams of TZ (0.57 µM) were dissolved in PBS and reacted with 2-iminothiolane hydrochloride (2.88µM) for 2 h. Thiolated TZ was purified by dialysis (MWCO 12000-14000) in PBS to remove 2-iminothiolane hydrochloride.

d) Bio-conjugation of thiolated TZ to PEGylated dendrimers

Finally, thiolated TZ was coupled with heterocross-linked conjugated FITC labeled dendrimers to give a bio-cojugate. NHS-PEG-MAL cross-linked dendrimer solution was mixed with thiolated TZ solution and allowed to react at room temperature overnight. The dendrimer-TZ conjugate (Dend-TZ) was purified by passing through a Sephadex column.

5.2.3. Characterization of Dend-TZ conjugate

5.2.3.1. Surface charge

Surface potential of various nanoconjugates was measured using a Malvern Zetasizer Nano-ZS (Malvern Instruments Ltd., UK). Samples were diluted in deionised water and analyzed at 25 $^{\circ}$C.

5.2.3.2. Polyacrylamide gel electrophoresis (PAGE)

TZ-Dend conjugates were also characterized by PAGE analysis. All gels were electrophoresed under reducing conditions using Mini-Protean II electrophoresis units from BioRad at a constant voltage of 200V in Tris/glycine/SDS buffer.

5.2.4. Drug loading

An excess (5 mg) of DTX was added to the dendrimer solution, sonicated for 30 sec and gently stirred overnight. For preparation of DTX loaded Dend-TZ formulations two approaches were used. In first method, DTX loaded dendrimers were conjugated to TZ. Alternatively, DTX was loaded into Dend-TZ solution. Formulations were equilibrated for 24, and then filtered through a 0.45 µm membrane cellulose filter. The concentration of DTX was determined using a HPLC, system.

5.2.5. In vitro drug release studies

In vitro drug release studies were performed by a dialysis method in phosphate buffer saline pH 7.4 (PBS). Taxotere and dendrimer formulations, equivalent to 2 mg of DTX, were placed in dialysis tubing (MWCO 2000) in release medium (100 mL of PBS) at 37 $^{\circ}$C stirring at 100 rpm. At different time intervals, an aliquot of one mL was withdrawn from the release medium and replaced with same volume of fresh medium. The samples were appropriately diluted, filtered through a 0.22 µm nylon filter and analyzed for DTX content by HPLC.

5.2.6. Cell culture

The human breast cancer cell lines-MDA-MB-453 (HER2 positive) and MDA-MB-231 (HER2 negative) were obtained from the American Type Culture Collection (ATCC) (Manassas, VA, USA). Cells were grown in DMEM medium supplemented with 10% fetal bovine serum, 100 U/mL penicillin, 100 mg/mL streptomycin and 2 mM/L L-glutamine. Cells were maintained at 37 °C in 5% CO_2.

5.2.7. Anti-proliferation assay

Cells were seeded in 96-well plates at a density of 5×10^3cells per well in 100 µL of medium and allowed to adhere overnight. Cells were then incubated with the DTX, Dend-DTX or TZ-Dend-DTX at equivalent drug concentrations, ranging from 5 to 250 ng/mL for 48 or 72 h. Media were then replaced with serum free DMEM containing MTT (0.5 mg/mL) and cells incubated for an additional 4 h. Media were removed and 150 µL of DMSO added to dissolve formazan crystals. Absorbance was measured at 570 nm using a microplate reader. Untreated cells were used as a negative control (100% viability). IC50 was calculated by fitting the curve of cell viability against drug concentration.

5.2.8. Cellular uptake studies

For qualitative uptake studies MDA-MB-453 cells were seeded in 12-well plates. After 24 h cells were incubated with FITC, Dend-FITC or TZ-Dend-FITC at an equivalent FITC concentration (25 µg/mL). At pre-determined time intervals culture media was removed, cells rinsed twice with cold PBS and observed by fluorescence microscopopy. For quantitative studies, 0.1% Triton X-100 in 0.2 M NaOH was added to each well to lyse cells. Fluorescence intensities were measured using a microplate reader at an excitation wavelength of 495 nm and an emission wavelength of 520 nm.

5.2.9. Acridine orange and Ethidium bromide (AO/EB) assays

AO/EB assay were used to visualize changes in cell morphology such as chromatin condensation and apoptotic body formation that are characteristic of apoptosis. MDA-MB-453 cells were seeded in 6 well plates at 5×10^5 cells per well in 2 mL of DMEM and cultured for 24 h. Cells were incubated with various DTX formulations (DTX, Dend-DTX or TZ-Dend-DTX), equivalent to 56.1 ng/mL of DTX.

After 24 h medium was removed and cells washed in PBS twice and incubated in PBS containing AO and EB (5 µg/mL of each) at 37 °C for 10 min. Cell viability was observed with a fluorescence microscope. In live cells chromatin is stained bright green by acridine orange, whilst dead cells it is stained orange by ethidium bromide.

5.2.10. Apoptosis

Annexin V-FITC/PI assays were used as per the manufacturer's protocols to evaluate apoptosis and necrosis. Briefly, MDA-MB-453 cells (1×10^6 cells/well) were seeded in 6-well plates and maintained at 37 °C in 5% CO_2 and a 95% humidified atmosphere. The medium was replaced with freshly prepared medium containing drug-loaded nanoparticles. Untreated cells were used as controls. After 24 h, cells were washed with PBS twice and resuspended in 500 µL of binding buffer. 5 µL of FITC-conjugated Annexin V and 10 µL of PI were added and cells incubated for 15 min at room temperature in the dark. Cells were then analyzed by a Muse™ Cell Analyzer (Merck-Millipore, Germany).

5.2.11. Pharmacokinetic studies

Female Balb/c mice were purchased from National Institute of Nutrition (Hyderabad, India). Experimental protocols for the study were approved by the Institutional Animal Ethics Committee (IAEC) of the CSIR-Indian Institute of Chemical Technology, Hyderabad and the animal studies were performed in accordance with the guidelines of the Committee for the Purpose of Control and Supervision of Experiments on Animals (CPCSEA). Animals were kept in polypropylene cages under standard laboratory conditions (12 h light/12h dark cycle).

Eighty four female mice (20-25 g) were randomly assigned to three groups for pharmacokinetics investigation. Taxotere, Dend-DTX, or TZ-Dend-DTX was injected

via the tail vein at an equivalent dose of 10 mg/kg DTX. At scheduled time intervals (0.25, 0.5, 1, 2, 4, 8, and 12 h) post-injection, 0.3 mL of blood was collected into heparinized polyethylene tubes from the retro-orbital plexus and centrifuged at 1500 rpm for 5 min to obtain plasma. The samples were stored at -80 °C until analysis.

An analytical method for the determination of the DTX content of plasma samples was validated using an HPLC system (Water, USA) equipped with a C18 column (Grace, 250 × 4.6 mm, 5 µm) and a photodiode array detector. The mobile phase consisted of acetonitrile (48%) and 0.1% orthophosphoric acid (52%). 5 µl of paclitaxel solution (1 mg/mL) was used as an internal standard. The flow rate was maintained at 1 mL/min and column temperature set at 25±5 °C. Peaks were monitored at a wavelength of 230 nm. The retention times for DTX and PTX were 9.1 min and 11.2 min, respectively.

5.2.12. Stability studies

For stability studies the final formulation (TZ-Dend-DTX) was stored at 2-8 °C for 60 days. The formulation was observed for changes in consistency and precipitation and analyzed for zeta potential and drug content.

5.2.13. Statistical analysis

Results are expressed as mean and standard deviation of three experiments (n=3). Pharmacokinetic and tissue distribution data are an average of four experiments (n=4). Statistical significance was analyzed using the student t-test for two groups and one-way ANOVA for multiple groups. A probability (p) of less than 0.05 was considered as statistically significant.

5.3. Results and discussion

5.3.1. Synthesis and characterization of TZ-Dend conjugate

Trastuzumab was conjugated onto the surface of dendrimers by a four step chemical reaction (Scheme 5.1).

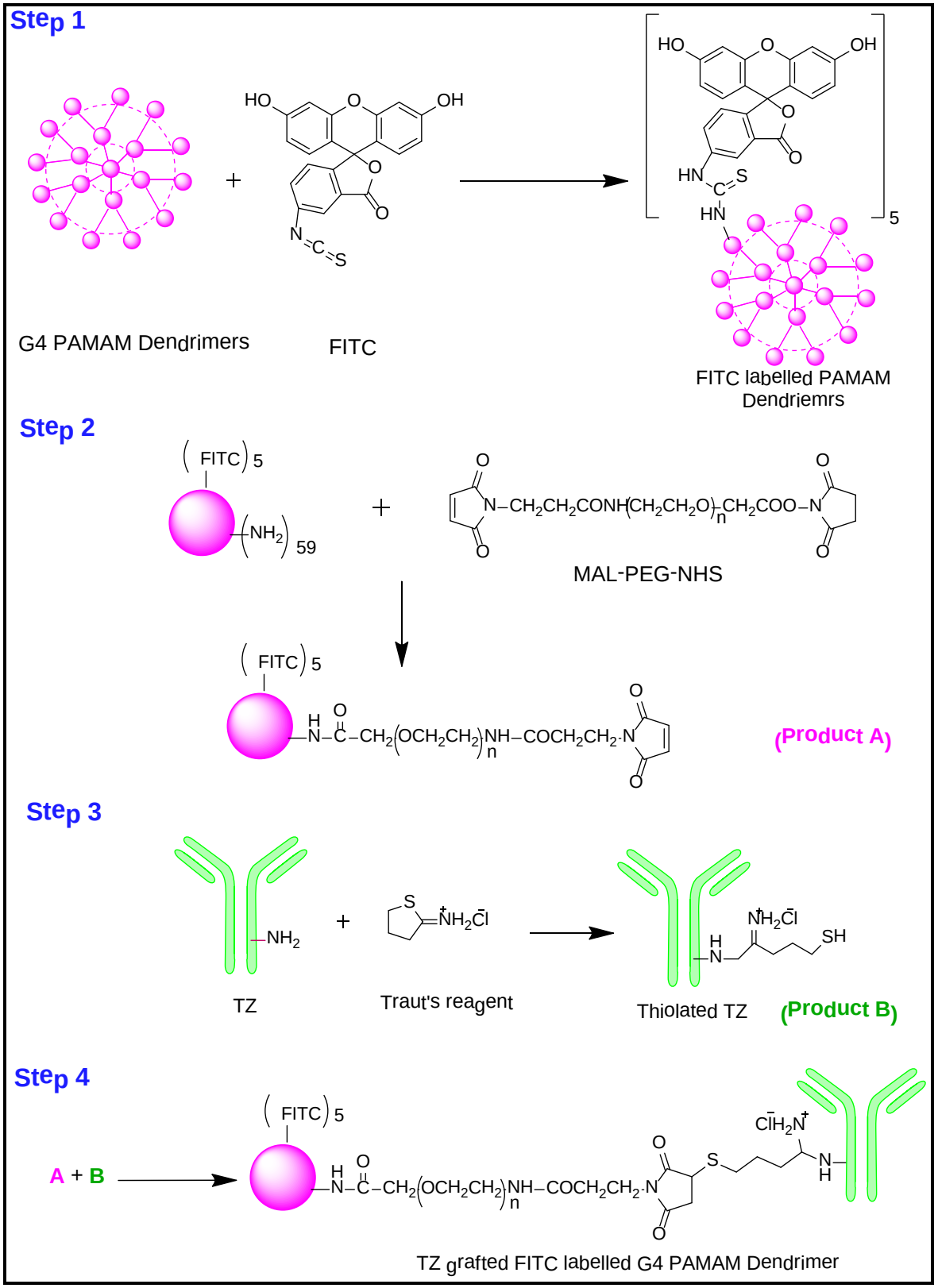

Scheme 5.1: Schematic diagram showing the various steps of bioconjugation of FITC and TZ on the surface of G4 PAMAM dendrimers

FITC labelled dendrimers were synthesized by reacting the primary amino groups of the dendrimers with the FITC isothiocyanate groups. This resulted in formation of a stable thiourea bond. Approximately 4.6 FITC molecules were attached per dendrimer molecule, as determined by UV/VIS spectrophotometric analysis (Figure 5.1). FITC labeled dendrimers were PEGylated with the NHS ester of PEG-Mal. ^{1}H NMR analysis confirmed the synthesis of pegylated dendrimers. Two new peaks appeared at 3.8 and 6.2 ppm, corresponding to the protons of the PEG chain and Mal group methylene groups, respectively. This confirmed substantial conjugation between dendrimers and NHS-PEG-Mal (Figure 5.2). In a separate reaction, TZ was thiolated using Traut's reagent (2-iminothiolane hydrochloride) and the number of thiol groups on the TZ dendrimer determined by the Ellmann's test. Finally, thiolated TZ was reacted with PEGylated dendrimers and conjugation confirmed by PAGE analysis. (Figure 5.3)

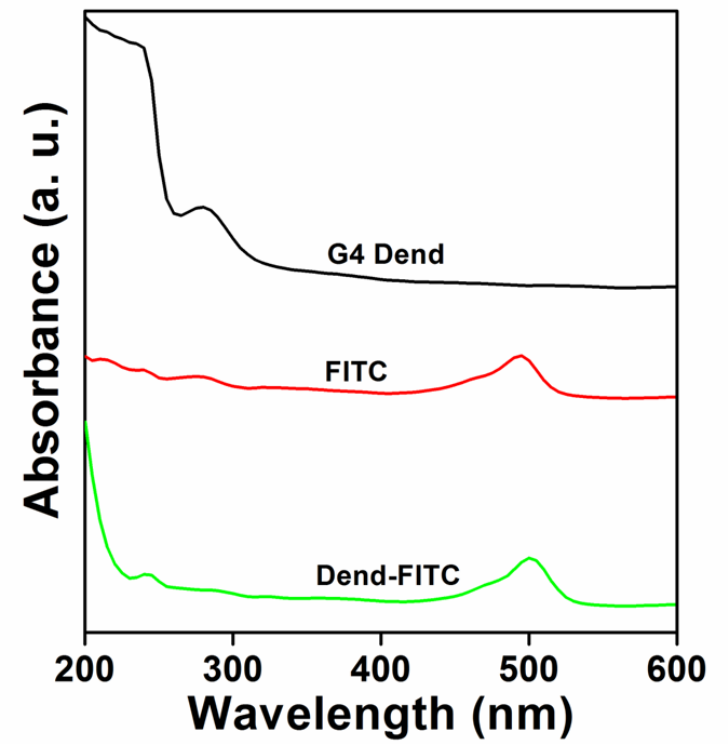

Figure 5.1: UV/VIS spectra of G4 PAMAM dendrimers (G4 Dend), FITC and FITC conjugated dendrimers (Dend-FITC)

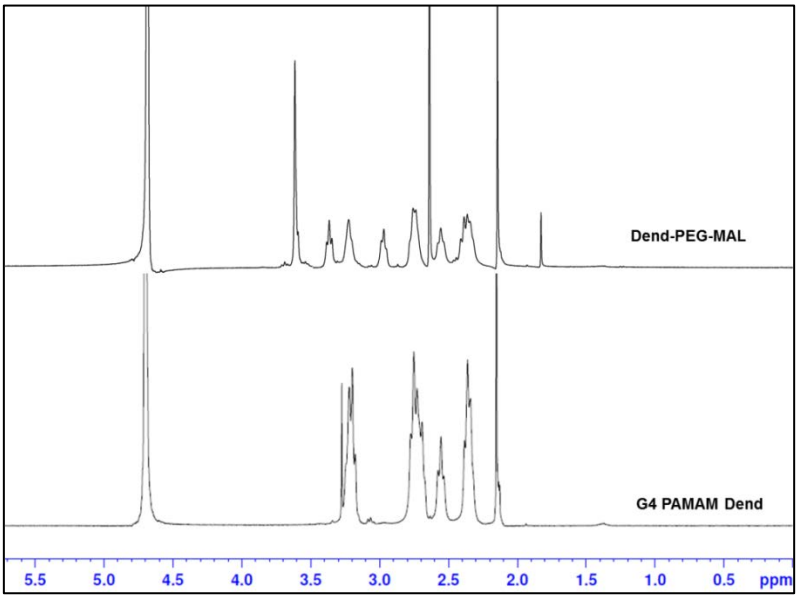

Figure 5.2: ^{1}H Nuclear magnetic resosnance spectra of G4 PAMAM dendrimers and MAL-PEG-NHS conjugated G4 PAMAM dendrimers (Dend-PEG-MAL)

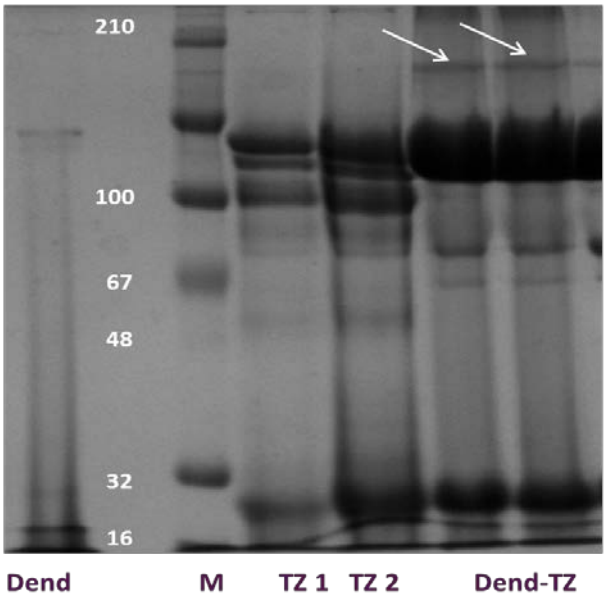

Figure 5.3: Polyacrylamide gel electrophoresis studies of Dendrimers (Dend), Trastuzumab (TZ) and TZ conjugated dendrimers (Dend-TZ)

Conjugation was also confirmed at various stages by the changes in surface charge of the dendrimers (Table 5.1). Due to presence of cationic 64 amine groups on surface, plain dendrimers showed a positive zeta potential of 12.7 mV. After

conjugation with NHS-PEG-Mal, the zeta potential was decreased to 6.8 mV and, after grafting of TZ to the dendrimer surface, to -2.3 mV.

Table 5.1: Zeta potential of plain dendrimers, dendrimer-PEG-NHS ester and dendrimer-Trastuzumab conjugate (Dend-TZ)

Step No.	Conjugate	Zeta Potential (mV)
1	Dendrimers	12.3 ± 0.9
2	Dendrimer PEG-NHS ester	6.8 ± 1.5
3	Dend-TZ conjugate	-2.3 ± 0.6

5.3.2. DTX loading

For the determination of drug loading, dendrimer formulations were appropriately diluted (50 times) with distilled water and then analyzed using a HPLC system. In plain dendrimers, DTX was loaded to a concentration of 241.7±3.82 µg/mL. In TZ-Dend conjugates, the DTX loading concentration was decreased significantly to 159.5±5.4 µg/mL. The decrease in DTX loading in the TZ-Dend conjugates may be due to the presence of TZ on the dendrimer surface which may restrict DTX molecules from reaching the interior cavities. DTX loaded dendrimers that were conjugated to TZ exhibited a DTX concentration of 216.4±2.79 µg/mL. In this case, the decrease in DTX loading concentration may be attributed to loss or release of drug during the conjugation process.

5.3.3. In vitro drug release studies

Release of DTX from Taxotere, Dend-DTX and TZ-Dend-DTX dendrimers was monitored in PBS. Results are shown in Figure 5.4. DTX was released faster from Taxotere than dendrimer-mediated formulations. About 94% of DTX was released from Taxotere dendrimers within 10 h. Dend-DTX and TZ-Dend-DTX

displayed controlled release of drug up to 48 h. Dend-DTX released 71.84% of drug after 24 h and 93.5% of drug after 48 h, respectively. DTX release from TZ-Dend-DTX was 58.6% and 73.9% after 24 and 48 h, respectively.

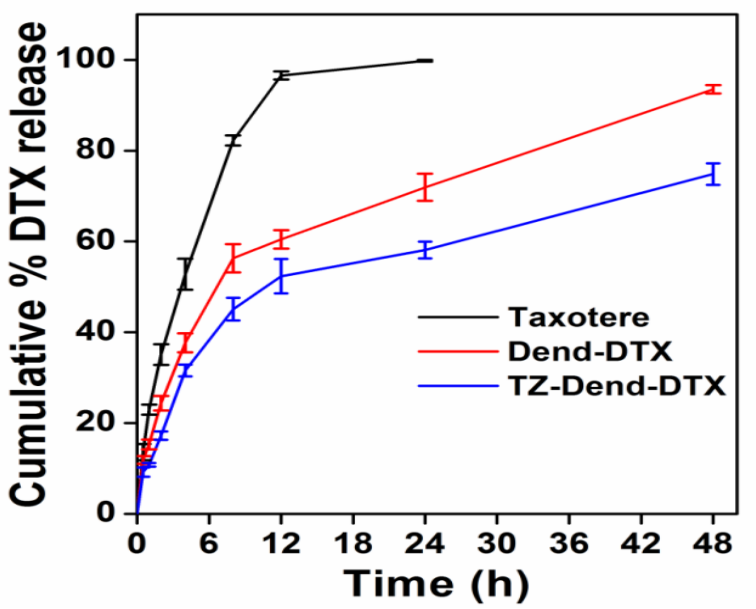

Figure 5.4: In vitro drug release profiles of Taxotere®, Dend-DTX and TZ-Dend-DTX up to 48 h

The slower release of DTX from TZ-Dend-DTX than Dend-DTX can be explained by the presence of TZ on the surface of the dendrimers. This could make a long release path for the drug or alternatively create a coat around the dendrimers.

5.3.4. Hemolytic toxicity

Biocompatibility of the drug delivery carriers were assessed by hemolytic toxicity studies. Plain dendrimers showed concentration-dependent hemolysis (Figure 5.5). TZ-conjugated dendrimers caused lower hemolysis than plain dendrimers. At 10 mg/mL dendrimers concentration, plain dendrimers caused 5.3% hemolysis compared to 1.5% by TZ-Dend conjugates. These results suggest TZ-Dend conjugates are more biocompatible than plain dendrimers. The decrease in toxicity of TZ-Dend conjugates compared to plain dendrimers can be explained by the presence of opposite charges on their surfaces (Table 1). Plain dendrimers

exhibited a high positive charge of 12.7 mV, whereas TZ-Dend conjugates were anionic in nature, with a zeta potential value of -2.3 mV. PAMAM dendrimers have been reported to cause hemolysis because of their cationic nature. They rapidly interact with anionic red blood cells (RBC) membranes, causing hemolysis (Domanski et al., 2004). This positive charge was neutralized by the TZ moiety on TZ-Dend conjugates, making them anionic and decreasing interaction between dendrimers and RBC membranes.

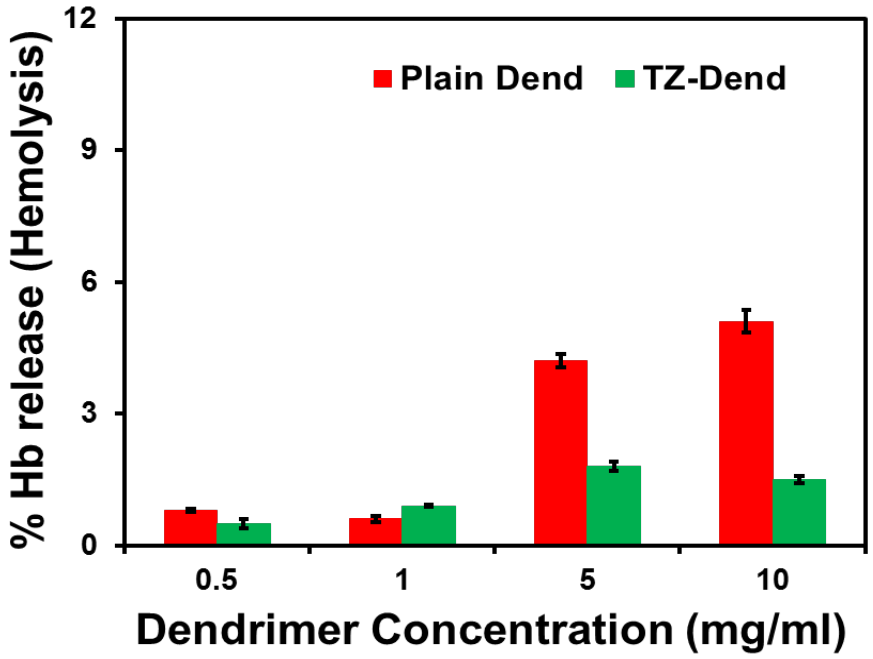

Figure 5.5: Hemolytic toxicity of plain dendrimers and TZ conjugated dendrimers

5.3.5. In vitro cytotoxicity

To investigate the anticancer actions of the DTX formulations two breast cancer lines (MDA-MB-453 and MDA-MB-231) were selected. The cell lines were chosen on the basis of their immuno-profiles. MDA-MB-453 cells are oestrogen receptor negative (ER^-), progesterone receptor negative (PR^-) and HER2 positive ($HER2^+$); whilst MDA-MB-231 cells are triple negative (ER^-, PR^- and $HER2^-$). Moreover, sensitivity of both cell lines to chemotherapy is comparable (Holliday and

Speirs, 2011; Liu et al., 2013). Therefore, a comparative evaluation of cytotoxicity against these cell lines could provide a better understanding of the contribution of TZ in drug targeting to $HER2^{+}$ breast cancers.

Cytotoxicity measures of DTX, Dend-DTX and TZ-Dend-DTX against MDA-MB-453 and MDA-MB-231 cells are shown in Figure 5.6a and b, respectively. At 125 ng/mL drug concentration, viability of MDA-MB-453 cells was 69, 57.6 and 36.2% for DTX, Dend-DTX and TZ-Dend-DTX, respectively. The results clearly indicated that DTX loaded dendrimers were more cytotoxic than plain DTX. Comparing the targeted and non-targeted dendrimers, cells treated with TZ-Dend-DTX showed enhanced cell death than with Dend-DTX. This may be attributed to the interaction between TZ and HER2 on MDA-MB-453 cells leading to internalization of TZ-Dend-DTX through receptor-mediated endocytosis. However, against MDA-MB-231, TZ-Dend-DTX did not cause significantly increased cytotoxicity over Dend-DTX. The Viability of MDA-MB-231 cells after 48 h of treatment was 61.9, 59.3 and 60.9% for DTX, Dend-DTX and TZ-Dend-DTX, respectively (Figure 5.6b).

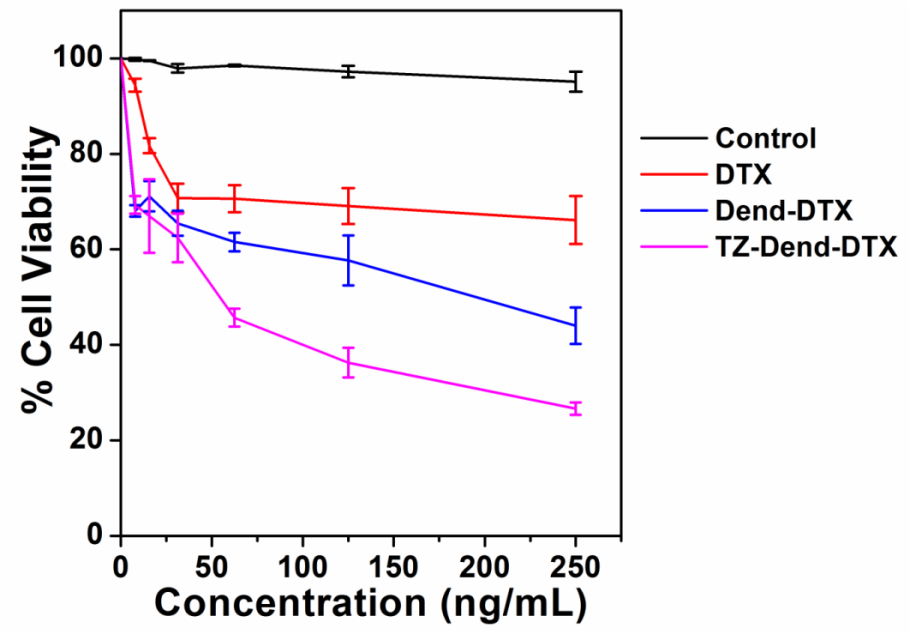

(a)

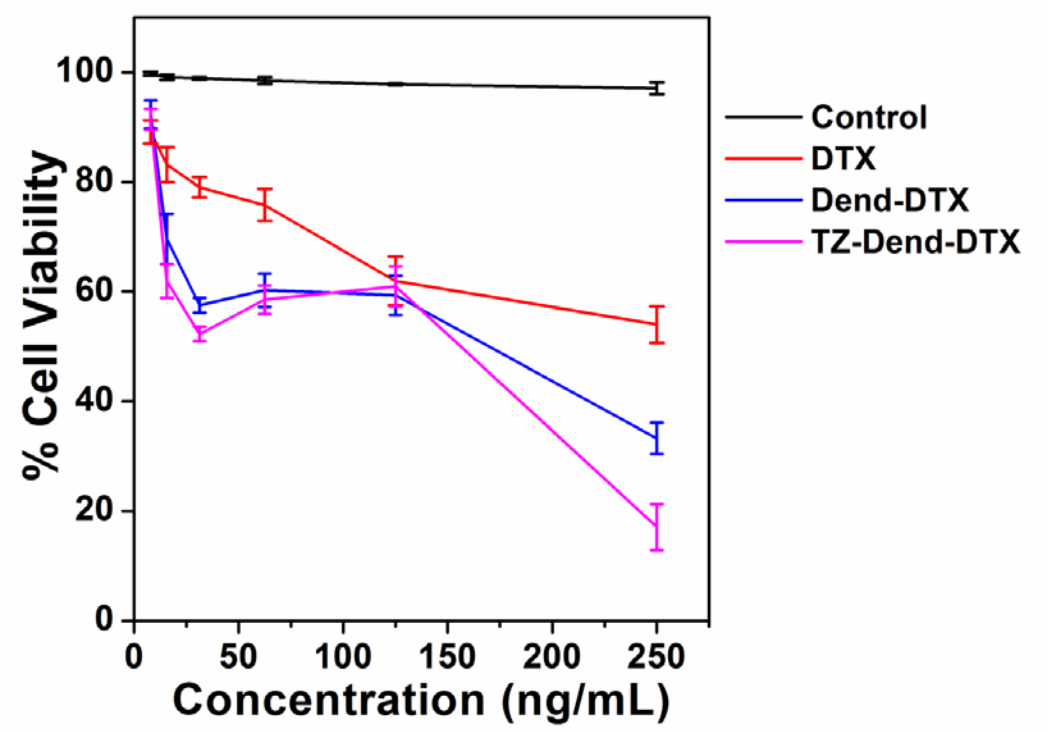

(b)

Figure 5.6: % Cell viability of a) HER$^+$ MDA-MB-453 human breast cancer cells and b) HER$^-$ human breast cancer cells MDA-MB-231 after 48 h incubation with varying concentrations of empty dendrimers (control), DTX, Dend-DTX and TZ-Dend-DTX

It was also noted that the different formulations caused dose-dependent decrease in the cell viability to both cell lines tested. Against MDA-MB-453 cells after 48 h treatment, the IC50 values for Dend-DTX and TZ-Dend-DTX were 201 ng/mL and 56.18 ng/mL, respectively. Therefore, TZ-Dend-DTX conjugate was 3.57 times more cytotoxic than unconjugated dendrimers. However, against HER2 negative MDA-MB-231 cells, the TZ-Dend-DTX conjugate did not show any increase in cytotoxicity compared to Dend-DTX. The IC50 value for Dend-DTX and TZ-Dend-TZ against MDA-MB-231 cells was 163.4 ng/mL and 149.5 ng/mL, respectively. These results demonstrate that TZ can specifically target and deliver DTX to HER2 positive tumor cells. After treatment with different DTX formulations, the changes in cell morphology of MDA-MB-453 cells are shown in Figure 5.7. Normal or untreated cells

formed loosely cohesive grape-like or stellate like structures and grew in a colony. Treated cells showed less colony formation and decrease in cell numbers.

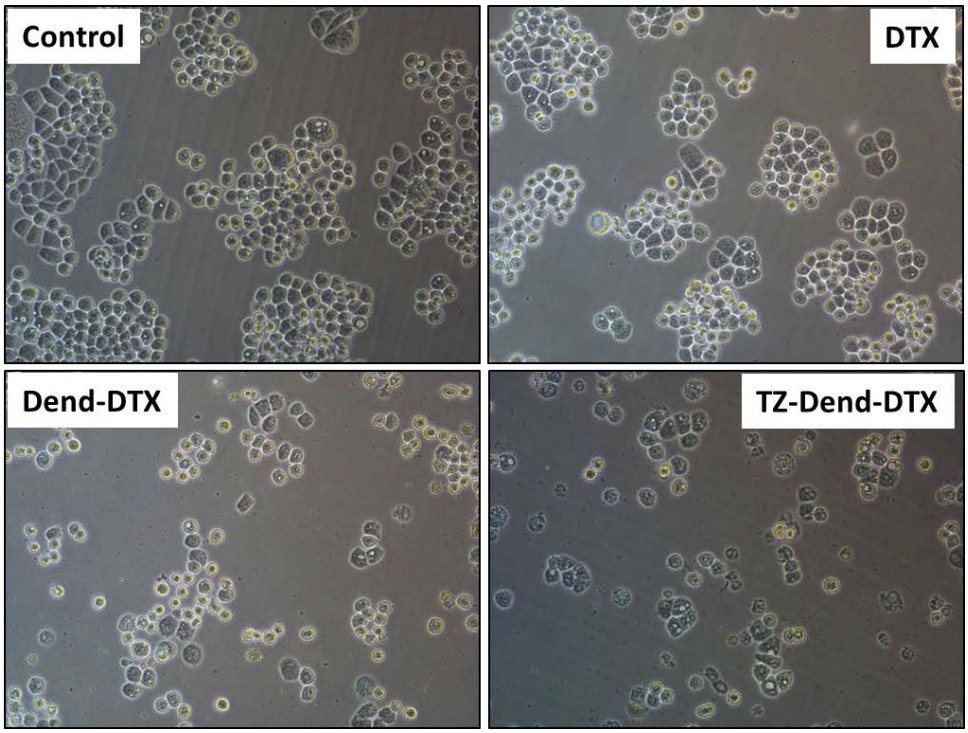

Figure 5.7: Cell morphology of HER$^+$ human breast cancer cells MDA-MB-453 after incubation with varying concentration of DTX, Dend-DTX and TZ-Dend-DTX for 24 h.

5.3.6. Cellular uptake of fluorescent dendrimer formulations

Cellular uptake studies are important tools to track internalization of fluorescent nanoparticles. Uptake of free FITC, Dend-FITC and TZ-Dend-FITC is shown in Figure 5.8. The fluorescent microscope images show that plain FITC was not taken up by the cells even after 4 h incubation, whereas fluorescence was detected in cells incubated with Dend-FITC and TZ-Dend-FITC after 1 h. Fluorescence intensity was significantly higher with TZ-Dend-FITC than Dend-FITC. The results were confirmed by quantitative analysis (Table 5.2). After 1 h of treatment, percentage uptake of free FITC, Dend-FITC and TZ-Dend-FITC was 1.6%, 11.4% and 23.5%, respectively. Dendrimer formulations also showed time-dependent uptake. After 4 h of incubation, uptake was increased to 34.2% and

57.9% for Dend-FITC and TZ-Dend-FITC, respectively. The increased uptake of TZ-Dend-FITC when compared to Dend-FITC, clearly demonstrates the contribution of TZ to the internalization of dendrimers.

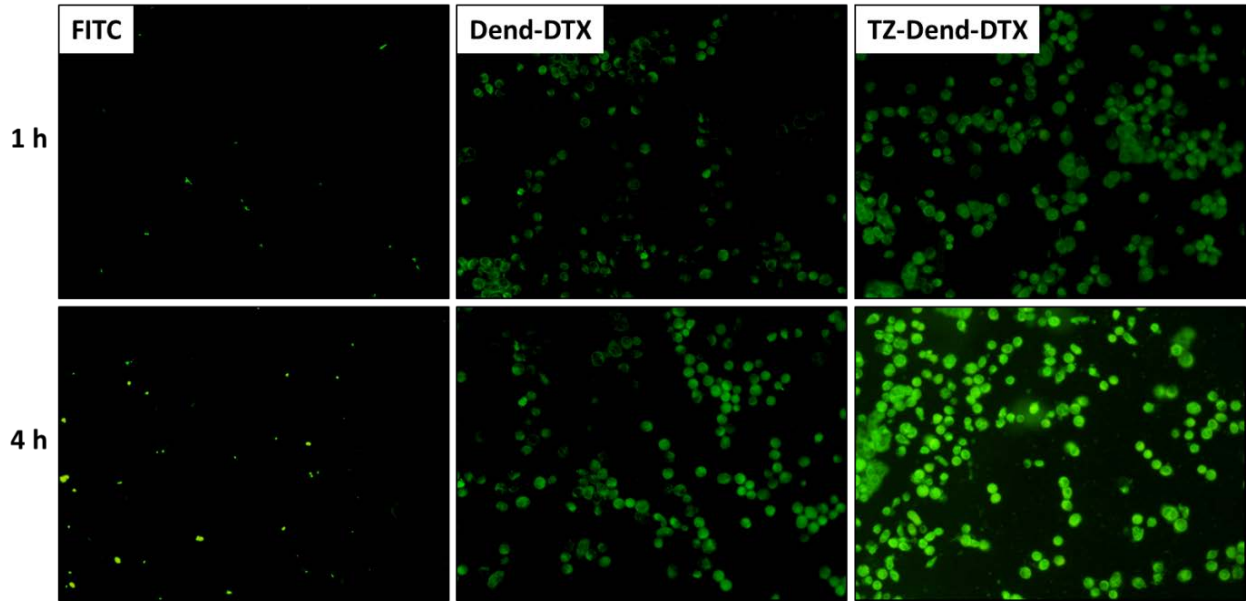

Figure 5.8: Fluorescent microscopic images of MDA-MB-453 human breast cancer cells incubated with free FITC, Dend-FITC and TZ-Dend-FITC for 1 and 4 h.

Table 5.2: Quantitative cellular uptake of free FITC, Dend-FITC and TZ-Dend-FITC by human MDA-MB-453 breast cancer cells after 1 and 4 h of incubation

Formulation	% Cell uptake after 1 h	% Cell uptake after 4 h
Free FITC	2.59 ± 0. 73	6.01 ± 0.48
Dend-FITC	11.28 ± 1.4	34.2 ± 1.95
TZ-Dend-FITC	23.49 ± 1.85	57.92 ± 2.71

5.3.7. AO/EB staining

AO stains both live and dead cells whereas EB stains only dead cells or the cells that have lost membrane integrity. Therefore, live cells appear as intense green colour while apoptotic and necrotic cells appear as orange colour. Figure 5.9 shows the fluorescent images of untreated MDA-MB-453 cells, cells treated with DTX,

Dend-DTX and TZ-Dend-DTX followed by AO/EB staining. Untreated cells showed evenly spread green color. Comparing the targeted and non-targeted dendrimers, cells treated with TZ-Dend-DTX showed enhanced apoptosis than with Dend-DTX.

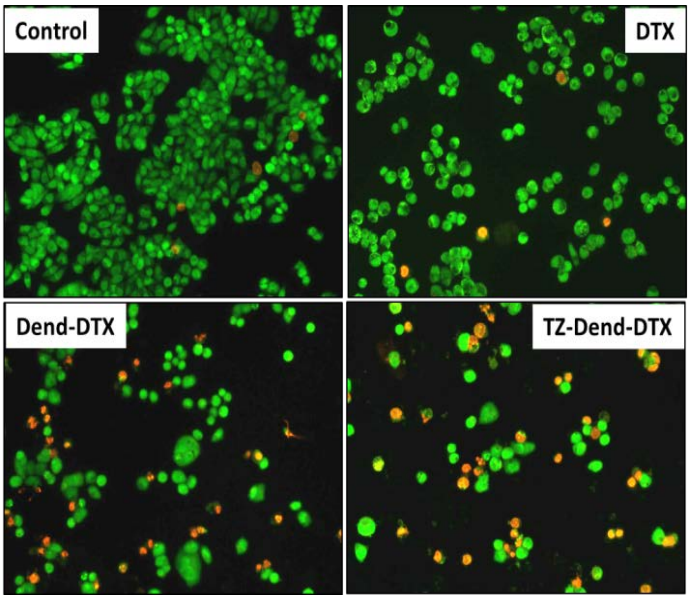

Figure 5.9: Fluorescent microscopic images of MDA-MB-453 human breast cancer cells incubated with free DTX, Dend-DTX and TZ-Dend-DTX for 24 h followed by staining with acridine orange and ethidium bromide

5.3.8. Annexin-V FITC/ PI assay

Quantitation of apoptosis induced by different DTX formulations were studied by Annexin-V FITC/ PI assay (Figure 5.10). A high percentage of live cells (94.8%) was observed in untreated cells. The percentage of live cells was decreased to 83% with Taxotere, 64.6% with Dend-DTX and 54.3% with TZ-Dend-DTX treatment. The data suggests TZ-Dend-DTX induced more apoptosis than unconjugated and Taxotere conjugated dendrimers. The total percentage of apoptotic cells was 42.5%, 32.6% and 16.4% with TZ-Dend-DTX, Dend-DTX and Taxotere, respectively. Higher levels of apoptosis with TZ-Dend-DTX compared to Dend-DTX treated cells can be attributed to more uptake and higher accumulation of DTX; thus leading to inhibition of cellular proliferation.

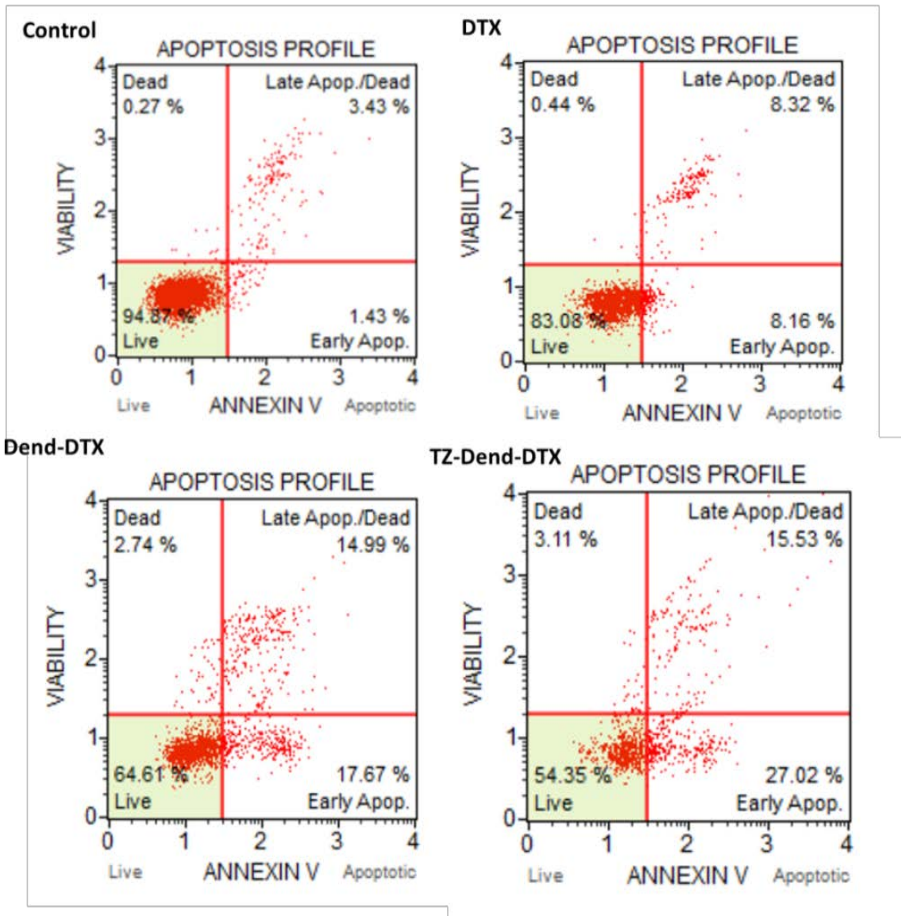

Figure 5.10: Quantification of apoptosis induced by free DTX, Dend-DTX and TZ-Dend-DTX using flow cytometer

5.3.9. Pharmacokinetic studies

Plasma-concentration profiles of DTX after intravenous injection of Taxotere, TZ-Dend-DTX and Dend-DTX are shown in shown in Figure 5.11 and correspond to the pharmacokinetic parameters presented in Table 5.3. Results suggest plasma pharmacokinetics of dendrimer formulations (TZ-Dend-DTX and Dend-DTX) were completely different from those of Taxotere. The area-under-the-curve ($AUC_{0-\infty}$) of TZ-Dend-DTX (271.6 µg.h/mL) and Dend-DTX (204.2 µg.h/mL) was approximately 4.7 and 3.5 times higher, respectively, than that of Taxotere (57.2 µg.h/mL). This could be explained by decreased clearance of DTX that is released from dendrimer-based formulations. The observed clearance values for Taxotere, Dend-DTX and TZ-Dend-DTX were 268.8, 48.9 (5.5 times less) and 36.8 mL/h (7.3 times less),

respectively. Mean residence time (MRT) increased approximately 3.4× and 2.5× for TZ-Dend-DTX and Dend-DTX, respectively.

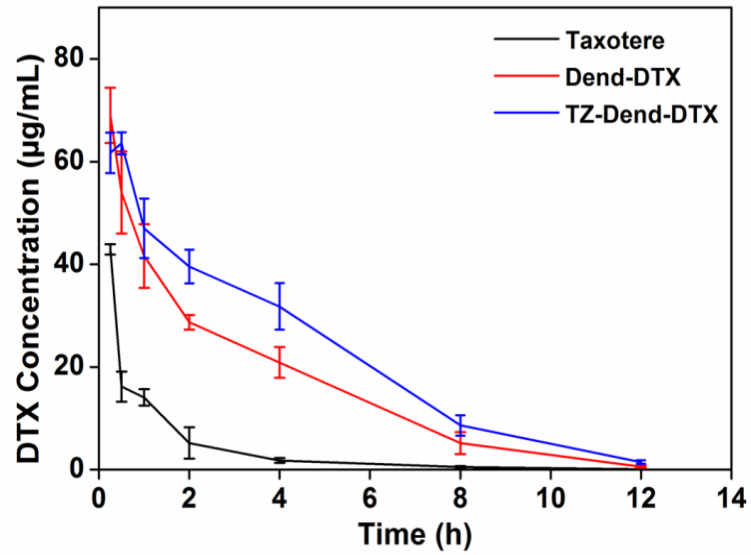

Figure 5.11: Pharmacokinetic profiles Taxotere, docetaxel loaded dendrimers (Dend-DTX) and Trastuzumab conjugated Dend-DTX (TZ-Dend-DTX) administered intravenously to Balb/c mice at a dose of 10 mg/Kg body weight.

Compared to unconjugated dendrimers, (Dend-DTX) and TZ-Dend-DTX induced significantly higher $AUC_{0-\infty}$ (271.6 versus 204.2, $p<0.005$), lower clearance (48.9 versus 36.8, $p<0.05$) and longer MRT values (6.85 versus 4.99; $p<0.05$). The differences between the two dendrimer formulations may be attributed to the presence of PEG-linkers and TZ on the surface of TZ-Dend-DTX. Polyethylene glycol (PEG) is a non-ionic hydrophilic polymer with an average molecular weight between 20 to 50 kDa. PEG is a well-documented molecule that could alter the pharmacokinetics of different nanocarrier systems (Zhu et al., 2010; Kim et al., 2009; Li et al., 2012; Zamboni et al., 2005). Being an antifouling molecule, PEG increases the circulation time of nanoparticles in the blood stream by delaying their capture by the reticulo-endothelial system. Additionally, TZ is a high molecular weight, clinically approved mAb (~ 145 KD), known for its high specificity for HER2 receptors (Raju et

al., 2013). It may therefore lengthen TZ-Dend-DTX circulation and slow release of DTX from conjugated dendrimers.

Table 5.3: Pharmacokinetic parameters for the three DTX formulations-Taxotere, DTX loaded dendrimers (Dend-DTX) and trastuzumab conjugated Dend-DTX (TZ-Dend-DTX)

PK Parameter	Taxotere	Dend-DTX	TZ-Dend-DTX
C_{max} (µg/mL)	42.7 ± 1.82	69.01 ± 4.38**	61.72 ± 3.92^{**,ns}
$T_{1/2}$ (h)	1.35 ± 0.21	1.99 ± 0.3*	3.24 ± 0.17$^{*,\#}$
Cl (mL/h)	268.81 ± 11.2	48.97 ± 5.65**	36.82 ± 4.06$^{**,\#}$
$AUC_{0-\infty}$	37.2 ± 2.94	204.16 ± 8.03***	271.58 ± 7.95$^{***, \#\#}$
MRT (h)	1.98 ± 0.08	4.99 ± 0.19**	6.85 ± 0.11$^{***,\#\#}$

C_{max}: peak plasma concentration; t1/2: terminal half-life; MRT: Mean residence time; Cl: Clearance; AUC: Area under the curve; MRT: Mean residence time

5.3.10. Stability studies

After 2 months of storage at 4 °C (specify), there was no sign of precipitation or significant change in consistency, zeta potential and drug content (Table 5.4).

Table 5.4: Physicochemical stability of TZ-Dend-DTX conjugate after 60 days of storage at refrigeration conditions (4 °C)

Parameter	Day 0	Day 60
Precipitation	No	No
Change in consistency	No	+
ZP (mV)	-2.3 ± 0.72	-3.89 ± 0.51
% DTX content	100	99.12

5.4. Conclusion

In summary, multifunctional TZ-conjugated dendrimers were synthesized using a heterocross-linker MAL-PEG-NHS and characterized by DLS, NMR and PAGE analysis. Targeted dendrimers selectively and specifically targeted DTX to HER2-positive breast cancer cells. Grafting TZ onto the surface of dendrimers could inhibit the growth of HER2-positive cancer cells, as demonstrated by our anti-proliferation and apoptosis studies. Furthermore, conjugation of TZ onto the surface of dendrimers decreased the hemolytic toxicity of unconjugated cationic PAMAM dendrimers and enhanced the circulation half-life of the conjugate. These findings could help to develop a better therapeutic profile for DTX and deliver better health outcomes for people with HER2-positive cancer.

5.5. References

- Bray F, Ren JS, Masuyer E, Ferlay J. Global estimates of cancer prevalence for 27 sites in the adult population in 2008. *Int J Cancer* 2013;**132(5)**:1133-45.
- Chauhan AS, Jain NK, Diwan PV. Solubility enhancement of indomethacin using dendrimer complex and bio-disposition profile of these complexes in arthritic rats. *J Drug Targeting* 2004;**12**:575–83.
- Domanski DM, Klajnert B, Bryszewska M. Influence of PAMAM dendrimers on human red blood cells. *Bioelectrochemistry* 2004;**63**:189-91.
- Feng S, Mei L, Anitha P, Gan CW, Zhou W. Poly(lactide)-vitamin E derivative/montmorillonite nanoparticle formulations for the oral delivery of docetaxel. *Biomaterials* 2009;**30**:3297-3306.
- Ferlay J, Soerjomataram I, Ervik M, Dikshit R, Eser S, Mathers C, Rebelo M, ParkinDM, Forman D, Bray F. GLOBOCAN 2012 v1.0, Cancer Incidence and Mortality Worldwide: IARCCancerBase No. 11 [Internet]. Lyon, France:

International Agency for Research on Cancer. 2012; Available at http://globocan.iarc.fr.

- Figueroa-Magalhaes MC, Jelovac D, Connolly RM, Wolff AC. Treatment of HER2-positive breast cancer. *The Breast* 2014;**23**:128-36.
- Gennari R, Menard S, Fagnoni F, Ponchio L, Scelsi M, Tagliabue E, Castiglioni F, Villani L, Magalotti C, Gibelli N, et al. Pilot study of the mechanism of action of preoperative trastuzumab in patients with primary operable breast tumors overexpressing HER2. *Clin Cancer Res* 2004;**10**:5650-5.
- Gschwind, Fischer OM, Ullrich A. The discovery of receptor tyrosine kinases: targets for cancer therapy. *Nat Rev Cancer* 2004;**4**:361-70.
- Holliday DL, Speirs V. Choosing the right cell line for breast cancer research. *Breast Cancer Research* 2011;**13(215)**:1-7.
- Isabel S, Birgit S, Klaus S, Klaus L. Trastuzumab-modified nanoparticles: optimization of preparation and uptake in cancer cells. *Biomaterials* 2006;27:4975-83.
- Kim C, Kim S, Oh WK, Choi M, Jang J. Efficient intracellular delivery of camptothecin by silica/titania hollow nanoparticles. *Chemistry* 2012;**18**:4902-8.
- Kim JY, Kim JK, Park JS, Byun Y, Kim CK. The use of PEGylated liposomes to prolong circulation lifetimes of tissue plasminogen activator. *Biomaterials* 2009;**30**:5751-6.
- Kulhari H, Pooja D, Prajapati SK, Chauhan AS. Performance evaluation of PAMAM dendrimer based simvastatin formulations. *Int J Pharm* 2011;**405**:203–9.
- Kulhari H, Kulhari DP, Prajapati SK, Chauhan AS. Pharmacokinetic and pharmacodynamic studies of poly(amido)amine dendrimer based simvastatin

oral formulations for the treatment of hypercholesterolemia. *Mol Pharm* 2013;**10**:2528-33.

- Kulhari H, Pooja D, Shrivastava S, Naidu VGM, Sistla R. Peptide conjugated polymeric nanoparticles as a carrier for targeted delivery of docetaxel. *Colloids Surf B* 2014;**117**:166-73.
- Kulhari H, Pooja D, Singh MK, Chauhan AS. Optimization of carboxylate-terminated poly(amidoamine) dendrimer-mediated cisplatin formulation. *Drug Dev Ind Pharm* 2013;1-7.
- Li A, Luehmann HP, Sun G, Samarajeewa S, Zou J, Zhang S, Zhang F, Welch MJ, Liu Y, Wooley KL. Synthesis and in vivo pharmacokinetic evaluation of degradable shell cross-linked polymer nanoparticles with poly(carboxybetaine) versus poly-(ethylene glycol) surface-grafted coatings. *ACS Nano* 2012;**6**:8970-82.
- Liu W, Xu J, Wu S, Liu Y, Yu X, et al. Selective anti-proliferation of HER2-positive breast cancer cells by anthocyanins identified by high-throughput screening. *PLoS ONE* 2013;**8(12)**: e81586.
- Miyano T, Wijagkanalan W, Kawakami S, Yamashita F, Hashida M. Anionic amino acid dendrimer-trastuzumab conjugates for specific internalization in HER2-positive cancer cells. *Mol Pharm* 2010;**7(4)**:1318-27.
- Moreno-Aspitia A, Perez EA. Treatment options for breast cancer Resistant to anthracycline and taxane. *Mayo Clinic Proceedings* 2009;**84**:533-45.
- Mosallaei N, Jaafari MR, Hanafi-Bojd MY, Golmohammadzadeh S, Malaekeh-NikoueiB. Docetaxel-loaded solid lipid nanoparticles: preparation, characterization, in vitro, and in vivo evaluations. *J Pharm Sci* 2013;**102(6)**:1994-2004.

- Pinto AC, Adesa F, de Azambuja E, Piccart-Gebhart M. Trastuzumab for patients with HER2 positive breast cancer: Delivery, duration and combination therapies. *The Breast* 2013;**22**:S152-55.
- Raju A, Muthu MS, Feng SS. Trastuzumab-conjugated vitamin E TPGS liposomes for sustained and targeted delivery of docetaxel. Ex*pert Opin Drug Deliv* 2013;**10(6)**:747-60.
- Senkusa E, Cardosob F, Pagani O. Time for more optimism in metastatic breast cancer? *Cancer Treatment Reviews* 2014;**40**:220-8.
- Shukla R, Thomas TP, Desai AM, Kotlyar A, Park SJ, Baker Jr JR. HER2 specific delivery of methotrexate by dendrimer conjugated anti-HER2 mAb. *Nanotechnology* 2008;**19**: 1-7.
- Yellepeddi VK, Pisal DS, Kumar A, Kaushik RS, Hildreth MB, Guan X, Palakurthi S. Permeability of surface modified polyamidoamine (PAMAM) dendrimers across Caco-2 cell monolayers. *Int J Pharm* 2008;**350**:113-21.
- Yousefpour P, Atyabi F, Vasheghani-Farahani E, Movahedi AAM, Dinarvand R. Targeted delivery of doxorubicin-utilizing chitosan nanoparticles surface-functionalized with anti-Her2 trastuzumab. *Int J Nanomed* 2011;**6**:1977-90.
- Zamboni WC. Liposomal, nanoparticle, and conjugated formulations of anticancer agents. *Clin Cancer Res* 2005;11:8230-4.
- Zhao P, Astruc D. Docetaxel nanotechnology in anticancer therapy. *ChemMedChem* 2012;**7(6)**:952-72.
- Zhu S, Hong M, Tang G, Qian L, Lin J, Jiang Y, Pei Y. Partly PEGylated polyamidoamine dendrimer for tumor-selective targeting of doxorubicin: the effects of PEGylation degree and drug conjugation style. *Biomaterials* 2010;31:1360-71.

CHAPTER

Cyclic-RGDfK peptide conjugated succinoyl-TPGS nanomicelles for targeted delivery of docetaxel to integrin receptor over-expressing angiogenic tumours

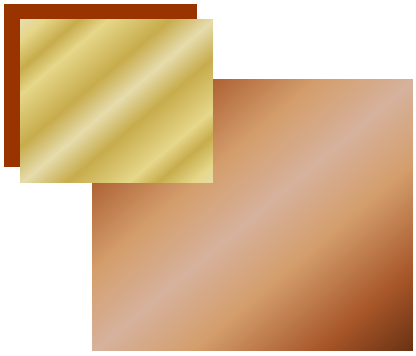

6.1. Background

Targeting angiogenesis is a strategy to better control tumour growth and metastasis (Zhaofei et al., 2008). Angiogenesis involves the formation of new blood vessels from pre-existing vessels and thus promotes tumor growth and metastasis. Angiogenesis is stimulated by hypoxia that causes up-regulation of proangiogenic proteins such as vascular endothelial growth factor, fibroblast growth factor, Ron, platelet derived growth factor, tumour necrosis factor-α and integrins (Thobe et al., 2010; Danhier et al., 2012; Carmeliet and Jain, 2000).

Among these, integrins are cell adhesion receptors which are over expressed on endothelial cells and tumour cells but poorly expressed in resting endothelial cells and normal tissues. Integrins expression in tumour cells promotes tumour progression and metastasis by increasing tumour cell migration, invasion, proliferation and survival. Thus, targeting a drug to integrin receptors can increase specificity and reduce the systemic toxicities of anticancer drugs (Danhier et al., 2012; Desgrosellier and Cheresh).

Among all integrins, $\alpha_v\beta_3$ is one of the most commonly involved integrins in the regulation of angiogenesis. It is over expressed in various cancers including breast, prostate, pancreatic and brain cancer. The RGD (Arg-Gly-Asp) based peptides, in general, have shown significant affinity towards integrin receptors. There is an increasing emphasis on employing cyclic RGD peptides for the development of targeted drug delivery systems because they are more stable, potent and specific than linear RGD peptides, which are otherwise highly susceptible to chemical degradation (Arosio et al., 2012). cRGDfK peptide has high specificity in particular towards $\alpha_v\beta_3$ integrin receptors making it a desirable targeting ligand for drug delivery applications (Danhier et al., 2012).

Docetaxel (DTX) is the semi-synthetic derivative of 10-deacetylbaccatin-III and widely used either alone or in combination with other drugs to treat breast, ovarian, prostate, non-small cell lung cancer, gastric and neck cancer (Zhao P, Astruc, 2012; Zhang and Zhang, 2013). The clinical application of DTX is limited owing to not only its poor aqueous solubility and low oral bioavailability (Cho et al., 2008), but also due to its intolerable side effects such as acute hypersensitivity reactions, fluid retention, neurotoxicity, and febrile neutropenia (Zhang and Zhang, 2013; Baker et al., 2009).

The use of nanocarrier-based drug delivery systems for anticancer drugs combines the advantages of passive and active targeting by enhancing permeability and retention, the EPR effect, avoidance of the reticulo-endothelial system, prolonged blood circulation time, controlled release of drug and providing an opportunity for surface modification for active drug targeting (Sultana et al., 2013; Farrell et al., 2011; Kulhari et al., 2015; Feng and Mumper, 2013).

D-α-tocopheryl polyethylene glycol succinate (TPGS or Vit E TPGS) is a water soluble derivative of natural D-α-tocopherol (Vit E). It is synthesized by the esterification of Vit E succinate with polyethylene glycol. TPGS is amphiphilic in nature with a hydrophilic-lipophilic balance (HLB) value of 13.2 that allows micelle formation above 0.02% w/w concentration. A HLB value indicates the relationship of the hydrophobic and hydrophilic groups of the surfactant. High HLB value means that the surfactant contains more hydrophilic groups and is soluble in water whereas a low HLB value represents lipophilicity of the surfactant. Compounds having HLB value in a range of 13-15 are categorized as detergents (Hait and Moulik, 2001). At a particular concentration, called as critical micellar concentration (CMC), these compounds self-aggregates in a defined orientation and form micelles. In an

aqueous system, micelles are arranged with an interior hydrophobic core and outer hydrophilic surface. Below CMC, surfactants enhance the aqueous solubility of poorly water soluble drugs by providing regions for hydrophobic drug interactions in solution. Above the CMC, drug is encapsulated in the hydrophobic core of the micelles resulting in to enhanced solubility (Narang et al., 2007). With a polar hydrophilic head (polyethylene glycol 1000) and a lipophilic tail (phytyl chain of d-α-tocopherol), TPGS has the HLB value about 13.2 and has been widely used as a solubiliser, emulsifier, and to enhance permeability and bioavailability. Several drug delivery systems have been developed using TPGS after it was approved by the FDA as pharmaceutically safe adjuvant (Sun and Feng, 2009; Raju et al., 2013; Muthu et al., 2012; Guo et al., 2013; Zhang et al., 2012; Mi et al., 2012; Pandey et al., 2013, Cao et al., 2008). Such TPGS-based engineered nanocarrier systems have been shown to transport and deliver anticancer drugs more efficiently than drug alone.

Notably, although TPGS nanomicelles and cRGDfK peptides have been independently employed for drug-delivery applications (Kutty et al., 2013; Zhu et al., 2014; Zhao et al., 2014; Wang et al., 2012; Graf et al., 2012), cyclic peptide (cRGDfK)-conjugated succinoyl TPGS nanomicelles have not been hitherto explored for their potential to target delivery of anticancer drugs to prostate cancer. The aim of this study was to successfully develop cRGDfK-conjugated succinoyl-TPGS nanomicelles for the targeted delivery of DTX in prostate cancer treatment.

6.2. Experimentation

6.2.1. Materials

TPGS, succinic anhydride (SA) and coumarin were purchased from Sigma Aldrich, (St. Louis, MO, USA). DTX was kindly provided by TherDose Pharma Pvt.

Ltd. (Hyderabad, India). Cyclic RGDfK was purchased from Peptide International (Kentucky, USA). Nylon membrane filters of pore size 0.22 µm were procured from Pall India Pvt. Ltd. (Mumbai, India). Human prostate cancer cell line (DU145) was obtained from American Type Culture Collection (ATCC) (Manassas, VA, USA). DMEM, Dulbecco's phosphate buffered saline (DPBS), fetal bovine serum (FBS) trypsin–EDTA, antibiotic anti-mycotic solution, phosphate buffered saline (Ca^{2+}, Mg^{2+} free), MTT and dimethyl sulfoxide (DMSO) were purchased from Sigma Aldrich, (St. Louis, MO, USA). Human umbilical vein endothelial cells (HUVECs) and EBM-2 media were purchased from Lonza (USA). Cell culture plastic wares were purchased from Tarson Ltd (Mumbai, India). All other chemicals were of analytical grade and used as received unless otherwise specified.

6.2.2. Synthesis and Characterization of Succinoyal-TPGS (TPSA)

TPGS was functionalized with a free carboxylic group by reaction with succinic anhydride. TPGS (200 mg), SA (13.2 mg) and 4-(Dimethylamino)pyridine (43.1 mg) were mixed in 20 mL of dichloromethane and stirred for 24 h at room temperature under strict anhydrous conditions. The reaction mixture was washed thrice with saturated NaCl aqueous solution. The organic layer was separated and dried with Na_2SO_4. The solvent was evaporated by rotary evaporation and lyophilized to remove traces of water. The activated TPGS was confirmed by proton nuclear magnetic resonance (^{1}HNMR), FTIR and mass analysis. For ^{1}HNMR analysis, samples were dissolved in $CDCl_3$ and scanned using Avance500 NMR. The presence of free carboxylic groups in TPSA was confirmed by FTIR analysis. The lyophilized TPSA was mixed with KBr, palletized and scanned for transmittance using a FTIR spectrophotometer (Perkin Elmer, Spectrum one) in the wave number range 4000 to 450 cm^{-1}.

6.2.3. Determination of Critical Micellar Concentration (CMC)

The CMC value of TPSA was determined by dynamic light scattering (DLS) using a Malvern Zetasizer Nano ZS (Malvern instrument Ltd., Malvern, UK). Different sample concentrations were prepared and particle diameter and intensity measured. Particle size and intensity were plotted against log concentration of sample. The concentration at which sharp changes in intensity or size appeared was considered the CMC.

6.2.4. Preparation and characterization of DTX loaded TPSA nanomicelles (DNM)

TPSA (50 mg) and DTX (2.5 mg) were dissolved in methanol (1 mL) and added to 5 mL of MilliQ water. The solution was kept stirring overnight in an open, round bottom flask to evaporate methanol. The excess or precipitated DTX was removed by filtration through a 0.22 µm filter and the filtrate used for further studies. For the preparation of FITC loaded fluorescent nanomicelles (FNM), FITC was dissolved in 0.2 mL acetone and mixed with TPSA solution without DTX.

The particle diameter and zeta potential of DNM were determined by DLS using a Zetasizer Nano-ZS. The samples were analyzed at 25 ºC with a backscattering angle of 173º. Thermal characteristics of pure DTX, TPSA and DNM were evaluated using DSC-Q100 (TA Instruments, USA). The samples were scanned from 25 ºC to 200 ºC at a speed of 10 ºC/min, under nitrogen environment. X-ray diffraction patterns of DTX, TPSA and DNM were obtained using an X-ray diffractometer (D8 Advance, Bruker, Germany) equipped with a Cu-Kα X-ray radiation source. The instrument was set at 40 KV and 30 mA and the diffraction angle (2θ) was measured at 2º to 60º. DTX content was determined by validated HPLC method. Encapsulation efficiency (EE) was calculated as follows:

% EE = (amount of drug present in nanomicelles / initial amount of drug added to the formulation) × 100

6.2.5. Bioconjugation of cRGDfK on the surface of DNM

Lyophilized DNM/FNM was dispersed in 0.5 mL phosphate buffer saline pH 7.4 (PBS) and incubated with 0.2 mL each of 0.1M EDC and 0.1M NHS for 30 min at room temperature with gentle stirring. The cRGDfK was dissolved in 0.3 mL PBS, added to the reaction mixture and stirred for another 2 h at room temperature. The cRGDfK-conjugated DNM (PDNM) and cRGDfK-conjugated FNM (PFNM) were purified by dialysis against a saturated solution of DTX or FITC.

cRGDfK conjugation onto the DNM surface was characterized by FTIR analysis. The FTIR spectra of PDNM, DNM and cRGDfK were obtained using a FTIR spectrophotometer (Perkin Elmer, Spectrum One, USA) in the wave number range of 4000 to 450 cm^{-1}.

6.2.6. In vitro drug release studies

In vitro release of DTX from peptide conjugated nanomicelles was studied in plasma, PBS, pH 7.4 and SAB, pH 5.0. A volume of PDNM equivalent to 1 mg DTX was placed in dialysis tubing and tubing incubated in 75 mL of release media. The release medium temperature was maintained at 37 ± 0.5 °C and stirred magnetically at 100 rpm. At predetermined time intervals, a 1 mL sample of release media was withdrawn and replaced with the same volume of fresh medium to maintain sink conditions and a constant volume of external release medium. The sample was filtered through a 0.22 µm nylon filter and analyzed for DTX content using HPLC.

6.2.7. Cell culture

DU145 prostate cancer cells were grown as an adherent layer in RPMI medium supplemented with 10% fetal bovine serum, 100 µg/mL penicillin, 200

µg/mL streptomycin and 2 mM L-glutamine. The culture was maintained at 37 °C in a humidified atmosphere with 5% CO_2. Dilutions were made with sterile PBS to the required concentration. Formulations were filtered with 0.22 µm sterile filter before adding to wells containing cells. HUVECs were cultured in complete EBM-2 media containing 5% FBS and maintained at 37 °C humidified incubator with 5% CO_2.

6.2.8. Cell proliferation assay

The MTT assay was used to determine the anti-cytoproliferative activity of different docetaxel formulations. About 1×10^4 cells (counted by Trypan blue exclusion dye method) per well were seeded in culture media in a 96 well plate and allowed to attach for 24 h. The cultured cells were then incubated with varying concentrations (7.8-500 ng/mL) of DTX, DNM and PDNM. After 24, 48 and 72 h incubation, the media was replaced with 90 µL of fresh serum free media and 10 µl of MTT reagent (5 mg/mL) and plates incubated at 37 ºC for 4 h, there after the above media was replaced with 200 µL of DMSO and incubated at 37 ºC for 10 min. The absorbance at 570 nm was measured on a spectrophotometer (Spectra max, Molecular Devices). The half maximum inhibitory concentration (IC50) values were determined. Cytotoxicity tests were repeated three times and data are expressed as mean and standard deviation of three replicates.

6.2.9. Cellular uptake of unconjugated and peptide conjugated fluorescent nanomicelles

Coumarin, a fluorescent compound, was loaded in nanomicelles to facilitate cell-uptake studies. Coumarin-loaded unconjugated and cRGDfK peptide conjugated nanomicelles are annotated as FNM and PFNM, respectively. About 5×10^4 cells were seeded in 24-wells plate and allowed to attach for 24 h. Cells were then exposed to 50 µl of Coumarin, FNM, and PFNM formulations and incubated for intervals of 1, 3, 6, 12 and 24 h. The culture media was removed, cells washed twice

with cold PBS, and fluorescence photographs taken with a digital camera (Nikon, Inc. Japan) at 200X magnification.

6.2.10. Assessment of cell morphology

Cells (1×10^6 cells/well) were grown in 24 well plates and treated with DTX, DNM and PDNM at concentration of 60 ng/mL (IC50 of PDNM) for 48 h. Morphological changes were observed with an inverted phase contrast microscope (Model: Nikon, Japan) and photographs taken with a digital camera (Nikon, Inc. Japan) at 200X magnification. Acridine orange/ethidium bromide (AO/EB) staining procedure was followed to differentiate live, apoptotic and necrotic cells. Briefly, treated or untreated cells were stained with AO (10 µg/mL) and EB (10 µg/mL) and analyzed with a fluorescence microscope with excitation (488 nm) and emission (550 nm) and 200X magnification.

6.2.11. Apoptosis studies

Cells were seeded in 6 well plates at a density of 3×10^6 cells per well and incubated overnight at 37 °C in a humidified atmosphere and 5% CO_2. Next day, DTX, DNM or PDNM (equivalent to 60 ng/mL of DTX) was added and cells incubated for another 48 h. Then cells were analyzed by a Muse™ Cell Analyzer (Merck-Millipore, Germany) according to the manufacturer instructions using Muse™Annexin-V and Dead Cell reagent (Merck-Millipore, Germany). Apoptosis and necrosis were analyzed with quadrant statistics on propidium iodide-negative cells, fluorescein positive cells and propidium iodide (PI)-positive cells, respectively.

6.2.12. Anti-angiogenic activity

Anti-angiogenic activity of DTX, DNM and PDNM was studied by two assays, namely cell viability assay and scratch wound directional migration assay using HUVEC cells. Cell viability assay was carried out in the presence of VEGF.

6.2.12.1. Endothelial cell proliferation assay

HUVEC cells (1 × 10^4 cells/well) were seeded into 96-wells cell culture plate for 24 h. Next day, the cells were starved with EBM-2 media containing 0.2% FBS for 8 h. Cells were then incubated with different materials at various concentrations for 24 h. After discarding the old media, fresh MTT solution (0.5 mg/mL) was added to each well and the plate was kept at 37 °C for 4 h. Media in each well was then replaced with DMSO-methanol mixture (1:1; v/v) to solubilise the purple formazan dye. Absorbance of the purple solution was measured using a multimode reader (Biotek Synergy) at 570 nm.

6.2.12.2. Scratch wound directional migration assay

HUVEC cells (4 ×10^4 cells/mL) were seeded in 24-wells plate for 24 h. The monolayers were then scratched with a sterile micro-tip. Cells were thoroughly washed with DPBS and incubated with different materials for up to 24 h. Phase images of cells were captured using a bright field microscope at different time points (0 h, 8 h and 24 h). The % of wound closure was calculated by measuring the wound area using Image J analysis software.

6.2.13. Stability Studies

The PDNM was stored at 2-8 °C and change in particle size, zeta potential and drug content were measured for up to 2 months.

6.2.14. Statistical analysis

The studies were performed in triplicate and results expressed as mean along with standard deviation (SD). Statistical significance was analysed using student t-test for two groups and one way ANOVA for multiple groups. P values of < 0.05 were considered significant.

6.3. Results and discussion

6.3.1. Synthesis and characterization of Succinoyl-TPGS (TPSA)

Carboxylic group functionalized succinoyl-TPGS (TPSA) was prepared by a ring opening reaction with succinic anhydride (Scheme 1). The activated TPGS showed two important characteristic ^{1}HNMR signals- one at 2.4 ppm assigned to succinoyl methylene (-CH_2) protons and a second at 3.6 ppm assigned to the –CH_2– protons of PEG moiety in TPGS (Figure 6.1) (Cao and Feng, 2008). The FTIR spectra of SA showed two sharp peaks at 1863 and 1784 cm^{-1} that are characteristic of cyclic anhydride group. However, in FTIR spectra of TPSA, we observed a new peak at 1735 cm^{-1} (characteristic –COOH group peak) instead of these peaks. The absence of cyclic anhydride group peaks and appearance of a characteristic –COOH group peak at 1735 cm^{-1} confirmed successful ring opening of SA and then functionalization of TPGS (Figure 6.2).

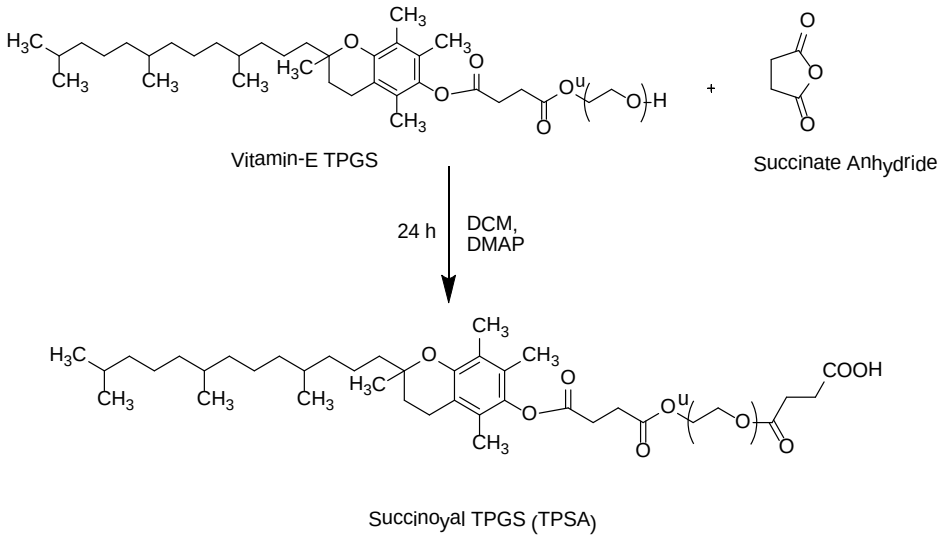

Scheme 6.1: Chemical synthesis of succinoyl TPGS (TPSA) by a ring opening reaction between Vit-E TPGS and succinic anhydride

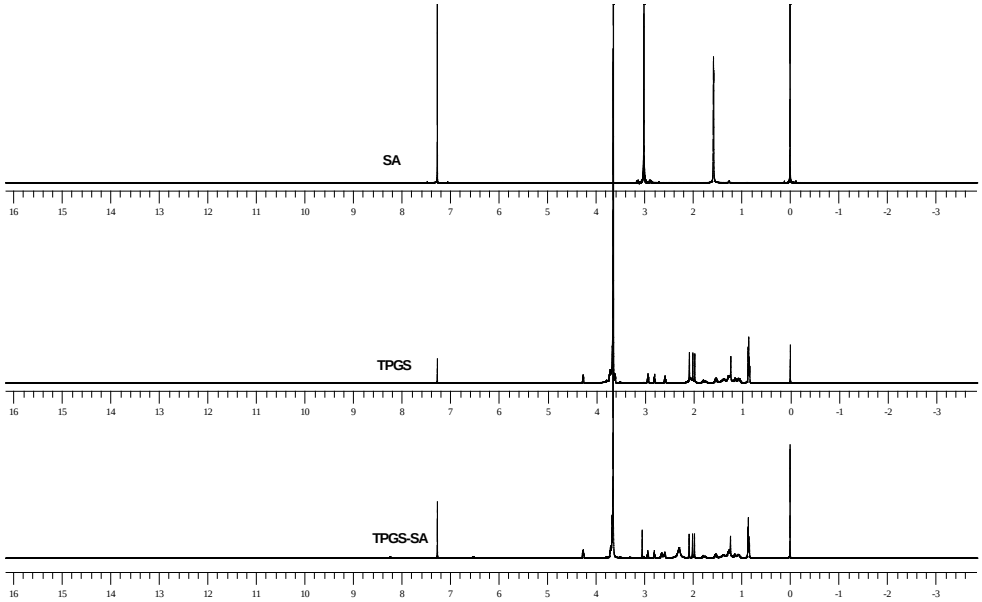

Figure 6.1: ^{1}H NMR spectra of stearic acid (SA), TPGS and stearic acid modified TPGS (TPSA)

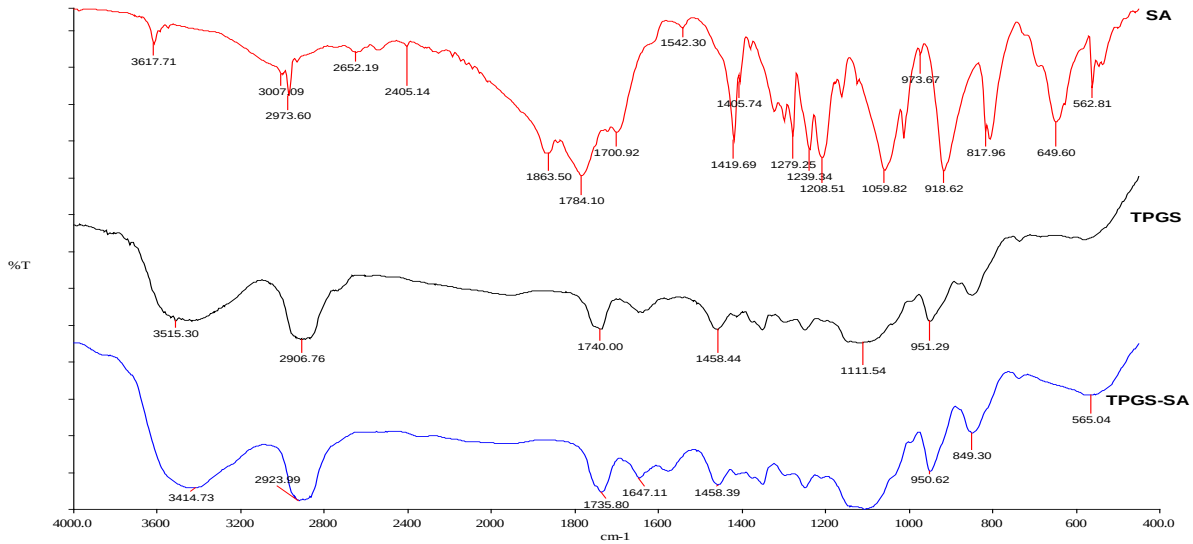

Figure 6.2: FTIR spectra of stearic acid (SA), D-α-tocopheryl polyethylene glycol succinate (TPGS) and SA functionalized TPGS (TPGS-SA)

6.3.2. Preparation and characterization of different nanomicelles

For surfactant molecules, the CMC value is an important parameter for determination of surface activity. TPSA is an amphiphile where its tocopherol part serves as a lipophilic tail, while polyethylene glycol serves as a polar head. The CMC value of TPSA was determined using the DLS technique and found to be 0.008%. A significant ($p<0.05$) decrease in CMC value of TPSA compared to TPGS (0.02%) could be attributed to surface modification of the stearate moiety to more a hydrophilic acid derivative. The lower CMC value indicated the high stability of TPSA. Determination of the CMC value for TPSA allowed simple synthesis of nanomicelles.

DTX-loaded TPSA nanomicelles (DNM) were prepared by the solvent loading and evaporation (SLE) method. In this method, DTX and TPSA were dissolved in methanol and added to the aqueous phase. However, to allow nanomicelle formation, the concentration of TPSA was kept higher than its CMC value (0.008%). As the methanol evaporated, excess DTX precipitated and after complete methanol evaporation (as determined by the total volume of the formulation) removed by filtration. Blank nanomicelles (BNM) were prepared without DTX. Coumarin-loaded fluorescent nanomicelles (FNM) were also prepared for cellular uptake studies. Coumarin was dissolved in acetone, mixed with TPSA methanol solution and then added to the water. The drug entrapment efficiencies of DNM and PDNM were found to be 79.55±2.98 and 73.42±1.54%, respectively.

The prepared nanomicelles were characterized by particle size, polydispersity, surface potential, DSC, XRD and FTIR analysis. Observed particle diameters and zeta potentials of different formulations are shown in Table 6.1. All the formulations exhibited very small sizes, ranging from 22.41 to 30.26 nm and with

narrow distribution (PDI< 0.25). Peptide conjugated formulations showed reduction in negative zeta potential values from those of unconjugated formulations, indicating the presence of cationic peptide on the surface. The zeta potential values for PDNM and PFNM were -10.3±1.5 and -13.3±2.2 mV, respectively, while these were 19.7±2.6 mV for DNM and -14.3±2.2 mV for FNM.

Table 6.1: Physicochemical characterization of various nanomicelles formulations (Mean ± SD, n=3)

Formulation	Particle Diameter (nm)	Polydispersity Index	Zeta potential (mV)	Entrapment efficiency (%)	Peptide conjugation efficiency (%)
BNM	23.80±0.56	0.21±0.016	-25.5±1.2	-	-
DNM	27.92±0.85	0.14±0.019	-19.7±2.6	79.55±2.98	-
PDNM	30.26±0.48	0.18±0.022	-10.3±1.5	73.42±1.54	84.21±2.59
FNM	22.41±0.73	0.22±0.038	-22.6±1.4	89.56±3.65	-
PFNM	26.95±1.06	0.23±0.027	-14.3±2.2	87.63±2.90	82.98±1.76

BNM: Blank nanomicelles; DNM: Docetaxel loaded nanomicelles; PDNM: cRGDfK peptide conjugated and docetaxel loaded nanomicelles; FNM: Coumarin loaded nanomicelles; PFNM: cRGDfK peptide conjugated and Coumarin loaded nanomicelles.

Nanomicelles showed high encapsulation efficiency (Table 6.1). The EE of 57.76% was considerably higher than that reported by Muthu et al, 2012. Increased EE of DNM can be attributed to the altered method of micelle preparation and to the functional group modification of TPGS. cRGDfK conjugation to nanomicelle surfaces was determined by the Bradford assay. The conjugation efficiencies were 84.21±2.59% and 82.98±1.76% for PDNM and PFNM, respectively. Bioconjugation of cRGDfK to the surface of DNM was confirmed by FTIR analysis (Figure 6.3). FTIR spectra of free DTX showed absorption bands of O-H at 3480 cm^{-1}, C=O stretching of ester group at 1741 cm^{-1} and a band corresponding to C-O band at 1109 cm^{-1}.

The C=O stretching of the carboxylic acid group of TPSA appeared at 1736 cm^{-1}. This carbonyl band disappeared from the spectra of PDNM and a new peak appeared at 1644 cm^{-1}, corresponding to C=O stretching of the amide bond formed between the -COOH group of DNM and the -NH_2 group of cRGDfK.

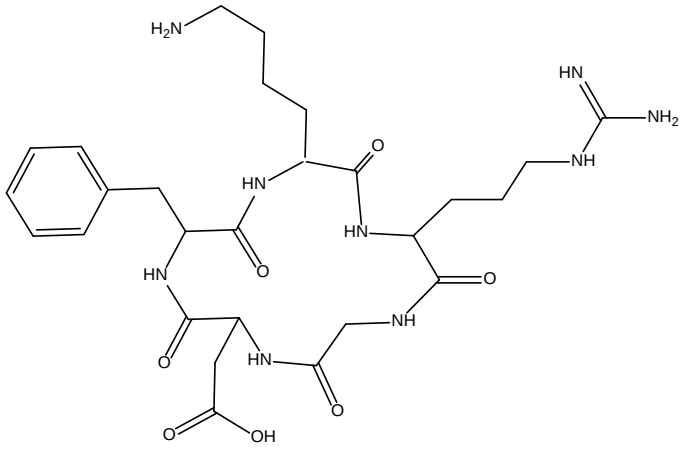

a)

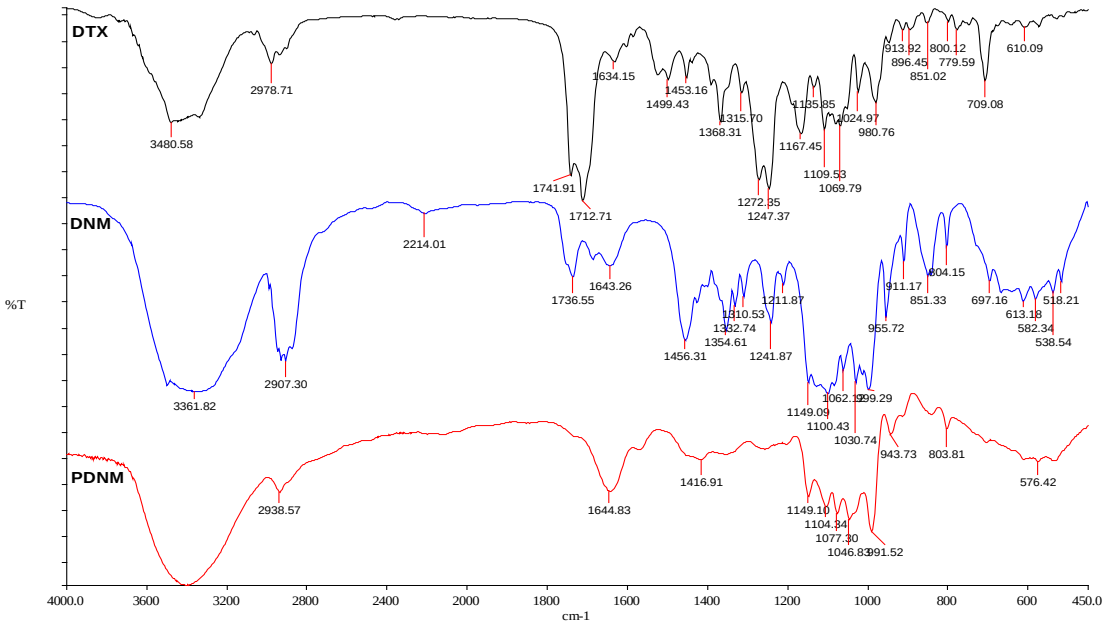

b)

Figure 6.3a-b: a) Chemical structure of Cyclo(Arg-Gly-Asp-D-Phe-Lys) (cRGDfK) b) FTIR spectra of docetaxel (DTX), DTX loaded nanomicelles (DNM) and cRGDfK peptide conjugated DNM (PDNM)

The thermal behaviour of pure DTX, TPSA and DNM was investigated by DSC analysis (Figure 6.4). DSC scanning of pure DTX showed sharp endothermic transition at 176 °C corresponding to its melting point. TPSA demonstrated the characteristic endothermic peak of TPGS at 38 °C. Therefore, surface group modification did not change the melting point of TPGS. The thermogram of DNM showed only the peak of TPSA at 36.5 °C. Absence of a DTX peak in the DSC spectra of DNM indicates phase transition of pure DTX from crystalline to amorphous, disordered crystalline or solid states. Such phase transformation of DTX has been observed in other nanocarrier systems (Kulhari et al., 2014; Roy et al., 2014).

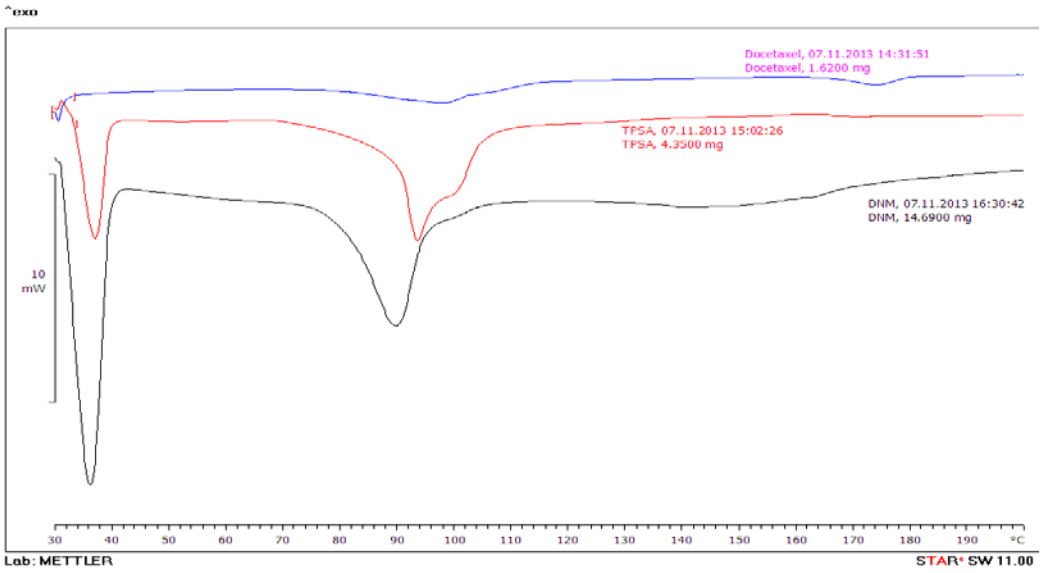

Figure 6.4: DSC spectra of docetaxel (DTX), TPSA and DTX loaded TPSA nanomicelles (DNM)

Figure 6.5 displays powder XRD patterns of DTX, TPSA and DNM. Native DTX spectra showed sharp peaks at 2θ angles at 5, 8.7, 9.8, 10.3, 11.5, 13.9 and at 16° showing the crystalline nature of DTX. These characteristic peaks of DTX were

absent in the DNM XRD pattern which instead showed peaks only at 19° and 23° corresponding to TPSA. Sharp and characteristic peaks of DTX were not observed in DNM spectra which suggest that during encapsulation DTX was transformed to the amorphous form.

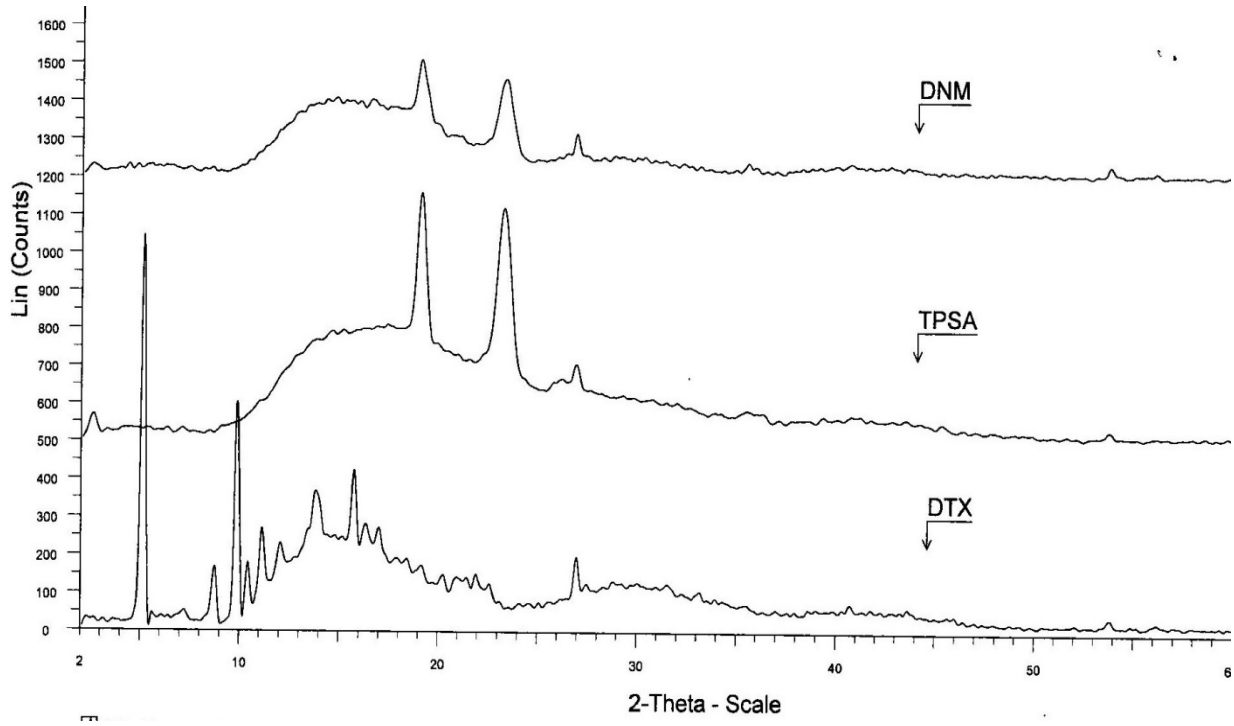

Figure 6.5: Powder XRD spectra of docetaxel (DTX), TPSA and DTX loaded TPSA nanomicelles

6.3.3. In vitro drug release studies

For the determination of the effect of pH and media on the release of DTX from nanomicelles, formulations were exposed to three different media—PBS pH 7.4, SAB pH 5 and plasma. Here, PBS represents the neutral to slightly alkaline pH of blood while SAB represents the acidic pH of cancer cells. The release of DTX from PDNM was faster in SAB than plasma and PBS (Figure 6.6). In SAB, 99.48% of encapsulated DTX was released within 48 h. However, about 70.53% and 76.9% of drug was released in PBS and plasma respectively, after 72 h. Drug release was faster at acidic pH (SAB pH 5). The slower drug release in plasma and faster release

in SAB would help to would enhance the therapeutic efficacy of the formulation. There was statistically no difference in the drug release rates in PBS and plasma.

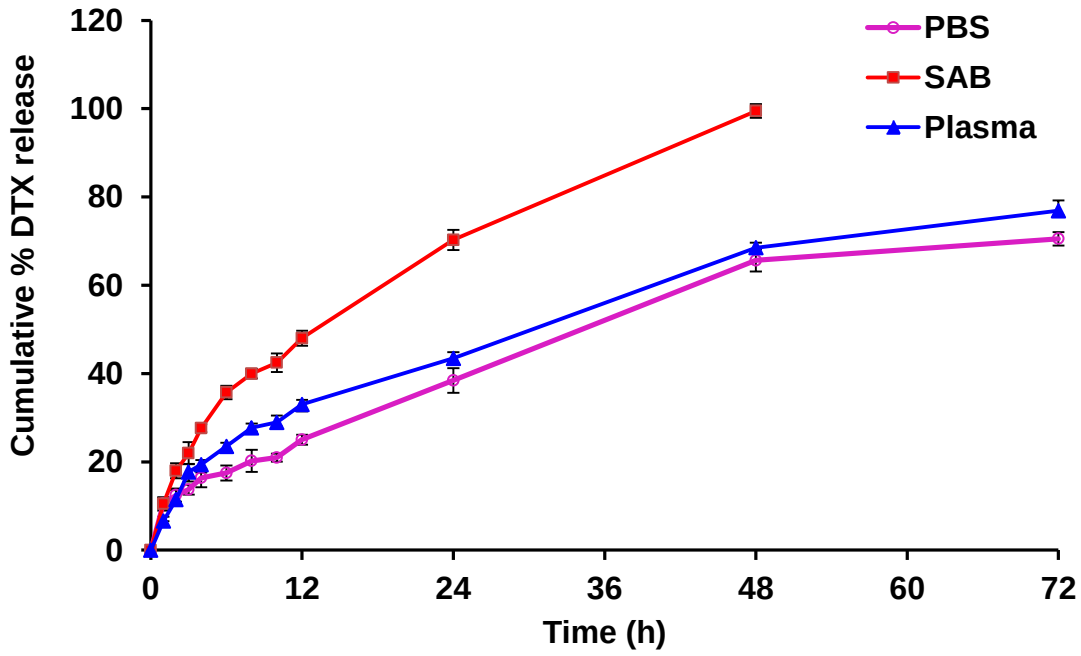

Figure 6.6: *In-vitro* drug release profiles of cRGDfK conjugated (PDNM) in plasma, phosphate buffer saline pH 7.4 (PBS) and sodium acetate buffer pH 4.5 (SAB) (Mean ± SD, n=3)

6.3.4. In vitro cytotoxicity

The potential for DNM and PDNM to inhibit cancer cell growth was tested in DU145 human prostate cancer cells and compared with that of DTX. As shown in Table 6.2, DNM and PDNM inhibited cell growth in a concentration and time-dependent manner. From the half-maximal inhibitory concentration (IC_{50}) values, it was found that DTX encapsulated in nanoformulations was more cytotoxic than plain DTX. Pure drug and nanomicelles displayed time-dependent anticancer activities against cancer cells and cytotoxicity was found to increase with exposure time. After 24 h incubation, IC_{50} values were >500 ng/mL for DTX, 325.9 ng/mL for DNM and 216.7 ng/mL for PDNM. The observed IC_{50} values of DTX, DNM and PDNM were 481.3, 179.6 and 56.3 ng/mL, respectively after 48 h of treatment. A further increase

in exposure time continued to decrease the amount of the drug required for the 50% growth inhibition of DU145 cells. After 72 h incubation, the IC_{50} values were decreased to 378.5 ng/mL for DTX, 70.7 ng/mL for DNM and 16.4 ng/mL for PDNM. Phase contrast images of DU145 human prostate cancer cells after 72 h exposure to different DTX formulations are shown in Figure 6.7.

Thus, at each time point (24, 48 and 72 h), nanomicelle formulations showed higher toxicity than pure DTX. The enhanced cytotoxicity of these formulations can be attributed to receptor mediated uptake of nanomicelles by the cells. In comparison to DNM, PDNM was 4.3 times more effective. Increased therapeutic efficacy of PDNM may be explained by increased intracellular delivery of DTX and active targeting through integrin receptors. The results were verified with comparative cellular uptake studies.

Table 6.2: IC_{50} (half-maximal inhibitory concentration) values for DTX, DTX loaded TPSA nanomicelles (DNM) and cRGDfK peptide conjugated DNM (PDNM) against DU145 human prostate cancer cells after treatment of 24, 48 and 72 h. The data represent the mean ± SD values for the three experiments performed in triplicate.

Time (h)	IC50 value (ng/ml)		
	DTX	DNM	PDMN
24	>500	325.9±12.5	216.7±11.8
48	481.3±16.3	179.6±14.9	56.3±4.3
72	378.5±12.9	70.7±2.5	16.4±1.1

6.3.5. Cellular uptake studies

Coumarin-loaded TPSA nanomicelles (FNM) and cRGDfK-conjugated FMN (PFNM) were separately formulated for cellular uptake studies. PFNM displayed higher cellular uptake than FNM and plain coumarin. Figure 6.8 shows the

fluorescent images of DU145 cells treated with coumarin, FNM and PFNM at different time intervals.

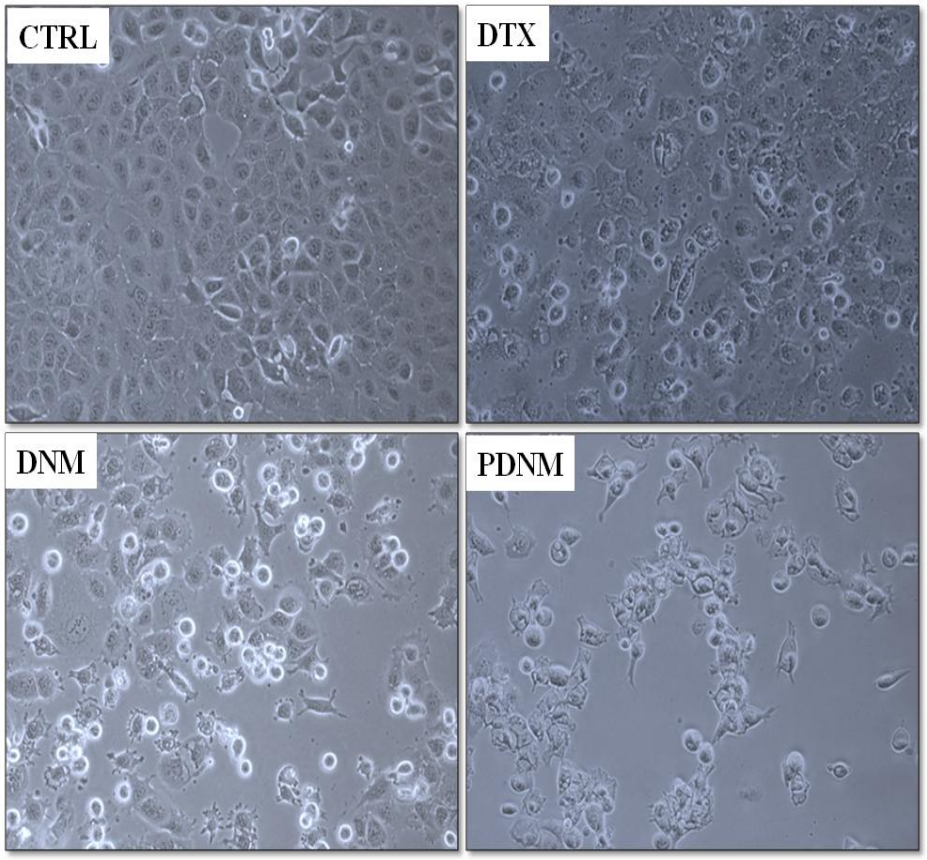

Figure 6.7: Phase contrast images of DU145 human prostate cancer cells after 72 h exposure of free docetaxel (DTX), docetaxel loaded nanomicelles (DNM) and cRGDfK conjugated DNM (PDNM) (Mean ± SD, n=3)

Nanomicelle uptake in cells was time-dependent, with maximum uptake observed after 12 h. The insets in Figure 6.8 show localization of nanomicelles in cells. Nanoparticles bind to the cell surface are then internalized to the cytoplasm and finally localized near the nucleus. Difference in cellular uptake of various formulations can be explained by their uptake mechanisms. Cellular uptake of free coumarin is through passive diffusion. Cellular uptake of PFNM is via integrin receptor-mediated endocytosis, while FNM enters the cell via nonspecific endocytosis.

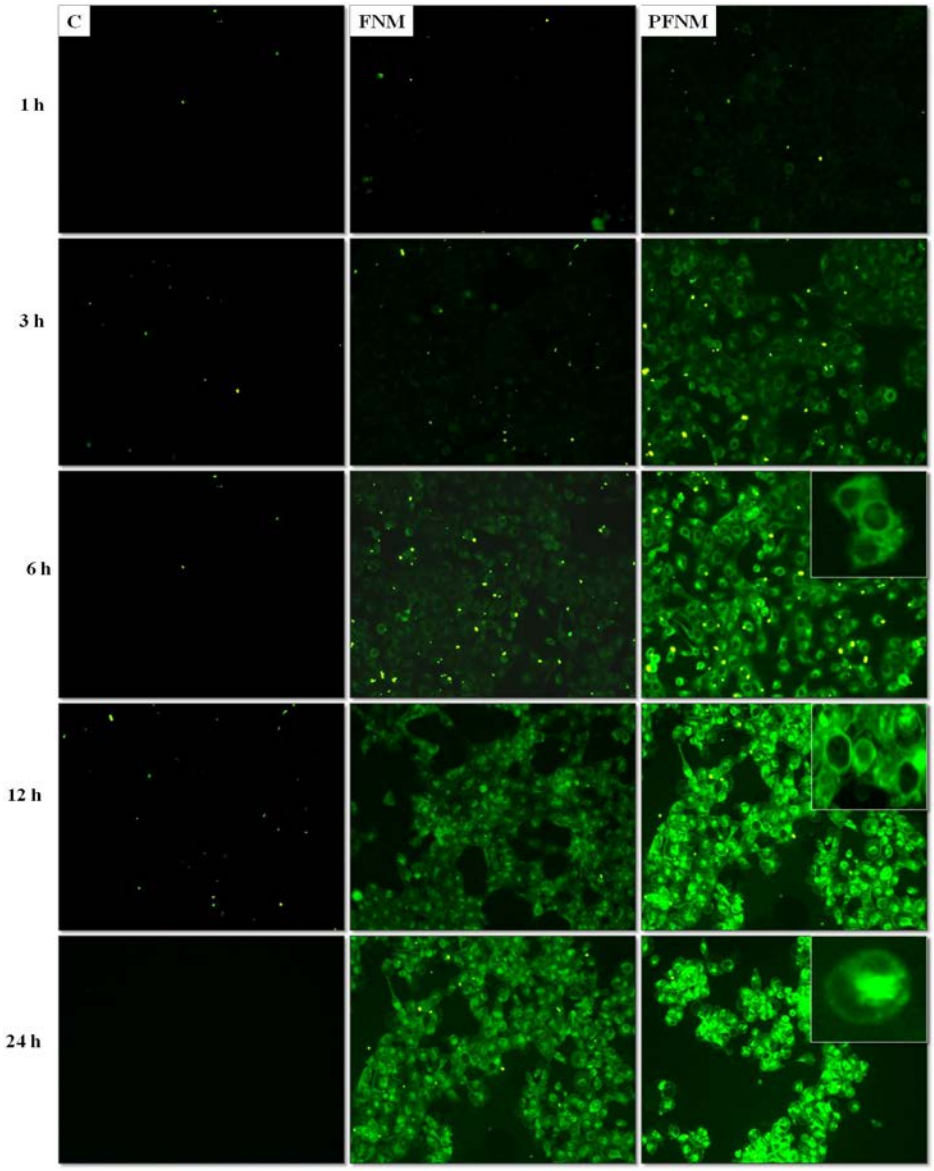

Figure 6.8: Cellular uptake of coumarin, coumarin loaded TPSA nanomicelles (FNM) and cRGDfK conjugated FNM (PFNM). Fluorescence microscope images of DU145 cells incubated for different time intervals.

6.3.6. Effect of nanomicelles on morphological changes

Obvious morphological changes were observed, with chromatin condensation, fragmentation and formation of apoptotic bodies in a dose-dependent manner. However, control cells exhibited a normal healthy shape with intact nuclei and no abnormalities. The results of phase contrast microscopy (Figure 6.9) were consistent

with those of the fluorescence microscope images using AO/EB. AO is only taken up by live cells while EB enters dead cells. Cells in apoptotic phase are stained by both AO and EB. Therefore, the AO/EB dual staining method differentiates condensed chromatin of dead apoptotic cells from the intact nuclei. Figure 9 shows the significant increase in apoptotic cells (orange fluorescence after treatment with nanomicelles. Green, intact nuclei were observed in control or untreated cells.

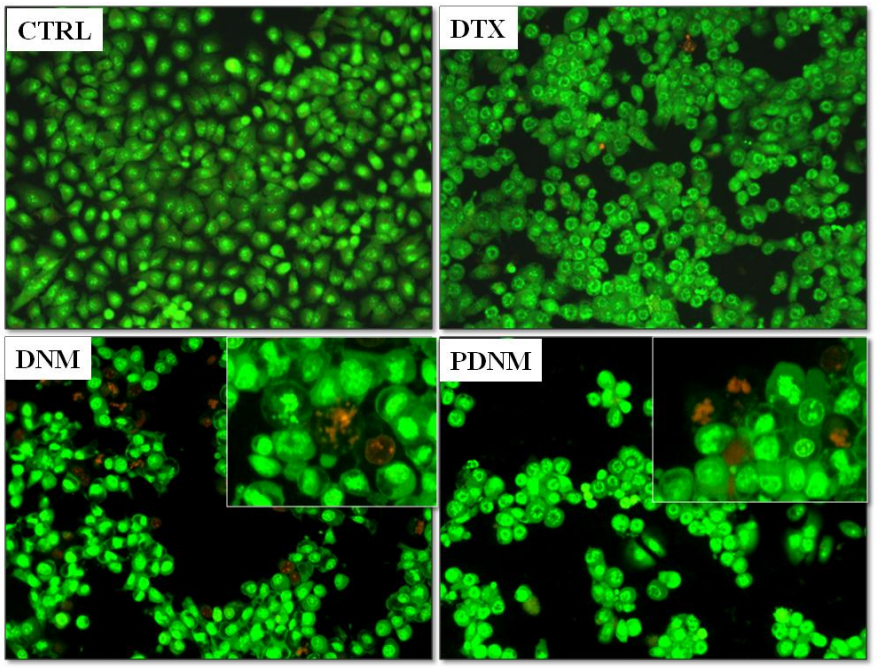

Figure 6.9: Fluorescence microscope images of DU145 human prostate cancer cells after 24 h incubation with acridine orange and ethidium bromide for the assessment of apoptotic morphology. Orange-red colour indicates the apoptosis while green colour indicates lack of apoptosis.

6.3.7. Apoptosis studies

Docetaxel induces apoptotic programmed cell death by interfering with microtubule dynamics during the cell division process. It binds to microtubules, stabilizes them and prevents their depolymerisation (Ting et al., 2007). The apoptotic stage can be determined by annexin-V FITC analysis. Cells are incubated with annexin-V FITC and propidium iodide (PI). Living or intact cells are stained negatively with both annexin-V FITC and PI, early apoptotic cells are stained only

with annexin-V FITC, cells at late apoptotic stage are stained with both annexin-V FITC and PI while necrotic cells are stain only with PI.

As shown in Figure 6.10, untreated, control DU145 cells had 87.17% of intact nuclei, 1.41% of cells were in early apoptosis, 4.84% were in the late apoptotic stage and 6.58% were necrotic. Pure DTX treatment did not induce a significant increase in apoptosis. However, significant apoptosis was observed when nanomicelles were used. With DNM, about 72.3% of cells were viable whereas 14.2% cells were in early apoptosis and 9.9% of cells in late apoptotic stages. Most apoptosis was observed with PDNM. In PDNM treated cells, only 41.13% of cells were viable and 57.12% were in apoptotic stages (39.87% in early apoptosis and 17.25% in late apoptosis).

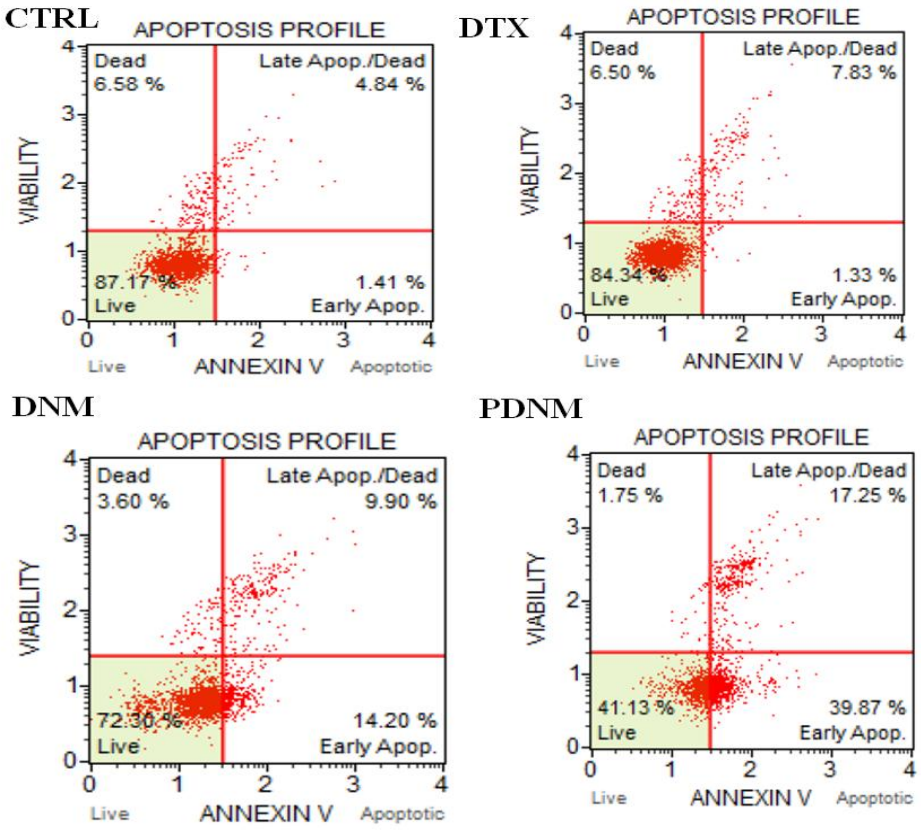

Figure 6.10: Quantification of docetaxel-induced apoptosis in DU145 human prostate cancer cells. Cells were incubated with DTX, DNM and PDNM for 48 h. Untreated cells served as controls.

6.3.8. Anti-angiogenic activities

Tumor growth and metastasis depend on angiogenesis thus it is an important factor in cancer progression (Rundhaug, 2005, Nethi et al., 2014). PDNM showed potential anti-angiogenic activities against HUVEC cells and in the presence of angiogenic factor VEGF. Endothelial cells are activated by VEGF which produces matrix metalloproteinases. These matrix metalloproteins aid in the development of a network of new blood vessels by multi-mechanism processes (Rundhaug, 2005).

Endothelial cell proliferation assays were performed in HUVECs and results are presented in Figure 6.11. After 24 h, cell viability was 86.6%, 61.4%, and 52% for DTX, DNM and PDNM, respectively. Cells incubated with VEGF exhibited 113% viability indicating angiogeneic activity of VEGF. Cells treated with PDNM in the presence of VEGF showed 61.2% cell viability. The results suggest anti-angiogenic activity for PDNM.

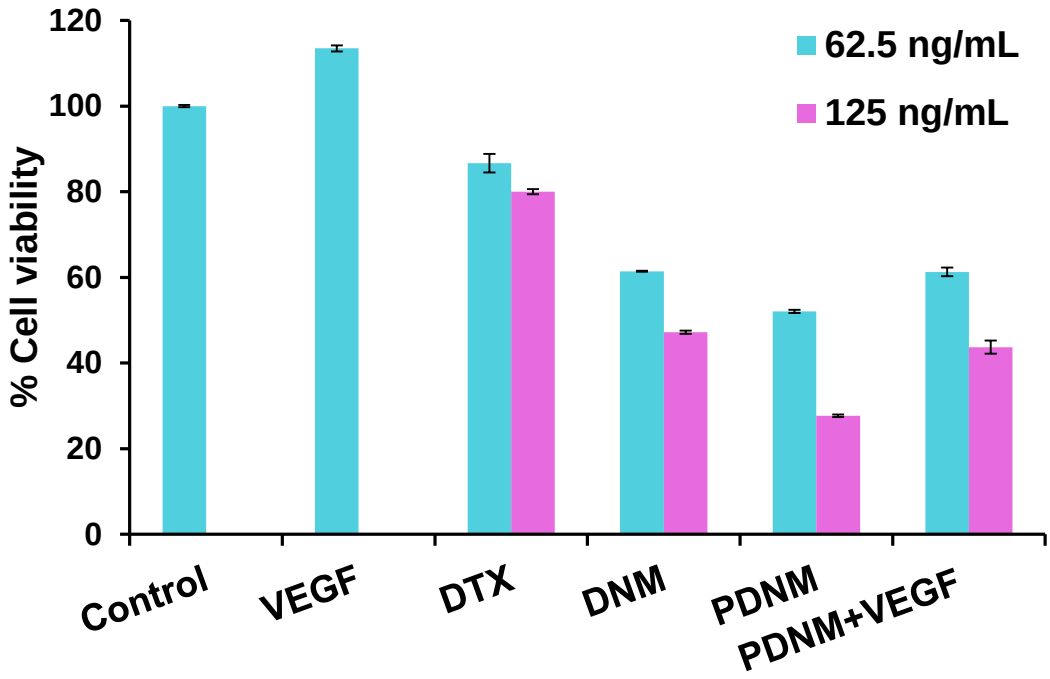

Figure 6.11. Endothelial cell proliferation assay: % cell viability of HUVECs treated with VEGF, DTX, DNM and PDNM after 24 h. (Mean ± SD, n=3)

In order to further elucidate the anti-angiogenic properties of PDNM, scratch wound directional migration assay was performed in HUVECs. Figure 6.12 shows that the untreated control HUVECs and cells treated with the positive control VEGF, migrate in a time dependent manner. The % of wound closure observed after 8 h was 25.3%, 44%, 14.8%, 4.44%, 2.3%, and 16.5% for control, VEGF, DTX, DNM, PDNM and VEGF with PDNM; respectively. A similar pattern was observed after 24 h incubation where the % wound closure was 54.4%, 95.5%, 28.1%, 13.2%, 7.47%, and 25.2% for control, VEGF, DTX, DNM, PDNM and VEGF with PDNM; respectively.

PDNM showed significant inhibition of endothelial cell proliferation in a dose dependent manner compared to untreated control HUVECs and cells treated with DTX or DNM (Figure 6.11). The results suggest anti-angiogenic properties for PDNM. It has been found that the potent angiogenic growth factor VEGF induces endothelial cell proliferation compared to untreated control cells (Barui et al., 2012). Interestingly, PDNM also significantly inhibits VEGF induced endothelial cell proliferation, supporting the anti-angiogenic potential of this drug delivery system.

Endothelial cell migration is also a key step of angiogenesis process (Nethi et al., 2014). In wound healing assays, cells incubated with VEGF showed rapid cell migration, with the wound area completely filled after 24 h (Figure 12a). However, cells treated with DTX, DNM or PDNM, did not migrate similarly. The wound area remained almost unaltered, especially for PDNM. Additionally, PDNM inhibits VEGF induced endothelial cell migration.

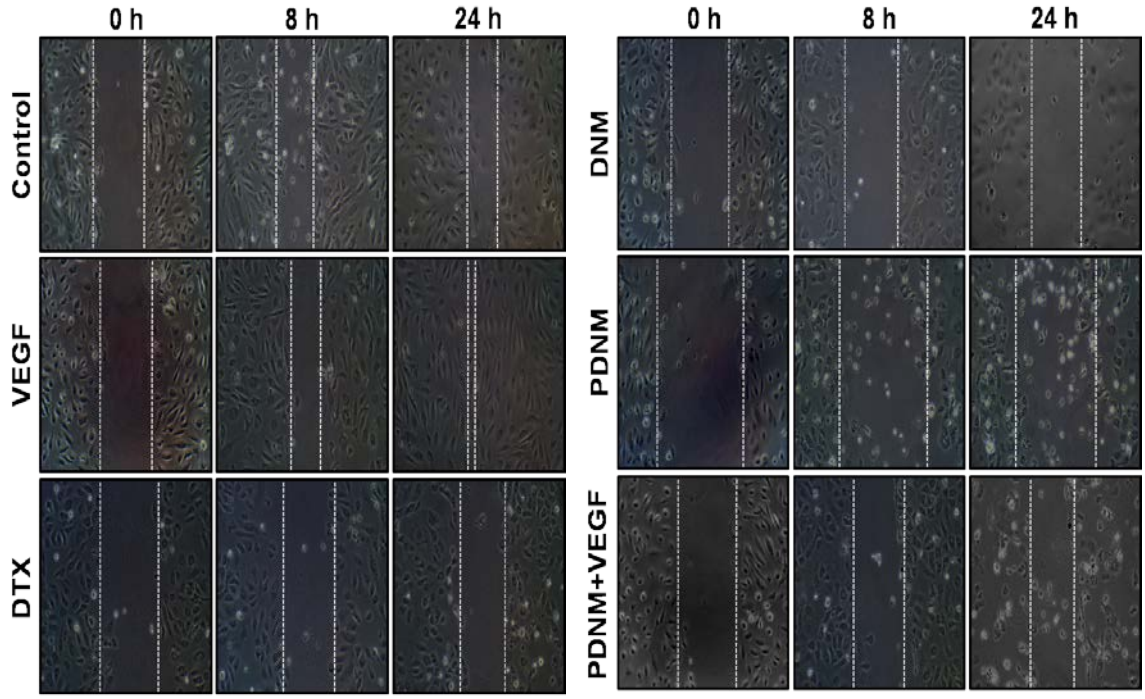

a)

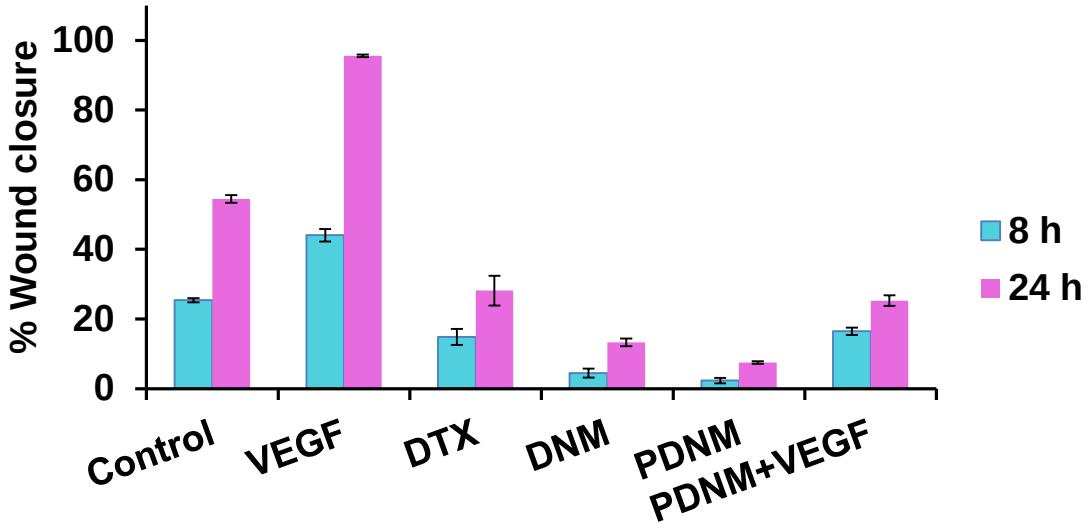

b)

Figure 6.12 (a-b): Scratch wound directional migration assay in HUVECs. (a) Untreated cells and cells treated with VEGF (100 ng/mL) migrated towards the wound area while cells treated with DTX, DNM and PDNM did not. PDNM also inhibited VEGF induced endothelial cell migration suggesting anti-angiogenic activity. (b) Quantification of wound healing activity using Image J Analysis software.

6.3.9. Stability Studies

PDNM showed high physical and chemical stabilities. After 2 months, nanomicelle size was 31.7 ± 0.59 nm, zeta potential -13. 2 ± 1.16 mV and DTX content was 93.52 ± 2.08%.

6.4. Conclusion

In summary, the present study reveals the enhanced cytotoxic potential of DTX against DU145 human prostate cancer cells when it is formulated in cRGDfK peptide conjugated succinoyl TPGS nanomicelles. The increased cytotoxicity of the nanomicelle system was further analysed by cellular uptake and apoptosis studies. Peptide-conjugated nanomicelles displayed controlled release of drug and good physicochemical stability in the colloidal state. Moreover, PDNM was able to inhibit endothelial cell proliferation and migration induced by angiogenic factors. Hence, the targeted nanomicelle system could be developed as a drug carrier for the site-specific delivery of DTX and other anticancer drugs to integrin receptor over-expressing angiogenic tumour vasculature.

6.5. References

- Arosio D, Casagrande C, Manzoni L. Integrin-mediated drug delivery in cancer and cardiovascular diseases with peptide-functionalized nanoparticles. *Curr Med Chem* 2012,**19**:3128-51.
- Baker J, Ajani J, Scotte F, Winther D, Martin M, Aapro MS, et al. Docetaxel-related side effects and their management. *Eur J Oncol Nurs* 2009,**13**:49–59.
- Barui AK, Veeriah V, Mukherjee S, Manna J, Patel AK, Patra S, Pal K, Murali S, Rana RK, Chatterjee S, Patra CR. Zinc oxide nanoflowers make new blood vessels. *Nanoscale* 2012,4:7861-9.
- Cao N, Feng, SS. Doxorubicin conjugated to D-alpha-tocopheryl polyethylene glycol 1000 succinate (TPGS): conjugation chemistry, characterization, in vitro and in vivo evaluation. *Biomaterials* 2008,**29**:3856–65.

- Carmeliet P, Jain RK. Review: Angiogenesis in cancer and other diseases. *Nature* 2000, **407**:249-57.
- Cho K, Wang X, Nie S, Chen ZG, Shin DM. Therapeutic nanoparticles for drug delivery in cancer. *Clin Cancer Res* 2008,**14**:1310-6.
- Danhier F, Le Breton A, Preat V. RGD-based strategies to target alpha(v) beta(3) integrin in cancer therapy and diagnosis. *Mol Pharm* 2012,**9**:2961-73.
- Desgrosellier JS, Cheresh DA. Integrins in cancer: Biological implications and therapeutic opportunities. *Nat Rev Cancer* 2010,**10**:9-22.
- Farrell D, Ptak K, Panaro NJ, Grodzinski P. Nanotechnology-based cancer therapeutics-promise and challenge-lessons learned through the NCI Alliance for nanotechnology in cancer. Pharm Res 2011,**28**:273-78.
- Feng L, Mumper RJA. critical review of lipid-based nanoparticles for taxane delivery. *Cancer Lett* 2013,**334**:157-75.
- Graf N, Bielenberg DR, Kolishetti N, Muus C, Banyard J, Farokhzad OC, et al. α(V)β(3) integrin-targeted PLGA-PEG nanoparticles for enhanced anti-tumor efficacy of a Pt(IV) prodrug. *ACS Nano* 2012,**6**:4530-9.
- Guo Y, Luo J, Tan S, Otieno BO, Zhang Z. The applications of Vitamin E TPGS in drug delivery. *Eur J Pharm Sci* 2013,**49**:175-86.
- Hait SK, Moulik SP. Determination of critical micelle concentration (CMC) of nonionic surfactants by donor-acceptor interaction with Iodine and correlation of CMC with hydrophile-lipophile balance and other parameters of the surfactants. J Surfactants Deterg 2001,4(3):303-9.
- Kulhari H, Deep Pooja Singh MK, Chauhan AS. Optimization of carboxylate-terminated poly(amidoamine) dendrimer-mediated cisplatin formulation. *Drug Dev Ind Pharm* 2015,**41(2)**:232-238.

- Kutty RV, Feng SS. Cetuximab conjugated vitamin E TPGS micelles for targeted delivery of docetaxel for treatment of triple negative breast cancers. *Biomaterials* 2013,**34**:10160-71.
- Mi Y, Zhao J, Feng SS. Vitamin E TPGS prodrug micelles for hydrophilic drug delivery with neuroprotective effects. *Int J Pharm* 2012,**438**:98-106.
- Muthu MS, Kulkarni SA, Liu Y, Feng SS. Development of docetaxel-loaded vitamin E TPGS micelles: formulation optimization, effects on brain cancer cells and biodistribution in rats. *Nanomedicine (Lond)* 2012,**7**:353-64.
- Narang AS, Delmarre D, Gao D. Stable drug encapsulation in micelles and microemulsions. *Int J Pharm* 2007,345(1-2):9-25.
- Nethi SK, Mukherjee S, Veeriah V, Barui AK, Chatterjee S, Patra CR. Bioconjugated gold nanoparticles accelerate the growth of new blood vessels through redox signaling. *ChemComm* 2014, 50:14367-70.
- Pandey P, Sinko PD, Bindra DS, Hamey R, Gour S, Vema-Varapu C. Processing challenges with solid dosage formulations containing vitamin E TPGS. *Pharm Dev Tech* 2013,**18**:296-304.
- Pooja D, Panyaram S, Kulhari H, Rachamalla SS, Sistla R. Xanthan gum stabilized gold nanoparticles: characterization, biocompatibility, stability and cytotoxicity. *Carbohydr Polym* 2014;110:1-9.
- Raju A, Muthu MS, Feng SS. Trastuzumab-conjugated vitamin E TPGS liposomes for sustained and targeted delivery of docetaxel. *Expert Opin Drug Deliv* 2013,**10**:747-60.
- Roy A, Murakami M, Ernsting MJ, Hoang B, Undzys E, Li SD. Carboxymethylcellulose-based and docetaxel-loaded nanoparticles circumvent P-glycoprotein-mediated multidrug resistance. *Mol Pharm* 2014;11:2592-9.

- Rundhaug JE. Matrix metalloproteinases and angiogenesis. *J Cell Mol Med* 2005;9:267-85.
- Sultana S, Khan MR, Kumar M, Kumar S, Ali M. Nanoparticles-mediated drug delivery approaches for cancer targeting: a review. *J Drug Target* 2013,**21**:107-25.
- Sun B, Feng SS. Trastuzumab-functionalized nanoparticles of biodegradable copolymers for targeted delivery of docetaxel. *Nanomedicine (Lond)* 2009, **4**:431-45.
- Thobe MN, Gurusamy D, Pathrose P, Waltz, SE. The Ron receptor tyrosine kinase positively regulates angiogenic chemokine production in prostate cancer cells. *Oncogene* 2010, **29**:214-26.
- Ting H, Jeffery Hsu J, Bao B, Lee Y. Docetaxel-induced growth inhibition and apoptosis in androgen independent prostate cancer cells are enhanced by 1α,25-dihydroxyvitamin D3. *Cancer Lett* 2007;247:122–9.
- Wang Z, Lee TY, Ho PC. A novel dextran-oleate-cRGDfK conjugate for self-assembly of nanodrug. *Nanomedicine* 2012,**8**:194-203.
- Zhang L, Zhang N. How nanotechnology can enhance docetaxel therapy. *Int J Nanomedicine* 2013,**8**:2927–41.
- Zhang Z, Tan S, Feng SS. Vitamin E TPGS as a molecular biomaterial for drug delivery. *Biomaterials* 2012,**33**,:4889-906.
- Zhao J, Feng SS. Effects of PEG tethering chain length of vitamin E TPGS with a Herceptin-functionalized nanoparticle formulation for targeted delivery of anticancer drugs. *Biomaterials* 2014,**35**:3340-7.
- Zhao P, Astruc D. Docetaxel nanotechnology in anticancer therapy. *ChemMedChem* 2012,7:952–72.

- Zhaofei L, Fan W, Xiaoyuan, C. Integrin $\alpha_v\beta_3$-Targeted Cancer Therapy. *Drug Dev Res* 2008,**69**:329–39.
- Zheng J, Tian X, Sun Y, Lu D, Yang W. pH-sensitive poly(glutamic acid) grafted mesoporous silica nanoparticles for drug delivery. *Int J Pharm* 2013,**450**:296-303.
- Zhu H, Chen H, Zeng X, Wang Z, Zhang X, Wu Y, et al. Co-delivery of chemotherapeutic drugs with vitamin E TPGS by porous PLGA nanoparticles for enhanced chemotherapy against multi-drug resistance. *Biomaterials* 2014,**35**:2391-400.

CHAPTER

Improving intracellular delivery of gemcitabine hydrochloride using cRGDfK peptide functionalized polymeric nanoparticles

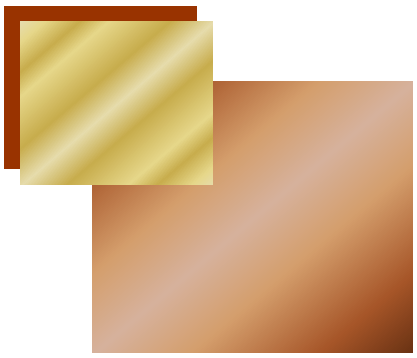

7.1. Introduction

Design and development of new drug delivery systems to achieve controllable targeted delivery of clinically approved anticancer drugs is an area of active investigation (Brannon-Peppas and Blanchette, 2012; Kanapathipillai et al;., 2014). It is well recognised that most of the clinically approved anticancer drugs face a major issue around the lack of biological target specificity (Kwon et al., 2012; Cheng et al., 2012). This leads to uncontrolled bio-distribution of anticancer drugs to non-specific tissues, resulting in severe unwanted side effects. To ensure safety and efficacy, these anticancer drugs are needed to be delivered to their target site selectively and at an optimal rate. In contrast to conventional drug delivery systems, a carefully designed targeted drug delivery system has the potential to deliver a therapeutic agent to the tissue of interest at higher dosages, while reducing the relative drug concentration in non-target tissues. Such delivery systems not only overcome the problems of non-specificity of anticancer drugs but also improve their therapeutic indices (Cunliffe et al., 2005; Cho et al., 2008; Zhang et al., 2008; Akhtar et al., 2014).

An example of such US-FDA approved chemotherapy is gemcitabine (GEM), which is used for the treatment of various cancers including breast, non-small cell lung, pancreatic and platinum-resistant ovarian cancer (Duenas-Gonzalez et al., 2011; Martín-Banderas et al., 2013). Being a pseudo-nucleotide, the efficacy of GEM relies on its incorporation into cellular DNA. This blocks DNA chain elongation, leading to cell arrest in the G1 phase and cytostatic effects (Huang and Plunkett, 1995; Lorusso et al., 2006). Although GEM offers an efficient chemotherapy option, its short plasma half-life (<20 min), enzymatic degradation in body fluids and non-specificity are major limitations in current clinical settings (Hodge et al., 2011; Tao et

al., 2012). The rapid clearance of GEM requires it to be administered at high doses, which leads to severe haematological and gastrointestinal side effects (Chu and Devita, 2007; Paolinoet al., 2010; Derakhshandeh and Fathi, 2012). Nano-engineered systems have shown considerable advances for a range of biomedical applications including imaging, diagnosis and delivery of therapeutic agents (Torchilin, 2012). As a drug carrier system, nanoparticles can deliver drugs at predetermined rates, thereby controlling clearance and maintaining drug concentration within the therapeutic index. In addition, nanoparticle surfaces can be modified with a ligand for specific targeting. Among various nanoparticle systems, polymeric nanoparticles exhibit some of the best characteristics for the delivery of hydrophilic drugs. For instance, they allow high payload, controllability over drug release, good physicochemical stability, biodegradability and opportunity for facile surface modification (Jia et al., 2013). Considering the importance of biocompatible polymers in drug delivery, it is not surprising that different types of nano-particulate polymers are regularly investigated as drug delivery platforms (Dend et al., 2012; Ye et al., 2014). These investigations are motivated by the rationale that the design principles of these nano-based drug delivery systems influence the biological fate of these materials, which remains predominantly unique for different drug candidates.

In the current study, a new targeted drug delivery platform was investigated for ovarian cancer by developing GEM-loaded poly(D,L-lactic-co-glycolic) acid [GEM-PLGA] nanoparticles, and functionalising them with cyclic RGDfK (cRGDfK), a five amino acid peptide [GEM-PLGA@cRGDfK], to achieve targetability. cRGDfK was chosen as a targeting ligand due to known high stability of cyclic peptides as well as high specificity of cRGDfK to the $\alpha_v\beta_3$ integrin receptors (Danhier et al., 2012). These integrin receptors are over-expressed in malignant ovarian cells and their levels are

strongly associated with tumour progression (Landen et al., 2008; Lossner et al., 2008). The reduced haemolytic toxicity accompanied with enhanced uptake and cytotoxicity of the proposed drug delivery system towards integrin-overexpressing SKOV-3 human ovarian cells suggests that up-regulation of integrin receptors may provide a unique opportunity to deliver anticancer drugs selectively to ovarian tumours.

7.2. Experimentation

7.2.1. Materials

Gemcitabine (GEM) was obtained as a gift from TherDose Pharma Pvt Ltd (Hyderabad, India). cRGDfK peptide was purchased from Peptide International (Kentucky, USA). Poly(D,L-lactic-co-glycolic) acid [PLGA, 30-60 kDa, lactide:glycolide - 50:50], polyvinyl alcohol [PVA, 89-98 kDA], sodium cholate, Pluronic F68 [8.5 kDa], RPMI-1640, trypsin–EDTA, antibiotic-antimycotic solution, 3-(4,5-dimethyl-2-thiazolyl)-2,5-diphenyltetrazolium bromide (MTT), dimethyl sulfoxide (DMSO), 1-ethyl-3-(3-dimethylaminopropyl)carbodiimide (EDC) and N-hydroxysuccinimide (NHS) were purchased from Sigma Aldrich (St. Louis, MO, USA). Tween® 80 was purchased from sd Fine Chemicals (Mumbai, India). Foetal bovine serum (FBS) was purchased from Gibco, USA. Mycoplasma-free SKOV-3 human ovarian cancer cells were kindly gifted by Prof. Rodney Hicks and Dr. Carleen Cullinane at Peter MacCallum Cancer Centre, Australia.

7.2.2. Synthesis of drug-loaded nanoparticles (GEM-PLGA)

GEM-loaded PLGA nanoparticles (GEM-PLGA) were synthesised by using a double emulsion solvent evaporation method. GEM (1 mg) was dissolved in 0.5 mL aqueous Pluronic F68 surfactant solution (1% w/v) and added to 2 mL of PLGA solution (5 mg/mL in ethyl acetate), followed by sonication for 1 min using a probe

sonicator. The resulting primary w/o emulsion was redispersed in 10 mL of Pluronic F68 surfactant solution (0.25% w/v), sonicated for 2 min and stirred for 3 h on a magnetic stirrer. This resulted in a w/o/w double emulsion that was centrifuged at 15,000 rpm for 30 min. The supernatant was collected and analysed for the quantification of free drug, whereas the pellet containing GEM-PLGA nanoparticles was washed three times with deionised MilliQ water and lyophilised. Preparation of drug-free PLGA nanoparticles was optimised to study the effects of organic solvent (dichloromethane, ethyl acetate, choloroform and mixture of solvents) and surfactant type (PVA, Tween® 80, pluronic F68, sodium cholate) on particle size and surface charge. GEM-PLGA formulations were also optimised for drug encapsulation efficiency and drug loading.

7.2.3. Estimation of entrapment efficiency and drug loading

GEM content in different samples was determined using a HPLC system (Agilent), wherein the analyses were carried out on a Chromolith Performance RP-18e column (100 mm × 4.6 mm, Merck). In HPLC, The optimal mobile phase was found to a mixture of acetonitrile and water (30:70, v/v), which was delivered at a flow rate of 1 mL per min. Sample injection volume was 20 µL and HPLC peaks were monitored at 269 nm using an UV detector. Linear calibration curves were obtained over 0.1–10 µg per mL concentration range (correlation coefficient, R^2 = 0.998). Entrapment efficiency (EE) and drug loading (DL) were calculated as follows:

$$EE\ (\%) = \frac{W_I - W_F}{W_I} \times 100 \qquad \ldots\ldots\ldots (1)$$

$$DL\ (\%) = \frac{W_E}{W_N} \times 100 \qquad \ldots\ldots\ldots (2)$$

wherein, W_I, W_F, W_E, and W_N correspond to the weights of initial amount of drug employed for nanoparticle synthesis, free drug in supernatant, drug encapsulated in nanoparticles, and drug-loaded nanoparticles, respectively.

For estimation of GEM drug content in lyophilised nanoparticles, 5 mg of nanoparticles were dissolved in 5 mL of acetone, followed by addition of 10 mL of water, subsequent evaporation of acetone to precipitate polymer, filtration of polymer through a 0.22 µm filter to obtain drug in the aqueous solution, and GEM estimation by HPLC.

7.2.4. Conjugation of cRGDfK peptide to drug-loaded nanoparticles

cRGDfK peptide-conjugated nanoparticles (GEM-PLGA@cRGDfK) were prepared by a carbodiimide reaction, in which GEM-PLGA nanoparticles (25 mg) were dispersed in phosphate buffer saline (PBS, pH 7.4, 5 mL) and incubated with EDC (20 mg) and N-hydroxysuccinimide (NHS, 12 mg) for 45 min at room temperature. To this solution, cRGDfK peptide (0.5 mg, 1 mL) was added and stirred for 6 h at room temperature. GEM-PLGA@cRGDfK nanoconjugates were obtained by centrifugation at 12,000 rpm for 30 min. The supernatant was collected to determine the amount of unconjugated peptide by measuring the arginine content, as per the previously reported protocol (Annett Schmitt et al., 2005).

7.2.5. Physico-chemical characterisation of nanoconjugates

Particle size distribution and surface charge of nanoparticles were analysed by Malvern Zetasizer Nano-ZS by appropriately diluting the samples with deionised water. The nanoparticle morphology was examined by TEM using a JEOL 1010 instrument operated at an accelerating voltage of 100 kV. For TEM, samples were prepared by drop casting the sample on a carbon-coated copper TEM grid, followed by air drying. FTIR spectra were obtained on a Perkin Elmer 1000 FTIR spectrometer at a resolution of 4 cm^{-1} by acquiring 8 scans and averaging them. DSC measurements of nanoparticles were carried out on DSC-Q100 (TA Instruments, USA) between 225-325 °C at a scan speed of 10 °C per min, under

nitrogen environment. XRD analysis of powder samples was performed using an X-ray diffractometer (D8 Advance, Bruker, Germany) using CuKα irradiation at 40 KV and 20 mA.

AFM measurements on nanoconjugates were obtained using a JPK Nanowizard 3 AFM, mounted on an inverted epifluorescence microscopy (Nikon TE2000). AFM images were made in AC (intermittent contact) mode using Bruker NCHV cantilevers that have a nominal resonant frequency and spring constant of 340 kHz and 40 N/m respectively. AFM images were acquired with a force set point of <1 nN and the same area were imaged repeatedly to ensure that no sample damage had occurred.

Small-angle neutron scattering (SANS) measurements were made on the Quokka instrument at the Bragg Institute, ANSTO, Lucas Heights, Australia. Samples were prepared in 2 mm thick quartz cells using D_2O as solvent, and scattering spectra were obtained at 25 °C. An incident neutron wavelength of 5 Å (with a typical Gaussian spread of 10%) was used, and scattering was measured at a two-dimensional array detector at three sample-to-detector distances: 2 m, 14 m and 20 m (in the latter of which a neutron optics system was used to detect scattering at lower q), giving an effective q range of 0.001–0.4 $Å^{-1}$. Data were modelled using a standard form factor for homogeneous ellipsoidal particles (Freigin and Svergu, 1987; Guinier and Fournet, 1995), assuming a simple hard-sphere structure factor.

7.2.6. In vitro drug release

In vitro drug release from drug-loaded nanoconjugates was studied by dialysis method at 37±0.5 ºC, in which an aqueous solution (2 mL) containing GEM-PLGA nanoparticles (equivalent to 2 mg of GEM) was placed in a 12 kDa dialysis bag. The

dialysis bag was suspended in 100 mL of PBS and the buffer was stirred at 100 rpm using a magnetic stirrer. Aliquots of 3 mL PBS were withdrawn at various time intervals over 72 h, which was replenished with equivalent volumes of fresh PBS buffer to maintain the volume and sink conditions. The obtained aliquots were filtered through a 0.22 µm filter, diluted appropriately and analysed by HPLC for released drug content. The experiments were repeated three times and average values calculated.

7.2.7. Hemolytic toxicity studies

Haemolytic toxicity studies on nanoparticles were performed as per our previously reported protocol (Pooja et at., 2014). Briefly, 5 mL of red blood cell (RBCs) suspension (2% v/v) in normal saline was incubated with 50-1000 µg/mL equivalent of drug in the form of either pristine GEM or GEM-PLGA@cRGDfK conjugate at 37 ºC for 1 h. Cells were centrifuged at 1000 rpm for 5 min and absorbance of supernatant was measured at 540 nm using a UV/VIS spectrophotometer. Cells incubated with distilled water and normal saline were considered to show 100% (standard) and 0% (control) hemolysis, respectively.

% Hemolysis was determined as follows:

$$\% \text{ Hemolysis} = \{(A_T - A_C) / (A_S - A_C)\} \times 100$$

Whereas; A_T is absorbance of test sample, A_S: absorbance of standard; and A_C: absorbance of control

7.2.8. Cell culture

Mycoplasma-free SKOV-3 human ovarian cancer cells were grown in RPMI-1640 medium supplemented with FBS (10%), glutamine (2 mM), penicillin (100 U per mL) and streptomycin (0.1 mg/mL). Cells were cultured under standard conditions at 37 °C in a humidified atmosphere (85% relative humidity) containing 5% CO_2.

7.2.9. Anti-proliferation assay

Cytotoxicity of free GEM as well as nanoconjugates was determined by MTT assay as described previously (Kulhari et al., 2014) Briefly, SKOV-3 cells (5×10^3) were seeded in 96-well culture plates and allowed to adhere for 24 h. The cells were then exposed to various concentrations (0.01-10 µg/mL) of free drug or nanoconjugates containing equivalent amounts of drug for 48 h in triplicates. Following treatment, culture media was replaced with serum-free media containing 0.5 mg/mL MTT and allowed to incubate for 4 h. This was followed by removal of MTT agent, addition of 200 µL of DMSO to each well and shaking the plates on a rocking shaker for 10 min at room temperature. The absorbance from the plates was then measured at 570 nm using a micro-plate reader (Perkin Elmer, USA). Untreated cells were also incubated under identical conditions and served as the controls. IC_{50} values were determined by probit analysis software package of MS-excel.

7.2.10. Cellular uptake studies

To study cellular uptake of nanoconjugates, fluorescent Rhodamine-B (RhB)-encapsulated polymeric nanoconjugates without any targeting ligand (RhB-PLGA) and with cRGDfK peptide as a targeting ligand (RhB-PLGA-cRGDfK) were prepared in a manner similar to that of GEM-PLGA and GEM-PLGA-cRGDfK, respectively. For uptake studies, SKOV-3 cells were seeded into 12-well plates up to 80% confluency, followed by incubation with 100 µL of these particles (20 µg/mL of RhB) for 2 h. Cells were then washed three times with chilled PBS and cellular uptake was assessed using fluorescent microscopy (Nikon, Inc. Japan).

7.2.11. Measurement of mitochondrial membrane potential (MMP)

SKOV-3 cells (2×10^5) were seeded in 24-well plates for 24 h, followed by treatment with GEM, GEM-PLGA and GEM-PLGA@cRGDfK at concentrations

equivalent to the IC50 value of GEM-PLGA@cRGDfK (0.1 µg/mL) for 24 h in 0.4 mL of RPMI-1640 medium. Cells were then washed twice with PBS and incubated with 0.4 mL of Rhodamine-123 (2 µg/mL) for 30 min in the dark under ambient conditions, followed by washing with PBS. Cells were observed using a Nikon fluorescence microscope. The changes in the MMP (Δψ) in response to different nanoconjugates were quantitatively estimated after adjusting cell counts for equal numbers and measuring Rhodamine-123 fluorescence at the excitation and emission wavelengths of 480 and 530 nm, respectively, using a Hitachi F-3010 spectrofluorometer.

7.2.12. Measurement of reactive oxygen species (ROS)

This was achieved using a protocol similar to that detailed above for the measurement of MMP. However, in this case, the Rhodamine-123 treatment step was replaced with an ROS-active reagent 2,7-dichlorofluorescin diacetate (DCFDA - 10 µg/mL). Cells were observed using a fluorescence microscope. For quantitative estimation, cell counts were adjusted for all formulations and fluorescence intensity of 2,7-dichlorofluorescin (DCF), an oxidised fluorescent product, was measured at excitation and emission wavelengths of 495 and 520 nm, respectively, using a Hitachi F-3010 spectrofluorometer.

7.2.13. Measurement of nuclear fragmentation by Hoechst 33242 staining

To assess the apoptotic nuclear morphology, SKOV-3 cells were grown and treated with various formulations, as elaborated above for the measurement of MMP and ROS. This was followed by fixing the cells using 4% paraformaldehyde in PBS for 15 min, washing with PBS, staining with Hoechst 33342 (5 µg/mL) in 0.4 mL PBS for 30 min, and washing the stained cells twice with PBS. Nuclear condensation was monitored using a fluorescent microscope through a UV excitation filter.

7.3. Results and Discussion

7.3.1. Synthesis and characterisation of drug-loaded nanoparticles

Gemcitabine (GEM), being a hydrophilic anticancer drug with serious side effects, it is not ideal for intravenous injection directly in the aqueous blood stream. Scheme 7.1 illustrates the double emulsification strategy for the encapsulation and targeting of GEM to the $\alpha_v\beta_3$ integrin receptors overexpressing SKOV-3 human ovarian cells. Initially, GEM is dissolved in aqueous Pluronic F68, an amphiphilic copolymer, followed by exposure to PLGA, a hydrophobic copolymer dissolved in ethyl acetate. In Pluronic F68, the alternating blocks of hydrophilic polyethylene oxide (PEO) and hydrophobic polypropylene oxide (PPO), arranged in the A-B-A tri-block structure, provides this copolymer with amphiphilic characteristics that allow Pluronic F68 to behave as a surfactant above its critical micellar concentration (CMC – 0.04 mM at 20-25 °C). Step 1, in the scheme, shows the spontaneous self-assembly of hydrophilic GEM drug molecules, amphiphilic Pluoronic F68 chains, and hydrophobic PLGA chains to form water-in-oil (w/o) micellar structures in ethyl acetate. Step 2 shows that when this primary w/o emulsion is re-exposed to amphiphilic Pluronic F68 chains in water, secondary micellar structures comprised of w/o/w double emulsions are formed. Further, Steps 3 and 4 show the functionalisation of cRGDfK (Arginine-Glycine-Aspartate-Phenylalanine-Lysine), an integrin-targeting cationic cyclic peptide to the GEM-loaded secondary micelles. In Step 3, when carboxylic groups of PLGA are activated using carbodiimide chemistry, this allows the primary amine of lysine residue in the cRGDfK peptide to act as a preferred conjugation site with PLGA, while the adjacent phenylalanine residue facilitates this conjugation through hydrophobic interactions with the Pluronic F68 chains.

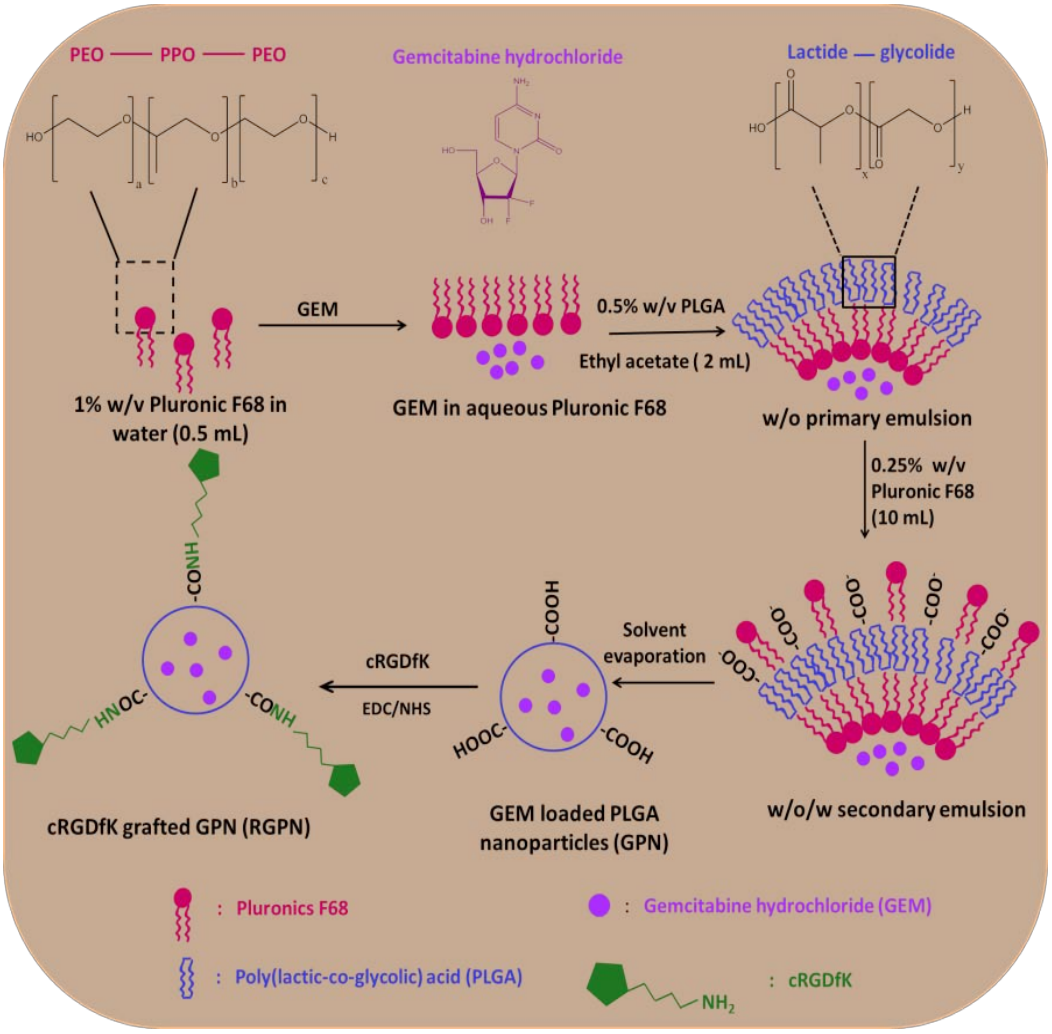

Scheme 7.1: Schematic diagram showing the preparation of cRGDfK conjugated and gemcitabine loaded PLGA nanoparticles by double emulsification method

The successful synthesis of integrin receptor targetable GEM-loaded nanoconjugates is evident from their physicochemical characteristics presented in Figure 1. DLS revealed that the hydrodynamic diameter of nanoconjugates prepared with or without GEM encapsulated in their cavity were 82.8 ± 3.1 nm and 89.7 ± 2.9 nm, respectively, with a PDI less than 0.2, indicating a narrow size distribution of these particles (Figure 1a). SANS measurements indicated that the particles were non-spherical in shape when dispersed in solvent, with the best fit being achieved

using an oblate spheroidal (ellipsoidal) model (Figure 1b). The PLGA particles (without GEM) indicated a semi-major radius of 23 nm and a semi-minor radius of 52 nm, suggesting a squat spheroid of aspect ratio approximately 2:1. Similar to the DLS measurements, a modest particle size increase when going from the drug-free PLGA to the drug-loaded GEM-PLGA particles was observed, where the semi-major and semi-minor axes increased to 24 nm and 58 nm respectively. Clearly the SANS data correlate well with the DLS measurements of particles when in dispersion, and corroborate their highly hydrated nature. TEM and AFM images of GEM-PLGA particles in Figures 1c and d, respectively, indicate that the particles shrink considerably when dried onto a surface, suggesting a high level of hydration when in solvated form. However, their collapsed size (50-75 nm in lateral dimension and ~4 nm in height), particularly the height may be an underestimate, as the particles are very soft and could be easily deformed by the AFM cantilever. The GEM-PLGA particles showed an impressive encapsulation efficiency of 93.16 ± 0.8%, while the drug loading was calculated to be 7.92 ± 0.17% of the total weight of these nanocarriers.

Zeta potential measurements revealed that drug-loading had insignificant effect on their highly negatively charged surface, with ζ-values corresponding to -25.9 ± 1.7 mV and -23.56 ± 1.93 mV for PLGA and GEM-PLGA particles, respectively. After conjugation of cRGDfK peptide, GEM-PLGA@cRGDfK nanoconjugates exhibited a slight increase in average DLS hydrodynamic diameter to 94.02 ± 2.3 nm along with concomitant decrease in the zeta potential value -13.7 ± 0.76 mV. This decrease in the negative zeta potential value results from the passivation of the negatively charged $–COO^-$ groups of PLGA after covalent conjugation with cationic cRGDfK peptide (Scheme 1), and therefore supports the

successful functionalization of GEM-PLGA nanoparticles with the integrin receptor targetable cationic peptide.

FTIR spectroscopy was employed to validate the successful drug loading and conjugation of targeting peptide on the nanoparticle surface (Figure 1e). FTIR spectrum of PLGA showed the characteristic carboxylic group (C=O stretching) vibration at 1751 cm^{-1}, whereas in the FTIR spectra of pristine GEM, signature bands appeared at 1676 cm^{-1} and 1061 cm^{-1}, corresponding to ureido and hydroxyl groups, respectively. FTIR spectrum of GEM-PLGA particles revealed characteristic peaks of PLGA alongside GEM, suggesting successful drug encapsulation. Further, the appearance of slightly shifted amide signatures (1646 and 1542 cm^{-1}) in GEM-PLGA@cRGDfK supports successful covalent conjugation of cRGDfK peptide on the nanoparticle surface, which otherwise appeared at 1641 and 1530 cm^{-1} in the pristine cRGDfK peptide.

DSC studies revealed that the physical state of GEM changes from crystalline to amorphous or a solid solution phase during drug loading (Figure 1f). While the DSC thermogram of pristine GEM shows an endothermic peak corresponding to its melting temperature at 291 °C, this peak is found absent in the thermogram for GEM-PLGA nanoparticles.

XRD analysis also confirmed this change in the physical state of the drug within nanoparticles (Figure 1g). Highly crystalline nature of pristine GEM is evident from sharp peaks in its XRD pattern, whereas the non-crystalline amorphous nature of GEM in GEM-PLGA nanoparticles leads to loss of these features.

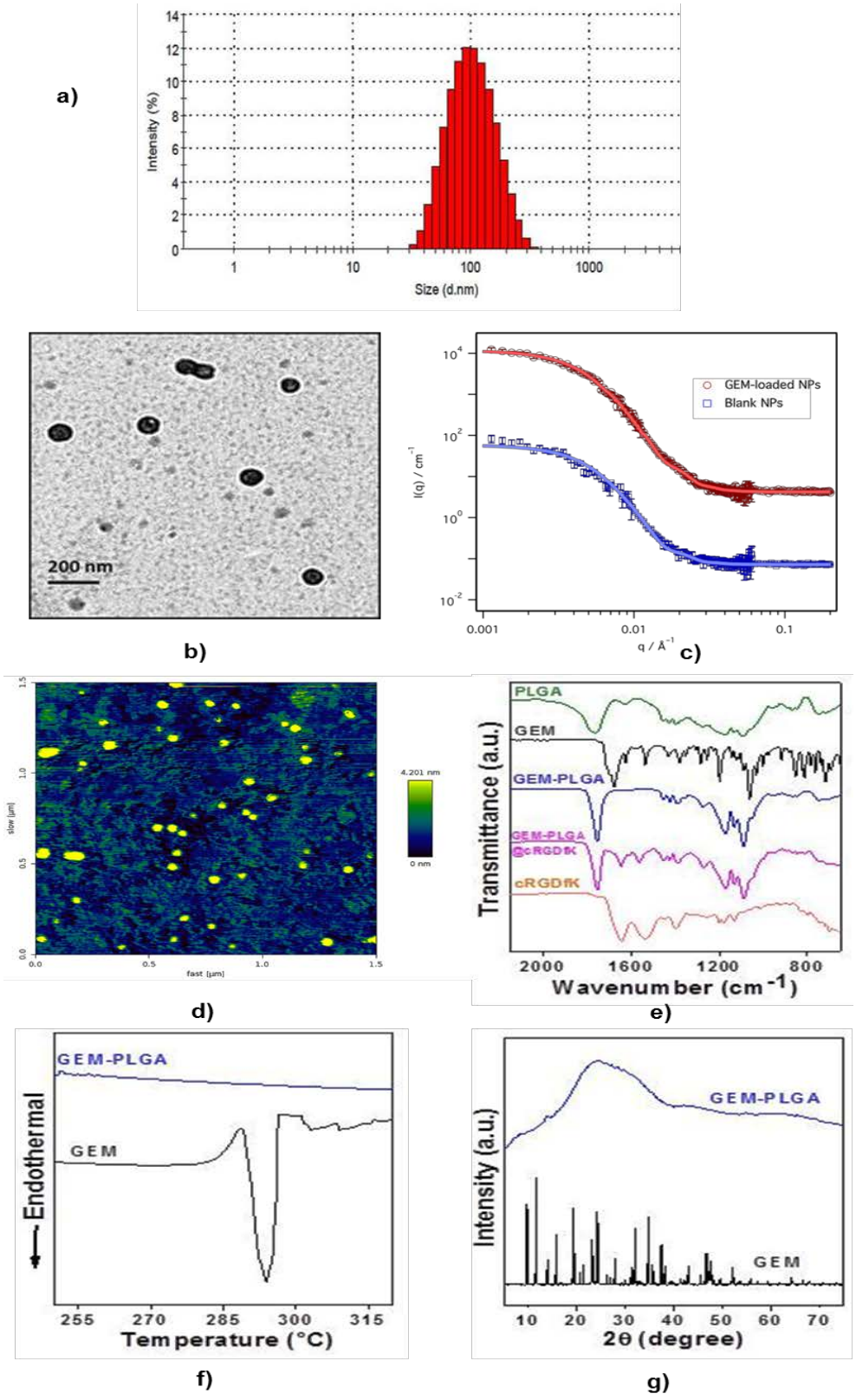

Figure 7.1: Characterization of nanoparticles by a) DLS b) TEM c) SANS d) AFM) e) FTIR f) DSC and g) XRD analysis

7.3.2. In vitro drug release

The cumulative release profile of GEM from pristine aqueous drug solution and from nanoparticles was evaluated *in vitro* (Figure 7.2). More than 90% of GEM was released from the pristine drug solution within 8 h. In contrast, drug release from GEM-PLGA and GEM-PLGA@cRGDfK particles showed a biphasic profile characterised by initial fast release, followed by a slower release phase. Approximately 40% of encapsulated drug was released in the first 8 h, with remaining drug released up to 96 h. The initial burst release may be attributed to the release of drug adsorbed on the surface of nanoparticles or present in the periphery of the polymeric matrix. The second phase could be due to drug diffusion through the matrix, or due to polymer degradation, or a combination both. Insignificant difference in the drug release profiles of GEM-PLGA and GEM-PLGA@cRGDfK particles indicate that the targeting peptide does not affect the release profiles of these drug-delivery carriers.

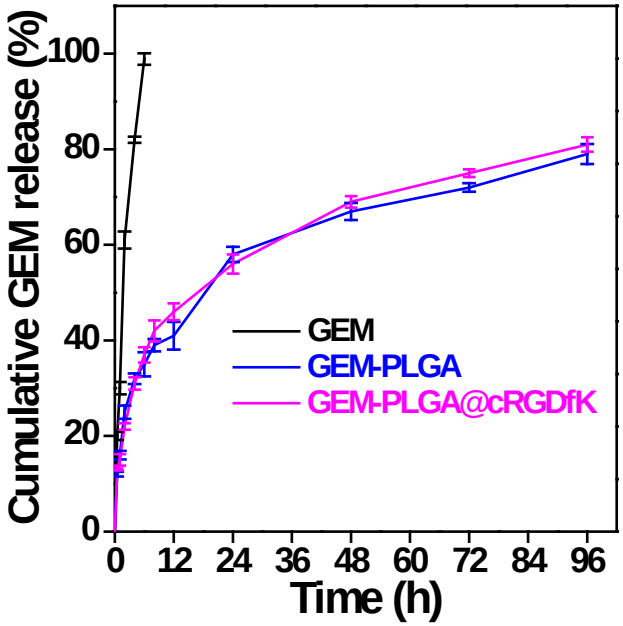

Figure 7.2: In vitro drug release profile of Gemcitabine (GEM), GEM loaded PLGA nanoparticles (GEM-PLGA) and cRGDfK conjugated GPN (GEM-PLGA@cRGDfK) in phosphate buffer saline pH 7.4 (PBS)

7.3.3. In vitro blood compatibility and tumour cytotoxicity

The *in vivo* efficacy of drug delivery systems relies on improved blood compatibility and higher specific toxicity against tumour cells. To assess these parameters, *in vitro* hemolytic toxicity assays were performed on RBCs and anti-proliferation assays were performed against SKOV-3 human ovarian cancer cells (Figure 7.3). Blood compatibility studies showed that while pristine GEM as well as peptide-grafted GEM-PLGA@cRGDfK nanoparticles caused concentration-dependent hemolysis, the amount of haemoglobin released from the rupture of RBCs was significantly less ($p<0.005$) in case of GEM-loaded nanoparticles in comparison to the pristine drug (Figure 7.3). For instance, at the highest concentration tested (1 mg/ml), pristine drug caused 5.2% hemolysis compared to 1.7% by GEM-PLGA@cRGDfK nanoparticles. This significant increase in blood compatibility may be attributed to efficient drug encapsulation within a nanoparticle that reduces direct contact of GEM with RBCs.

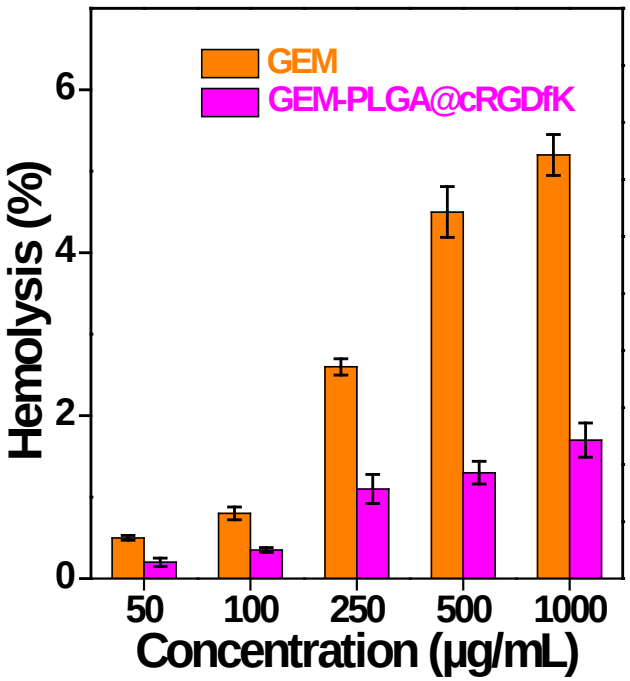

Figure 7.3: Hemolytic toxicity assay of gemcitabine (GEM), GEM loaded PLGA nanoparticles (GEM-PLGA) and cRGDfK conjugated GPN (GEM-PLGA@cRGDfK)

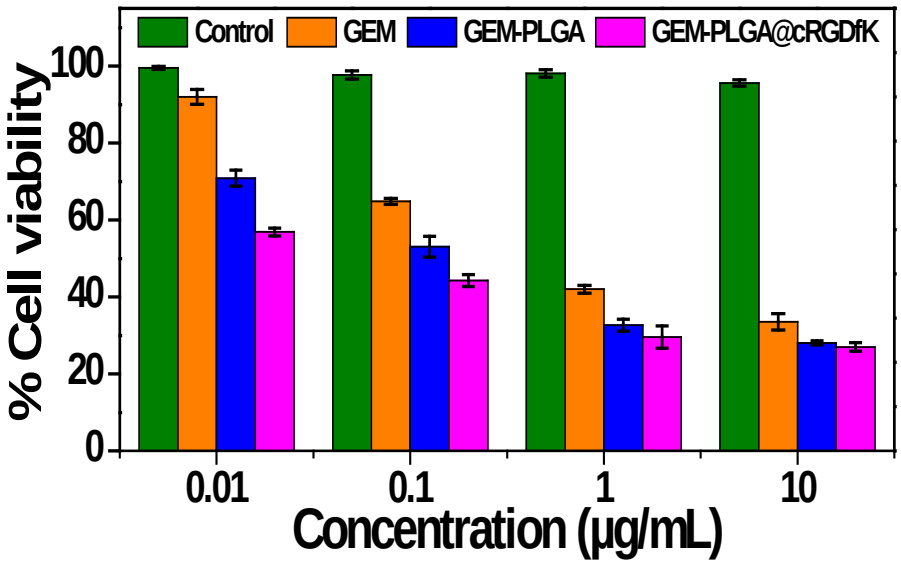

Figure 7.4: % Cell viability of SKOV-3 human ovarian cancer cells incubated with *Gemcitabine (GEM), GEM loaded PLGA nanoparticles (GEM-PLGA) and cRGDfK conjugated GPN (GEM-PLGA@cRGDfK)*

The relative anti-cancer efficacy of pristine GEM, GEM-PLGA and GEM-PLGA@cRGDfK is evident from Figure 7.4, which shows that all these formulations inhibited cell proliferation in a dose-dependent manner. At the lowest tested concentration (0.01 µg/mL), cell viability was 92.1%, 70.8% and 56.9% for GEM, GEM-PLGA and GEM-PLGA@cRGDfK, respectively. After 48 h incubation, the IC_{50} of GEM-PLGA@cRGDfK (0.034 ± 0.004 µg/mL) was 16.4 fold and 3.8 fold lesser than pristine GEM (0.572 ± 0.013 µg/mL; $p < 0.001$) and GEM-PLGA (0.148 ± 0.01 µg/mL; $p < 0.05$), respectively. These results clearly indicate that cRGDfK-conjugated nanoparticles exhibit significantly higher cytotoxicity than free drug or targeting peptide-free nanoparticles against SKOV-3 human ovarian cancer cells. This improved anticancer efficacy of GEM-PLGA@cRGDfK particles is due to the ability of cRGDfK peptide to bind to $\alpha_v\beta_3$ integrin receptors. This allows enhanced uptake of drug-loaded particles through integrin receptor-mediated endocytosis while

avoiding drug efflux pumps, leading to sustained intracellular drug concentration resulting in greater cytotoxic effects (Liu et al., 2008; Danhier et al., 2012). In contrast, regular efflux of free drug from the cytoplasm via P-glycoprotein pumps leads to the lower cytotoxicity of pristine GEM (Alexander et al., 2005). This is supported by the observation that as the drug concentration is increased, the three formulations start showing similar cytotoxicity effects due to a sustained intracellular drug concentration. For instance, at the highest tested drug concentration (10 µg/mL), cell viability was 32.5%, 28% and 26.9% for GEM, GEM-PLGA and GEM-PLGA@cRGDfK, respectively. Therefore, our findings suggest that while GEM-based chemotherapy offers high potential against SKOV cancer cells, conventional GEM formulation (pristine drug solution) is not effective as it requires high dosage treatment that leads to systematic toxicity, as evident from the blood compatibility studies. Conversely, the ability of targeted nanoparticles to allow high intracellular drug concentrations even following a low dosage administration offers an efficient drug delivery platform for gemcitabine.

7.3.4. Influence of intracellular drug uptake on mitochondrial membrane potential (MMP), reactive oxygen species (ROS), and apoptosis

Cellular uptake studies were performed to validate whether integrin receptor targeting ability of cRGDfK peptide is indeed responsible for higher intracellular drug concentrations achieved by cRGDfK-conjugated particles over that of unconjugated PLGA particles. Since gemcitabine does not have fluorescence properties, a set of two new fluorescent particles, viz. RhB loaded PLGA (RPN) and cRGDfK conjugated RPN (RRPN) were prepared in a manner similar to that of drug-loaded particles; however in this case GEM was replaced with RhB, a red fluorescent dye. On exposure of these particles to SKOV-3 cells for 2 h, it becomes clear that conjugation of cRGDfK peptide on the particle surface significantly improves their intracellular

uptake, most likely due to the overexpression of $\alpha_v\beta_3$ receptors in these ovarian cancer cells (Figure 7.5). These results also validate the effectiveness of our cRGDfK peptide grafting strategy onto the nanoparticle surface, as the ability of $\alpha_v\beta_3$ integrin receptors to specifically recognize cRGDfK peptide and promote its internalisation is well-established (Danhier et al., 2012). Further, the Hoechst nuclear staining of particle-treated cells suggests that particles remain in the cytoplasm post-internalisation. Control experiments revealed that SKOV-3 cells treated with these drug-free particles retained more than 95% cell viability, indicating high biocompatibility of polymers and surfactants employed to prepare the proposed nanocarrier system.

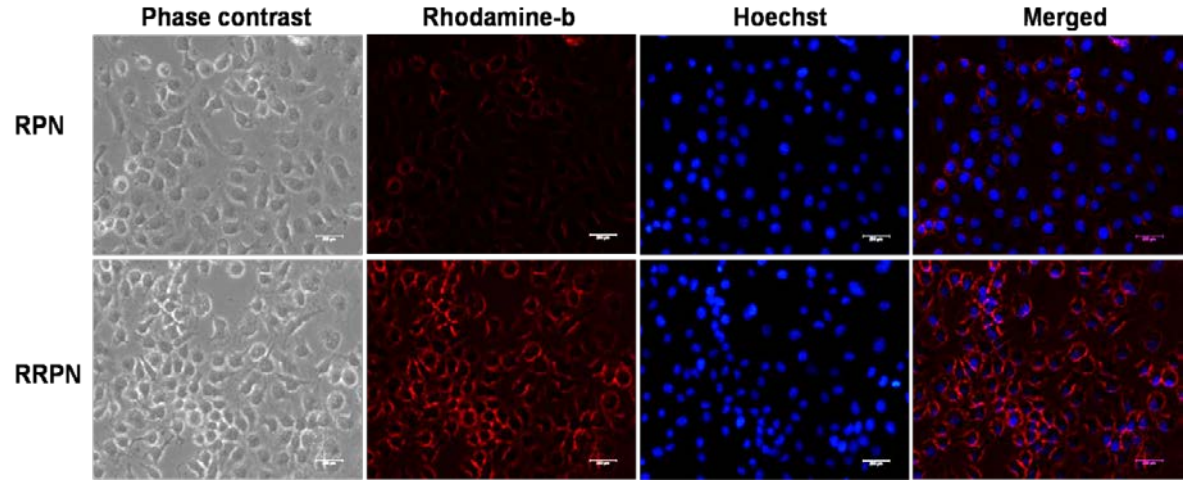

Figure 7.5: Comparative cellular uptake of Rhodamine-b loaded PLGA nanoparticles (RPN) and cRGDfK conjugated RPN (RRPN) after 2 h of incubation

The higher effective intracellular drug concentration achieved by cRGDfK peptide functionalised nanocarriers may influence important intracellular processes such as MMP and ROS generation, both of which jointly participate in promoting cancer cell death via apoptosis (Pelicano et al., 2004; Kuznetsov et al., 2011). Mitochondria are the major cellular organelles that involved in regulation of cell death and a decrease in MMP provides an early indication of the initiation of cellular

apoptosis (Baracca et al., 2003). Figure 7.6 shows the effect of various formulations of gemcitabine on MMP of SKOV-3 cells, as evaluated using Rh-123, a mitochondria-specific fluorescent dye. When SKOV-3 cells are exposed to 0.1 µg/mL equivalent of gemcitabine in the form of pristine GEM, GEM-PLGA and GEM-PLGA@cRGDfK nanoparticles, respectively, a sequential decrease in the cellular uptake of Rh-123 dye is observed (Figure 7.6). This reduction in dye uptake corresponds to 71.49%, 68.35% and 53.65% fluorescence intensity, respectively, for these three formulations with respect to 100% fluorescence in untreated cells. This shows that among different formulations, peptide-conjugated particles cause the highest reduction in the MMP of SKOV-3 cells, most likely due to the highest effective drug concentration per cell achieved by high cellular uptake.

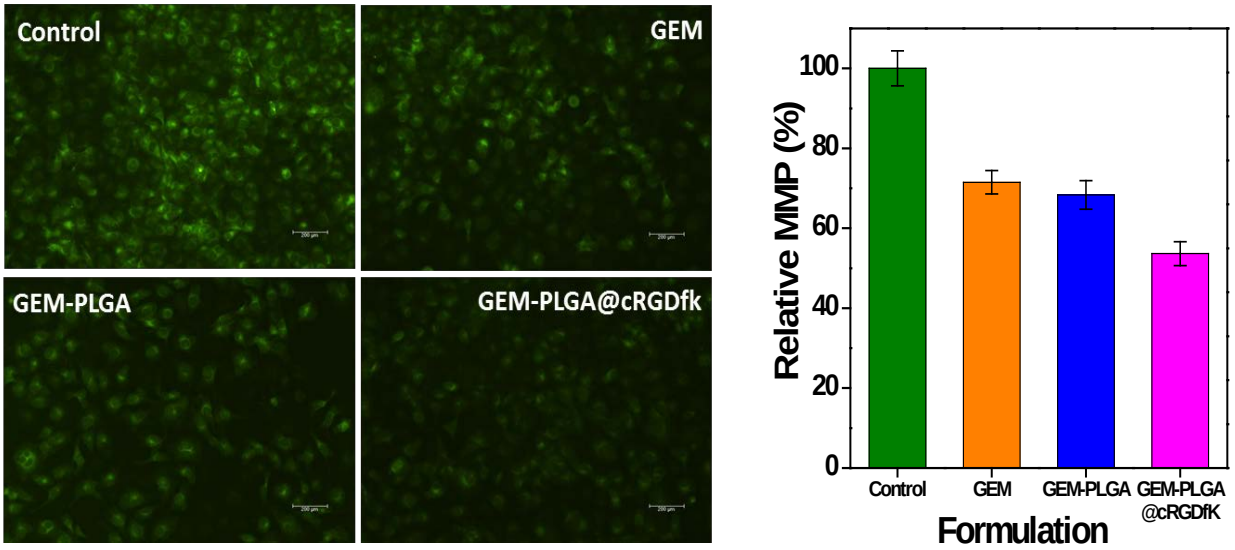

a) *b)*

Figure 7.6 a-b: Change in mitochondrial membrane potential (MMP) determined qualitatively a) and quantitatively b) using rhodamine-123

Induction of ROS is another mechanism by which it elicits antitumor activity (Donadelli et al., 2007). ROS activity in cells can be monitored by DCFDA, which is a cell-permeable, fluorogenic dye that gets deacetylated by cellular esterases to a non-

fluorescent compound in healthy cells. However, ROS produced in the stressed cell environment can oxidise, this non-fluorescent compound into fluorescent 2',7'-dichlorofluorescein (DCF) (Eruslanov and Kusmartsev, 2010). Therefore, an increase in DCF fluorescence indicates increased levels of intracellular ROS. While untreated cells showed minimal ROS generation; among three formulations, GEM-PLGA@cRGDfK particles generated the highest levels of ROS, followed by GEM-PLGA particles and pristine GEM drug, as evident from the levels of fluorescence in the respective image (Figure 7.7a). Quantitative assay shows that in comparison to control cells, the DCF fluorescence intensity was enhanced by 3.31, 2.54 and 1.91 times, in cells treated with GEM-PLGA@cRGDfK, GEM-PLGA and free GEM, respectively (Figure 7.7b). The highest level of ROS generation in those ovarian cancer cells that were treated with targeting peptide-conjugated nanoparticles further supports the importance of high intracellular uptake of drug in improving its chemotherapeutic potential.

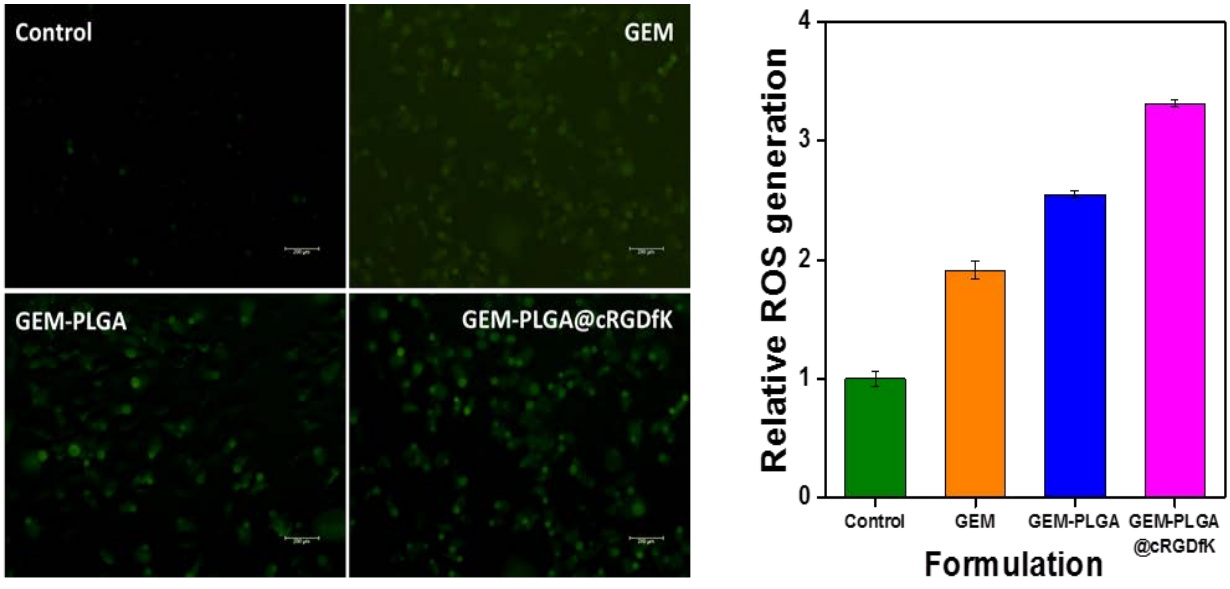

a) ***b)***

Figure 7.7a-b: a) Qualitative and b) quantitative estimation of reactive oxygen species (ROS) generation by various gemcitabine formulations

After treatment with an anticancer drug, apoptosis is the most common mode of cell death (Doonan et al., 2008). Apoptosis can be assessed by changes in biochemical and morphological features such as cell shrinkage, chromatin condensation, DNA fragmentation, and breakdown of the cell into apoptotic bodies (Doonan et al., 2008). Nuclear or DNA fragmentation, a late event in apoptosis, was assessed in SKOV-3 cells with a nucleus-specific Hoechst 33342 dye (Figure 7.8). The nuclei of untreated SKOV-3 cells were spherical and integral with homogenous fluorescence, whereas the nuclei of cells treated with different GEM formulations became increasing condensed and severely fragmented on exposure to pristine GEM (9.8%), GEM-PLGA nanoparticles (23.7%) and GEM-PLGA@cRGDfK nanoparticles (42.3%). Apoptosis studies therefore further validate the importance of cRGDfK peptide in achieving high anticancer activity of gemcitabine formulations against integrin-overexpressing ovarian cancer cells.

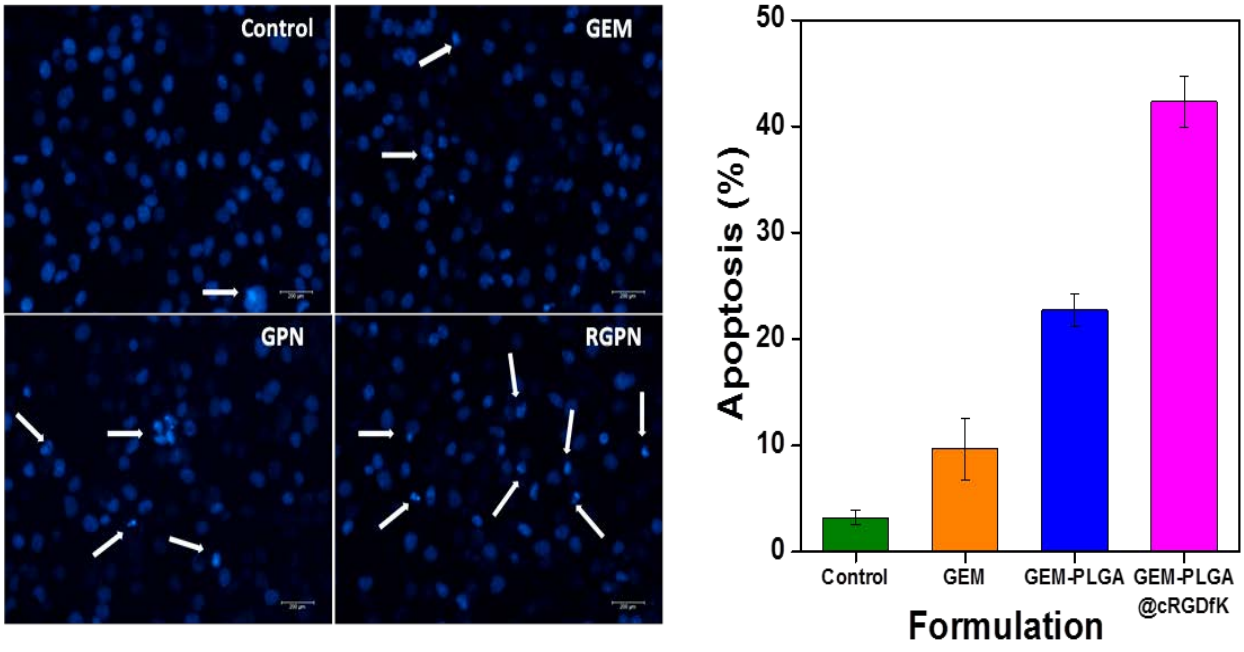

a) *b)*

Figure 7.8a-b: a) Qualitative and b) quantitative determination of apoptosis using Hoechst 33342 staining

7.4. Conclusion

To summarise, new targetable drug delivery system was developed to enhance the efficacy of an FDA-approved water-soluble chemotherapeutic drug (Gemcitabine hydrochloride) against ovarian cancers. The proposed nanoparticle formulations demonstrate narrow size distribution, high encapsulation efficiency, sustained release of drug and high biocompatibility. Our nanocarrier utilises the outstanding ability of a cationic cyclic pentapeptide (cRGDfK) to specifically target the $\alpha_v\beta_3$ integrin receptors overexpressed in ovarian cancer cells (SKOV-3). This targeting ability promotes the receptor-mediated internalisation of nanocarriers in SKOV-3 cells while remaining relatively safer towards non-target cells, such as that observed via low hemolytic toxicity against RBCs. The efficient uptake of nanocarriers by SKOV-3 cells leads to a high effective intracellular concentration of drug, even at low dosages treatments. This efficient drug uptake, in turn enhances the antiproliferative activity of gemcitabine hydrochloride by influencing important intracellular processes such as reduction in MMP, increase in intracellular ROS and cellular apoptosis. Considering the increasingly recognised association of integrin receptors with ovarian tumour progression, our findings provide a good basis for future preclinical and clinical studies, along with future development of smart targeted drug delivery systems for newly approved hydrophilic anticancer drugs-based chemotherapeutics.

7.5. References

- Akhtar MJ, Ahamed M, Alhadlaq HA, Alrokayan SA, Kumar S. Targeted anticancer therapy: Overexpressed receptors and nanotechnology. *Clin Chim Acta* 2014,**436**:78–92.

- Alexander RL, Greene BT, Torti SV, Kucera GL. A novel phospholipid gemcitabine conjugate is able to bypass three drug-resistance mechanisms. *Cancer Chemother* Pharmacol 2005,**56(1)**:15-21.
- Baracca A, Sgarbi G, Solaini G, Lenaz G. Rhodamine 123 as a probe of mitochondrial membrane potential: evaluation of proton flux through F(0) during ATP synthesis. *Biochim Biophys Acta* 2003,**1606**:137-46.
- Hodge LS, Taub ME, Tracy TS. Effect of its deaminated metabolite, 2',2'-difluorodeoxyuridine, on the transport and toxicity of gemcitabine in HeLa cells. *Biochem Pharmacol* 2001,**81(7)**, 950-6.
- Brannon-Peppas L, Blanchette JO. Nanoparticle and targeted systems for cancer therapy. *Adv Drug Deliv Rev* 2012,**64**:206–12.
- Cheng Z, Zaki AA, Hui JZ, Muzykantov VR, Tsourkas A. Multifunctional Nanoparticles: Cost Versus Benefit of Adding Targeting and Imaging Capabilities. *Science* 2012,**338**:903-10.
- Cho K, Wang X, Nie S, Chen ZG, Shin DM. Therapeutic nanoparticles for drug delivery in cancer. *Clin Cancer Res* 2008,**14**:1310–6.
- Chu, E., Devita, V. T., Physicians' Cancer Chemotherapy Drug Manual. Jones and Bartlett Publishers, Toronto, 201–204 (2007).
- Cunliffe D, Kirby A, Alexander C. Molecularly imprinted drug delivery systems. *Adv Drug Deliv Rev* 2005,**57**:1836–53.
- Danhier F, Le Breton A, Préat V. RGD-based strategies to target alpha (v) beta(3) integrin in cancer therapy and diagnosis. *Mol Pharm* 2012,**9(11)**:2961-73
- Deng C, Jiang Y., Cheng R, Meng F, Zhong Z. Biodegradable polymeric micelles for targeted and controlled anticancer drug delivery: Promises, progress and prospects. *Nano Today* 2012,**7(5):**467–80.

- Derakhshandeh K, Fathi S. Role of chitosan nanoparticles in the oral absorption of Gemcitabine. *Int J Pharm* 2012,**437**:172– 7.
- Donadelli M, Costanzo C, Beghelli S, Scupoli MT, Dandrea M, Bonora A, Piacentini P, Budillon A, Caraglia M, Scarpa A, Palmieri M. Synergistic inhibition of pancreatic adenocarcinoma cell growth by trichostatin A and gemcitabine. *Biochim Biophys Acta* 2007,**773**:1095–1106.
- Doonan F, Cotter TG. Morphological assessment of apoptosis. *Methods* 2008,**44(3)**:200-4.
- Duenas-Gonzalez A, Coronel J, Cetina L. Pharmacokinetic evaluation of gemcitabine hydrochloride for the treatment of cervical cancer. *Expert Opin Drug Metab Toxicol* 2011,**7:**1601–12.
- Eruslanov E, Kusmartsev S. Identification of ROS using oxidized DCFDA and flow-cytometry. *Methods Mol Biol* 2010,**594**:57-72.
- Feigin LA, Svergu DA. Structure Analysis by Small-Angle X-Ray and Neutron Scattering. Plenum Press, New York 1987.
- Guinier A, Fournet G. Small-Angle Scattering of X-Rays. John Wiley and Sons, New York 1995.
- Huang P, Plunkett W. Fludarabine- and gemcitabine-induced apoptosis: Incorporation of analogs into DNA is a critical event. *Cancer Chemother Pharmacol* 1995,**36**:181–8.
- Jia F, Liu X, Li L, Mallapragada S, Narasimhan B, Wang Q. Multifunctional nanoparticles for targeted delivery of immune activating and cancer therapeutic agents. *J Control Release* 2013,**172(3)**:1020-34.
- Kanapathipillai M, Brock A, Ingber, DE. Nanoparticle targeting of anti-cancer drugs that alter intracellular signaling or influence the tumor microenvironment. *Adv Drug Deliv Rev* 2014,**79–80**:107–18.

- Kulhari H, Pooja D, Shrivastava S, VGM N, Sistla R. Peptide conjugated polymeric nanoparticles as a carrier for targeted delivery of docetaxel. *Colloids Surf, B* 2014,**117**:166-73.
- Kuznetsov AV, Margreiter R, Amberger A, Saks V, Grimm M. Changes in mitochondrial redox state, membrane potential and calcium precede mitochondrial dysfunction in doxorubicin-induced cell death. *Biochim Biophys Acta* 2011,**1813(6)**:1144-52.
- Kwon, I. K., Lee, S. C., Han, B., Park, K. Analysis on the current status of targeted drug delivery to tumors. *J Control Release* 2012,**164(2)**:108-14.
- Landen CN, Kim TJ, Lin YG, Merritt WM, Kamat AA, Han LY, Spannuth WA, Nick AM, Jennnings NB, Kinch MS, Tice D, Sood AK. Tumor-selective response to antibody-mediated targeting of $\alpha_v\beta_3$ Integrin in ovarian cancer. *Neoplasia* 2008;**10**:1259–67.
- Liu Z, Wang F, Chen X. Integrin $\alpha_v\beta_3$-Targeted Cancer Therapy. *Drug Dev Res* 2008,**69(6)**:329–39.
- Lorusso D, Di Stefano A, Fanfani F, Scambia G. Role of gemcitabine in ovarian cancer treatment. *Ann Oncol* 2006 **17**:v188–94.
- Lossner D, Abou-Ajram C, Benge A, Reuning U. Integrin $\alpha_v\beta_3$ mediates upregulation of epidermal growth-factor receptor expression and activity in human ovarian cancer cells. Int. J. Biochem. *Cell Biol* 2008,**40**:2746–61.
- Martín-Banderas L, Sáez-Fernández E, Holgado MA, Durán-Lobato MM, Prados JC, Melguizo C, Arias JL. Biocompatible gemcitabine-based nanomedicine engineered by Flow Focusing for efficient antitumor activity. *Int J Pharm* 2013,**443**:103-9.
- Paolino D, Cosco D, Racanicchi L, Trapasso E, Celia C, Iannone M, Puxeddu E, Costante G, Filetti, S, Russo, D, Fresta, M. Gemcitabine-loaded PEGylated

unilamellar liposomes vs GEMZAR®: Biodistribution, pharmacokinetic features and in vivo antitumor activity. *J Control Release* 2010,**144**:144–50.

- Pelicano H, Carney D, Huang P. ROS stress in cancer cells and therapeutic implications. *Drug Resist Updat* 2004,**7**:97–110.
- Pooja D, Panyaram S, Kulhari H, Rachamalla SS, Sistla R. Xanthan gum stabilized gold nanoparticles: characterization, biocompatibility, stability and cytotoxicity. *Carbohydr Polym* 2014,**110**:1-9.
- Schmitt A, Schmitt J, Munch G, Gasic-Milencovic J. Characterization of advanced glycation end products for biochemical studies: side chain modifications and fluorescence characteristics. *Anal Biochem* 2005,**338**:201-15.
- Tao XM, Wang JC, Wang JB, Feng Q, Gao SY, Zhang LR, Zhang Q. Enhanced anticancer activity of gemcitabine coupling with conjugated linoleic acid against human breast cancer in vitro and in vivo. *Eur J Pharm Biopharm* 2012,**82(2)**:401-9.
- Torchilin VP. Multifunctional nanocarriers. *Adv Drug Deliv Rev* 2012,**64**:302–15.
- Ye F, Barrefelt A, Asem H, Abedi-Valugerdi M, El-Serafi I, Saghafian M, Abu-Salah K, Alrokayan S, Muhammed M, Hassan M. Biodegradable polymeric vesicles containing magnetic nanoparticles, quantum dots and anticancer drugs for drug delivery and imaging. *Biomaterials* 2014,**35**:3885–94.
- Zhang L, Gu FX, Chan JM, Wang AZ, Langer RS, Farokhzad OC. Nanoparticles in medicine: therapeutic applications and developments. *Clin Pharmacol Ther* 2008**,83**:761–9.

CHAPTER

Peptide grafted and self-assembled poly(glutamic acid) nanoparticles for active targeting of Camptothecin to glioblastoma cells

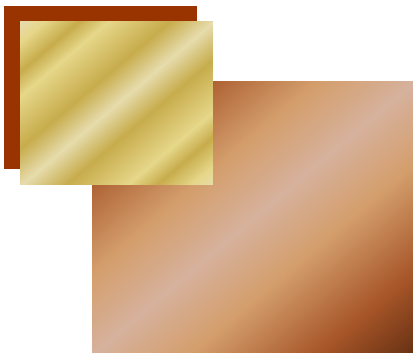

8.1. Background

Glioblastoma (GBM) is the most common type of brain tumor, accounting for 29% of primary brain cancers (Tirapelli et al., 2010). Among all types of cancer, GBM is the most difficult to treat as it localizes in brain that has limited capacity to repair itself. In addition GBM tumors show inherent resistance to conventional therapy and have poor blood supply; thus drug delivery is inhibited (Mrugala, 2013). Tumor infiltration into brain tissue makes it very difficult to treat GBM with conventional surgical removal. Because of this diffusive invasion, recurrence from residual tumors is also very common (Nikki et al., 2012). Therefore, multiple therapies are needed to treat GBM. Currently, the best approach for the management of GBM is initial surgery followed by radiation and adjuvant chemotherapy (Reardon and Wen, 2006; Chang et al., 2006; Kanu et al., 2009). Chemotherapy plays an important role in the treatment of GBM especially in recurrent GB, however, the blood brain barrier, drug resistance and systemic toxicity of anticancer drugs decrease the therapeutic efficacy of available agents (Harr et al., 2012).

In recent years, ligand-mediated, targeted drug delivery has shown promise in effective delivery of drugs to brain tumors (Huile Gao et al., 2013; Chen and Liu, 2012). In ligand-mediated drug delivery, nanoparticle surfaces are modified with a ligand that selectively binds to specific receptors on cancer cells. Receptors for molecules such as glucose (Dhanikula et al., 2008), folate (Beduneau et al., 2007), human epidermal growth factor (Kuo et al., 2011), lectins (Du et al., 2009; He at el., 2011), lactoferrin (Pang et al., 2010;), transferrin (Tianet al., 2010; Pang et al., 2011) and integrin have been studied as a potential targets for chemotherapy to treat brain cancer (Gabathuler, 2010; Ulbrich et al., 2009; Demeule et al., 2008; Quin et al., 2011; Hu et al., 2009; Morris and Sharma, 2011; Bies et al., 2004; Wu et al., 2006).

Peptides, such as TAT-peptide, that can penetrate cells have also been used to target brain tumor (Qin et al., 2011; Han et al., 2010). However, these cell penetrating peptides may also enhance the penetration of nanocarriers into normal cells resulting in toxicity. $\alpha_v\beta_3$ integrins are over-expressed on endothelial and tumor cells in both primary and recurrent GBM. RGD-based peptides have high affinity towards $\alpha_v\beta_3$integrins and cyclic RGD peptides have been used successfully for in vivo imaging, magnetic resonance imaging and drug delivery to GBM (Jiang et al., 2011; Zhan et al., 2010; Xie et al., 2008). Kim et al., (2011) used RGD-conjugated peptide and radioactive iodine-labelled gold nanoparticles for imaging of tumor sites. Jin et al., (2013) synthesised cRGDyK conjugated paramagnetic nanoprobes for the imaging of $\alpha_v\beta_3$ overexpressing U87MG tumor xenografts.

In this study, cRGDfK conjugated poly(glutamic) acid nanoparticles were synthesized for the selective delivery of camptothecin (CPT) to GBM. CPT is a natural quinone alkaloid that has high efficacy against malignant gliomas (Lee et al., 2010; Cirpanli et al., 2011; Martins et al., 2013). CPT binds to the topoisomerase I-DNA complex during cell division, stabilizing the complex and therefore prevents the replication processes (Li et al., 2006). Moreover, CPT acts only in the S-phase of cell cycle. As cancer cells have longer S-phase compared to normal healthy cells, s-phase selectivity makes CPT a suitable drug candidate in the development of a targeted drug delivery system for GBM (Pizzolato and Saltz, 2003).

8.2. Experimentation

8.2.1. Materials

cRGDfK was purchased from Peptide International (Kentucky, USA). CPT, Poly (glutamic) acid (PGA), phenyl alanine (PA), EDC, NHS, DMEM, trypsin–EDTA, penicillin, streptomycin, MTT, dimethyl sulfoxide (DMSO) and propidium iodide (PI)

were purchased from Sigma Aldrich (Australia). FBS was purchased from Gibco, USA. DCFDA and Hoechst 33342 were purchased from Life Technologies Australia Pty Ltd. (Australia).

8.2.2. Synthesis and characterization of phenylalanine ester (PAE)

Thionyl chloride (0.87 mL, 12.1 mM) was added to a solution of phenylalanine (1 g, 6.05 mM) in methanol. The reaction was continued for 30 min in an ice-bath and then stirred for 24 h at room temperature. After completion of the reaction (as monitored by thin layer chromatography), an excess of thionyl chloride was removed under reduced pressure using a rota-evaporator. PAE was obtained as a white solid powder and characterized by ^{1}H NMR and FTIR analysis.

8.2.3. Synthesis and characterization of PGA-PA conjugate

PGA-PA conjugate was synthesized as described previously (Matsusaki et al., 2004). Briefly, 200 mg of PGA was dissolved in 30 mL of sodium bicarbonate solution (50 mM) and placed in an ice-bath on a magnetic stirrer. Then, EDC (300 mg) was added and stirred for 1 h. Thereafter, PAE (310 mg) was added to the reaction mixture and stirred overnight. PGA-PA conjugate was purified by dialysis against distilled water for three days, freeze-dried and stored. The conjugate was characterized by ^{1}HNMR and FTIR analysis.

8.2.4. Preparation and characterization of CPT loaded PGA-PA nanoparticles (CPN)

For the preparation of CPT loaded PGA-PA nanoparticles (CPN), CPT and PGA-PA were dissolved in DMSO and mixed with surfactant solution (1.5% w/v Tween 80). The dispersion was dialyzed against distilled water for 24 h and then centrifuged for 30 min at 15,000 rpm. The nanoparticle pellet was redispersed in distilled water and again centrifuged to remove free or non-encapsulated drug. Drug loaded nanoparticles were freeze-dried and stored at 4 °C. The amount of drug in

the supernatant was determined using an Ultra performance liquid chromatography (UPLC) system (Waters Acquity UPLC, AUS). A reversed-phase column (Acquity C18, 1.7 µm, 2.5 × 50 mm) was used at 30 °C. The mobile phase was composed of methanol and water (45:55). The flow rate was set at 0.45 mL/min and the detection wavelength was 256 nm.

Particle size and zeta potential were determined by photon correlation spectroscopy using a Zetasizer Nano-ZS. The surface morphology of nanoparticles was studied by TEM. DSC analysis of native CPT and CPN were carried out on a DSC-Q100 (TA Instruments, USA). The samples were scanned from 220 to 300 °C at a speed of 10 °C/min, under nitrogen environment. XRD patterns of CPT and CPN were obtained in the range of 5–45º using an X-ray diffractometer, equipped with a graphite crystal monochromator (CuKa). The instrument was set at a voltage of 40 KV and a current of 40 mA.

8.2.5. Bioconjugation of cRGDfK to CPN

Nanoparticles (50 mg) were dispersed in 5 mL of PBS and incubated with EDC (35 mg) and NHS (21 mg). After 30 min, cRGDfK was added and stirred for 4 h at room temperature. cRGDfK conjugated nanoparticles were obtained by centrifugation and washed three times with PBS. The supernatant was used to determine the amount of unconjugated cRGDfK.

8.2.6. Cell culture

U87MG Human glioblastoma cells were obtained from Peter MacCallum Cancer Institute, Australia. Cells were grown in DMEM media supplemented with 10% FBS, 2 mM glutamine, penicillin (100 U/mL), and streptomycin (0.1 mg/mL). Cells were cultivated under standard conditions at 37 °C in a humidified atmosphere (85% relative humidity) containing 5% CO_2.

8.2.7. In vitro cytotoxicity assay

The cytotoxicity of the pure CPT and drug-loaded nanoparticles was evaluated by the MTT assay. U87MG cells (5×10^3) were seeded in 96-well plates and incubated for 24 h. Cells were then treated with CPT, CPN or RCPN (1-400 ng/mL) for 24 and 48 h at 37 °C. Untreated cells served as controls. After incubation, 100 µL of DMEM medium containing MTT reagent (0.5 mg/mL) was added to each well. The plate was then incubated at 37 °C for 4 h. The violet-colour formazan crystals were dissolved in 150 µL of DMSO. Absorbance was measured at 570 nm using a microplate reader and the percentage viability of cells was calculated as the ratio of absorbance of sample to control wells.

8.2.8. Cellular uptake of nanoparticles in cells

Comparative uptake of unconjugated (RPN) and cRGDfK conjugated nanoparticles (RRPN) was studied using rhodamine-b loaded nanoparticles. Cells were incubated with RPN and RRPN for 2 h at 37 °C. Cells were washed twice with PBS and stained with 5 µg/mL of Hoechst 33342 to stain nuclei. After 30 min incubation, cells were washed with PBS and observed by fluorescence microscopy.

8.2.9. Estimation of apoptosis

Apoptosis in cells treated with CPT, CPN and RCPN was estimated by an Annexin V PE Cys5.5 and PI assays. Concentration of all three reagents was 50 ng/mL. Cells were seeded in 6-well plates at 1×10^6 cells/well and incubated for 24 h to allow adherence to the plate surface. Cells were treated with 50 ng/mL of CPT, CPN or RCPN for 24 h. The cells were then collected, washed with PBS, stained according to the manufacturer's instructions and analyzed using a flow cytometer (BD FACSCanto™ II).

8.2.10. Nuclear staining with Hoechst 33242

Nuclear morphology of CPT, CPN or RCPN treated cells was studied by Hoechst 33342 staining. Hoechst 33342 is a DNA specific fluorescent dye used to study nuclear morphology. U87MG cells (1×10^5) were seeded in 24-well microplates and incubated overnight. Cells were then incubated with free drug or nanoparticles (CPT concentration 20 ng/mL). After washing with PBS, cells were stained with Hoechst 33342 (5 µg/mL) at 37 °C for 30 min in the dark. Cells were washed again with PBS and observed under afluorescence microscope. % Apoptosis was determined as follows:

% Apoptosis = (Number of apoptotic cells/ Total number of cells) × 100

8.2.11. Measurement of reactive oxygen species (ROS)

U87MG cells were seeded at a density of 1×10^5 cells per well in 24-well plates and incubated for 24 h at 37 °C. Cells were then treated with CPT formulations equivalent to 20 ng/mL of CPT for 24 h, washed twice with PBS and fixed with 4% paraformaldehyde for 10 min. After washing two times with PBS, cells were incubated with DCFDA (10 µM) for 30 min in the dark. Cells were finally washed with PBS and observed using a fluorescence microscope (Nikon, Japan).

For quantitative estimation of ROS, cells were harvested using 0.25% trypsin-EDTA and washed with PBS. Cell counts were adjusted for all formulations. Cells were incubated with DCFDA (10 µM) for 30 min in the dark and fluorescence intensity was measured at excitation and emission wavelengths of 495 and 520 nm, respectively, using a Hitachi F-3010 spectrofluorometer.

8.2.12. Wound healing scratch assay

The effect of CPT formulations on wound healing or the migration of cells was analyzed by the scratch-wound healing assay, with slight modification as reported by Ma et al., 2014. U87MG cells were cultured to form an approximate80% confluent

monolayer. The monolayers were scratched with a sterile 200-µL pipette tip to form a "wound". Cells were washed twice with PBS to remove cellular debris. Cells were then incubated with CPT, CPN or RCPN in serum-free media for 24 h. Images were captured at 0 and 24 h to monitor the migration of cells into the wound area using a photomicroscope (Nikon, Japan). The % of wound closure was determined by measuring the wound area using Image J analysis software.

8.2.13. Statistical analysis

All studies were performed in triplicate and results are expressed as Mean ± SD (standard deviation). Statistical significance was determined using the student t-test for two groups and one-way ANOVA for multiple groups. Statistical significance was assumed at $p < 0.05$.

8.3. Results and discussion

8.3.1. Synthesis and characterization of PGA-PA conjugates

PGA is a water soluble, biodegradable, naturally occurring poly(amino acid) composed of glutamic acid molecules linked through the amide bonds between α-amino and γ-carboxylic acid groups (Kim et al., 2009; Moncha and Mararitis, 2008). Because of aqueous solubility, native PGA is not suitable as drug delivery carrier. Therefore, it was conjugated with hydrophobic PA to produce an amphiphilic copolymer which spontaneously forms nanoparticles in aqueous solution. The structure of PGA-PA nanoparticles is a shell type with a hydrophobic PA core and an outer hydrophilic cortex of PGA (Scheme 1).

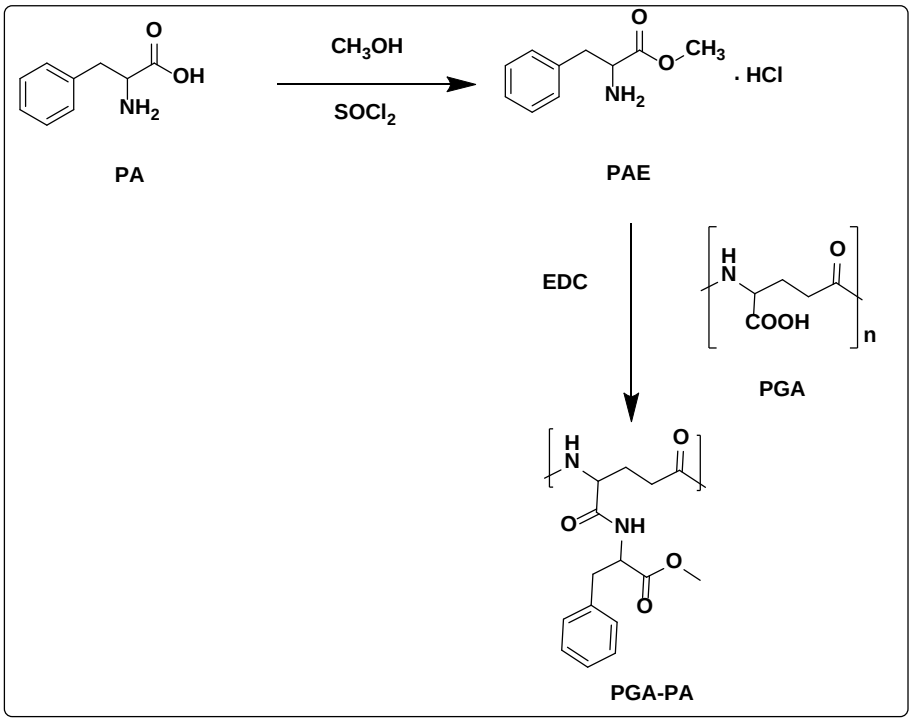

a)

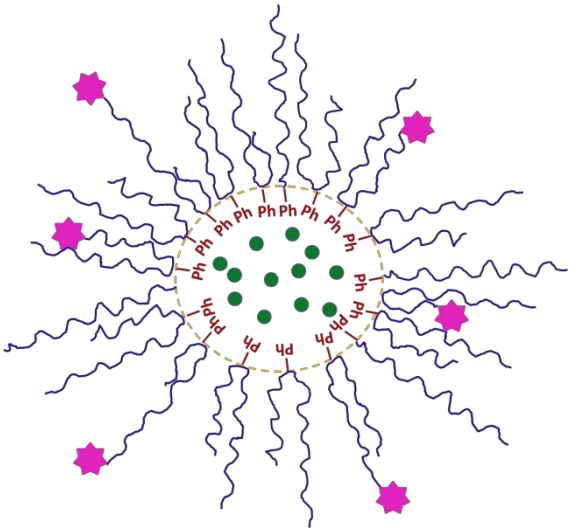

b)

Scheme 8.1: a) Chemical synthesis of phenyl alanine ester (PAE) from phenyl alanine (PA) and then conjugation of PAE to poly (glutamic) acid (PGA) to form PGA-PA conjugate b) Schematic diagram showing cRGDfK conjugated and Camptothecin loaded self-assembled PGA-PA nanoparticles

For the synthesis of poly (glutamic acid)-phenyl alanine conjugate (PGA-PA) firstly, phenyl alanine (PA) was converted to phenylalanine ester (PAE). Esterified PA was conjugated to PGA through a carbodiimide reaction and conjugation efficiency was determined by NMR analysis (Figure 1a). The peaks corresponding to the methylene protons (δ 2.1) of PGA and the aromatic protons of the benzene ring (δ 7.3) of PA were compared. The conjugation efficiency was 52.9%. The PGA-PA conjugate was also confirmed by FTIR analysis (Figure 1b). The FTIR spectrum of PA showed two characteristic N-H stretching vibration bands at 3078 cm^{-1} and 3030 cm^{-1}. Bands corresponding to asymmetric and symmetric stretching vibrations of the carboxylic group (COO^-) were observed at 1557 cm^{-1} and 1409 cm^{-1}, respectively. The stretching vibration band of benzene appeared at 745 cm^{-1}. After esterification of the carboxylic group of PA, a sharp band was observed at 1736 cm^{-1}indicative of C=O stretching of the ester bond. The FTIR spectrum of PGA showed bands at 3263 cm^{-1} (NH stretching), 1644 cm^{-1} (amide I) and 1551 cm^{-1} (amide II).

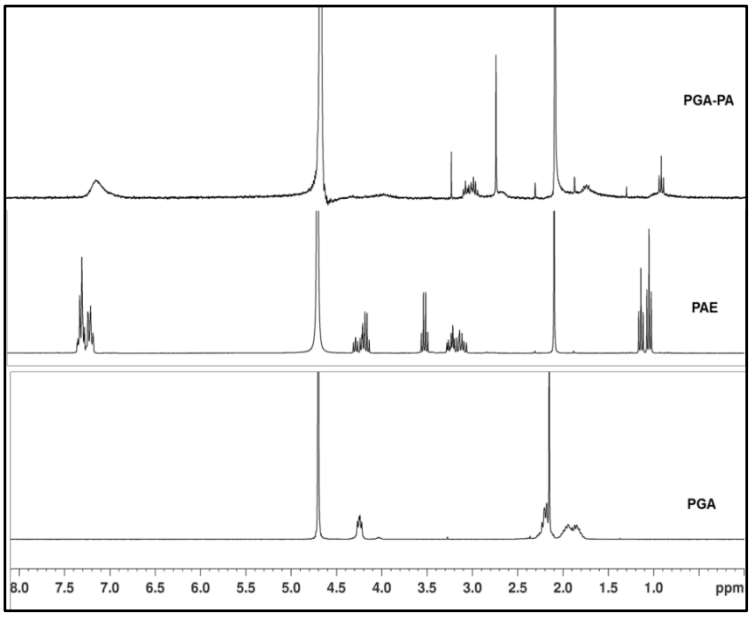

a)

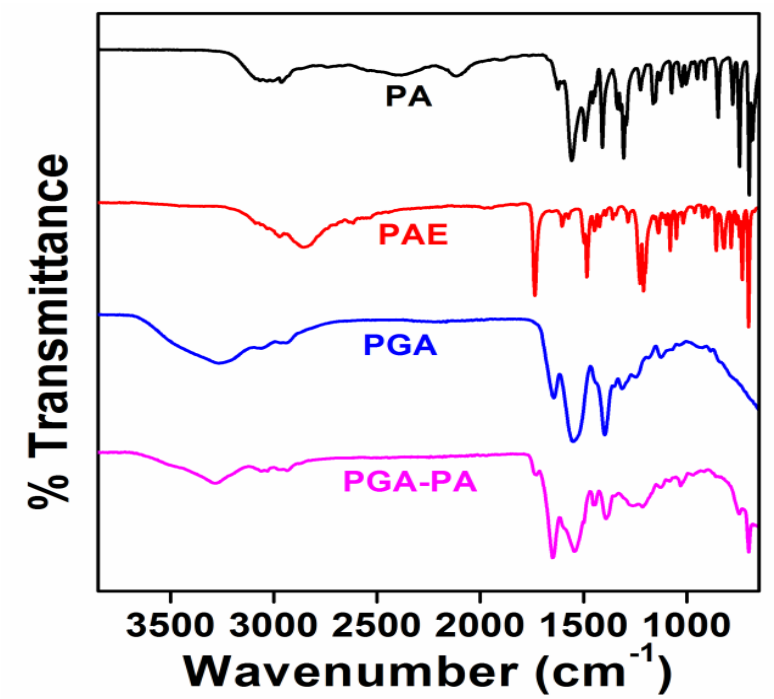

b)

Figure 8.1a-b. a).^{1}H NMR spectra of phenylalanine ester (PAE), poly(glutamic acid) (PGA) and poly(glutamic acid)-phenylalanine conjugate (PGA-PA) b). FTIR spectra of phenyl alanine (PA), phenylalanine ester (PAE), poly(glutamic acid) (PGA) and poly(glutamic acid)-phenylalanine conjugate (PGA-PA)

PGA was conjugated to PA through amide coupling between the amine group of PA and carboxylic group of PGA. The FTIR spectrum of the PGA-PA conjugate showed a shift in the PGA peaks (3263 to 3278, 1644 to 1648 and 1551 to 1544 cm^{-1}). A new peak at 746 cm^{-1} corresponding to the benzene ring of PA confirmed successful conjugation of PA to PGA.

8.3.2. Characterization of nanoparticles

BPN and CPN were prepared by the dialysis method. Physicochemical parameters of different nanoparticles are presented in Table 1. BPN showed particle size of 66 nm with very low polydispersity 0.08 and high negative zeta potential -30.9 mV. After CPT loading, the particle size of nanoparticles was increased slightly to 81.6 nm without a significant change in polydispersity (0.09) and zeta potential (-29.7

mV). cRGDfK grafted nanoparticles were of 89.7 nm in size and -16.7 mV zeta potential (Table 1). A decrease in negative zeta potential of RCPN confirmed the conjugation of cRGDfK on the surface of CPN. The size of the nanoparticles after drug loading and cRGDfK conjugation was less than 100 nm; an ideal size for a nanocarrier system to across the blood-brain barrier (Chen and Liu, 2012).

Table 8.1: Physicochemical characterization of empty poly(glutamic acid) nanoparticles (BPN), campatothecin-loaded PGA nanoparticles (CPN) and cRGDfK conjugated CPN (RCPN)

Formulation	Particle size (nm)	PDI	ZP (mV)	%EE
BPN	66.07 ± 2.41	0.08 ± 0.03	-30.9 ± 2.36	-
CPN	81.68 ± 1.79	0.09 ± 0.02	-29.7 ± 1.14	68.41 ± 3.95
RCPN	89.76 ± 2.58	0.10 ± 0.02	-16.4 ± 1.86	65.22 ± 1.47

Morphology of nanoparticles was studied using TEM analysis (Figure 2). The size of the nanoparticles after drug loading and cRGDfK conjugation was less than 100 nm; an ideal size for a nanocarrier system to cross the blood-brain barrier (Chen and Liu, 2012). RCPN were also characterized by FTIR analysis (Figure 3). % encapsulation efficiency for CPN and RCPN was 68.4% and 65.2%, respectively.

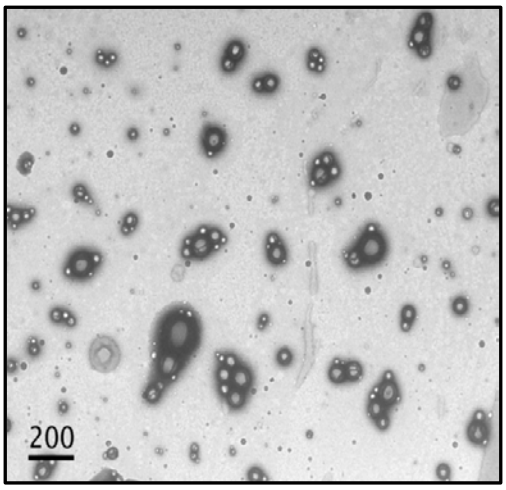

Figure 8.2. Transmission electron microscopic image of PGA-PA nanoparticles. The scale represent diameter in nanometer.

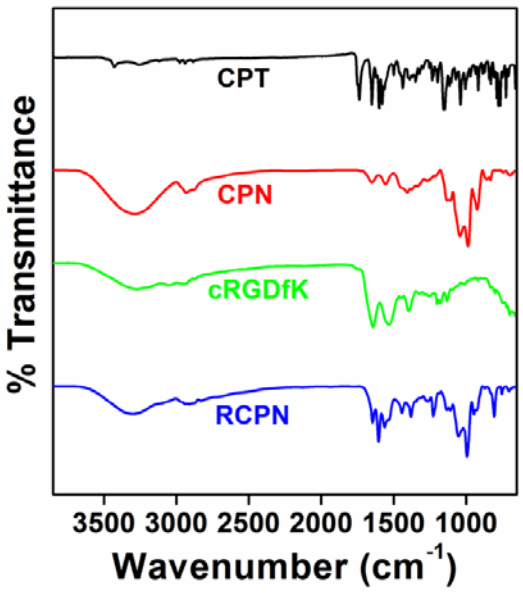

Figure 8.3: FTIR spectra of CPT, CPN, cRGDfK peptide and cRGDfK conjugated CPN.

Drug loaded nanoparticles were also characterized for differential scanning calorimetry (DSC) and x-ray diffraction (XRD) analysis. DSC spectra of CPT and CPN are presented in Figure 4a. The DSC spectra of CPT showed a sharp endothermic peak at 268 °C corresponding to its melting point. However, the absence of a CPT peak in may be due to its amorphous or disordered crystalline sate or to solid solution in polymeric matrix of nanoparticles.

Figure 4b demonstrates the XRD patterns of pure CPT, PGA-PA conjugate, a physical mixture of CPT and PGA-PA, and CPN. The XRD pattern of raw CPT showed characteristic high-intensity diffraction peaks at diffraction angles of 2θ 6.2°, 8.5°, 11.5°,12.1°, 13.6°, 17.8° and 25° suggesting the crystalline nature of the drug (Guijin et al., 2013). Due to its amorphous nature, the XRD patterns of PGA-PA did not show any sharp peaks. We observed all the characteristic peaks of CPT in the XRD pattern of the physical mixture of CPT and PGA-PA, demonstrating a lack of chemical interaction between CPT and PGA-PA. However, owing to transformation

of CPT from a crystalline to an amorphous phase during nanoparticle preparation, the peaks representing CPT were absent in the CPN XRD pattern.

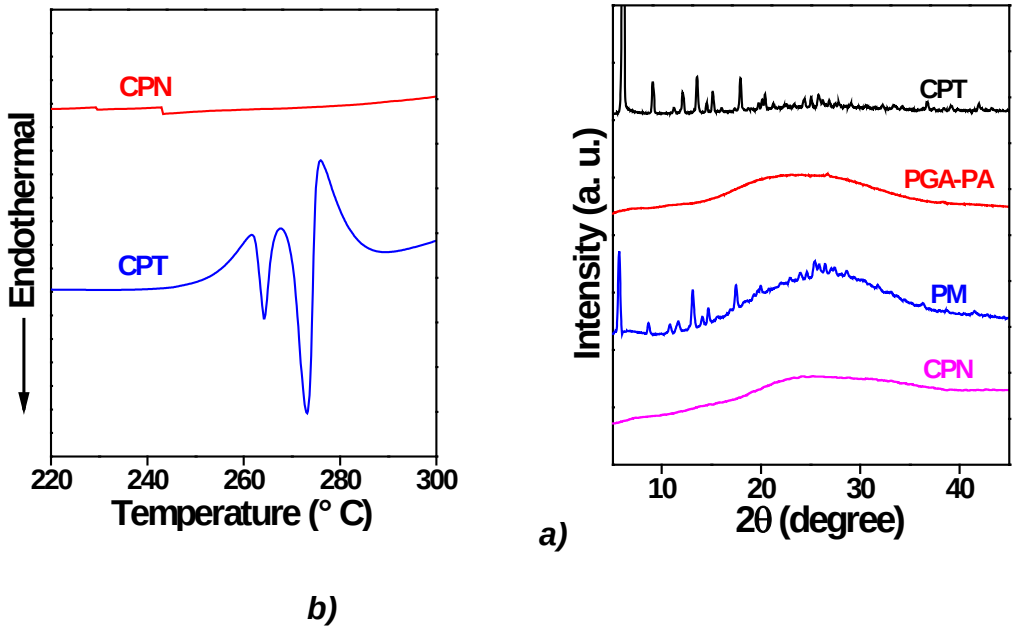

Figure 8.4a-b. a) Differential scanning calorimetry spectra of camptothecin (CPT), Poly(glutamic acid)-phenylalanine conjugate (PGA-PAE) and CPT loaded PGA-PAE nanoparticles (CPN). b) X-ray diffraction pattern of CPT, PGA-PA, physical mixture of CPT and PGA-PA (PM) and CPN.

8.3.3. In vitro cytotoxicity

In order to investigate the anti-proliferation activity of native CPT and CPT loaded formulations (CPN and RCPN), cell viability of U87MG human glioblastoma cells was determined using the MTT assay. Anticancer activities of pure drug as well as drug-loaded nanoparticles depend on both the dose of drug and time of incubation. Therefore, U87MG cells were incubated with free CPT, CPN or RCPN, equivalent to 1-400 ng/mL of CPT, for 24 and 48 h. The cell viability of U87MG cells after 24 h and 48 h are shown in Figure 5a and 5b, respectively. All three formulations showed caused a significant decrease in cell viability. IC50 values for the three formulations are presented in Table 2. After 24 h, targeted nanoparticles (RCPN, IC50 30.46 ng/mL) were more effective than non-targeted nanoparticles

(CPN, IC50 168.29 ng/mL) and native CPT (IC50 552.21 ng/mL). A similar pattern was observed after 48 h incubation where the IC50 value of RCPN (11.34 ng/mL) was 2.3 and 5.4 times lower than CPN (27.05) and CPT (61.78 ng/mL), respectively. The results suggest RCPN not only inhibits cell growth at higher efficiency than native CPT but also lowers the minimum effective dose required for cytotoxicity.

Table 8.2: IC_{50} value of pure campatothecin (CPT), CPT loaded PGA nanoparticles (CPN) and cRGDfK conjugated CPN (RCPN) against U87MG human glioblastoma after 24 and 48 h incubation.

Formulation	IC_{50} (ng/mL)	
	After 24 h	After 48 h
CPT	552.21 ± 7.38	54.51 ± 2.06
CPN	168.29 ± 4.92	22.57 ± 0.98
RCPN	30.46 ± 1.59	11.34 ± 1.25

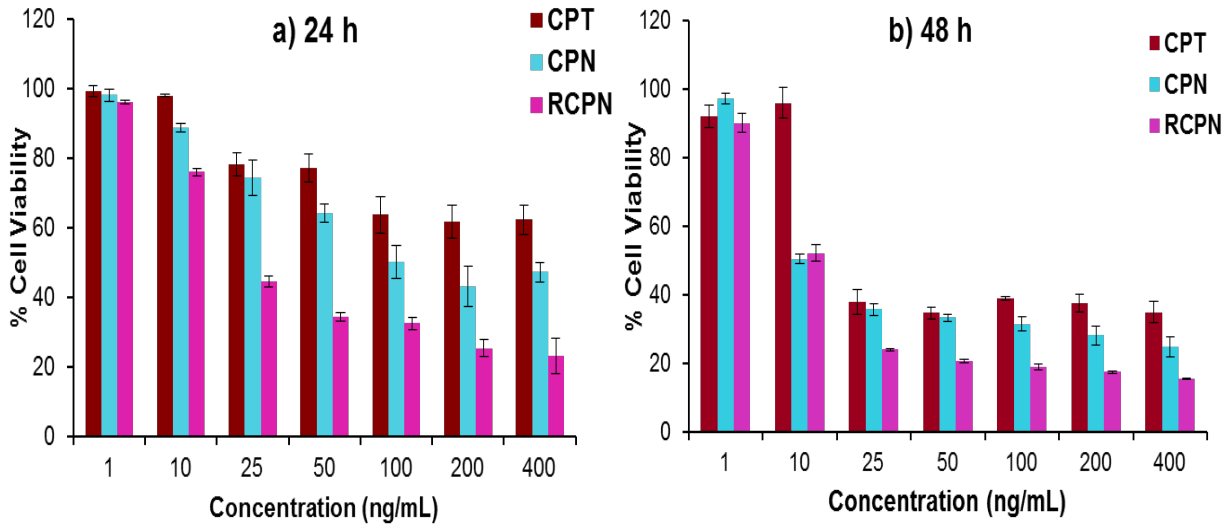

Figure 8.5a-b. % Cell viability of U87MG human glioblastoma cells treated with Camptothecin (CPT), CPT loaded PGA-PAE nanoparticles (CPN) and cRGDfK conjugated loaded CPN (RCPN) for a) 24 h and b) 48 h.

8.3.4. Uptake of nanoparticles by U87MG cells

Internalization of nanoparticles was studied using Rho-b loaded nanoparticles. Nuclei were visualized by Hoechst 33342 staining. Figure 6 shows fluorescence microscopic images of U87MG cells after 2 h of incubation with nanoparticles. cRGDfK conjugated and Rho-b loaded PGA nanoparticles (RRPN) showed higher intracellular accumulation of Rho-b than unconjugated nanoparticles (RPN). The increased uptake of targeted nanoparticles could be attributed to the presence of cRGDfK on the surface of nanoparticles. Peptide containing RGD moieties have been reported to be taken uptake by U87MG cells more efficiently than unconjugated nanoparticles (Chen et al., 2009; Rangger et al., 2013). Therefore, the enhanced cytotoxicity of RCPN formulation than CPN can be correlated to the higher uptake of RRPN.

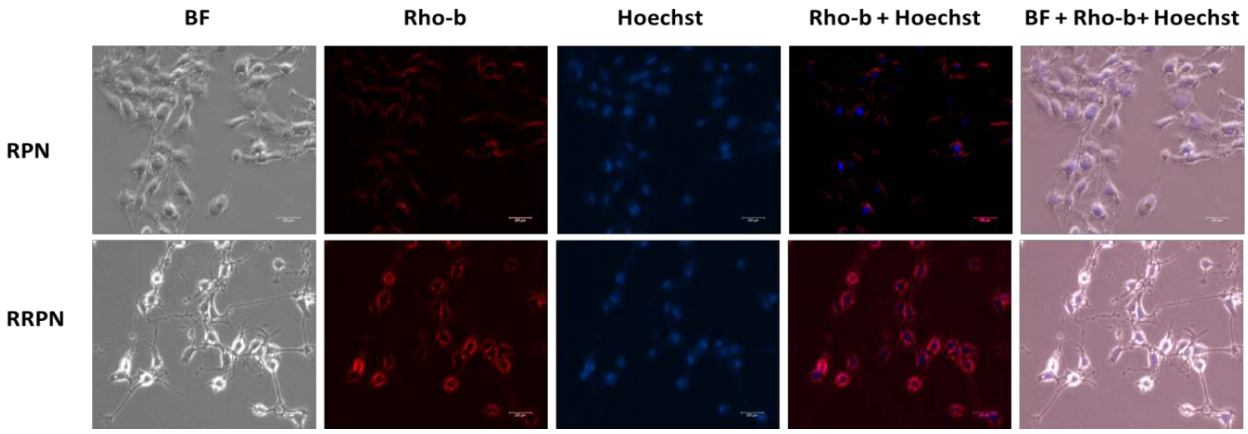

Figure 8.6: Cellular uptake of Rhodamine-b loaded PGA nanoparticles (RPN) and cRGDfK conjugated RPN (cRGDfK) by U87MG human glioblastoma cells.

8.3.5. Analysis of apoptosis

GBM cells exhibit less apoptosis than normal cells (Kesari, 2013). Apoptosis induced by targeted CPT nanoparticles was also analysed by flow cytometer analysis. As shown in Figure 7a, the percentage of live U87MG cells was decreased

with the three CPT formulations. The percentage of live cells in control, CPT, CPN and RCPN was 98.4%, 71.6%, 62.4% and 52.5%, respectively. The ability of the different CPT formulations to induce cell death followed the order: RCPN>CPN>CPT (Figure 4a). Cells treated with RCPN were more apoptotic compared to those treated with native drug and CPN. The percentage of apoptotic cells after treatment with RCPN (46.9%), was much higher than with CPN (35.6%) and CPT (26.9%) treatment. Thus, RCPN induced more apoptosis than CPN or non-encapsulated CPT; most likely due to enhanced intracellular delivery of drug.

Apoptosis was also studied qualitatively and quantitatively using Hoechst staining. Cells treated with CPT, CPN or RCPN showed fragmented nuclei whilst control or untreated cells demonstrated intact nuclei (Figure 7b, c). The findings are consistent with those from Annexin Cys5.5 PI assays.

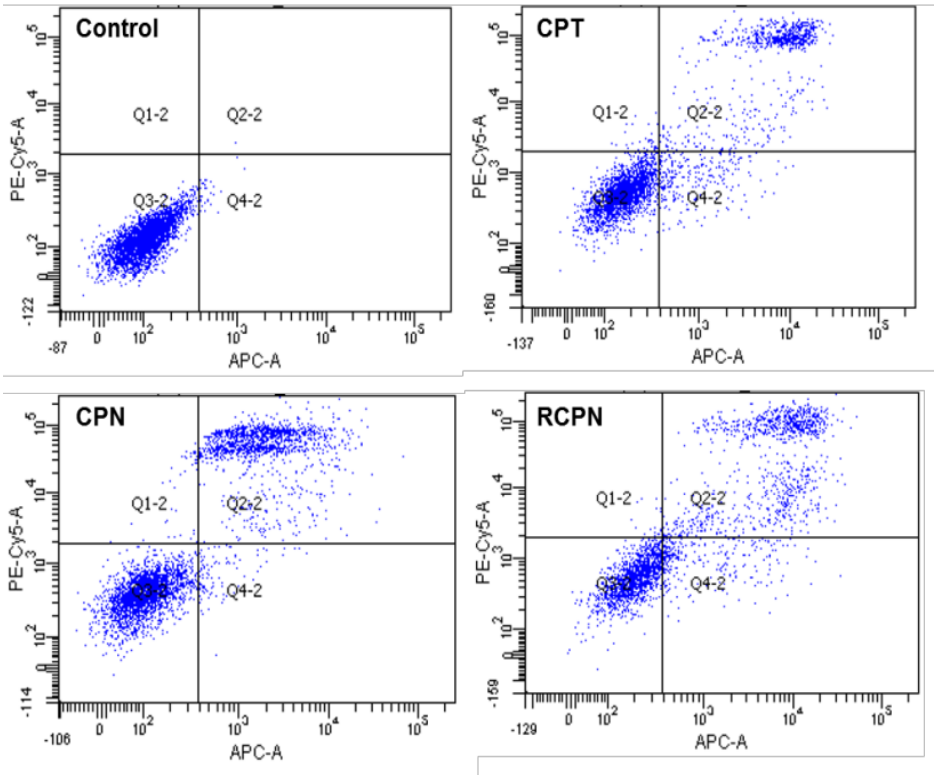

a)

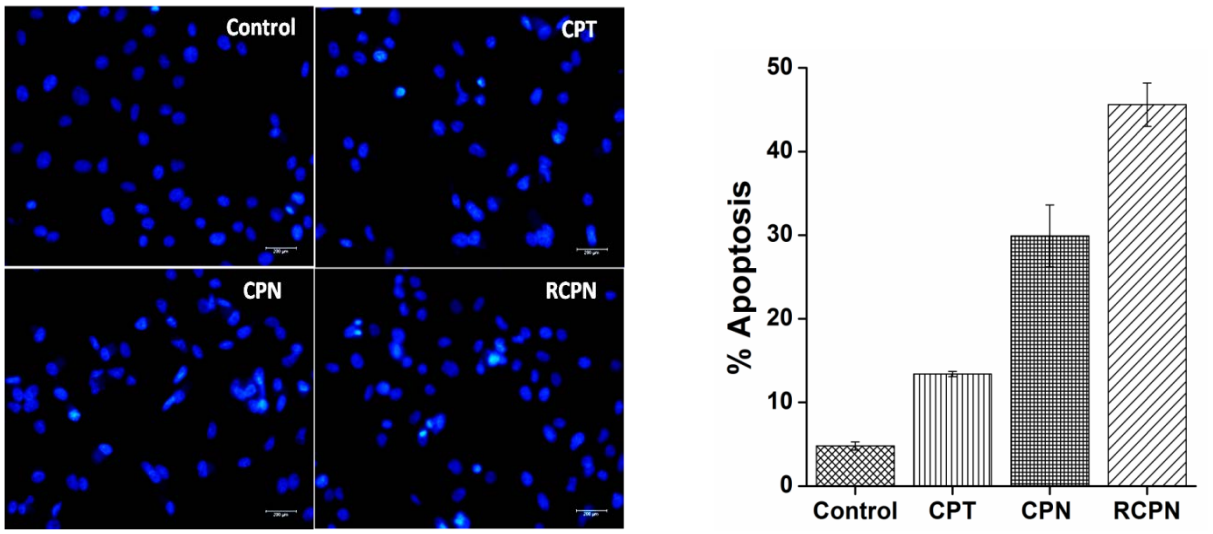

b) ***c)***

Figure 8.7a-c: Apoptosis studies: a) Quantitative analysis of apoptosis induced by camptothecin (CPT), CPT loaded PGA-PA nanoparticles (CPN) and cRGDfK conjugated loaded CPN (RCPN) in U87MG human glioblastoma cell. (b) Fluorescent microscopic images of nucleus of U87MG cells stained with Hoechst 33342 stained after treatment with CPT, CPN and RCPN and (c) % apoptosis determined by Hoechst 33342 staining after treatment 24 h of treatment with CPT, CPN and RCPN.

8.3.6. Intracellular ROS generation

Anticancer drugs, including CPT, generate ROS (Hollomon et al., 2013; Pizzolato and Saltz, 2003; Mizutani et al., 2002, 2005). Intracellular generation of ROS can be measured using the DCFDA dye. Fluorescent intensity of DCFDA is directly related to intracellular ROS levels. In present study, fluorescence intensity was measured both qualitatively and quantitatively (Figure 8a, b). Control, or untreated cells, showed less green fluorescence than drug treated cells. Among the three CPT formulations, RCPN showed 2.51 and 1.48 times higher fluorescence intensity than CPT and CPN, respectively. This may be explained by the enhanced intracellular delivery of CPT by targeted nanoparticles.

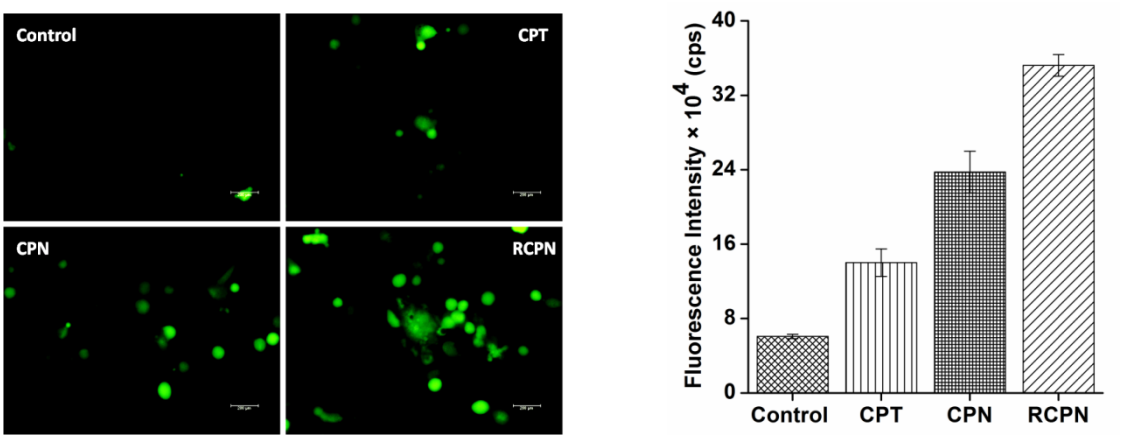

a) *b)*

Figure 8.8a-b: a) Qualitative and b) Quantitative determination of reactive oxygen species (ROS) generation in U87MG human glioblastoma cell after treatment with camptothecin (CPT), CPT loaded PGA-PA nanoparticles (CPN) and cRGDfK conjugated loaded CPN (RCPN).

8.3.7. Wound-healing assay

Gliomas exhibit significant angiogenesis that is induced by vascular endothelial growth factor (VEGF). VEGF is responsible for the formation of new blood vessels required for tumor growth and cell migration (Kesari et al., 2011; Hoeben et al., 2004). To study the effect of targeted delivery of RCPN on the cell migration of U87MG, wound-healing or scratch assays were performed. Cells were observed by light microscopy. Figure 9 shows the migration distance observed after 0 and 24 h of wound creation. % closure of wound area observed after 24 h of treatment was 98.1%, 63.8%, 47.4% and 5.7% for control, CPT, CPN and RCPN, respectively.

Control or untreated U87MG cells exhibit self-healing and migration. RCPN significantly diminishes cell migration, while CPN and CPT show slight inhibitory activity. The greater inhibition of cell migration by RCPN can be attributed to higher anti-angiogenic activity via $\alpha_v\beta_3$integrin receptors that are up regulated on vascular endothelial cells in tumors (Hoeben et al., 2004).

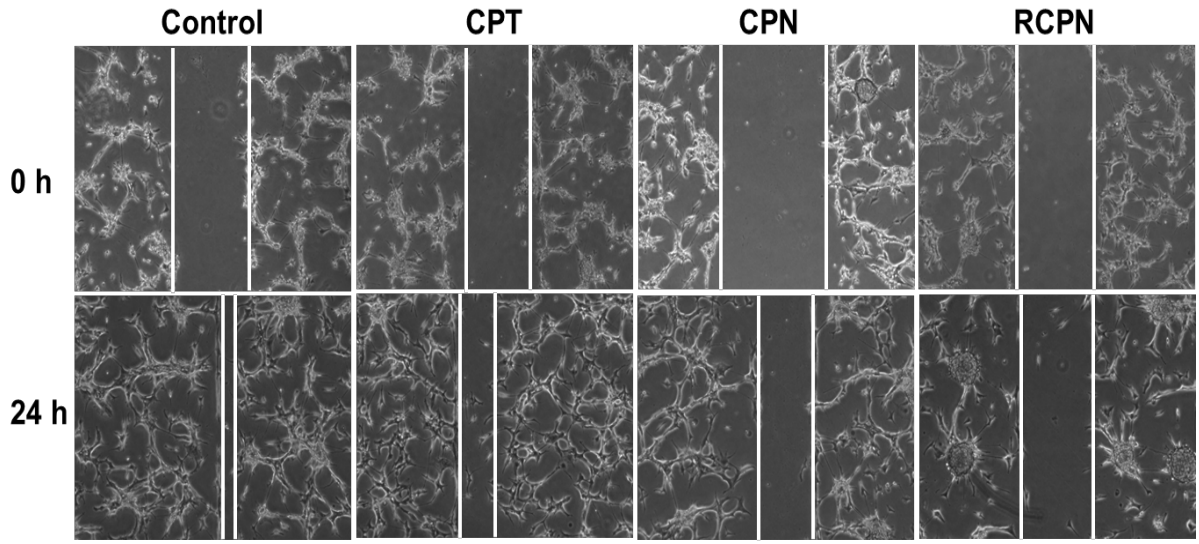

Figure 8.9: Wound healing scratch assay: Figure shows the wound area in U87MG cells after 0 and 24 h of treatment with different formulations. Campatothecin formulations showed inhibition of wound healing by decreasing the migration of the cells. However, inhibition of cell migration was more in cRGDfK peptide conjugated nanoparticles (RCPN) than plain CPT and unconjugated nanoparticles (CPN). Control or untreated cells showed almost complete healing of wound after 24 h.

8.3.8. Stability of nanoparticles

Lyophilized RCPN were stable up to 2 months. RCPN did not show a significant change in the physicochemical parameters such particle size, surface charge and drug content.

8.4. Conclusion

In summary, self-assembled poly(amino acid) based nanoparticles were successfully prepared for the targeted delivery of CPT to glioma cells. The nanoparticles contain a hydrophobic phenylalanine core and a hydrophilic surface corona of poly(glutamic acid). Antitumor effects of RCPN are shown by anti-proliferation activity, cell morphology and induction of apoptosis. Targeted nanoparticles show higher cellular uptake, induced apoptosis through ROS generation and better control over cell migration than non-targeted nanoparticles.

8.5. References

- Beduneau A, Saulnier P, Benoit JP. Active targeting of brain tumors using nanocarriers. *Biomaterials* 2007;**28(33):**4947-67.
- Bies C, Lehr CM, Woodley JF. Lectin-mediated drug targeting: history and applications. *Adv Drug Deliv Rev* 2004;**56**(4):425-35.
- Chen K, Xie J, Chen X. RGD-human serum albumin conjugates as efficient tumor targeting probes. *Mol Imaging* 2009;**8(2)**:65-73.
- Chen Y, Liu L. Modern methods for delivery of drugs across the blood–brain barrier. *Adv Drug Deliv Rev* 2012;**64**:640–65.
- Cupaioli FA, Zucca FA, Boraschi D, Zecca L. Engineered nanoparticles. How brain friendly is this new guest? *Prog Neurobiol* 2014;**119-120**:20-38.
- Demeule M, Currie JC, Bertrand Y, Che C, Nguyen T, Regina A, Gabathuler R, Castaigne JP, Beliveau R. Involvement of the low-density lipoprotein receptor-related protein in the transcytosis of the brain delivery vector Angiopep-2. *J Neurochem* 2008;**106**:1534–44.
- Dhanikula RS, Argaw A, Bouchard J-F, Methotrexate loaded polyether-copolyesterdendrimers for the treatment of gliomas: enhanced efficacy and intratumoral transport capability. *Mol Pharm* 2008;**5**:105-16.
- Di X, Shiu RP, Newsham IF, Gewirtz DA. Apoptosis, autophagy, accelerated senescence and reactive oxygen in the response of human breast tumor cells to Adriamycin. *Biochem Pharmacol* 2009;**77**:1139–50.
- Doi A, Kawabata S, Iida K, Yokoyama K, Kajimoto Y, Kuroiwa T, Shirakawa T, Kirihata M, Kasaoka S, Maruyama K, Kumada H, Sakurai Y, Masunaga S, Ono K, Miyatake S. Tumor-specific targeting of sodium borocaptate (BSH) to malignant glioma by transferrin-PEG liposomes: a modality for boron neutron capture therapy. *J Neurooncol* 2008;**87**:287–94.

- Du J, Lu W-L, Ying X. Dual-targeting topotecan liposomes modified with tamoxifen and wheat germ agglutinin significantly improve drug transport across the blood-brain barrier and survival of brain tumor-bearing animals. *Mol Pharm* 2009;**6**:905-17.
- Gabathuler R. Approaches to transport therapeutic drugs across the blood–brain barrier to treat brain diseases. *Neurobiol Dis* 2010; **37:** 48–57.
- Gao H, Yang Z, Zhang S, Cao S, Shen S, Pang Z, Jiang X. Ligand modified nanoparticles increases cell uptake, alters endocytosis and elevates glioma distribution and internalization. *Sci Rep* 2013;**3**:1-8.
- Han L, Zhang A, Wang H. Tat-BMPs-PAMAM conjugates enhance therapeutic effect of small interference RNA on U251 glioma cells in vitro and in vivo. *Hum Gene Ther* 2010;**21**:417-26.
- He H, Li Y, Jia X-R. PEGylated poly(amidoamine) dendrimer-based dual-targeting carrier for treating brain tumors. *Biomaterials* 2011;**32**:478-87.
- Hu K, Li J, Shen Y, Lu W, Gao X, Zhang Q, Jiang X. Lactoferrin-conjugated PEG-PLA nanoparticles with improved brain delivery: In vitro and in vivo evaluations. *J Control Release* 2009;**134:**55–61.
- Jiang X, Sha X, Xin H, Chen L, Gao X, Wang X, Law K, Gu J, Chen Y, Jiang Y, Ren X, Ren Q, Fang X. Self-aggregated pegylated poly (trimethylene carbonate) nanoparticles decorated with c(RGDyK) peptide for targeted paclitaxel delivery to integrin-rich tumors. *Biomaterials* 2011;**32(35):**9457-69.
- Jin J, Xu Z, Zhang Y, GuYJ, Lam MH, Wong WT. Up conversion nanoparticles conjugated with Gd(3+) -DOTA and RGD for targeted dual-modality imaging of brain tumor xenografts. *Adv Healthc Mater* 2013;**2(11):**1501-12.
- Kim H, Akagi T, Akashi M.Preparation of size tunable amphiphilic poly(amino acid) nanoparticles. *Macro Mol Biosci* 2009;**9(9)**:842-8.

- Kim YH, Jeon J, Hong SH, Rhim WK, Lee YS, Youn H, Chung JK, Lee MC, Lee DS, Kang KW, Nam JM. Tumor targeting and imaging using cyclic RGD-PEGylated gold nanoparticle probes with directly conjugated iodine-125. *Small* 2011;**7(14):**2052-60.
- Krex D, Klink B, Hartmann C, von Deimling A, Pietsch T, Simon M, Sabel M, Steinbach JP, Heese O, Reifenberger G, Weller M, Schackert G. Long term survival with glioblastoma multiforme. *Brain* 2007;**13**:2596-2606.
- KuoYC, Liang CT. Inhibition of human brain malignant glioblastoma cells using carmustine-loaded catanionic solid lipid nanoparticles with surface anti-epithelial growth factor receptor. *Biomaterials* 2011;**32**:3340-50.
- Li L, Ishdorj G, Gibson SB. Reactive oxygen species regulation of autophagy in cancer: Implications for cancer treatment. *Free Radic Biol Medic* 2012;**53**:1399–1410.
- Li QY, Zu YG, Shi RZ, Yao LP. Review camptothecin: current perspectives. *Curr Med Chem* 2006;**13(17)**:2021-39.
- Ma J, Fang B, Zeng F, Pang H, Zhang J, Shi Y, Wu X, Cheng L, Ma C, Xia J, Wang Z. Curcumin inhibits cell growth and invasion through up-regulation of miR-7 in pancreatic cancer cells. *Toxicol Lett* 2014;**231(1)**:82-91.
- Manocha B, Margaritis A. Production and characterization of gamma-polyglutamic acid nanoparticles for controlled anticancer drug release. *Crit Rev Biotechnol* 2008;**28(2)**:83-99.
- Matsusaki M, Hiwatari K, Higashi M, Kaneko T, Akashi M. Stably-dispersed and surface-functional bionanoparticles prepared by self-assembling amphipathic polymers of hydrophilic poly(γ-glutamic acid) bearing hydrophobic amino acids. *Chem Lett* 2004;**3**:398–99.

- Morris VB, Sharma CP. Folate mediated l-arginine modified oligo (alkylaminosiloxane) graft poly (ethyleneimine) for tumor targeted gene delivery. *Biomaterials* 2011;**32**:3030-41.
- Mrugala MM. Advances and challenges in the treatment of glioblastoma: a clinician's perspective. *Discov Med* 2013;**15(83):**221-30.
- Nikki A. Charles, Eric C. Holland, Richard Gilbertson, Rainer Glass, Helmut Kettenmann. The brain tumor microenvironment. *Glia* 2012,**60**:502–14.
- Olsztynska S, Komorowska M, Vrielunck L, Dupuy N. Vibrational Spectroscopic Study of L-Phenylalanine: Effect of pH. *Appl Spectrosc* 2001;**55**:901-7.
- Pang Z, Feng L, Hua R. Lactoferrin-conjugated biodegradable polymersome holding doxorubicin and tetrandrine for chemotherapy of glioma rats. *Mol Pharm* 2010;**7**:1995-2005.
- Pang Z, Gao H, Yu Y. Enhanced intracellular delivery and chemotherapy for glioma rats by transferrin-conjugated biodegradable polymersomes loaded with doxorubicin. *Bioconjug Chem* 2011;**22**:1171-80.
- Pardridge WM. Drug transport across the blood-brain barrier. *J Cereb Blood Flow Metab* 2012;**32(11):**1959-72.
- Pinzon-Daza ML, Campia I, Kopecka J, Garzón R, Ghigo D, Riganti C. Nanoparticle- and liposome-carried drugs: new strategies for active targeting and drug delivery across blood-brain barrier. *Curr Drug Metab* 2013;**14:**625-40.
- Qin Y, Chen H, Yuan W, Kuai R, Zhang Q, Xie F, Zhang L, Zhang Z, Liu J, He Q. Liposome formulated with TAT-modified cholesterol for enhancing the brain delivery. *Int J Pharm* 2011;**420**:304–12.
- Rangger C, Helbok A, Sosabowski J, Kremser C, Koehler G, Prassl R, Andreae F, Virgolini IJ, von Guggenberg E, Decristoforo C. Tumor targeting and imaging

with dual-peptide conjugated multifunctional liposomal nanoparticles. *Int J Nanomedicine* 2013;**8**:4659-71.

- Sun X, Ai M, Wang Y, Shen S, Gu Y, Jin Y, Zhou Z, Long Y, Yu Q. Selective induction of tumor cell apoptosis by a novel P450-mediated reactive oxygen species (ROS) inducer methyl 3-(4-nitrophenyl) propiolate. *J Biol Chem* 2013;**288(13):**8826-37.
- Tian W, Ying X, Du J. Enhanced efficacy of functionalized epirubicin liposomes in treating brain glioma-bearing rats. *Eur J Pharm Sci* 2010;**41**:232-43.
- Tirapelli LF, Bolini PH, Tirapelli DP, Peria FM, Becker AN, Saggioro FP, Carlotti Jr CG. Caspase-3 and Bcl-2 expression in glioblastoma: an immunohistochemical study. *Arq Neuropsiquiatr* 2010;**68(4)**:603-7.
- Ulbrich K, Hekmatara T, Herbert E, Kreuter J. Transferrin- and transferrin-receptor-antibody-modified nanoparticles enable drug delivery across the blood–brain barrier (BBB). *Eur J Pharm Biopharm* 2009,**71**:251–6.
- Wong RS. Apoptosis in cancer: from pathogenesis to treatment. *J Exp Clin Cancer Res* 2011;**30**:87.
- Wu G, Barth RF, Yang W, Kawabata S, Zhang L, Green-Church K. Targeted delivery of methotrexate to epidermal growth factor receptor-positive brain tumors by means of cetuximab (IMC-C225) dendrimer bioconjugates. *Mol Cancer Ther* 2006;**5**(1):52-59.
- Xie J, Chen K, Lee HY, Xu C, Hsu AR, Peng S, Chen X, Sun S. Ultrasmall c(RGDyK)-coated Fe3O4 nanoparticles and their specific targeting to integrin alpha(v)beta3-rich tumor cells. *J Am Chem Soc* 2008;**130(24):**7542-3.
- Zhan CY, Gu B, Xie C, Li J, Liu Y, Lu WY. Cyclic RGD conjugated poly(ethylene glycol)-co-poly(lactic acid) micelle enhances paclitaxel anti-glioblastoma effect. *J Control Release* 2010;**143**:136–142.

➢

CHAPTER

Summary and Future Prospective

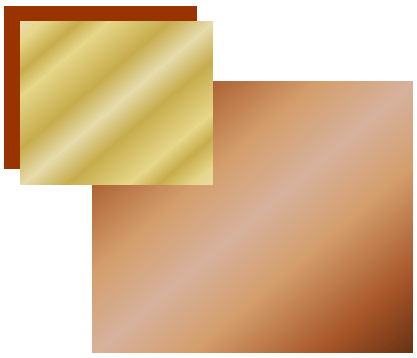

Cancer is one of the most deadly diseases world-wide. After the discovery of nitrogen mustard as first anticancer drug in 1940's, various anticancer drugs have been synthesized or isolated from natural sources (DeVita and Chu, 2008). These anticancer drugs have significant potential against various types of cancer. Taxanes, podophyllotoxins, platinum derivatives and anthracyclines are most commonly used anticancer drugs (Smith and Clark, 2011). However, all of these suffer from several drawbacks such as non-specificity, poor physicochemical properties, poor bioavailability and increasing drug resistance over the course of treatment (Krishna and Mayer, 2000; Ross et al., 2204; Cho et al., 2008). To enhance the aqueous solubility of water insoluble anticancer drugs, pharmaceutical companies use solubilizers such as tween 80 and cremophore EL that cause severe anaphylactic hypersensitivity reactions, neutropenia, hepatotoxicity and fluid retention (Pooja et al., 2014).

This thesis was planned to develop peptide and monoclonal antibody mediated targeted nanoparticles for delivery of current anticancer drugs. Nanoparticles have the ability to deliver the anticancer drugs through enhanced permeability and retention (EPR) effect due to defective vasculature in tumor tissues (Peer et al., 2007). However, when EPR approach is applied, the specificity of the nanoparticles towards cancer cells is only about 30% (Kobayashi et al., 2014). Therefore, there is a strong need for innovative strategies such as ligand-mediated targeted drug delivery systems to deliver anticancer drugs more specifically to cancer cells. Among various targeting ligands, peptides and monoclonal antibodies have high binding affinity towards the specific receptors over-expressed on tumor cells.

Therefore, the work presented in thesis originally aimed to focus on the development of targeted nanoparticles using two peptides, Bombesin (BBN) and cRGDfK, and a monoclonal antibody Trastuzumab (TZ) for the delivery of docetaxel, a hydrophobic anticancer drug (**Chapters 2-6**). Among different targeting ligands, the promising results of cRGDfK-conjugation allowed further studies on delivery of two additional clinically approved anticancer drugs. In those studies, gemcitabine hydrochloride, a hydrophilic drug was utilised for the chemotherapy of ovarian tumor (**Chapter 7**); and Camptothecin, a hydrophobic drug, for the treatment of glioblastoma (**Chapter 8**).

Bombesin conjugated PLGA nanoparticles as drug delivery carrier for docetaxel

PLGA is a clinically-approved biodegradable polymer and has been extensively explored as a component of drug delivery carriers. As demonstrated in **Chapter 2**, the preparation of PLGA nanoparticles was optimized using three surfactants, *viz.*, Tween 80, sodium cholate and PVA. Nanoparticles prepared with sodium cholate showed the smallest particle size with low polydispersity index and high negative zeta potential. These nanoparticles were conjugated with BBN through carbodiimide chemistry to provide them with a breast targeting ability. During stability studies of these nanoparticles, it was observed that BBN conjugated nanoparticles, even though showed reduced zeta potential, were more stable than unconjugated nanoparticles. Detailed investigations revealed that the increase in stability of conjugated nanoparticles was attributed to change in the surface properties and stabilization mechanism of nanoparticles, as conjugated nanoparticles were less hydrophobic than unconjugated nanoparticles. Further, the conjugated nanoparticles

were found to be stabilized by steric stabilization in contrary to electrostatically stabilized unconjugated nanoparticles.

Nanoparticles optimized from chapter 2 were used for the encapsulation of docetaxel **(Chapter 3)**. Docetaxel is a highly potent anticancer agent and being used for the treat of various types of cancer. Encapsulation of docetaxel in nanoparticles was optimized for drug loading and entrapment efficiency. In-vitro cytotoxicity studies in GRP receptors over-expressing MDA-MB-231 human breast cancer cells revealed that BBN peptide conjugated nanoparticles had significantly higher cytotoxicity than unconjugated nanoparticles and pure docetaxel. As GRP receptors are also overexpressed on prostate cancer, the above formulations were also tested against DU145 and PC3 human prostate cancer cells (**Chapter 4**). It was observed that BBN-conjugated docetaxel loaded nanoparticles exhibited higher cytotoxicity and inhibition of cell migration and colony formation than non-targeted nanoparticles and docetaxel alone. Moreover, BBN-conjugated nanoparticles showed faster cellular uptake than unconjugated nanoparticles. During pharmacokinetic and tissue-distribution studies in male Balb/c mice, BBN-conjugated nanoparticles displayed improved pharmacokinetics of docetaxel by increasing mean residence time and decreasing clearance. This suggests that the prepared formulations have significant potential to treat GRP overexpressing breast and prostate cancers.

Trastuzumab conjugated dendrimers for targeted delivery of docetaxel to HER2 receptor overexpressing breast cancer

Another type of receptors that are overexpressed in breast cancer cells includes human epidermal growth factor 2 receptors (HER2). About 20-30% of breast cancer cells overexpress HER2 receptors. Trastuzumab, a monoclonal

antibody, has high affinity towards HER2 receptors. Using a hetero crosslinker MAL-PEG-NHS, transtumuzab was conjugated to PAMAM dendrimers for the selective delivery of docetaxel to HER2 positive breast cancer cells (**Chapter 5**). TZ conjugated dendrimer formulations showed higher cellular uptake and toxicity than unconjugated dendrimers against MDA-MB-453, the HER2 positive breast cancer cells. However, no significant difference between toxicities of both the formulations against MDA-MB-231, the HER2 negative breast cancer cells. This confirmed that the transtuzumab antibody present on the surface of conjugated dendrimers was responsible for its high efficacy. During docetaxel-induced apoptosis studies, cells treated with transtuzumab conjugated formulation were more apoptotic than unconjugated dendrimers. This effect could be attributed to enhanced intracellular delivery of docetaxel by conjugated dendrimers.

Pure PAMAM dendrimers, particularly those with amine surface groups are known to cause hemolysis of red blood cells. Hemolysis assays showed that conjugation of trastuzumab to dendrimers significantly reduce their hemolysis toxicity. Plain PAMAM dendrimers with amine surface groups are cationic in nature and therefore interact with anionic RBC membranes to cause hemolysis. After conjugation with trastuzumab, the surface of PAMAM dendrimers became negatively charged which reduced their interaction with RBC membrane. In-vivo studies revealed higher plasma docetaxel concentration and half-life, decreased clearance and longer mean residence time in trastuzumab-conjugated dendrimers than Taxotere®, a marketed formulation of docetaxel. Therefore, the prepared trastuzumab-mediated dendrimers formulation has the potential as an improved drug delivery platform for the treatment of HER2 positive breast cancer.

Cyclic-RGDfK peptide conjugated succinoyl-TPGS nanomicelles for targeted delivery of docetaxel to integrin receptor over-expressing angiogenic tumours

In a series of development of targeted drug delivery systems, **Chapter 6** investigated the role of cyclic-RGDfK peptide conjugated succinoyl-TPGS nanomicelles for the targeting of docetaxel to integrin receptor over-expressing angiogenic tumours. cRGDfK is a cyclic pentapeptide and has affinity to integrin receptors, particularly $\alpha_v\beta_3$ that are overexpressed in various cancers including breast, prostate, ovarian, pancreatic and brain cancer (Danhier et al., 2012). TPGS is a water soluble derivative of natural Vitamin E. As a drug delivery carrier, TPGS has several advantages like enhancement of aqueous solubility of water-insoluble compounds, simple method of preparation, small micellar size, and opportunity for surface modification (Pooja et al., 2014). The surface of TPGS was modified with succinic anhydride to achieve free carboxylic group bearing TPGS. Docetaxel was encapsulated by solvent casting method and nanomicelles were conjugated to cRGDfK to prepare integrin targeted nanomicelles. The prepared nanomicelles were found to be more effective than plain drug against DU145 human prostate cancer cells. Anti-angiogenic assays revealed strong ability of peptide conjugated nanomicelles to inhibit VEGF-induced proliferation and migration of endothelial cells (HUVEC).

Improving intracellular delivery of hydrophilic gemcitabine hydrochloride (GEM) using cRGDfK peptide functionalized PLGA nanoparticles

With the promising results of cRGDfK conjugated and docetaxel loaded TPSA nanomicelles, cRGDfK conjugated PLGA nanoparticles were developed for the delivery of gemcitabine hydrochloride for the treatment of ovarian cancer. Being a

hydrophilic drug, GEM cannot be encapsulated in hydrophilic TPGS, and therefore PLGA-based drug carriers were developed in this study (**Chapter 7**). GEM loaded PLGA nanoparticles (GPN) were prepared by a double emulsification method and cRGDfK peptide attached to the nanoparticle surface via a carbodiimide reaction. Anticancer efficacy of different GEM formulations was evaluated against integrin receptor over-expressing, SKOV-3 human ovarian cancer cells. cRGDfK conjugated GPN (RGPN) improved the intracellular accumulation of GEM in SKOV-3 cells, leading to an increased anti-proliferative activity and induction of apoptosis. Mitochondrial membrane potential, intracellular reactive oxygen species (ROS) levels and apoptosis-mediated nuclear fragmentation were also evaluated. Overall, this study revealed that this targeted drug delivery system may also have substantial promise for effective delivery and targeting of hydrophilic chemotherapeutics.

cRGDfK conjugated PGA nanoparticles for the targeted delivery of camptothecin to integrin over expressing brain tumors

It has always been challenging to treat brain diseases due to presence of blood brain barrier. As $\alpha_v\beta_3$ integrin receptors are also overexpressed on brain tumor cells, particularly glioblastoma (Danhier et al., 2012), in this last sub-project of this thesis (**Chapter 8**), cRGDfK-based targeted drug delivery system was prepared for the targeting and specific delivery of camptothecin to brain cancer cells. Poly(glutamic acid)-phenyl alanine conjugate was employed for the preparation of nanoparticles. Peptide conjugated nanoparticles (RCPN) with a particle size of less than 100 nm and 65% drug encapsulation efficiency exhibited a dose and time dependent cytotoxicity to U87MG human glioblastoma cells. U87MG cells show high angiogenesis and are one of the best model cancer cells for the anti-angiogenesis studies. RCPN showed induced apoptosis, increase in ROS generation and greater

inhibition of cell migration of U87MG than native camptothecin and unconjugated nanoparticles. In summary, cRGDfK-mediated and amphiphilic copolymer based nanomedicine could offer a promising approach for the delivery of anticancer drugs against glioblastoma and cGRDfK peptide could be a versatile targeting ligand against different cancers including ovarian, prostate and brain cancer.

Future Prospective

Overall, the work presented in this thesis provides an understanding towards development of new nanocarrier systems by employing a number of drug encapsulation and bioconjugation strategies. The results of these studies could be a strong basis for future preclinical studies in tumor-bearing mice and clinical studies. For examples:

- During tissue-distribution studies, it was observed that bombesin grafted PLGA nanoparticles were preferentially accumulated in lungs in comparison to other body tissues. Therefore, the use of bombesin conjugated nanocarriers for delivery of anticancer drugs to lung cancer could be a research interest.
- Additionally, trastuzumab has also been approved by FDA for the treatment of the gastric cancers. Therefore, the efficacy of docetaxel loaded dendrimer-trastuzumab conjugate could be tested for efficacy against HER-2 over expressing gastric cancer.
- The future work could be focused on real-time biodistribution studies using a near-infrared active dye loaded nanoparticles and efficacy studies of drug loaded nanoparticles in tumor bearing mice.
- In recent years, combination therapy (delivering multiple therapeutic agents with a single nanocarrier) has been motivated to overcome some of the problems associated with chemo-resistance. By administering two drugs simultaneously,

the resistance acquired by cells to one of the drugs could be immediately eliminated by another. Therefore, higher therapeutic efficacy could be achieved by simultaneous delivery of multiple drugs targeting the same cellular pathway. The prepared various types of nanocarrier systems in this thesis could be explored as delivery vehicle for combination cancer chemotherapy.

- Last but not the least; it is commonly observed that a particular chemotherapy is effective only for a subset of population. For instance, trastuzumab is found to be effective only against 20% of breast cancer patients that overexpress HER2 receptors (Senkusa et al., 2014). Since, cancer cells typically overexpress more than one type of receptors simultaneously; a unique approach may involve co-grafting of two or more targeting ligands on a single nanocarrier system. This approach many not only further improve the specificity of targeted drug delivery systems, this may also potentially offer an interesting avenue to successfully implement targeted chemotherapy against a larger set of population.

References

- Chanda N, Kattumuri V, Shukla R, Zambre A, Katti K, Upendran A, Kulkarni RR, Kan P, Fent GM, Casteel SW, Smith CJ, Boote E, Robertson JD, Cutler C, Lever JR, Katti KV, Kannan R. Bombesin functionalized gold nanoparticles show in vitro and in vivo cancer receptor specificity. *Proc Natl Acad Sci USA*. 2010;**107(19)**:8760-5.
- Cho K, Wang X, Nie S, Chen ZG, Shin DM. Therapeutic nanoparticles for drug delivery in cancer. *Clin Cancer Res* 2008;**14(5)**:1310-6.
- Danhier F, Le Breton A, Preat V. RGD-based strategies to target alpha(v) beta(3) integrin in cancer therapy and diagnosis. *Mol Pharm* 2012,**9**:2961-73.

- DeVita VT Jr, Chu E. A history of cancer chemotherapy. Cancer Res 2008;68(21):8643-53.
- Guo Y, Luo J, Tan S, Otieno BO, Zhang Z. The applications of Vitamin E TPGS in drug delivery. *Eur J Pharm Sci* 2013,**49**:175-86.
- Kobayashi H, Watanabe R, Choyke PL. Improving Conventional Enhanced Permeability and Retention (EPR) Effects; What Is the Appropriate Target? *Theranostics* 2014;**4(1)**:81–9.
- Krishna R, Mayer LD. Multidrug resistance (MDR) in cancer. Mechanisms, reversal using modulators of MDR and the role of MDR modulators in influencing the pharmacokinetics of anticancer drugs. *Eur J Pharm Sci* 2000;**11(4)**:265-83.
- Peer D, Karp JM, Hong S, Farokhzad OC, Margalit R, Langer R. Nanocarriers as an emerging platform for cancer therapy. *Nat Nanotech* 2007;**2**:751-60.
- Pooja D, Kulhari H, Singh MK, Mukherjee S, Rachamalla SS, Sistla R. Dendrimer-TPGS mixed micelles for enhanced solubility and cellular toxicity of taxanes. *Colloids Surf B Biointerfaces* 2014;**121**:461-8.
- Ross JS, Schenkein DP, Pietrusko R, Rolfe M, Linette GP, Stec J, Stagliano NE, Ginsburg GS, Symmans WF, Pusztai L, Hortobagyi GN. Targeted therapies for cancer. *Am J Clin Pathol* 2004;**122(4)**:598-609.
- Senkusa E, Cardosob F, Pagani O. Time for more optimism in metastatic breast cancer? *Cancer Treatment Reviews* 2014;**40**:220-8.
- Smith FT, Clark CR. Antineoplastic agents. In Beale JM and Block JH, Wilson and Gisvold's Textbook of Organic medicinal and pharmaceutical chemistry. Lippincot Wiliams and Wilkins. 2011, Twelfth edition, 355-412.

Appendices

Appendix 1

My contribution in each chapter of the thesis

Chapter 1: I wrote full chapter and drew the figures (apart from those taken from already published papers) and chemical structures. (Overall contribution 90%)

Chapter 2: Experimentation and data analysis followed by manuscript writing. (Overall contribution 85%)

Chapter 3: Preparation and characterization of formulations, validation of analytical method of estimation of docetaxel content, and manuscript writing. (Overall contribution 80%)

Chapter 4: Cell culture experiments and in-vivo studies and manuscript writing. (Overall contribution 70%)

Chapter 5: Design of project, formulation development and in vivo studies and manuscript writing. (Overall contribution 65%)

Chapter 6: Formulation development, characterization, analysis of data and manuscript writing. (Overall contribution 75%)

Chapter 7: Design of project, cell culture experiments and manuscript writing. (Overall contribution 75%)

Chapter 8: Formulation development and characterization, cell culture experiments and manuscript writing. (Overall contribution 70%)

Appendix 2

List of Publications, Conferences and Workshops during PhD

Published Research and Review Papers

(1) **H Kulhari**, D Pooja, MK Singh, M Kuncha, DJ Adams, R Sistla. (2015) Bombesin-conjugated nanoparticles improve the cytotoxic efficacy of docetaxel against gastrin-releasing but androgen-independent prostate cancer. **Nanomedicine UK** 10:2847-2859. (IF: 5.413)

(2) **H Kulhari,** D Pooja, RSV Kiran, DJ Adams, R Sistla. (2015). Biomedical applications of trastuzumab: as a therapeutic agent and a targeting ligand. **Medicinal Research Reviews** 35(4):849-876. (IF: 8.431)

(3) **H Kulhari**, D Pooja, S Shrivastava, SR Telukutala, AK Barui, CR Patra, N VGM., DJ Adams, R Sistla. (2015). Cyclic-RGDfK peptide conjugated succinoyl-TPGS nanomicelles for targeted delivery of docetaxel to integrin receptor over-expressing angiogenic tumours. **Nanomedicine:NBM** 11(6) 1511–1520. (IF: 6.155)

(4) D Pooja**,** S Panyaram, **H Kulhari**, S Chinde, SS Rachamalla, R Sistla. (2015). Natural gum capped biocompatible gold nanoparticles as drug delivery carrier for anticancer drugs. **International Journal of Biological Macromolecules** 80:48-56. (IF: 3.096)

(5) R Swami, I Singh, **H Kulhari**, MK Jeengar, W Khan, R Sistla. (2015) Docetaxel encapsulated surface modified PAMAM dendrimers for effective delivery to brain. **Journal of Nanoparticle Research** 17:265. (IF: 2.184)

(6) TS Reddy, **H Kulhari**, VG Reddy, V Bansal, A Kamal, R Shukla. (2015) Design, Synthesis and Biological evaluation of 1, 3-diphenyl-1H-Pyrazole derivatives containing benzimidazole skeleton as potential anticancer agents and apoptosis inducing agents. **European Journal of Medicinal Chemistry** 101:790-805. (IF: 3.447)

(7) TS Reddy, **H Kulhari**, VG Reddy, AV Subba Rao, V Bansal, A Kamal, R Shukla. (2015) Synthesis and biological evaluation of pyrazolo–triazole hybrids as cytotoxic and apoptosis inducing agents. **Organic and Biomolecular Chemistry**. (Accepted) (IF:3.562)

(8) D Pooja, **H Kulhari**, L Tunki, S Chinde, M Kuncha, Paramjit Grover, SS Rachamalla, R Sistla. (2015) Nanomedicines for targeted delivery of etoposide to non-small cell lung cancer using transferrin functionalized nanoparticles. **RSC Advances** 5, 49122-49131. (IF: 3.840)

(9) **H Kulhari**, D Pooja, MK Singh, AS Chauhan. (2015) Optimization of carboxylate-terminated poly (amidoamine) dendrimer-mediated cisplatin formulation. Drug

Development and Industrial Pharmacy 41(2) 232-238. **(IF: 2.101)**

(10) **H Kulhari**, D Pooja, S. Srivastava, VGM Naidu, R Sistla. (2014) Peptide conjugated polymeric nanoparticles as a carrier for targeted delivery of docetaxel. **Colloids and Surfaces B: Biointerfaces** 117, 166–173. (IF: 4.152)

(11) **H Kulhari**, D Pooja, MK Singh, R Sistla. (2014) Colloidal stability and physicochemical characterization of bombesin conjugated biodegradable nanoparticles. **Colloids and Surfaces A: Physicochemical and Engineering Aspects** 443, 459-466. **(IF: 2.752)**

(12) D Pooja, **H Kulhari**, Mayank K. Singh, Sudip Mukherjee, SS Rachamalla, R Sistla. (2014). Dendrimer–TPGS mixed micelles for enhanced solubility and cellular toxicity of taxanes. **Colloids and Surfaces B: Biointerfaces** 121, 461-468. (IF: 4.152)

(13) D Pooja, DJ Babu Bikkina, **H Kulhari**, Nikhila N, S Chinde, AK Tiwari. (2014) Fabrication, characterization and bioevaluation of silibinin loaded chitosan nanoparticles. **International Journal of Biological Macromolecules** 69, 267–273. (IF: 3.096)

(14) D Pooja, S Panyaram, **H Kulhari**, RS Sunder, R Sistla. (2014) Xanthan gum stabilized gold nanoparticles: characterization, biocompatibility, stability and cytotoxicity. **Carbohydrate Polymers** 110, 1–9. (IF: 4.074)

(15) **H Kulhari**, DP Kulhari, SK Prajapati, AS Chauhan. (2013) Pharmacokinetic and Pharmacodynamic studies of PAMAM dendrimer based Simvastatin oral formulations for treatment of hypercholesterolemia. **Molecular Pharmaceutics** 10, 2528−2533. (IF: 4.384)

(16) G Swami, D Pooja, **H Kulhari**, KM Kymonil, SA Saraf. (2013) Surface modification of poly (l-lactic acid) microspheres for site-specific delivery of ketoprofen for chronic inflammatory disease. **Journal of Drug Targeting** 21 (3), 232-239. (IF: 2.741)

Manuscripts submitted to the journals

(19) **H Kulhari**, D Pooja, R Kota, SR Telukutla, R Tabor, R Shukla, DJ Adams, R Sistla, V Bansal. Cyclic RGDfK peptide functionalized polymeric nanocarriers for targeted anticancer applicability of gemcitabine. Submitted to Nanoscale.

(20) D Pooja, **H Kulhari,** DJ Adams, R Sistla. Formulation and dosage of therapeutic nanosuspension for active targeting of docetaxel (WO 2014210485A1). Submitted to Expert Opinion on Therapeutic Patent.

(21) D Pooja, L Tunki, **H Kulhari**, B Reddy, R Sistla. Characterization, biorecognitivity and stability of WGA grafted and rifampicin loaded lipid nanostructures. Submitted to Chemistry and Physics of Lipids.

Manuscripts under preparation

(22) **H Kulhari**, D Pooja, S Shrivastava, M Kuncha, VGM Naidu, V Bansal, DJ Adams, R Sistla. Synthesis of trastuzumab grafted PAMAM dendrimers for the selective delivery of anticancer drug to HER2-positive breast cancer.

(23) **H Kulhari**, SR Telukutala, D Pooja, R Shukla, DJ Adams, R Sistla, V Bansal. Peptide grafted, self-assembled poly(glutamic acid)-phenylalanine nanoparticles for active targeting of camptothecin to brain glioblastoma.

(24) TS Reddy, **H Kulhari**, VG Reddy, R Shukla, A Kamal, V Bansal. Design, Synthesis and biological evaluation of novel pyrazole-anilino hybrid derivatives as anticancer and apoptosis inducing agents.

(25) TS Reddy, **H Kulhari**, BD Sahu, S Nekkanti, VG Reddy, S Ponnepalli, N Jain, N Shankaraiah, R Shukla, A Kamal, V Bansal. Design, synthesis and biological evaluation of phenanthrene based tylophorine derivatives containing triazole nucleus as NF-κB inhibitors and apoptosis inducing agents.

(26) D Pooja, **H Kulhari**, SS Rachamalla, V Bansal, R Sistla. Lectin conjugated solid lipid nanoparticles for targeted delivery of paclitaxel to lung cancer.

(27) MK Singh, **H Kulhari**, S K. Jain, AS Chauhan. Development and evaluation of PAMAM dendrimer-mediated combination therapy of ramipril and hydrochlorthiazide.

(28) V Mistry, **H Kulhari**, V Bansal, R Shukla. Dendrimer-based nanoformulations for enhanced solubility, stability and anticancer activity of thymoquinone.

Book chapters (Under preparation)

(1) **H Kulhari**, D Pooja, S Shrivastava, SR Telukutala, AK Barui, CR Patra, N VGM., DJ Adams, R Sistla.
Chapter title: Cyclic-RGDfK directed docetaxel loaded nanomicelles for angiogenic tumour targeting
Book: Integrin targeting systems for tumor diagnosis and therapy.
Publisher: Humana Press, a part of Springer Science and Business Media

(2) D Pooja, **H Kulhari**, SS Rachamallas, R Sistla.
Chapter title: Nano-therapeutic strategies for lung cancer management.
Book: Therapeutic Nanostructures;
Publisher: Elsevier

Conference presentations

(1) 6th **International Nanomedicine Conference**, held at University of New South Wales, Sydney from 6-8th July 2016.

(2) 5th FIP **Pharmaceutical Sciences World Congress** (PSWC), held at **Melbourne**, Australia, from 13 – 16th April 2014.

(3) AICTE sponsored National Seminar on-**Recent Advances in Pharmaceutical Education and Research**, held at BNIPS, **Udaipur** dated on 5-6th March 2014.

(4) 27th **International Carbohydrate Symposium**, held at Indian Institute of Science, **Bangalore** dated on 12-17thJanuary 2014.

(5) AICTE sponsored National seminar on **Recent trends in development of novel drug delivery systems** held at Jaipur College of Pharmacy, **Jaipur** on 16-17th March 2013.

Workshop

(1) Workshop on **Drug Development: Conceptualization to Commercialization** (D2 @C2 - 2012), National Institute of Pharmaceutical Education and Research (NIPER), **Hyderabad**, October, 18-20, 2012.